



Universiteit
Leiden
The Netherlands

Phenotypic screening with 3D cell-based assays

Booij, T.H.

Citation

Booij, T. H. (2017, December 20). *Phenotypic screening with 3D cell-based assays*. Retrieved from <https://hdl.handle.net/1887/59503>

Version: Not Applicable (or Unknown)

License: [Licence agreement concerning inclusion of doctoral thesis in the Institutional Repository of the University of Leiden](#)

Downloaded from: <https://hdl.handle.net/1887/59503>

Note: To cite this publication please use the final published version (if applicable).

Cover Page



Universiteit Leiden



The following handle holds various files of this Leiden University dissertation:

<http://hdl.handle.net/1887/59503>

Author: Booij, T.H.

Title: Phenotypic screening with 3D cell-based assays

Issue Date: 2017-12-20

2017

Phenotypic screening with 3D cell-based assays

dissertation

Tijmen Harmen Booij

Leiden Academic Centre for Drug Research | LACDR |
Leiden, The Netherlands

Phenotypic screening with 3D cell-based assays

Tijmen H. Booij

Phenotypic screening with 3D cell-based assays

Tijmen Booij

September 2017

ISBN: 978-94-028-0871-1

© 2017, Tijmen Booij. All rights reserved. No part of this thesis may be reproduced or transmitted in any form, by any means, electronic or mechanical, without prior written permission from the author.

Design and lay-out by Studio Amy Guijt

Phenotypic screening with 3D cell-based assays

Proefschrift

Ter verkrijging van de graad van Doctor aan de Universiteit Leiden,
op gezag van Rector Magnificus prof.mr. C.J.J.M. Stolker,
volgens besluit van het College voor Promoties
te verdedigen op woensdag 20 December 2017
klokke 10:00 uur

door

Tijmen Harmen Booij

Geboren te Den Helder, Nederland
in 1988

Promotor

Prof. Dr. Bob van de Water	(Universiteit Leiden/LACDR)
Prof. Dr. Dorien J.M. Peters	(Leids Universitair Medisch Centrum)

Co-promotor

Dr. Leo S. Price	(Universiteit Leiden/Ocello B.V.)
------------------	-----------------------------------

Promotiecommissie

Prof. Dr. Hubertus Irth	(Universiteit Leiden/LACDR) (voorzitter)
Prof. Dr. Joke A. Bouwstra	(Universiteit Leiden/LACDR) (secretaris)

Overige leden

Prof. Dr. Ad P. IJzerman	(Universiteit Leiden/LACDR)
Prof. Dr. Huib Ovaa	(Leids Universitair Medisch Centrum)
Prof. Dr. Roos Masereeuw	(Universiteit Utrecht)
Prof. Dr. Paul Jennings	(VU Amsterdam)

The investigations described in this thesis were performed at Division of Toxicology of the Leiden Academic Centre for Drug Research, Leiden University, Leiden, the Netherlands and at the Human Genetics department, Leiden University Medical Center, Leiden, the Netherlands

This research was funded by the Dutch Technology Foundation STW (project 11823), which is part of the Netherlands Organization for Scientific Research (NWO).

To my parents

INDEX

CHAPTER 1	11
General introduction	
CHAPTER 2	35
Getting the most out of 3D cell based assays with high content image analysis and phenotypic profiling	
CHAPTER 3	55
Development of a 3D tissue culture-based high-content screening platform that uses phenotypic profiling to discriminate selective inhibitors of receptor tyrosine kinases	
CHAPTER 4	83
High-throughput phenotypic screening of kinase inhibitors to identify drug targets for polycystic kidney disease	
CHAPTER 5	113
Phenotypic profiling of 3D-cultured micro-tissues to identify selective inhibitors of cyst growth	
CHAPTER 6	145
<i>In vitro</i> 3D phenotypic drug screen identifies celastrol as an effective <i>in vivo</i> inhibitor of polycystic kidney disease	
CHAPTER 7	173
General discussion and future perspectives	
CHAPTER 8	189
Appendices	

chapter 1

General introduction

Tijmen H. Booij

Challenges in drug research & development

Over the past decades, it has become clear that the increasing investments in pharmaceutical research and development (R&D) have not translated into an anticipated increase in approved new drugs. With new drugs being discovered at a steady rate by the pharmaceutical industry and the exponentially rising R&D costs, it is becoming more difficult to obtain a return of R&D investments and to fund new research. It is possible that the current R&D strategies are exhausted and that the only solution to this problem is a radical change towards more innovative strategies to improve success rates of new drugs.¹ Additionally, when older patents of important blockbuster drugs expire, the pharmaceutical industry will be required to address R&D productivity to remain viable.

As a brief summary of the steps in current drug discovery, novel drug candidates are typically discovered after the identification of a new drug target. Drug targets are often proteins that are aberrantly active or inactive in a pathophysiological process, and modulation of these targets, or their signalling cascade, could therefore be used to alleviate or reverse disease symptoms. Not surprisingly, the identification of new drug targets typically requires many years of intensive study of disease-associated cellular signalling pathways. After a disease target has been identified, potential drug candidates that bind to the target protein, often many thousands, can be synthesised and assayed on cell culture models for the disease. This pre-selection on cell culture models is required in order to preselect a small number of molecules for *in vivo* efficacy measurement and clinical development (figure 1).

This particular drug discovery workflow is target-based: it relies on known information of disease targets.² A drawback associated with this strategy is the assumption that modulation of a single protein target is sufficient for the alleviation of disease symptoms: many diseases are much more complex than this and require a broader targeting approach, which can for example be overcome by treatment with multiple drugs. Another consequence of this target-driven drug discovery is that only the most potent inhibitors or activators for certain potentially druggable targets will progress through drug development. While these molecules may be curative for a certain disease, many diseases do not require complete abolishing of one molecular target, but rather require fine-tuning of multiple target proteins, which is often the most challenging to achieve. Importantly, entirely abolishing a single disease target can also lead to drug side effects. Antineoplastic drugs (chemotherapeutics) are an example of this: while these drugs mostly interfere with cell division or promote programmed cell death and thereby inhibit tumour growth, they can also have similar effects on healthy cells, with side effects as a result.

In addition to the increasing R&D costs, high drug attrition rates pose a large challenge. Most drugs initially introduced in the drug development pipeline will never reach the clinical evaluation stage. However, even for drugs that enter clinical trials, the average success rate is only around 11%.³ Because this phase in drug development is associated with the highest costs, it is essential for the pharmaceutical industry to

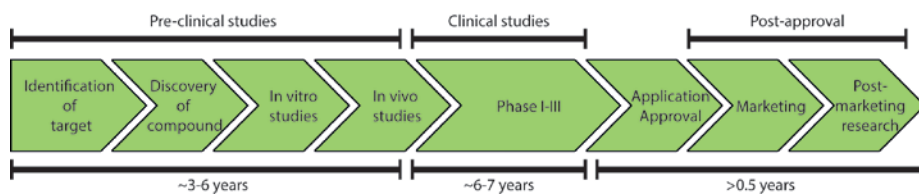


FIGURE 1 Schematic representation of the drug discovery pipeline resulting from the identification of druggable targets.

ensure that new drugs do not fail during this phase, or after the clinical trials. However, many drugs that are introduced in clinical trials suffer from lack of efficacy or toxicity that was not predicted.⁴ Additionally, the success rate of clinical trials highly differs between therapeutic areas. For example, drugs for cardiovascular indications have an approximate 20% chance of success, while this is only 8% for drugs targeting diseases of the central nervous system.³ These differences are likely, at least in part, attributable to our knowledge of the etiology of the disease, the complexity of the biology and the predictive value of disease models. Also after drug approval by the Food and Drug Administration (FDA, USA) or European Medicines Agency (EMA, Europe), unexpected toxicity or lack of clinical benefit remains an important factor for drug withdrawal.³ Therefore, in order to make better and safer drugs and to achieve higher success rates in the clinic, it is necessary that better drugs are pre-selected before these reach clinical development.

Physiological relevance of 2D *in vitro* disease models to predict drug efficacy

In order to pre-select better drugs for clinical development, it is necessary to have a more detailed look at the earlier stages of the R&D pipeline. After the identification of a druggable target for a disease, potential drug candidates that modulate the activity of the target can be developed, and can eventually be tested in a biological model.

When potential drug candidates are first investigated in cell-based biological models (*in vitro*), generally their efficacy is assessed on two-dimensional (2D) cell culture models, which are often named monolayers (figure 2). In such a cell culture system, cells that are relevant to the investigated disease or process are cultured on culture plastic in growth medium, supplemented with animal serum and often antibiotics. These cell models are generally easy to maintain and cheap to use, the latter of which is extremely important when testing many thousands of candidate molecules at once, often referred to as high-throughput screening (HTS). However, in recent years it has become increasingly clear that for many diseases, these monolayer cultures often fail to predict drug efficacy in animal models (*in vivo*) or in clinical trials.

A large problem associated with this poor translation is that many drug candidates that appear to be successful in such an *in vitro* model, fail in the later, more

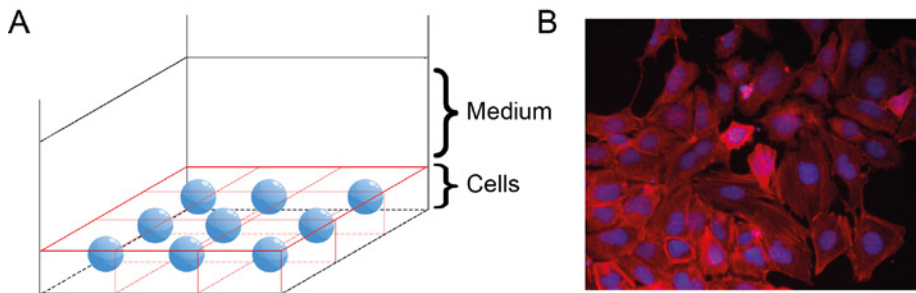


FIGURE 2 Cells cultured as a monolayer are poor simulators of human biology.

A) Schematic representation of cells cultured as a monolayer on culture plastic. Red lines represent the cortical cytoskeleton and nuclei are shown as blue spheres. **B)** Immunofluorescence image of 2D-cultured mIMCD3 cells (BD Pathway 855, 10x objective). Red colour shows cytoskeleton (rhodamine-phalloidin) and blue colour shows nuclei (Hoechst 33258).

expensive, drug development stages. Conversely, it is possible that potentially good drugs fail to show desirable effects in monolayer cell cultures, causing these to be filtered out and never progress into further development. A key concept in this problem is that monolayer cultures cannot adequately recapitulate the complex conditions in the body, since tissues are comprised of many cell types that interact within a three-dimensional environment. Hence, the tissue architecture that is observed in the body cannot be adequately recapitulated using monolayer cell culture models, since these fail to reflect the tissue architecture and its relevance in various disease processes. This, coupled to the implementation of the three R's (reduction, refinement, replacement) to reduce the use of animals in drug testing⁵ means that more relevant *in vitro* evaluation models are required to select better drugs.

In order to provide a background for the different disease areas described throughout this dissertation, the following subchapters give a brief overview on two neoplastic disorders, cancer and polycystic kidney disease (PKD), where tissue architecture is essential for the pathophysiology and thereby providing a rationale for the development of new *in vitro* disease models on which to test candidate drugs.

CANCER

Disease background

Cancer is a neoplastic disorder that is characterized by abnormal cell proliferation and is among the most common causes of death worldwide.⁶ The process by which healthy cells can transform into cancer cells and form a tumour is a multistep process by which cells need to acquire properties that confer a proliferative advantage, such as self-stimulatory growth signals, insensitivity to anti-growth signals, the ability to evade apoptosis and avoid immune destruction and the ability to induce angiogenesis. These

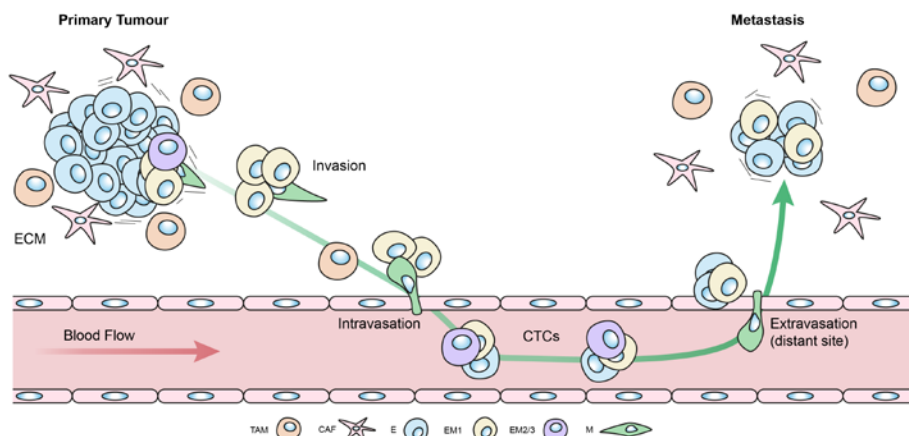


FIGURE 3 Schematic representation of the metastatic cascade showing the processes of invasion, intravasation and extravasation at a distant site to establish a metastasis. Extracellular matrix, ECM; Circulating tumour cells, CTCs; cancer-associated fibroblast, CAF; tumour-associated macrophage/M2-type macrophage, TAM. E (epithelial), EM1-3 (intermediate stages/partial EMT) and M (mesenchymal) represent different stages of EMT. Figure based on Nieto et al, 2016.⁹

factors, amongst many more, contribute to the origin and growth of a primary tumour⁷⁻⁸ and are generally the result of acquired mutations that confer a growth advantage.

Importantly, the main cause of cancer-related deaths generally is not the presence of the primary tumour, but rather the metastasis of tumour cells to distant sites, where the growth of tumours can interfere with normal organ function. In order for metastasis to occur, tumour cells need to acquire migratory properties. These properties can then allow the cells to escape from the primary tumour into the blood stream (or lymphatic system), and eventually extravasate at a distant site. This metastatic cascade is illustrated in figure 3, and describes the process of invasion of tumour cells into the extracellular matrix, the intravasation into the blood stream and eventual extravasation at a distant site.⁹ In general, the cause of this migratory phenotype is the loss of cell-cell contacts and changes in cell-matrix contacts and the secretion of matrix-remodelling enzymes. Collectively, this switch in cellular behaviour is often termed epithelial- to mesenchymal transition (EMT). It is currently becoming clearer that the tumour extracellular matrix¹⁰⁻¹¹ and many immune cells¹²⁻¹⁵ play a role in carcinogenesis. Importantly, the causes of cancer are highly diverse, and range from genetic predisposition to DNA damage to diet.¹⁶ Specific signalling pathways that are involved in this process are therefore highly variable and also depend on the tumour type and its underlying mutations. It is therefore not feasible and also not the scope of this chapter to discuss all these properties in detail, and the reader is referred to other relevant literature.^{7-9, 16-18}

Current therapeutic strategies and limitations

Surgery is often the first line of treatment against a primary tumour that has not yet metastasized, sometimes supplemented with radiation- or chemotherapy, if required. Whether this strategy is successful depends highly on the tumour type, its underlying mutations and the tumour stage. For tumours that have already metastasized, surgery on its own is often not sufficient to cure the patient, and it is therefore often supplemented with radiation-, chemo- or immunotherapy. These additional therapies generally function to inhibit tumour cell proliferation, taking advantage of the tumours' defective DNA repair mechanisms, or to eradicate tumour cells by the immune system. However, such therapies, with the possible exception of immunotherapy, usually have side effects related to their effects on healthy cells. For example, the chemotherapeutic drug cisplatin (cis- diamminedichloroplatinum(II), CDDP) is a molecule that intercalates directly into the tumour cells' DNA,¹⁹ thereby preventing cell division and tumour growth. However, the use of this molecule is limited by its nephrotoxic effects,²⁰ which are, at least in part, attributable to active cisplatin uptake in the kidneys by high affinity copper uptake protein 1 (Ctr1)²¹ and organic cation transporter OCT2 (SLC22A2),²² causing the local increase in intracellular cisplatin concentrations that is responsible for its nephrotoxic side effects. While molecules such as cisplatin can be effective at preventing the growth of tumours and their metastases, many such molecules do not effectively eradicate 100% of the tumour cells. Such drugs have mostly been developed using 2D-cultured, immortalized (and rapidly proliferating), tumour cell lines, most of which have retained little resemblance to the tumour they were originally derived from. Critically, because tumours are comprised of more than one cell type, some cell types are often unaffected by these proliferation-inhibiting drugs, which can in turn be responsible for tumour re-growth and therapy resistance.

Another strategy to improve patient survival is to prevent cancer metastasis, by blocking processes such as angiogenesis, cancer cell invasion into the surrounding matrix, intravasation or extravasation. Especially in this context, conventional 2D cell culture models represent a poor representation of the *in vivo* situation, since they lack the presence of extracellular matrix to model these processes. As one of the main topics of this thesis, we describe the development of a more physiologically relevant cell culture assay that can be used to study cancer cell invasion (the first step of the metastatic cascade) and to test treatments to prevent this process.

POLYCYSTIC KIDNEY DISEASE

Genetic background

Polycystic kidney disease (PKD) is a genetic disorder in which fluid-filled cysts develop in the kidneys (figure 4). In principal, these cysts develop in all segments of the nephron,²³ the kidney's smallest functional unit, but have been described to originate more often from the collecting duct.²⁴ As more and more cysts develop and grow over a patient's lifetime, kidney function deteriorates to end-stage renal disease (ESRD), the point where a patient requires kidney transplantation for survival. PKD exists as

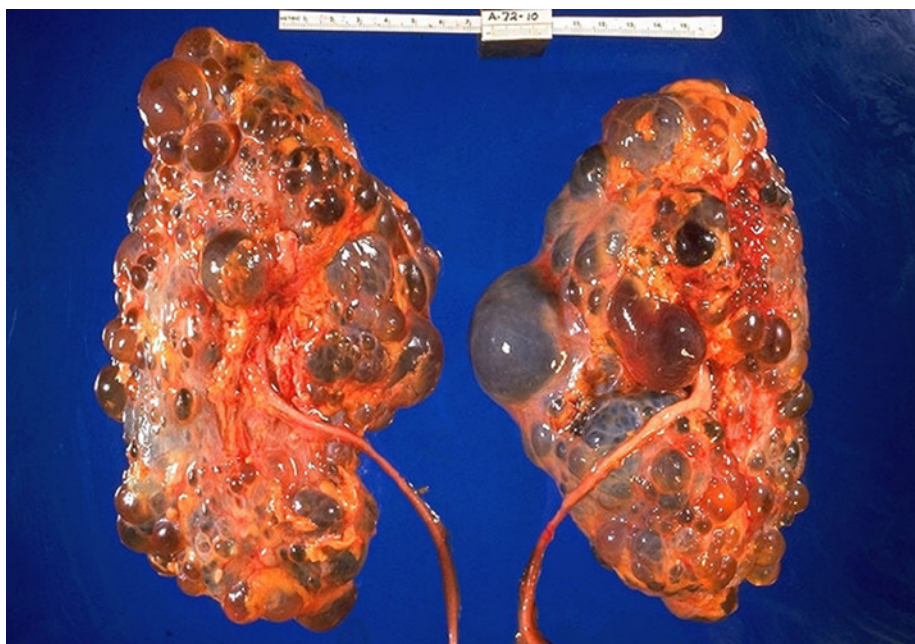


FIGURE 4 Pathology of polycystic kidney disease. Image provided by CDC/Dr. Edwin P. Ewing, Jr., 1972.

an autosomal dominant (ADPKD) and autosomal recessive (ARPKD) form. ADPKD is the most common form of the disease, which affects approximately 1 in 2500 people,²⁵ and thereby also places a large burden on society. The autosomal recessive form is much less prevalent (only approximately 1 in 20000 people²⁶), but has a more severe nature. This specific form of PKD is often referred to as childhood PKD, because kidney function declines much faster than in the autosomal dominant form. Approximately half of the newborns that survive the neonatal period will develop ESRD within the first decade of life.²⁷

In the case of ADPKD, a heterozygous genetic defect in either the *PKD1* gene on chromosome 16, or the *PKD2* gene on chromosome 4, underlies cyst formation, although the precise mechanism by which these mutations can cause the development of cysts remains largely unknown. One hypothesis that supports the slow progression of ADPKD is that heterozygous mutation of *PKD1* or *PKD2* is not sufficient to cause the formation of cysts, and inactivation of the second allele during life is required. This is supported by the finding that homozygous *Pkd1* or *Pkd2* inactivation in mice is embryonic lethal.²⁸ Additionally, renal injury may be an important contributor²⁹ to initiate cyst formation, as it is known that the presence of cysts can obstruct neighbouring tubules, likely leading to a cystic snowball effect that aggravates the cyst formation.³⁰

PKD1 encodes the protein polycystin-1, which is a 467kDa transmembrane re-

ceptor-like molecule thought to be involved in mechanosensing³¹ and cell-cell and cell-matrix interactions.³² Moreover, this protein was recently identified as a receptor for various WNT ligands.³³ Polycystin-2 is a 110kDa polypeptide encoded by the *PKD2* gene, and this protein is known as a non-selective cation channel that is permeable to calcium ions.³⁴ Polycystin-2 is often named transient receptor potential polycystic 2 (TRPP2). ADPKD as a result from mutations in *PKD2* is generally milder, since cysts develop later.³⁵ The polycystin proteins can bind to each other³⁶ and form a functional complex³⁷⁻³⁸ which is thought to be involved in the translation of mechanical stimuli to an influx of Ca^{2+} into the cell. This process is thought to be mediated by the localization of this complex to the tubular cells primary cilium, an organelle protruding from the cell membrane. However, the polycystin proteins localize also to different parts of the cell, such as the endoplasmic reticulum and cell-cell and cell-matrix contacts,³⁹⁻⁴¹ where they likely perform different functions ranging from mechanotransduction to regulating planar cell polarity (PCP).

For the autosomal recessive form of PKD, mutations in the *PKHD1* gene are responsible for the early onset and rapid progression of cystic kidney disease. It is estimated that such mutations are carried by approximately 1:70 people.^{27, 42} The *PKHD1* gene encodes for the protein fibrocystin, also known as polyductin. Fibrocystin is a receptor-like protein for which ligands are currently unknown, and it can form a complex with polycystin-2.⁴³ Due to the lower prevalence of ARPKD, the following sections of this subchapter will focus instead on ADPKD. For more insight into the mechanistic background of ARPKD and its similarities with ADPKD, the reader is referred to other literature.²⁶

Signalling alterations in ADPKD

Inactivating mutations in the genes responsible for ADPKD result in dysregulated cellular signalling pathways, with reduced intracellular Ca^{2+} levels as a central mediator. This reduction of Ca^{2+} can in turn activate calcium-inhibitable adenylyl cyclase (AC), to stimulate 3'-5'-cyclic adenosine monophosphate (cAMP) production. Conversely, reduced Ca^{2+} levels can also inhibit calcium-dependent phosphodiesterases (PDEs) to prevent cAMP breakdown. Alternatively, abnormal activation of the vasopressin V2 receptor (V2R) by antidiuretic hormone arginine vasopressin (AVP) can also drive the accumulation of cAMP through the activation of AC. This mechanism, together with the alterations in calcium homeostasis, has a central role in the pathophysiology of ADPKD.⁴⁴

cAMP is an important second messenger, and the increased levels lead to many changes in cellular signalling, including increased activity of B-Raf, ERK, mTOR and PI3K pathways and of various proteins involved in the cell cycle and fluid transport (figure 5).⁴⁴⁻⁴⁷ Together, these changes lead to increased cell proliferation, dedifferentiation and increased fluid secretion. These signalling alterations likely lead to the initiation of cyst formation and the consequent expansion that eventually causes renal failure.

Current therapeutic strategies

Currently, treatment for polycystic kidney disease is mainly aimed at alleviating fre-

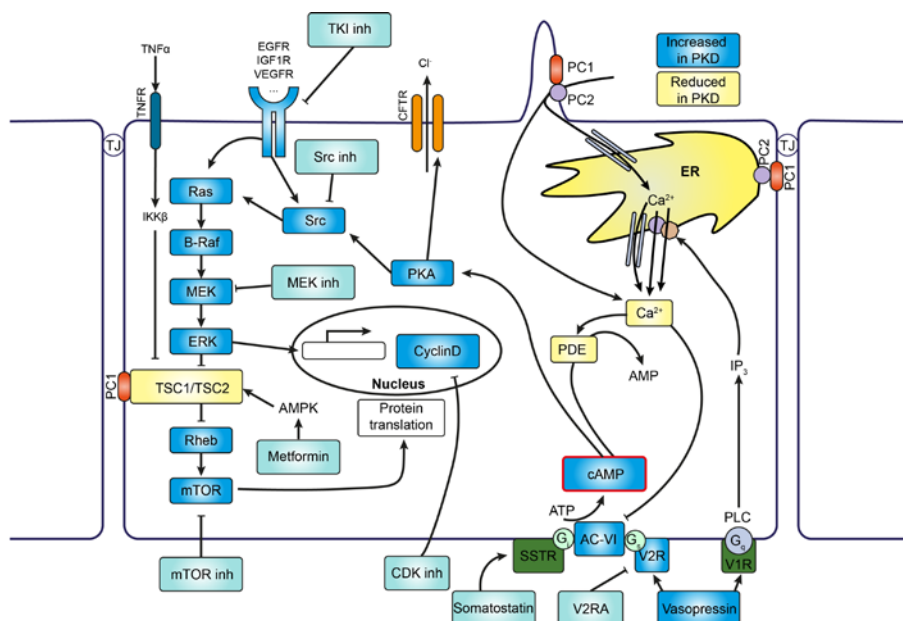


FIGURE 5 Schematic representation of known signalling alterations in ADPKD. Figure based on Torres et al, 2007 and Torres, 2010.^{45, 110} Adenosine monophosphate (AMP), 5'AMP-activated protein kinase (AMPK), Adenylyl cyclase 6 (AC-VI), 3',5'-cyclic AMP (cAMP), cyclin-dependent kinase (CDK), cystic fibrosis transmembrane conductance regulator (CFTR), endoplasmic reticulum (ER), epidermal growth factor receptor (EGFR), extracellular regulated kinase (ERK), inositol triphosphate (IP₃), insulin-like growth factor 1 receptor (IGF-1R), mammalian target of rapamycin (mTOR), mitogen-activated protein-kinase/ERK kinase (MEK), phosphodiesterase (PDE), phospholipase c (PLC), polycystin 1 (PC1), polycystin 2 (PC2), protein kinase A (PKA), somatostatin receptor (SSTR), tuberlin (TSC2), hamartin (TSC1), tyrosine kinase inhibitor (TKI), tumour necrosis factor alpha (TNF α), TNF receptor (TNFR), vascular endothelial growth factor receptor (VEGFR), vasopressin V1 receptor (V1R), vasopressin V2 receptor (V2R), V2R antagonist, (V2RA).

quent disease-associated symptoms such as hypertension,⁴⁸⁻⁵⁰ cyst infection,⁵¹ and pain.^{45, 52-53} The patient will ultimately require renal transplantation, when the kidney function has deteriorated to the point of ESRD. However, as kidneys for transplantation are not always available, there have been many efforts to find a medicinal treatment to prevent disease progression. Due to the genetic background of the disease, it is amenable that genetic screening to allow early detection of the disease combined with pharmacological treatment that delays progression of the disease is sufficient to allow for a lifetime without disease symptoms. However, due to the extensive pathway deregulations in PKD (figure 5), the identification of effective drug treatments has been problematic.

Currently, the only therapy approved in the EU to slow disease progression is tolvaptan (marketed under the name *Jinarc*). This V2R inhibitor slowed down increases

in kidney volume and the decline in renal function in a recent Phase III clinical trial.⁵⁴ Blockade of the V2R prevents the binding of AVP to the receptor and prevents the consequent activation of AC, thereby delaying the growth of cysts. However, treatment with tolvaptan is also correlated with extensive side-effects that could limit patient compliance. These side-effects are largely related to the pharmacological action of tolvaptan and require patients to consume excessive amounts of water due to increased urine production. In addition, even though liver injury as a result of tolvaptan treatment is infrequent, patients receiving long-term tolvaptan treatment may be at risk of serious irreversible liver injury.⁵⁵⁻⁵⁷ This illustrates that novel therapies are still needed.

In the past, there have been several clinical trials for mTOR inhibitors such as sirolimus (rapamycin) or everolimus. While mTOR inhibitors have often been proven effective in *in vivo* PKD models,⁵⁸⁻⁶¹ there have also been conflicting results.⁶² In line with this, the clinical trials that have been performed for such inhibitors, have failed to show a clinical benefit.⁶³⁻⁶⁸ However, it is possible that renal targeting of mTOR inhibitors like rapamycin can improve therapeutic response due to local increases in concentration.⁶⁹

Other therapies currently undergoing clinical evaluation include somatostatin analogues (ALADIN trial), niacinamide, epidermal growth factor (EGF) inhibitors, and triptolide, (although a recent study with triptolide, NCT00801268, has been terminated due to high patient drop-out). A more detailed overview of the clinical trials undertaken for ADPKD has recently been published elsewhere.⁷⁰

Limitations of 2D in vitro models

Even though 2D *in vitro* models for PKD have been useful to investigate signalling pathways, there are limits to their usefulness in evaluating the effects of potential therapeutics. Principally, the main pathophysiological characteristic, the growth of cysts, cannot be simulated in 2D, since a cyst is a three-dimensional structure. Very importantly, when test molecules are provided to 2D-cultured monolayers, the cells will be exposed to the test molecules on their *apical* side (figure 6A), whereas a closed cyst is more likely to take up a test molecule through its *basolateral* side (figure 6B). These differences in administration route could in turn lead to differences in intracellular concentrations, depending on transporter localization differences between *apical* and *basal* membranes.

Therefore, while the signalling pathways in PKD have often been investigated on 2D cell culture models, pharmacological treatment evaluation for PKD has traditionally been pursued in animal models, as treatment efficacy cannot adequately be measured using 2D cell culture. With the desire to reduce animal experimentation in mind,⁵ new, more relevant, *in vitro* cell culture models for PKD need to be developed to facilitate preclinical testing of potential drugs. The development of relevant *in vitro* assays for PKD is therefore an important topic in this thesis.

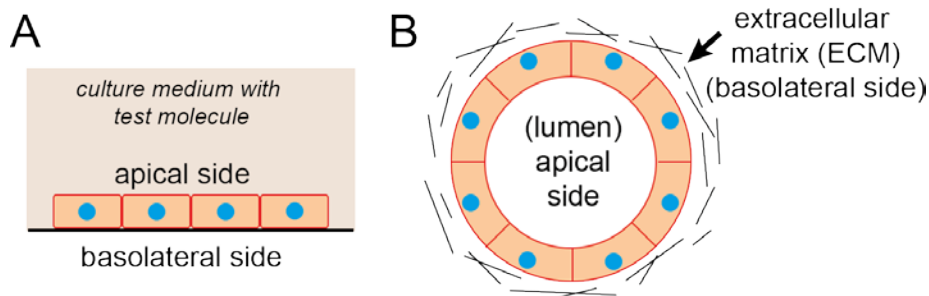


FIGURE 6 2D monolayers poorly recapitulate renal cysts. A) Schematic representation of cell polarity when cells are cultured as a monolayer. Apical side of cells is in contact with culture medium with test molecules. B) Schematic representation illustrating inverted orientation of cysts cultured in hydrogels. Basolateral side is in contact with the culture medium and test molecules.

3D cell culture models in drug discovery

In order to overcome problems traditionally associated with 2D cell cultures and to improve physiological relevance of *in vitro* cell models, the past couple of decades have witnessed the development of three-dimensional (3D) cell culture models. These models were developed in order to better model disease biology and bridge the gap between 2D *in vitro* models and the *in vivo* situation.⁷¹ A great example that cells, when confined to a monolayer, display unnatural behaviour was proven when Bissell and colleagues showed that non-cancerous breast epithelial cells developed similarly to breast carcinoma cell lines when grown in 2D monolayers. However, when these cells were grown in reconstituted basement membrane (BM), non-cancerous cells responded to the presence of the BM by growth arrest, lumen formation and correct cell polarity, whereas the cancer cell lines were not growth-inhibited by the presence of BM.⁷² Since then, several groups have proven large differences between 2D- and 3D-cultured cells, such as increased metabolic enzyme expression in liver cells which, may have profound consequences for *in vitro* toxicity assessment.⁷³⁻⁷⁴ Additionally, the growth of tumour cells in 3D is known to enhance *in vivo*-like gene expression and structural properties.⁷⁵⁻⁷⁸

3D cell culture models in drug screening

Over the years, many different technologies have been optimized to allow compound screening on 3D cultured micro-tissues. Broadly, these techniques can be divided into scaffold-free and scaffold-based technologies, while the first category is largely comprised of multicellular tumour spheroids suspended in media, the second category comprises all matrix-embedded models such as the models used throughout this thesis.

Multicellular spheroids are clusters of cells that grow in suspension media. These media do not provide a rigid extracellular matrix and the cells are forced to aggregate

to a multicellular spheroid because cell-cell interactions dominate the cell-substrate interactions.⁷⁹⁻⁸⁰ These cultures are known to be easy to prepare and provide physiologically relevant responses.⁸¹ The cultures can be easily adapted in most labs, since there are many commercially available solutions, such as the hanging-drop microtiter plate (HDM) technology developed by InSphero AG. This technology can be readily scaled up to 96⁸² and even 384 well plate formats.⁸³ Additionally, spheroids can be grown in the ultra-low attachment 96-well or 384-well plates commercially available from Corning as used here.⁸⁴ These 3D culture systems therefore have large potential in 3D high-throughput screening. Drawbacks of using such systems is that cells are required to produce their own extracellular matrix as they receive no support from the suspension media, and the limitation to the number of spheroids that are present in each well. Additionally, such a spheroid model may not recapitulate some aspects of tissue biology, since processes such as tubulogenesis, fibrosis and many more are not dependent on spheroid formation in the body. As an upside, the presence of suspension media rather than a gel makes it easier to collect 3D cultured cells for other techniques in molecular biology such as western blotting for the detection of proteins.

In contrast to the scaffold-free techniques, scaffold-embedded cell cultures are often used to prepare 3D cultures. These scaffolds are discussed further in more detail below, but mostly function to provide an extracellular matrix (ECM) to the cultured cells. Advantages of these scaffold-embedded cell cultures are that they are generally compatible with regular 96- and 384 well plates, and that the morphology of the cultured multicellular structures is not limited to the formation of spheroids. Additionally, the scaffold can often be modified to accommodate different cell types and behaviour, and multicellular structures can grow in all planes of the scaffold. While the increased number of structures in each scaffold can be considered as an advantage, it also poses new challenges for the analysis of results, as will be discussed in more detail in **chapter 2**. However, due to the presence of a scaffold, which is often rich in proteins, these 3D culture techniques are often not easily compatible with standard techniques such as western blotting, nucleic acid (RNA/DNA) extraction or immunofluorescent labelling.

ECM-mimicking scaffolds for 3D cell culturing

It is important to realise that the ECM that cells grow in are not 'passive', but highly contribute to cellular signalling. Consequently, a large effort was directed to the development of different ECM-mimics that simulate biological ECM properties.⁸⁵⁻⁸⁸ Cell behaviour in 3D cell systems can be influenced by different matrix types. Importantly, the choice of matrix will depend on the cell type and aim of the study. In order to provide 3D cultured cells with more physiologically relevant microenvironments, hydrogels comprise a highly convenient and highly popular material for 3D culturing. However, many different types of hydrogel exist, and these gels can either be purely natural or synthetic.^{85, 88} Natural hydrogels are derived from natural sources and thereby inherently support cell viability and promote cellular signalling. As a disadvantage of this type of natural gel, it is often impossible to completely define the matrix and due to their nat-

ural background, they can also suffer from batch-to-batch variability, which can induce biological variation in cultured cells.⁸⁵ The most popular types of natural gels include agarose, collagen (often collagen type I derived from rat tail tendons), fibronectin, laminin, silk fibroin, fibrin and matrigel,⁸⁹ the latter containing natural ECM components and proteins.⁹⁰ An advantage of these natural materials is that by altering the concentration it is possible to alter the gel rigidity or pore size, making it easy to modify the gel properties, which in turn alters cell behaviour.⁹¹ Synthetic hydrogels, in contrast, are comprised of non-natural molecules, which have the advantage that the chemical composition of the resulting gels is highly reproducible and very well-defined.⁸⁵ An example of a synthetic hydrogel is poly-ethylene glycol (PEG), which can support cell viability.^{85, 92-95} These gels, however, do not always have desirable biological properties and generally lack important factors to support cell viability and *in vivo*-like cell growth. In order to improve their biocompatibility, synthetic hydrogels may be readily altered to incorporate, for example, relevant integrin-binding domains by incorporating ECM proteins or relevant peptide sequences. In addition, it is possible to generate 3D matrices using a combination of natural and synthetic polymers, and these can be designed to resemble the natural ECM. For a more detailed review on the different synthetic and natural hydrogels and their properties, the reader is referred elsewhere.^{85-86, 90}

Towards more relevant screening assays

Even though the currently available 3D culturing techniques have greatly improved physiological relevance of *in vitro* models, these models still have to be incorporated for routine drug screening.⁹⁶ Currently, the most common use of 3D cell culture assays is to validate observations made in 2D cultured cells. This can range from the validation of certain signalling cascades to validating selected hits obtained from compound screens. However, when validating hits from compound screens, it is possible that potentially good molecules have been filtered out due to screening in 2D cell cultures. It is therefore important to use more physiologically relevant assays in (primary) compound screening.

The main drawbacks for the incorporation of 3D cell culture assays in screening have traditionally been that such assays are often much more expensive than their 2D counterparts, making 3D assays unsuitable for large-scale compound screening. Additionally, 3D assays can encompass more biological variation, sometimes making it harder to obtain meaningful measurements. A solution to these problems has been provided by the adaptation of robotics for cell culture automation, and also the large-scale production of scaffolds in which to culture cells. Aside from these technological drawbacks, a case can be made against the use of transformed or immortalized cell lines in 3D assays. These immortalized cell lines are often used, also in this thesis, because they are relatively cheap to use and have little variation between batches. While these cells are therefore convenient for screening, it is important to mention that tissues are not composed of a single cell type, and more physiological characteristics may be captured by using a different cell model. Additionally, immortalized cell lines have often been passaged many times, which can change their (epi-)genetic and physiological

characteristics.⁹⁷⁻⁹⁸ Even though, in 3D cultures, these cell lines may display more *in vivo*-like behaviour, the relevance to a functional organ may be improved by the incorporation of multiple (non-immortalized) cell types. On the other hand, for screening large molecule libraries, this addition of multiple cell types may induce undesirable variation into the model, making efficacy readouts less consistent.

In recent years, there also has been an increased interest in the use of tissue-derived stem cells and induced pluripotent stem cells (iPSC) for drug screening. Indeed, such cell types can be used to more accurately simulate organ function,⁹⁹⁻¹⁰¹ but often also require extensive differentiation procedures, which means that they can be more expensive to work with. Additionally, these cells often require fresh patient-tissue supplies, meaning that they are not always readily available for screening and may also vary more between different sources. However, such stem cells do open the door for more personalized medicine, and it is possible that, eventually, these cell types will become more popular than cultured cell lines.

Alongside the selection of the correct cell type, it is important to also select the correct matrix to culture cells in, so that they can organize in a functional way to form tissue-like structures. An interesting recent development has been the use of de-cellularized organs, where the cells have been removed and the extracellular matrix can be solubilized to form hydrogels. This approach has been applied for multiple organs,¹⁰² such as colon,¹⁰³ heart,¹⁰⁴ kidney,¹⁰⁵ liver,¹⁰⁶ lung¹⁰⁷ and skin.¹⁰⁸ In its current status however, it is not likely that this can be applied in routine screening purposes. Another use for these de-cellularized organs can be found in organ replacement therapy, since de-cellularized organs can potentially be re-seeded with a patient's own cells to again form functional organs.¹⁰⁹

Aim and outline of this thesis

In **chapter 2**, we discuss, in addition to the importance of screening in biologically relevant *in vitro* models, the importance of having a biologically relevant assay readout. As many groups that make use of 3D cultured cells still use relatively simple measurements to assess compound efficacy, such as biochemical toxicity measurements, or single phenotypic parameter readouts of 3D cultures, the complexity that is provided inherently by 3D cultures can be exploited by the application of phenotypic profiling of drug effects.

In **chapter 3**, we use a 3D cultured prostate cancer cell line to model tumour cell invasion as a result of growth factor stimulation. As mentioned earlier in this chapter, cancer cell invasion is one of the first steps that eventually leads to cancer metastasis. This 3D culture model was scaled up for use with 384 well plates and automated liquid handlers, so that many compounds could be screened simultaneously. This screening platform was applied to measure the activity and selectivity of inhibitors of the c-Met and epidermal growth factor (EGF) receptor (EGFR) tyrosine kinases. We could identify selective inhibitors of both c-Met and EGFR, and could also identify dual kinase

inhibitors. These findings were subsequently confirmed after *in vitro* enzyme activity measurements.

In **chapter 4**, we describe the development of a 3D cell culture-based high-throughput screening platform for PKD. This screening platform was applied to screen a tyrosine kinase inhibitor library of 273 small molecules with pre-described targets, to identify new druggable targets for PKD. Using multiparametric phenotypic classification of compound effects, we could discriminate desirable compound effects from potentially toxic molecules. Using this strategy, we identified many molecules that targeted kinases that are known to be involved in PKD, such as mTOR, CDK and Chk, but we failed to identify PI3K inhibitors as effective molecules, even though this pathway is known to be dysregulated in PKD. Additionally, we found targets that have not been previously described in PKD, such as Syk. In this chapter, we show that using *in vitro* models with high pathophysiological relevance coupled to phenotypic profiling can be used to predict and validate molecular targets.

In **chapter 5**, we further applied the methodology developed in **chapter 4** to screen a kinase inhibitor library to investigate pathways involved in cystogenesis. We discovered that most active molecules overlapped in target specificity with **chapter 4**. However, in order to discriminate potentially non-specific molecules, we screened the entire molecule library using a tumour cell invasion model. This strategy allowed us to prioritize molecules that affected cystogenesis but not tumour cell phenotype.

In **chapter 6**, we applied the 3D cell culture model developed in **chapter 4** to screen a SPECTRUM compound library containing over 2320 molecules to find potentially new therapeutics against PKD. We found that 81 of the 2320 molecules potentially inhibited cyst growth, and using multiparametric phenotypic measurements we excluded potentially cytotoxic molecules. We selected two molecules, pyrinium pamoate, an antihelminthic drug, and celastrol, a triterpenoid derived from *Tripterygium Wilfordii*, for *in vivo* evaluation in an iKspCre-*Pkd1*^{lox,lox} mouse model of PKD. In contradiction with the effects observed *in vitro*, we did not observe beneficial effects of pyrinium pamoate on kidney volume and function. However, we discovered that cyst growth was markedly reduced after treatment with celastrol. In addition, celastrol prevented the associated decline in renal function and also ameliorated tissue fibrosis that normally accompanies cyst growth.

Chapter 7 provides a general discussion to discuss the conclusions in this work and the implications of the work presented in this thesis.

References

1. Munos B: Lessons from 60 years of pharmaceutical innovation. *Nat Rev Drug Discov* 8(12): 959-968, 2009
2. Swinney DC, Anthony J: How were new medicines discovered? *Nat Rev Drug Discov* 10(7): 507-519, 2011

3. Kola I, Landis J: Can the pharmaceutical industry reduce attrition rates? *Nat Rev Drug Discov* 3(8): 711-715, 2004
4. Waring MJ, Arrowsmith J, Leach AR, Leeson PD, Mandrell S, Owen RM, Pairaudeau G, Pennie WD, Pickett SD, Wang J, Wallace O, Weir A: An analysis of the attrition of drug candidates from four major pharmaceutical companies. *Nat Rev Drug Discov* 14(7): 475-486, 2015
5. Lindsjo J, Fahlman A, Tornqvist E: ANIMAL WELFARE FROM MOUSE TO MOOSE--IMPLEMENTING THE PRINCIPLES OF THE 3RS IN WILDLIFE RESEARCH. *J Wildl Dis* 52(2 Suppl): S65-77, 2016
6. Jemal A, Bray F, Center MM, Ferlay J, Ward E, Forman D: Global cancer statistics. *CA Cancer J Clin* 61(2): 69-90, 2011
7. Hanahan D, Weinberg RA: The hallmarks of cancer. *Cell* 100(1): 57-70, 2000
8. Hanahan D, Weinberg RA: Hallmarks of cancer: the next generation. *Cell* 144(5): 646-674, 2011
9. Nieto MA, Huang RY, Jackson RA, Thiery JP: EMT: 2016. *Cell* 166(1): 21-45, 2016
10. Pietras K, Ostman A: Hallmarks of cancer: interactions with the tumor stroma. *Exp Cell Res* 316(8): 1324-1331, 2010
11. Tarin D: Role of the host stroma in cancer and its therapeutic significance. *Cancer Metastasis Rev* 32(3-4): 553-566, 2013
12. Corthay A: Does the immune system naturally protect against cancer? *Front Immunol* 5 197, 2014
13. Lakshmi Narendra B, Eshvendar Reddy K, Shantikumar S, Ramakrishna S: Immune system: a double-edged sword in cancer. *Inflamm Res* 62(9): 823-834, 2013
14. Silver DJ, Sinyuk M, Vogelbaum MA, Ahluwalia MS, Lathia JD: The intersection of cancer, cancer stem cells, and the immune system: therapeutic opportunities. *Neuro Oncol* 18(2): 153-159, 2016
15. Candeias SM, Gaipal US: The Immune System in Cancer Prevention, Development and Therapy. *Anticancer Agents Med Chem* 16(1): 101-107, 2016
16. Blackadar CB: Historical review of the causes of cancer. *World J Clin Oncol* 7(1): 54-86, 2016
17. Ravegnini G, Sammarini G, Hrelia P, Angelini S: Key Genetic and Epigenetic Mechanisms in Chemical Carcinogenesis. *Toxicol Sci* 148(1): 2-13, 2015
18. Jia LT, Zhang R, Shen L, Yang AG: Regulators of carcinogenesis: emerging roles beyond their primary functions. *Cancer Lett* 357(1): 75-82, 2015
19. Chválová K, Brabec V, Kašpárková J: Mechanism of the formation of DNA-protein cross-links by antitumor cisplatin. *Nucleic Acids Res* 35(6): 1812-1821, 2007
20. Miller RP, Tadagavadi RK, Ramesh G, Reeves WB: Mechanisms of Cisplatin Nephrotoxicity. *Toxins (Basel)* 2(11): 2490-2518, 2010
21. Pabla N, Murphy RF, Liu K, Dong Z: The copper transporter Ctr1 contributes to cisplatin uptake by renal tubular cells during cisplatin nephrotoxicity. *Am J Physiol Renal Physiol* 296(3): F505-511, 2009
22. Ciarimboli G, Ludwig T, Lang D, Pavenstadt H, Koepsell H, Piechota HJ, Haier J, Jaehde U, Zisowsky J, Schlatter E: Cisplatin nephrotoxicity is critically mediated via the human organic cation transporter 2. *Am J Pathol* 167(6): 1477-1484, 2005

23. Devuyst O, Burrow CR, Smith BL, Agre P, Knepper MA, Wilson PD: Expression of aquaporins-1 and -2 during nephrogenesis and in autosomal dominant polycystic kidney disease. *Am J Physiol* 271(1 Pt 2): F169-183, 1996
24. Verani RR, Silva FG: Histogenesis of the renal cysts in adult (autosomal dominant) polycystic kidney disease: a histochemical study. *Mod Pathol* 1(6): 457-463, 1988
25. Willey CJ, Blais JD, Hall AK, Krasa HB, Makin AJ, Czerwiec FS: Prevalence of autosomal dominant polycystic kidney disease in the European Union. *Nephrol Dial Transplant*, 2016
26. Sweeney WE, Jr., Avner ED: Molecular and cellular pathophysiology of autosomal recessive polycystic kidney disease (ARPKD). *Cell Tissue Res* 326(3): 671-685, 2006
27. Sweeney WE, Jr., Avner ED: Pathophysiology of childhood polycystic kidney diseases: new insights into disease-specific therapy. *Pediatr Res* 75(1-2): 148-157, 2014
28. Lu W, Peissel B, Babakhanlou H, Pavlova A, Geng L, Fan X, Larson C, Brent G, Zhou J: Perinatal lethality with kidney and pancreas defects in mice with a targeted Pkd1 mutation. *Nat Genet* 17(2): 179-181, 1997
29. Kurbegovic A, Trudel M: Acute kidney injury induces hallmarks of polycystic kidney disease. *Am J Physiol Renal Physiol* 311(4): F740-F751, 2016
30. Leonhard WN, Zandbergen M, Veraar K, van den Berg S, van der Weerd L, Breuning M, de Heer E, Peters DJ: Scattered Deletion of PKD1 in Kidneys Causes a Cystic Snowball Effect and Recapitulates Polycystic Kidney Disease. *J Am Soc Nephrol* 26(6): 1322-1333, 2015
31. Forman JR, Qamar S, Paci E, Sandford RN, Clarke J: The remarkable mechanical strength of polycystin-1 supports a direct role in mechanotransduction. *J Mol Biol* 349(4): 861-871, 2005
32. Polycystic kidney disease: the complete structure of the PKD1 gene and its protein. The International Polycystic Kidney Disease Consortium. *Cell* 81(2): 289-298, 1995
33. Kim S, Nie H, Nesin V, Tran U, Outeda P, Bai CX, Keeling J, Maskey D, Watnick T, Wessely O, Tsiokas L: The polycystin complex mediates Wnt/Ca(2+) signalling. *Nat Cell Biol* 18(7): 752-764, 2016
34. Giamarchi A, Padilla F, Crest M, Honore E, Delmas P: TRPP2: Ca2+-permeable cation channel and more. *Cell Mol Biol (Noisy-le-grand)* 52(8): 105-114, 2006
35. Harris PC, Bae KT, Rossetti S, Torres VE, Grantham JJ, Chapman AB, Guay-Woodford LM, King BF, Wetzel LH, Baumgarten DA, Kenney PJ, Consugar M, Klahr S, Bennett WM, Meyers CM, Zhang QJ, Thompson PA, Zhu F, Miller JP: Cyst number but not the rate of cystic growth is associated with the mutated gene in autosomal dominant polycystic kidney disease. *J Am Soc Nephrol* 17(11): 3013-3019, 2006
36. Giamarchi A, Feng S, Rodat-Despoix L, Xu Y, Bubenshchikova E, Newby LJ, Hao J, Gaudio C, Crest M, Lupas AN, Honore E, Williamson MP, Obara T, Ong AC, Delmas P: A polycystin-2 (TRPP2) dimerization domain essential for the function of heteromeric polycystin complexes. *EMBO J* 29(7): 1176-1191, 2010

37. Xu GM, Gonzalez-Perrett S, Essafi M, Timpanaro GA, Montalbetti N, Arnaout MA, Cantiello HF: Polycystin-1 activates and stabilizes the polycystin-2 channel. *J Biol Chem* 278(3): 1457-1462, 2003
38. Newby LJ, Streets AJ, Zhao Y, Harris PC, Ward CJ, Ong AC: Identification, characterization, and localization of a novel kidney polycystin-1-polycystin-2 complex. *J Biol Chem* 277(23): 20763-20773, 2002
39. Scheffers MS, van der Bent P, Prins F, Spruit L, Breuning MH, Litvinov SV, de Heer E, Peters DJ: Polycystin-1, the product of the polycystic kidney disease 1 gene, co-localizes with desmosomes in MDCK cells. *Hum Mol Genet* 9(18): 2743-2750, 2000
40. Huan Y, van Adelsberg J: Polycystin-1, the PKD1 gene product, is in a complex containing E-cadherin and the catenins. *J Clin Invest* 104(10): 1459-1468, 1999
41. Wilson PD, Geng L, Li X, Burrow CR: The PKD1 gene product, "polycystin-1," is a tyrosine-phosphorylated protein that colocalizes with alpha2beta1-integrin in focal clusters in adherent renal epithelia. *Lab Invest* 79(10): 1311-1323, 1999
42. Sweeney WE, Avner ED: Polycystic Kidney Disease, Autosomal Recessive. In: edited by Pagon RA, MP Adam, HH Ardinger, SE Wallace, A Amemiya, LJH Bean, TD Bird, N Ledbetter, HC Mefford, RJH Smith and K Stephens, Seattle WA, University of Washington, Seattle. GeneReviews is a registered trademark of the University of Washington, Seattle, 1993,
43. Wang S, Zhang J, Nauli SM, Li X, Starremans PG, Luo Y, Roberts KA, Zhou J: Fibrocystin/polyductin, found in the same protein complex with polycystin-2, regulates calcium responses in kidney epithelia. *Mol Cell Biol* 27(8): 3241-3252, 2007
44. Devuyst O, Torres VE: Osmoregulation, vasopressin, and cAMP signaling in autosomal dominant polycystic kidney disease. *Curr Opin Nephrol Hypertens* 22(4): 459-470, 2013
45. Torres VE, Harris PC, Pirson Y: Autosomal dominant polycystic kidney disease. *Lancet* 369(9569): 1287-1301, 2007
46. Boca M, Distefano G, Qian F, Bhunia AK, Germino GG, Boletta A: Polycystin-1 induces resistance to apoptosis through the phosphatidylinositol 3-kinase/Akt signaling pathway. *J Am Soc Nephrol* 17(3): 637-647, 2006
47. Yamaguchi T, Nagao S, Wallace DP, Belibi FA, Cowley BD, Pelling JC, Grantham JJ: Cyclic AMP activates B-Raf and ERK in cyst epithelial cells from autosomal-dominant polycystic kidneys. *Kidney Int* 63(6): 1983-1994, 2003
48. Schrier RW, Johnson AM, McFann K, Chapman AB: The role of parental hypertension in the frequency and age of diagnosis of hypertension in offspring with autosomal-dominant polycystic kidney disease. *Kidney Int* 64(5): 1792-1799, 2003
49. Chapman AB, Schrier RW: Pathogenesis of hypertension in autosomal dominant polycystic kidney disease. *Semin Nephrol* 11(6): 653-660, 1991
50. Ecder T, Schrier RW: Hypertension in autosomal-dominant polycystic kidney disease: early occurrence and unique aspects. *J Am Soc Nephrol* 12(1): 194-200, 2001

51. Sallee M, Rafat C, Zahar JR, Paulmier B, Grunfeld JP, Knebelmann B, Fakhouri F: Cyst infections in patients with autosomal dominant polycystic kidney disease. *Clin J Am Soc Nephrol* 4(7): 1183-1189, 2009
52. Bajwa ZH, Sial KA, Malik AB, Steinman TI: Pain patterns in patients with polycystic kidney disease. *Kidney Int* 66(4): 1561-1569, 2004
53. Bajwa ZH, Gupta S, Warfield CA, Steinman TI: Pain management in polycystic kidney disease. *Kidney Int* 60(5): 1631-1644, 2001
54. Torres VE, Chapman AB, Devuyst O, Gansevoort RT, Grantham JJ, Higashihara E, Perrone RD, Krasa HB, Ouyang J, Czerwiec FS: Tolvaptan in patients with autosomal dominant polycystic kidney disease. *N Engl J Med* 367(25): 2407-2418, 2012
55. Watkins PB, Lewis JH, Kaplowitz N, Alpers DH, Blais JD, Smotzer DM, Krasa H, Ouyang J, Torres VE, Czerwiec FS, Zimmer CA: Clinical Pattern of Tolvaptan-Associated Liver Injury in Subjects with Autosomal Dominant Polycystic Kidney Disease: Analysis of Clinical Trials Database. *Drug Saf* 38(11): 1103-1113, 2015
56. Wu Y, Beland FA, Chen S, Liu F, Guo L, Fang JL: Mechanisms of tolvaptan-induced toxicity in HepG2 cells. *Biochem Pharmacol* 95(4): 324-336, 2015
57. Baur BP, Meaney CJ: Review of tolvaptan for autosomal dominant polycystic kidney disease. *Pharmacotherapy* 34(6): 605-616, 2014
58. Ravichandran K, Zafar I, Ozkok A, Edelstein CL: An mTOR kinase inhibitor slows disease progression in a rat model of polycystic kidney disease. *Nephrol Dial Transplant* 30(1): 45-53, 2015
59. Shillingford JM, Murcia NS, Larson CH, Low SH, Hedgepeth R, Brown N, Flask CA, Novick AC, Goldfarb DA, Kramer-Zucker A, Walz G, Piontek KB, Germino GG, Weimbs T: The mTOR pathway is regulated by polycystin-1, and its inhibition reverses renal cystogenesis in polycystic kidney disease. *Proc Natl Acad Sci U S A* 103(14): 5466-5471, 2006
60. Tao Y, Kim J, Schrier RW, Edelstein CL: Rapamycin markedly slows disease progression in a rat model of polycystic kidney disease. *J Am Soc Nephrol* 16(1): 46-51, 2005
61. Zafar I, Belibi FA, He Z, Edelstein CL: Long-term rapamycin therapy in the Han:SPRD rat model of polycystic kidney disease (PKD). *Nephrol Dial Transplant* 24(8): 2349-2353, 2009
62. Belibi F, Ravichandran K, Zafar I, He Z, Edelstein CL: mTORC1/2 and rapamycin in female Han:SPRD rats with polycystic kidney disease. *Am J Physiol Renal Physiol* 300(1): F236-244, 2011
63. Stallone G, Infante B, Grandaliano G, Bristogiannis C, Macarini L, Mezzopane D, Bruno F, Montemurno E, Schirinzi A, Sabbatini M, Pisani A, Tataranni T, Schena FP, Gesualdo L: Rapamycin for treatment of type I autosomal dominant polycystic kidney disease (RAPYD-study): a randomized, controlled study. *Nephrol Dial Transplant* 27(9): 3560-3567, 2012

64. Ruggenenti P, Gentile G, Perico N, Perna A, Barcella L, Trillini M, Cortinovis M, Ferrer Siles CP, Reyes Loaeza JA, Aparicio MC, Fasolini G, Gaspari F, Martinetti D, Carrara F, Rubis N, Prandini S, Caroli A, Sharma K, Antiga L, Remuzzi A, Remuzzi G: Effect of Sirolimus on Disease Progression in Patients with Autosomal Dominant Polycystic Kidney Disease and CKD Stages 3b-4. *Clin J Am Soc Nephrol* 11(5): 785-794, 2016
65. Liu YM, Shao YQ, He Q: Sirolimus for treatment of autosomal-dominant polycystic kidney disease: a meta-analysis of randomized controlled trials. *Transplant Proc* 46(1): 66-74, 2014
66. He Q, Lin C, Ji S, Chen J: Efficacy and safety of mTOR inhibitor therapy in patients with early-stage autosomal dominant polycystic kidney disease: a meta-analysis of randomized controlled trials. *Am J Med Sci* 344(6): 491-497, 2012
67. Serra AL, Poster D, Kistler AD, Krauer F, Raina S, Young J, Rentsch KM, Spanaus KS, Senn O, Kristanto P, Scheffel H, Weishaupt D, Wuthrich RP: Sirolimus and kidney growth in autosomal dominant polycystic kidney disease. *N Engl J Med* 363(9): 820-829, 2010
68. Walz G, Budde K, Mannaa M, Nurnberger J, Wanner C, Sommerer C, Kunzendorf U, Banas B, Horl WH, Obermuller N, Arns W, Pavenstadt H, Gaedeke J, Buchert M, May C, Gscheidmeier H, Kramer S, Eckardt KU: Everolimus in patients with autosomal dominant polycystic kidney disease. *N Engl J Med* 363(9): 830-840, 2010
69. Shillingford JM, Leamon CP, Vlahov IR, Weimbs T: Folate-conjugated rapamycin slows progression of polycystic kidney disease. *J Am Soc Nephrol* 23(10): 1674-1681, 2012
70. Yu ASL, El-Ters M, Winklhofer FT: Clinical Trials in Autosomal Dominant Polycystic Kidney Disease. In: edited by Li X, Brisbane AU, : The Authors., 2015,
71. Pampaloni F, Reynaud EG, Stelzer EH: The third dimension bridges the gap between cell culture and live tissue. *Nat Rev Mol Cell Biol* 8(10): 839-845, 2007
72. Petersen OW, Ronnov-Jessen L, Howlett AR, Bissell MJ: Interaction with basement membrane serves to rapidly distinguish growth and differentiation pattern of normal and malignant human breast epithelial cells. *Proc Natl Acad Sci U S A* 89(19): 9064-9068, 1992
73. Takahashi Y, Hori Y, Yamamoto T, Urashima T, Ohara Y, Tanaka H: 3D spheroid cultures improve the metabolic gene expression profiles of HepaRG cells. *Biosci Rep* 35(3), 2015
74. Ramaiahgari SC, den Braver MW, Herpers B, Terpstra V, Commandeur JN, van de Water B, Price LS: A 3D in vitro model of differentiated HepG2 cell spheroids with improved liver-like properties for repeated dose high-throughput toxicity studies. *Arch Toxicol* 88(5): 1083-1095, 2014
75. Ghosh S, Spagnoli GC, Martin I, Ploegert S, Demougin P, Heberer M, Reschner A: Three-dimensional culture of melanoma cells profoundly affects gene expression profile: a high density oligonucleotide array study. *J Cell Physiol* 204(2): 522-531, 2005

76. Kenny PA, Lee GY, Myers CA, Neve RM, Semeiks JR, Spellman PT, Lorenz K, Lee EH, Barcellos-Hoff MH, Petersen OW, Gray JW, Bissell MJ: The morphologies of breast cancer cell lines in three-dimensional assays correlate with their profiles of gene expression. *Mol Oncol* 1(1): 84-96, 2007
77. Birgersdotter A, Baumforth KR, Porwit A, Sundblad A, Falk KI, Wei W, Sjoberg J, Murray PG, Bjorkholm M, Ernberg I: Three-dimensional culturing of the Hodgkin lymphoma cell-line L1236 induces a HL tissue-like gene expression pattern. *Leuk Lymphoma* 48(10): 2042-2053, 2007
78. Birgersdotter A, Sandberg R, Ernberg I: Gene expression perturbation in vitro--a growing case for three-dimensional (3D) culture systems. *Semin Cancer Biol* 15(5): 405-412, 2005
79. Hirschhaeuser F, Menne H, Dittfeld C, West J, Mueller-Klieser W, Kunz-Schughart LA: Multicellular tumor spheroids: an underestimated tool is catching up again. *J Biotechnol* 148(1): 3-15, 2010
80. Lin RZ, Chang HY: Recent advances in three-dimensional multicellular spheroid culture for biomedical research. *Biotechnol J* 3(9-10): 1172-1184, 2008
81. Fennema E, Rivron N, Rouwkema J, van Blitterswijk C, de Boer J: Spheroid culture as a tool for creating 3D complex tissues. *Trends Biotechnol* 31(2): 108-115, 2013
82. Drewitz M, Helbling M, Fried N, Bieri M, Moritz W, Lichtenberg J, Kelm JM: Towards automated production and drug sensitivity testing using scaffold-free spherical tumor microtissues. *Biotechnol J* 6(12): 1488-1496, 2011
83. Hsiao AY, Tung YC, Qu X, Patel LR, Pienta KJ, Takayama S: 384 hanging drop arrays give excellent Z-factors and allow versatile formation of co-culture spheroids. *Biotechnol Bioeng* 109(5): 1293-1304, 2012
84. Robertson FM, Ogasawara MA, Ye Z, Chu K, Pickei R, Debeb BG, Woodward WA, Hittelman WN, Cristofanilli M, Barsky SH: Imaging and analysis of 3D tumor spheroids enriched for a cancer stem cell phenotype. *J Biomol Screen* 15(7): 820-829, 2010
85. Tibbitt MW, Anseth KS: Hydrogels as extracellular matrix mimics for 3D cell culture. *Biotechnol Bioeng* 103(4): 655-663, 2009
86. Lee J, Cuddihy MJ, Kotov NA: Three-dimensional cell culture matrices: state of the art. *Tissue Eng Part B Rev* 14(1): 61-86, 2008
87. Magin CM, Alge DL, Anseth KS: Bio-inspired 3D microenvironments: a new dimension in tissue engineering. *Biomed Mater* 11(2): 022001, 2016
88. Cushing MC, Anseth KS: Materials science. Hydrogel cell cultures. *Science* 316(5828): 1133-1134, 2007
89. Benton G, Arnautova I, George J, Kleinman HK, Koblinkski J: Matrigel: from discovery and ECM mimicry to assays and models for cancer research. *Adv Drug Deliv Rev* 79-80 3-18, 2014
90. Ravi M, Paramesh V, Kaviya SR, Anuradha E, Solomon FD: 3D cell culture systems: advantages and applications. *J Cell Physiol* 230(1): 16-26, 2015
91. Baker EL, Bonnecaze RT, Zaman MH: Extracellular matrix stiffness and architecture govern intracellular rheology in cancer. *Biophys J* 97(4): 1013-1021, 2009

92. Bryant SJ, Anseth KS: Hydrogel properties influence ECM production by chondrocytes photoencapsulated in poly(ethylene glycol) hydrogels. *J Biomed Mater Res* 59(1): 63-72, 2002
93. Raic A, Rodling L, Kalbacher H, Lee-Thedieck C: Biomimetic macroporous PEG hydrogels as 3D scaffolds for the multiplication of human hematopoietic stem and progenitor cells. *Biomaterials* 35(3): 929-940, 2014
94. Zhou W, Stukel JM, Cebull HL, Willits RK: Tuning the Mechanical Properties of Poly(Ethylene Glycol) Microgel-Based Scaffolds to Increase 3D Schwann Cell Proliferation. *Macromol Biosci* 16(4): 535-544, 2016
95. Pradhan S, Hassani I, Seeto WJ, Lipke EA: PEG-fibrinogen hydrogels for three-dimensional breast cancer cell culture. *J Biomed Mater Res A* 105(1): 236-252, 2017
96. Horvath P, Aulner N, Bickle M, Davies AM, Nery ED, Ebner D, Montoya MC, Ostling P, Pietiainen V, Price LS, Shorte SL, Turcatti G, von Schantz C, Carragher NO: Screening out irrelevant cell-based models of disease. *Nat Rev Drug Discov* 15(11): 751-769, 2016
97. Masters JR, Stacey GN: Changing medium and passaging cell lines. *Nat Protoc* 2(9): 2276-2284, 2007
98. Nestor CE, Ottaviano R, Reinhardt D, Cruickshanks HA, Mjoseng HK, McPherson RC, Lentini A, Thomson JP, Dunican DS, Pennings S, Anderton SM, Benson M, Meehan RR: Rapid reprogramming of epigenetic and transcriptional profiles in mammalian culture systems. *Genome Biol* 16 11, 2015
99. Kretzschmar K, Clevers H: Organoids: Modeling Development and the Stem Cell Niche in a Dish. *Dev Cell* 38(6): 590-600, 2016
100. Drost J, Artegiani B, Clevers H: The Generation of Organoids for Studying Wnt Signaling. *Methods Mol Biol* 1481 141-159, 2016
101. Broutier L, Andersson-Rolf A, Hindley CJ, Boj SF, Clevers H, Koo BK, Huch M: Culture and establishment of self-renewing human and mouse adult liver and pancreas 3D organoids and their genetic manipulation. *Nat Protoc* 11(9): 1724-1743, 2016
102. Saldin LT, Cramer MC, Velankar SS, White LJ, Badylak SF: Extracellular matrix hydrogels from decellularized tissues: Structure and function. *Acta Biomater*, 2016
103. Keane TJ, Dziki J, Castelton A, Faulk DM, Messerschmidt V, Londono R, Reing JE, Velankar SS, Badylak SF: Preparation and characterization of a biologic scaffold and hydrogel derived from colonic mucosa. *J Biomed Mater Res B Appl Biomater*, 2015
104. Johnson TD, Dequach JA, Gaetani R, Ungerleider J, Elhag D, Nigam V, Behfar A, Christman KL: Human versus porcine tissue sourcing for an injectable myocardial matrix hydrogel. *Biomater Sci* 2014 60283D, 2014
105. Nagao RJ, Xu J, Luo P, Xue J, Wang Y, Kotha S, Zeng W, Fu X, Himmelfarb J, Zheng Y: Decellularized Human Kidney Cortex Hydrogels Enhance Kidney Microvascular Endothelial Cell Maturation and Quiescence. *Tissue Eng Part A* 22(19-20): 1140-1150, 2016

106. Lee JS, Shin J, Park HM, Kim YG, Kim BG, Oh JW, Cho SW: Liver extracellular matrix providing dual functions of two-dimensional substrate coating and three-dimensional injectable hydrogel platform for liver tissue engineering. *Biomacromolecules* 15(1): 206-218, 2014
107. Pouliot RA, Link PA, Mikhael NS, Schneck MB, Valentine MS, Kamga Gninzeko FJ, Herbert JA, Sakagami M, Heise RL: Development and characterization of a naturally derived lung extracellular matrix hydrogel. *J Biomed Mater Res A* 104(8): 1922-1935, 2016
108. Wolf MT, Daly KA, Brennan-Pierce EP, Johnson SA, Carruthers CA, D'Amore A, Nagarkar SP, Velankar SS, Badylak SF: A hydrogel derived from decellularized dermal extracellular matrix. *Biomaterials* 33(29): 7028-7038, 2012
109. Seetapun D, Ross JJ: Eliminating the organ transplant waiting list: The future with perfusion decellularized organs. *Surgery*, 2016
110. Torres VE: Treatment strategies and clinical trial design in ADPKD. *Adv Chronic Kidney Dis* 17(2): 190-204, 2010

chapter 2

Getting the most out of 3D cell based assays with high content image analysis and phenotypic profiling

Tijmen H. Booij¹, Bram Herpers² Kuan Yan² and
Leo S. Price^{1,2#}

1 Leiden Academic Centre for Drug Research, Leiden University,
Leiden, The Netherlands

2 Ocello B.V., Leiden, The Netherlands

Corresponding Author

Manuscript in preparation

Abstract

Introduction of more relevant cell models in early pre-clinical drug discovery, combined with high-content imaging and automated analysis are expected to increase the quality of compounds progressing to pre-clinical stages in the drug development pipeline. In this review we discuss the current switch to more relevant 3D cell culture models and associated challenges for high-throughput screening and high content analysis. We propose that overcoming these challenges will enable front-loading the drug discovery pipeline with better biology, extracting the most from that biology and in general, improve translation between *in vitro* and *in vivo* models. This is expected to reduce the proportion of compounds that fail *in vivo* testing due to lack of efficacy or due to toxicity.

Introduction

Declining drug success rates and increasing costs suggest that alternative strategies are required in early drug discovery. Traditional drug discovery has favoured a target-based approach where drugs were selected to manipulate a single molecular target. Since good targets are often not identified or inhibition of single targets is often not sufficient for effective therapy, phenotypic screening represents an alternative approach that has proved successful in recent years.¹⁻³ Phenotypic drug screening techniques typically combine simple single end-point measurements, such as cell viability, with 2D monolayer cultures of cell lines. Such pleiotropic endpoints limit their sensitivity and selectivity for the most promising drugs.⁴ Furthermore, cells cultured as a monolayer often respond differently to drugs compared to native tissues.⁵

Reasons underlying the aberrant responses of 2D cultured cell lines compared to tissues include the grossly distorted architecture of cells stretched on rigid plastic, the absence of natural ligands with which to attach to and the lack of multiple different cell types found within a tissue that are typically closely intertwined to regulate cellular behaviour. These cellular interactions can dramatically influence cell differentiation and signalling and thus the ability to accurately recapitulate the situation in the body. For example, cancer cells grown as a monolayer have a deregulated cell cycle, often doubling every 24 hours, while tumours *in vivo* typically show only a few percent of actively cycling cells and only have a marginally higher rate of proliferation compared to healthy tissue. As a result, cancer drugs selected on this basis often show adverse effects in healthy tissues. These problems indicate that different, more biologically-relevant strategies, will be more effective in developing successful medicines.

Three-dimensional cell culture models simulate aberrant tissue organization in pathology

Over the last three decades or so, three-dimensional (3D) cell culture techniques have been developed that have resulted in models that more accurately mimic physiological and diseased states than their 2D counterparts.⁶⁻¹¹ These have the potential to provide a more physiologically relevant context for drug screening, as culturing cells in a 3D environment allows the formation of complex multicellular micro-tissues or organoids that display cell-cell and cell-matrix attachment that drive differentiation and normal tissue function.¹²⁻¹⁹

The resulting biological complexity of these multicellular micro-tissues makes them particularly well suited for phenotypic drug discovery. Traditional end-points, such as proliferation and viability can be combined with 3D assays – either using biochemical assays or specific fluorescent labels.²⁰ But just as modern histopathology relies on a diverse range of cell and tissue architectural characteristics of patient material for decision making, maximum leverage of the more complex biology of 3D-cultured tissues can also be gained from analysis of diverse morphological characteristics. This can be of particular value when aberrant tissue organization is directly associated with pathology, for example, with neurodegenerative disorders,²¹⁻²² tissue fibrosis,²³ cancer,²⁴⁻²⁷

and ciliopathies such as polycystic kidney disease (PKD).²⁸⁻²⁹ In the context of these diseases, 2D cultured cell lines fail profoundly to capture properties critically associated with the pathophysiology. The modelling of cystopathies is a particularly clear example since cysts, such as those formed in the kidneys of PKD patients, are 3D structures that cannot be recapitulated in 2D cell cultures. Therefore, mechanistic studies and compound efficacy testing can only effectively be studied in a 3D environment or *in vivo*. Similarly, to evaluate tumour dysplasia and invasion, 2D cell cultures lack the required physical environment. These and many other examples underscore the need for the more disease-relevant 3D cell culture models (Figure 1).

Front-loading the early *in vitro* stages of drug discovery with more disease-relevant biological models will inevitably increase the quality of molecules entering the pipeline.³⁰ A more faithful *in vitro* representation of the pathways and processes in disease *in vivo* will improve drug testing even with simple end-point measurements such as cell viability. However, maximum potential of 3D cultured tissues can be realized by exploiting the phenotypic complexity with high-content endpoints.

3D cell culture models for high-throughput screening

Many different options to culture cells in 3D have emerged, each with specific limitations and advantages for evaluation of compound effects.³¹⁻³⁵ 3D culture techniques often make use of immortalized cell lines due to ease of culturing and relative lack of heterogeneity and, while convenient for high-throughput screens, these cells may not accurately represent tissues, since these generally require the interaction of multiple cell types for normal function. This problem may be circumvented by introduction of co-cultures,³⁶ as has been shown for different co-culture systems.³⁷⁻³⁹ However, co-culture systems also introduce an increased level of complexity to the culture system, which can be undesirable for high-throughput screens. For example, cell ratios and cell culture media require optimization to support growth of both co-cultured cell types to obtain functional tissues.^{36, 38} It may only be worth considering this approach if the interaction between the co-cultured cell types is of particular significance for the disease, such as the interaction of fibroblasts and epithelial cells in fibrosis.⁴⁰⁻⁴¹

Additional improvement of the relevance of cell models can be gained by the incorporation of primary cells obtained from specific tissues.¹² However, as these can only be passaged a few times before they cease proliferating, their capacity to develop into functional tissues is limited. Furthermore, the cost, logistics and lack of prior characterization of patient tissues limits their suitability for *in vitro* testing.³⁶

Induced pluripotent stem cells (iPSCs) are an attractive alternative to the direct use of primary cells in screening, since iPSCs can be generated from virtually any adult cell type reprogrammed with a combination of transcription factors (e.g. Oct4, Sox2, Klf4 and c-Myc⁴²). The resulting pluripotent stem cells can be differentiated to generate a desired tissue type. As a result, iPSC-derived tissues have been used to model a variety of different diseases⁴³ such as cardiovascular, neurological⁴⁴ and hepatic⁴⁵ disorders.

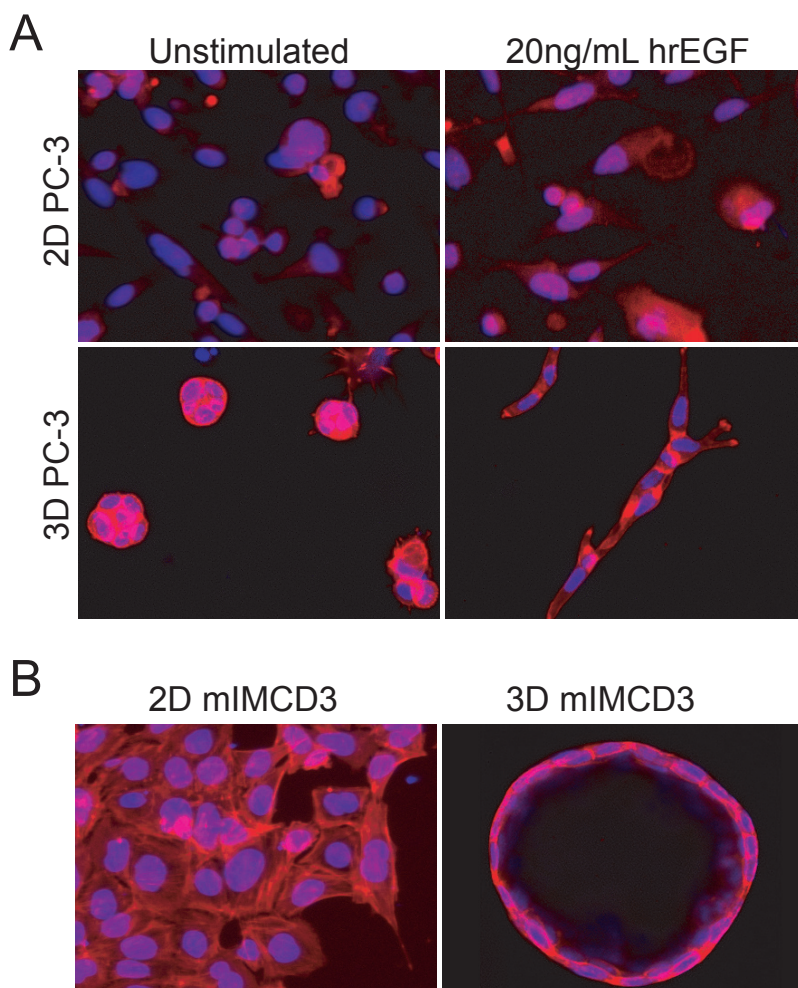


FIGURE 1 3D cell cultures provide a more physiologically relevant context for drug screening. **A)** Prostate Carcinoma (PC-3) cells cultured as 2D monolayer (top) or embedded in 3D hydrogels (bottom) display differential morphology and response to growth factors.⁷⁵ Images in top panel obtained using wide-field BD pathway 855 with a 10x objective and images in bottom panel obtained using a Nikon Ti Eclipse confocal microscope with 20x objective. **B)** mIMCD3 cells transduced with a short-hairpin targeting *Pkd1*, deactivation of which is responsible for cyst growth in polycystic kidney disease, cannot form cysts in 2D culture conditions (left panel, BD pathway 855 with 10x objective), whereas they can in 3D hydrogels (right panel, Nikon Ti Eclipse confocal microscope with 20x objective). F-actin (rhodamine-phalloidin), red; Nuclei (Hoechst 33258), blue.

Although the popularity of using iPSC-derived tissues in high-throughput screens is rapidly increasing, significant hurdles for routine use of iPSCs for this purpose are still posed by extensive differentiation procedures that are required and also the possibility of incomplete differentiation.⁴⁶ In addition, slow growth⁴⁷ and challenging culture conditions can complicate screening procedures.⁴⁸ Interestingly, because 3D culturing of iPSC-derived tissues is known to facilitate rapid reprogramming,⁴⁹ growing iPSC-derived tissues in 3D assays may overcome some of these hurdles.

In the context of neoplastic disorders, an attractive possibility is the use of patient derived xenograft (PDX) tumour material as a source of cells for 3D culture assays.⁵⁰⁻⁵² These tumours are typically well characterized genetically with respect to drug sensitivity *in vivo* and the availability is not restricted as with primary patient tumour material. Practically, dissociated tumour cells can be allowed to reform as tumour spheroids in extracellular matrix hydrogels for the screening of small molecules and biologics (figure 2). The use of PDX derived tumour material for *in vitro* tests also offers the possibility to subsequently test compounds in the autologous *in vivo* model. Such approaches are expected to improve the concordance between *in vitro* and *in vivo* data although to what extent remains to be established. Recent advances in tissue culture technology have also enabled the generation of 3D organoid cultures of normal and diseased tissues from stem cells derived from tissue biopsies. Studies on panels of patient derived organoids have shown that these can preserve the histology and genetic profile of the primary tissue and maintain an additional level of physiological relevance by forming more complex structures comprised of cells with different functions.^{9-10,53} While expansion of these tissue cultures is demanding compared to standard cell lines, they can still be used for compound screening.⁵⁴

Despite a number of successful studies showing the practical implementation of 3D cultures in routine screening,⁵⁵⁻⁵⁷ adoption of these model systems in routine drug discovery pipelines has been slow. Generally, high reagent costs and low-throughput experimental procedures have long hampered the development of high-throughput screening platforms, and as a result, 3D cultures have mostly been used for small-scale experimentation and validation with single end-point measurements, rather than for primary screens. Although several technical challenges remain, the appearance of a wide range of new reagents, technologies and published methods have resulted in increasing adoption of 3D cultures for compound screening and testing.

Matrix composition and automation

To provide a physiologically relevant context for 3D-cultured micro-tissues to develop and interrogate the effects of compounds, a micro-environment is required that provides cells with mechanical and physical interactions that normally occur *in vivo*.⁵⁸ For this purpose, scaffolds have been used that can mimic the extracellular matrix (ECM).⁵⁹⁻⁶¹ The most commonly used scaffolds include hydrogels, which can be natural, synthetic, or a combination.⁶² Natural hydrogels are animal-derived basement-membrane (BM) extracts, which have fixed chemical and physical properties, but an un-

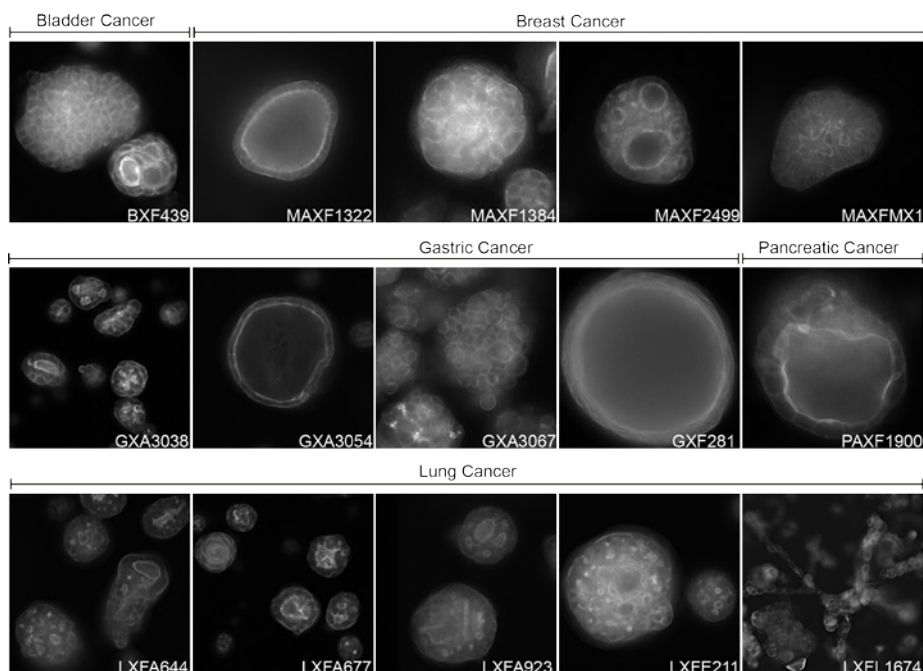


FIGURE 2 3D cultures of patient-derived xenograft (PDX) material. PDX material from different tumours can be cultured in 3D hydrogels to form complex micro-tissues that can be used for compound screening in a physiologically- and patient-relevant context. Actin cytoskeleton visualised with rhodamine-phalloidin. Image materials provided by Ocello B.V. (Leiden, the Netherlands).

defined composition that varies between batches with unforeseen consequences. Examples of such natural hydrogels are collagen or the laminin-rich extracts produced from Engelbreth-Holm-Swarm (EHS) mouse sarcoma cells (Matrigel). These gels contain many endogenous factors that can support viability of cell cultures.⁶³ Synthetic hydrogels, in contrast, are well-defined and can be readily modified and manufactured, thereby overcoming many problems associated with natural hydrogels. However, synthetic hydrogels often do not support cell growth since these lack endogenous factors and first require remodelling to support cell adhesion and other cellular behaviour.⁶⁴ In order to adequately recapitulate the natural microenvironment, these gels need to present various different ligand types at different densities.⁶⁵ Probably most critical is the absence of functional laminin mimetics which are required to engage at multiple sites on the laminin binding integrins⁶⁶ and subsequently drive differentiation.⁶⁷ Cells that grow under conditions where integrin-mediated interactions with the extracellular environment are compromised, such as in synthetic hydrogels, but also in hanging-drop, suspension media, or ultra-low adhesion systems, fail to differentiate adequately or require extended culture periods to enable secretion of endogenous ECM proteins to support differentiation.

Automation of liquid handling for 3D culturing techniques is a more technical challenge that can hamper the adoption of 3D micro-tissues in primary high-throughput screens. While liquid handling for suspension media and ultra-low attachment micro-plates can be conveniently automated, this can be challenging for more viscous liquids such as collagen- and Matrigel-containing hydrogels.⁶⁸ The polymerization of these gels is typically temperature sensitive, requiring extensive environment control to avoid premature polymerization and rapid liquid handling to avoid blocked pipette tips. While automation of 3D culturing techniques can often be achieved for 96- or 384 well plates, further miniaturization may be problematic due to pipetting of smaller volumes.⁶⁹

Sample preparation

Additional challenges arise due to the environment in which cells are cultured. For example, for the detection of fluorescent signals, or for absorption measurements, the culture matrix often interferes with measurement, and this can be especially important for colorimetric measurements of cell viability or proliferation. Also, protein- or RNA/DNA sample preparation techniques are often not compatible with the use of natural hydrogels that contain many endogenous factors, as the presence of matrix proteins can interfere with antibody labelling of protein or purification and detection of RNA and DNA.

Alternatively, the specific composition of the matrix can interfere with free diffusion of certain compounds, especially large molecules, such as antibodies, or molecules that bind to ECM-proteins. For sample preparation, this means that standard procedures for immunofluorescent labelling have to be modified to allow sufficient time for diffusion of antibodies through the gel. Similarly, washing steps need to be prolonged to allow excess antibody removal. Importantly, these properties of gels can also mimic specific physiological processes, such as poorly perfused tissues.

Developments in 3D culture reagents and liquid handling technology will help to overcome these challenges and the adoption of 3D cell cultures in high-throughput screening, will inevitably continue to grow.

Phenotypic profiling of 3D-cultured micro-tissues

High throughput screens typically use single-endpoint measurements for hit selection, such as cell viability or a single fluorescent reporter. This can compromise the quality of the selected hits, since only a narrow view of the cellular response to a treatment is reported. Automated microscopy and image analysis enables multiple features to be measured and allows a better differentiation of biological responses. The greater morphological complexity of tissues cultured in 3D make this type of high content analysis particularly valuable, retrieving rich information that would be overlooked by single end-point assays. The fluorescent reporters in 2D assays can also typically be incorporated in the 3D assays. Recent years have witnessed the development of (ultra-)high content phenotypic screening and multiparametric analysis techniques that can fully exploit the complex cellular response patterns to classify compound effects.⁷⁰⁻⁷⁴ While currently used extensively for 2D cultured cells, high-content screening of 3D cell-based

assays presents challenges for imaging, image analysis, computation and data storage and also data visualisation.

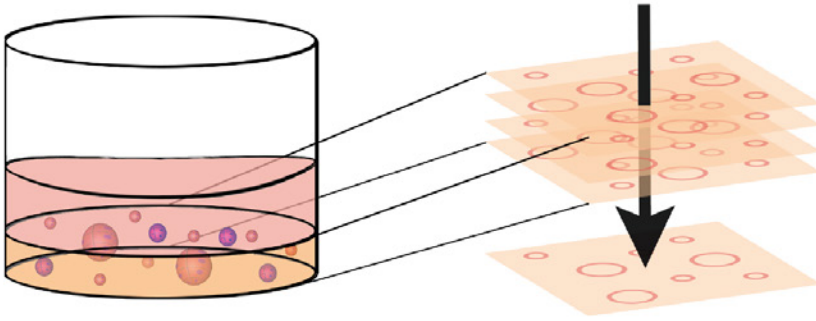
Imaging of 3D-cultured micro-tissues

To analyse cellular phenotypes, fixed and stained cultures are typically imaged using conventional wide-field or confocal fluorescence microscopy. Because single *xy*-images taken from gel-embedded micro-tissues capture only a fraction of the objects in a well (with the majority captured in a sub-optimum plane), to retrieve sufficient information from 3D cultures it is necessary to capture a series of *xy*-images at fixed steps in the vertical direction using automated microscopes,⁷⁵ to obtain a *z*-stack from each well (Figure 3A). Although the entire well of a 384-well plate is typically captured with a 4x objective, stepping up to a 10x lens to capture more (sub)cellular detail multiplies the number of *xy*-fields and *z*-planes required to capture the same number of objects – increasing the image capture time perhaps 10-fold. Using multiple fluorescent channels similarly multiplies image capture time. Wide-field fluorescence imaging can speed up image capture time compared to confocal imaging, but requires post-imaging deconvolution to reduce out-of-focus signal.

Since 3D cultures in multi-well plates require the capture of multiple *xy*-images, often with multiple image channels, data volumes can rise considerably. For example, a 384 well plate of 3D cultures imaged with a 4x lens can typically yield 50GB-100GB of image data. Maximum focus or –intensity projection algorithms are available in several software packages such as ImageJ⁷⁶ and CellProfiler⁷⁷ and convert 3D image stacks to 2D images, dramatically reducing data volume and the complexity of analysis (Figure 3A). However, collapsing a 3D image stack to a single *xy*-image results in a significant corruption of architecture, mis-measurement of objects blended from different *z*-planes and loss of the spatial association of objects between fluorescence channels, compromising co-localisation measurements; analysis of intact 3D image stacks is necessary to retain this phenotypic information (Figure 3B).⁷⁸⁻⁷⁹ 2D cell cultures typically provide thousands of cells for phenotypic analysis. 3D cultures, however, often only provide one object (in the case of spheroids generated using the hanging-drop technology or ultra-low attachment plates²⁰) or perhaps a hundred objects per well (cells embedded in gel) for analysis. Low object numbers, coupled with heterogeneity of cell seeding and growth, can be potentially problematic when measuring single-endpoints such as cell viability. Multiparametric high-content analysis can overcome these problems by allowing for normalization to object (spheroid) number and can additionally exploit heterogeneity to study the effect of treatments on specific cellular subpopulations.⁷⁸⁻⁷⁹

While it is clear that adding a third dimension increases the image capture and computational demands, including live-cell 3D imaging in a multi-well screening format pushes the demands beyond the capacity of the available technology. However, such techniques could provide valuable information on tissue dynamics over time in more relevant biological systems.⁸⁰ With advances in image analysis software and

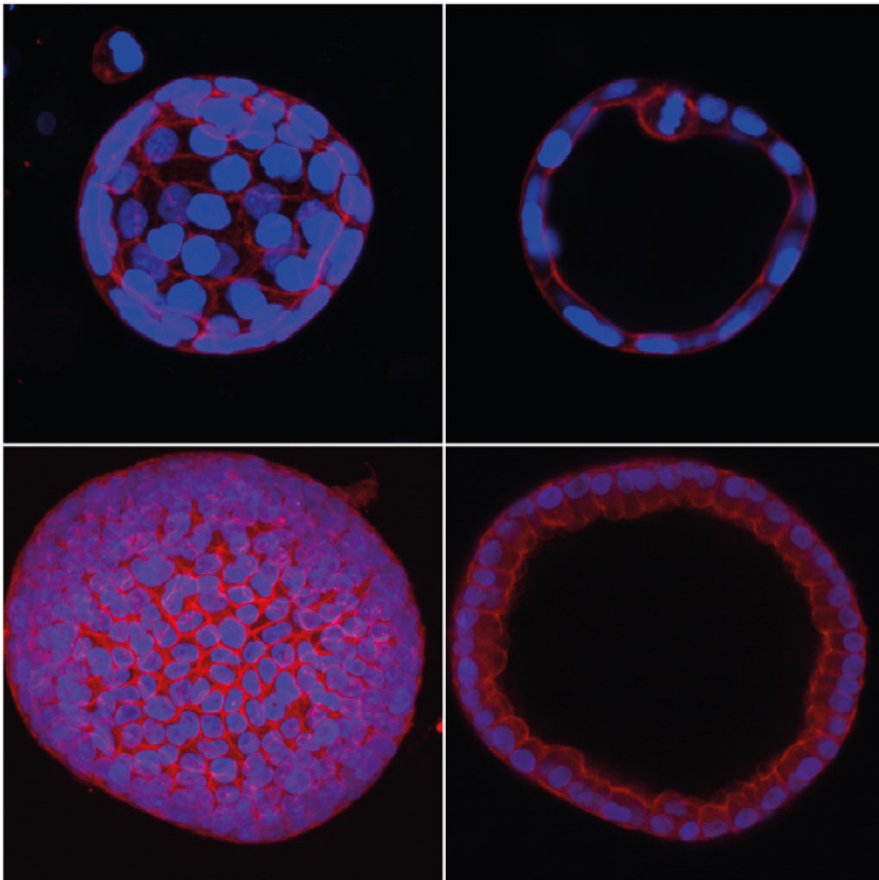
A



B

Max-IP

Individual Section



◀ **FIGURE 3** Maximum-intensity projections can cause loss of phenotypic information in 3D cultures. **A)** Schematic representation of 2D maximum-intensity projections modified from Booi et al, 2016.⁷⁵ Structures embedded in hydrogels are captured in xy and z directions using automated microscopy and in-focus regions from all sections are projected into a 2D reconstruction. **B)** 2D projections from 3D structures can cause loss of important phenotypic characteristics. These images display human kidney cyst-derived organoids, cultured in Matrigel and stained for F-actin (rhodamine-phalloidin, red) and nuclei (Hoechst 33258, blue) and imaged on a Nikon Ti Eclipse confocal microscope. Maximum-intensity projection performed with ImageJ software prevents lumen and cell shape detection.

automated microscopy systems and the increases in computational power, live 3D image capture is also expected to become accessible.

Image analysis and multiparametric end-points

Despite the availability of advanced image analysis tools through software such as ImageJ⁷⁶ and CellProfiler,⁷⁷ the true phenotypic complexity of 3D-cultured micro-tissues is often not exploited to its full extent.⁴ Although often requiring the use of high magnification lenses and multiple z-planes when imaging, it is relatively straightforward to capture single-cell-resolution images from cells cultured in a monolayer and apply this in an automated high throughput format. However it is not yet feasible to achieve this with 3D cultures – largely due to the inability of imager software to detect objects ‘on-the-fly’ and home in for high magnification image capture. However, this may be compensated by the additional features that can be measured from multicellular organotypic structures using lower magnification lenses in a high-throughput format.

For many research questions, a simple parameter, such as spheroid size, may be adequate to discriminate a treatment response. As an advantage of using only a few parameters, readouts are generally simpler to interpret. But the use of a limited number of parameters ignores an abundance of the information that can be extracted from the 3D image stacks. We showed previously that the integration of multiple phenotypic descriptors can improve classification of compounds according to phenotypic response.⁷⁹ The analysis of high-dimensional data (often containing over 500 different phenotypic measurements) requires the use of more advanced data processing and visualisation software, such as KNIME, R and Spotfire. As a result of using hundreds of phenotype-derived parameters, it can be difficult to extrapolate individual parameters to biological observations.⁸¹ To integrate high-dimensional data and generate meaningful visualisations, dimensionality-reduction methods such as principal components analysis (PCA) can be useful. PCA linearly transforms high-dimensional data to a space of fewer dimensions, while retaining most of the variance of the data. We have previously applied this dimensionality reduction technique to differentiate between c-Met and epidermal growth factor receptor (EGFR)-specific inhibitors in a cancer cell invasion assay⁷⁵ and also, more recently, to identify new potentially drugable targets for PKD.⁸²

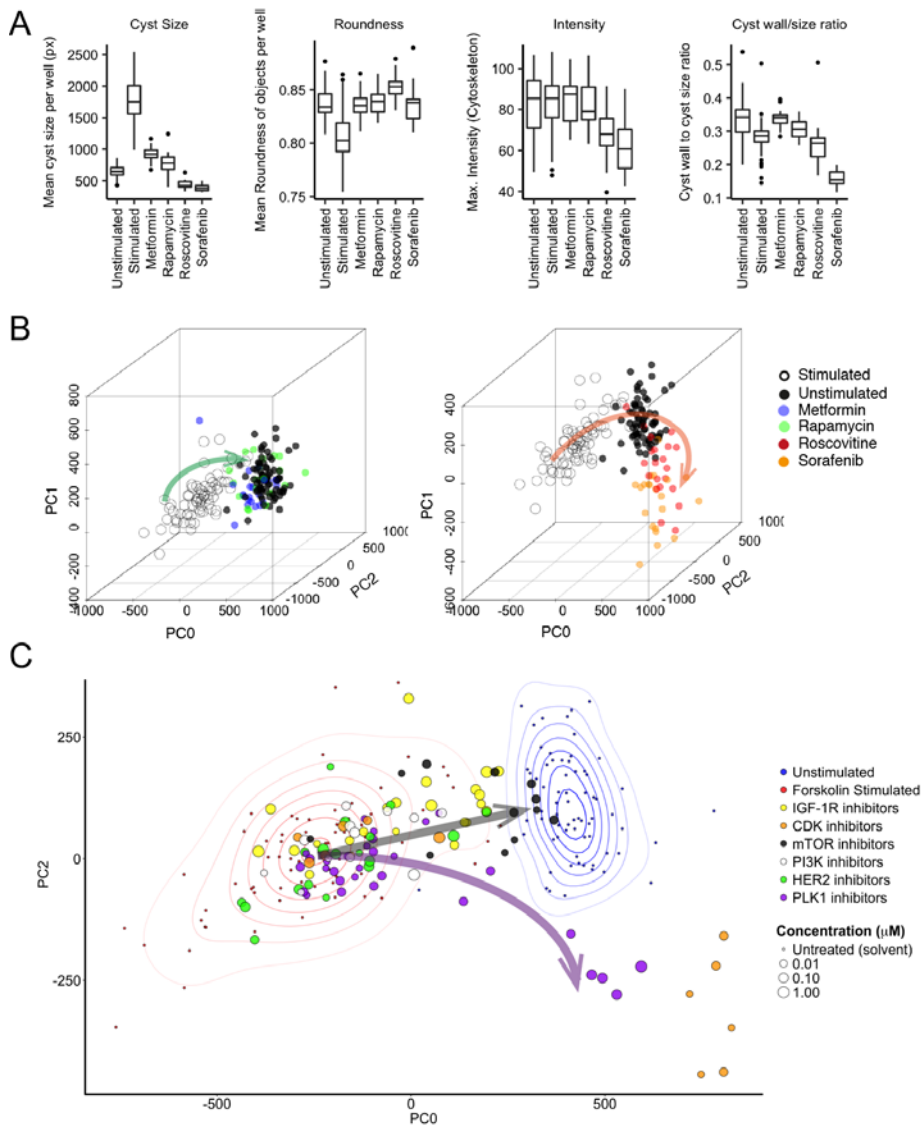


FIGURE 4 Extracting the value of 3D-image stacks with multiparametric end-points.

A) Metformin, rapamycin, roscovitine and sorafenib inhibit forskolin-induced ('stimulated') cyst growth and roscovitine and sorafenib would be classified as the most potent inhibitors on the basis of single parameters (left to right: cyst size, roundness, perimeter and distance of cyst wall to cyst centre). **B)** Three principal components summarizing 84% of variance in the data show a desirable phenotypic change (left panel, green arrow) from stimulated (empty circles [2.5μM forskolin-exposed large cysts]) to unstimulated (black circles [solvent-exposed small cysts]) for exposure to 5mM metformin + 2.5μM forskolin (purple) or 10nM rapamycin (green) + (legend continues on next page)

2.5 μ M forskolin. The right panel shows that despite efficacy of roscovitine and sorafenib on the basis of single parameters as shown in A, multiparametric analysis reveals additional phenotypic alterations (orange arrow).⁸² **C**) Two principal components from figure B showing inhibitors for cyclin-dependent kinases (CDK), mammalian target of rapamycin (mTOR), phosphatidylinositol-4,5-bisphosphate 3-kinase (PI3K), human epidermal growth factor receptor 2 (HER2) and polo-like kinase (PLK1). Density estimations in red and blue shown to emphasize the locations of 2.5 μ M forskolin-stimulated and unstimulated controls, respectively). Grey arrow represents desirable compound efficacy (from forskolin-stimulated control to unstimulated) and purple arrow represents novel phenotypes that are observed after treatment with PLK1 inhibitors or high dose CDK inhibitors.

As an example of this approach, in figure 4A we show the efficacy of four control molecules at inhibiting forskolin-induced cystogenesis.⁸² On the basis of single parameters such as cyst size and perimeter, all inhibitors show inhibition of cyst growth, with roscovitine and sorafenib being most potent. However, if a PCA-based visualization is used, such as shown in figure 4B,⁸² the inhibitory effects of metformin and rapamycin can be discriminated from those of roscovitine and sorafenib, which induce a novel phenotype indicative of toxicity (figure 4B). This type of approach can also be useful in the classification of previously untested compounds (figure 4C).^{73, 75, 82}

The use of multiparametric end-points to profile compounds therefore represents an opportunity to extract more information from primary 3D screens and exploit this phenotypic information to better discriminate promising compounds at the earliest stage of the discovery process.

Conclusion and perspectives

We propose that inclusion of biologically relevant *in vitro* model systems early in pre-clinical development will aid in selection of the best drugs, especially when these model systems are coupled to multiparametric phenotypic analysis strategies. Based on the progress in the development of tissue culture matrices, improvement of cell culture techniques and the incorporation of laboratory automation equipment over the past decade, we anticipate a steep rise in the popularity of 3D cell culture techniques in primary high-throughput screens, and also expect a move away from immortalized cell lines in favour of more physiologically relevant iPSC-, PDX-, co-culture- and organoid models, or even *in vitro* -generated and -cultured organs. It is likely that the current switch from single cell lines to more challenging iPSC-, PDX-, co-culture- and organoid models, or even *in vitro* -generated and -cultured organs, will also increase the demand for high-content analysis methods due to increased tissue complexity that cannot be exploited when using well-based measurements.

With the increases in computational power and improvements in data storage, but also now that better image analysis tools are available, we anticipate that morphological analysis of 3D cell cultures will become more accessible and will eventually allow object-based phenotypic analysis and classification, perhaps eventually also allowing 3D-volume analysis of multi-well plates, rather than analysis of image stacks.

However, there currently is a high need to validate these technologies and to demonstrate that using biologically relevant *in vitro* systems actually improves the efficiency of early drug discovery. Rather than waiting to see sufficient evidence, a comparison of the predictive value of 2D and 3D models for *in vivo* efficacy is required. Ideally such an effort should include collections of molecules that have previously passed and failed in pre-clinical and clinical studies to determine the phenotypic footprint of successful medicines, and apply this knowledge in our search for more effective medicines.

Acknowledgments and conflicts of interest

Leo S. Price is founder and major shareholder of Ocello B.V. T.H. Booij was supported by the Dutch Technology Foundation STW (Project 11823).

References

1. Zheng W, Thorne N, McKew JC: Phenotypic screens as a renewed approach for drug discovery. *Drug discovery today* 18(21-22): 1067-1073, 2013
2. Swinney DC, Anthony J: How were new medicines discovered? *Nature reviews Drug discovery* 10(7): 507-519, 2011
3. Swinney DC: Phenotypic vs. target-based drug discovery for first-in-class medicines. *Clinical pharmacology and therapeutics* 93(4): 299-301, 2013
4. Singh S, Carpenter AE, Genovesio A: Increasing the Content of High-Content Screening: An Overview. *Journal of biomolecular screening* 19(5): 640-650, 2014
5. Howes AL, Richardson RD, Finlay D, Vuori K: 3-Dimensional culture systems for anti-cancer compound profiling and high-throughput screening reveal increases in EGFR inhibitor-mediated cytotoxicity compared to monolayer culture systems. *PloS one* 9(9): e108283, 2014
6. Lee GY, Kenny PA, Lee EH, Bissell MJ: Three-dimensional culture models of normal and malignant breast epithelial cells. *Nature methods* 4(4): 359-365, 2007
7. Simian M, Bissell MJ: Organoids: A historical perspective of thinking in three dimensions. *J Cell Biol* 216(1): 31-40, 2017
8. Sakurai H, Nigam SK: In vitro branching tubulogenesis: implications for developmental and cystic disorders, nephron number, renal repair, and nephron engineering. *Kidney Int* 54(1): 14-26, 1998
9. Clevers H: Modeling Development and Disease with Organoids. *Cell* 165(7): 1586-1597, 2016
10. Takasato M, Er PX, Chiu HS, Maier B, Baillie GJ, Ferguson C, Parton RG, Wolvetang EJ, Roost MS, Chua de Sousa Lopes SM, Little MH: Kidney organoids from human iPS cells contain multiple lineages and model human nephrogenesis. *Nature* 526(7574): 564-568, 2015

11. Fang Y, Eglén RM: Three-Dimensional Cell Cultures in Drug Discovery and Development. *SLAS DISCOVERY: Advancing Life Sciences R&D* 0(o): 2472555217696795,
12. Sokol ES, Miller DH, Breggia A, Spencer KC, Arendt LM, Gupta PB: Growth of human breast tissues from patient cells in 3D hydrogel scaffolds. *Breast cancer research : BCR* 18(1): 19, 2016
13. Petersen OW, Ronnov-Jessen L, Howlett AR, Bissell MJ: Interaction with basement membrane serves to rapidly distinguish growth and differentiation pattern of normal and malignant human breast epithelial cells. *Proceedings of the National Academy of Sciences of the United States of America* 89(19): 9064-9068, 1992
14. Shaw KR, Wrobel CN, Brugge JS: Use of three-dimensional basement membrane cultures to model oncogene-induced changes in mammary epithelial morphogenesis. *Journal of mammary gland biology and neoplasia* 9(4): 297-310, 2004
15. Debnath J, Brugge JS: Modelling glandular epithelial cancers in three-dimensional cultures. *Nat Rev Cancer* 5(9): 675-688, 2005
16. Martin-Belmonte F, Yu W, Rodriguez-Fraticelli AE, Ewald AJ, Werb Z, Alonso MA, Mostov K: Cell-polarity dynamics controls the mechanism of lumen formation in epithelial morphogenesis. *Curr Biol* 18(7): 507-513, 2008
17. Nguyen-Ngoc KV, Cheung KJ, Brenot A, Shamir ER, Gray RS, Hines WC, Yaswen P, Werb Z, Ewald AJ: ECM microenvironment regulates collective migration and local dissemination in normal and malignant mammary epithelium. *Proceedings of the National Academy of Sciences of the United States of America* 109(39): E2595-2604, 2012
18. Lee JL, Streuli CH: Integrins and epithelial cell polarity. *Journal of cell science* 127(Pt 15): 3217-3225, 2014
19. Muschler J, Streuli CH: Cell-matrix interactions in mammary gland development and breast cancer. *Cold Spring Harb Perspect Biol* 2(10): a003202, 2010
20. Sirenko O, Mitlo T, Hesley J, Luke S, Owens W, Cromwell EF: High-content assays for characterizing the viability and morphology of 3D cancer spheroid cultures. *Assay and drug development technologies* 13(7): 402-414, 2015
21. Hopkins AM, DeSimone E, Chwalek K, Kaplan DL: 3D in vitro modeling of the central nervous system. *Progress in neurobiology* 125 1-25, 2015
22. D'Avanzo C, Aronson J, Kim YH, Choi SH, Tanzi RE, Kim DY: Alzheimer's in 3D culture: challenges and perspectives. *BioEssays : news and reviews in molecular, cellular and developmental biology* 37(10): 1139-1148, 2015
23. Porras AM, Hutson HN, Berger AJ, Masters KS: Engineering approaches to study fibrosis in 3-D in vitro systems. *Current opinion in biotechnology* 40 24-30, 2016
24. Kimlin LC, Casagrande G, Virador VM: In vitro three-dimensional (3D) models in cancer research: an update. *Molecular carcinogenesis* 52(3): 167-182, 2013
25. Levinger I, Ventura Y, Vago R: Life is three dimensional-as in vitro cancer cultures should be. *Advances in cancer research* 121 383-414, 2014
26. Yamada KM, Cukierman E: Modeling tissue morphogenesis and cancer in 3D. *Cell* 130(4): 601-610, 2007

27. Smalley KS, Lioni M, Herlyn M: Life isn't flat: taking cancer biology to the next dimension. *In vitro cellular & developmental biology Animal* 42(8-9): 242-247, 2006
28. Desrochers TM, Palma E, Kaplan DL: Tissue-engineered kidney disease models. *Advanced drug delivery reviews* 69-70 67-80, 2014
29. Subramanian B, Rudym D, Cannizzaro C, Perrone R, Zhou J, Kaplan DL: Tissue-engineered three-dimensional in vitro models for normal and diseased kidney. *Tissue engineering Part A* 16(9): 2821-2831, 2010
30. Bickle M: The beautiful cell: high-content screening in drug discovery. *Analytical and bioanalytical chemistry* 398(1): 219-226, 2010
31. Horvath P, Aulner N, Bickle M, Davies AM, Nery ED, Ebner D, Montoya MC, Ostling P, Pietiainen V, Price LS, Shorte SL, Turcatti G, von Schantz C, Carragher NO: Screening out irrelevant cell-based models of disease. *Nature reviews Drug discovery*, 2016
32. Joshi P, Lee MY: High Content Imaging (HCI) on Miniaturized Three-Dimensional (3D) Cell Cultures. *Biosensors* 5(4): 768-790, 2015
33. Edmondson R, Broglie JJ, Adcock AF, Yang L: Three-dimensional cell culture systems and their applications in drug discovery and cell-based biosensors. *Assay and drug development technologies* 12(4): 207-218, 2014
34. Kimlin L, Kassis J, Virador V: 3D in vitro tissue models and their potential for drug screening. *Expert opinion on drug discovery* 8(12): 1455-1466, 2013
35. Klinghammer K, Walther W, Hoffmann J: Choosing wisely - Preclinical test models in the era of precision medicine. *Cancer Treat Rev* 55 36-45, 2017
36. Abbott RD, Kaplan DL: Strategies for improving the physiological relevance of human engineered tissues. *Trends in biotechnology* 33(7): 401-407, 2015
37. Wang PC, Takezawa T: Reconstruction of renal glomerular tissue using collagen vitrigel scaffold. *Journal of bioscience and bioengineering* 99(6): 529-540, 2005
38. Kang JH, Gimble JM, Kaplan DL: In vitro 3D model for human vascularized adipose tissue. *Tissue engineering Part A* 15(8): 2227-2236, 2009
39. Hussain A, Collins G, Yip D, Cho CH: Functional 3-D cardiac co-culture model using bioactive chitosan nanofiber scaffolds. *Biotechnology and bioengineering* 110(2): 637-647, 2013
40. Nowinski D, Lysheden AS, Gardner H, Rubin K, Gerdin B, Ivarsson M: Analysis of gene expression in fibroblasts in response to keratinocyte-derived factors in vitro: potential implications for the wound healing process. *J Invest Dermatol* 122(1): 216-221, 2004
41. Nomoto Y, Kobayashi K, Tada Y, Wada I, Nakamura T, Omori K: Effect of fibroblasts on epithelial regeneration on the surface of a bioengineered trachea. *Ann Otol Rhinol Laryngol* 117(1): 59-64, 2008
42. Takahashi K, Yamanaka S: Induction of pluripotent stem cells from mouse embryonic and adult fibroblast cultures by defined factors. *Cell* 126(4): 663-676, 2006
43. Park IH, Arora N, Huo H, Maherali N, Ahfeldt T, Shimamura A, Lensch MW, Cowan C, Hochedlinger K, Daley GQ: Disease-specific induced pluripotent stem cells. *Cell* 134(5): 877-886, 2008

44. Dimos JT, Rodolfa KT, Niakan KK, Weisenthal LM, Mitumoto H, Chung W, Croft GF, Saphier G, Leibel R, Goland R, Wichterle H, Henderson CE, Eggan K: Induced pluripotent stem cells generated from patients with ALS can be differentiated into motor neurons. *Science (New York, NY)* 321(5893): 1218-1221, 2008
45. Rashid ST, Corbineau S, Hannan N, Marciniak SJ, Miranda E, Alexander G, Huang-Doran I, Griffin J, Ahrlund-Richter L, Skepper J, Semple R, Weber A, Lomas DA, Vallier L: Modeling inherited metabolic disorders of the liver using human induced pluripotent stem cells. *J Clin Invest* 120(9): 3127-3136, 2010
46. Passier R, van Laake LW, Mummery CL: Stem-cell-based therapy and lessons from the heart. *Nature* 453(7193): 322-329, 2008
47. Narsinh KH, Sun N, Sanchez-Freire V, Lee AS, Almeida P, Hu S, Jan T, Wilson KD, Leong D, Rosenberg J, Yao M, Robbins RC, Wu JC: Single cell transcriptional profiling reveals heterogeneity of human induced pluripotent stem cells. *J Clin Invest* 121(3): 1217-1221, 2011
48. Ebert AD, Liang P, Wu JC: Induced Pluripotent Stem Cells as a Disease Modeling and Drug Screening Platform. *J Cardiovasc Pharmacol* 60(4): 408-416, 2012
49. Caiazzo M, Okawa Y, Ranga A, Piersigilli A, Tabata Y, Lutolf MP: Defined three-dimensional microenvironments boost induction of pluripotency. *Nat Mater* 15(3): 344-352, 2016
50. Xie BY, Wu AW: Organoid Culture of Isolated Cells from Patient-derived Tissues with Colorectal Cancer. *Chin Med J (Engl)* 129(20): 2469-2475, 2016
51. Fong EL, Wan X, Yang J, Morgado M, Mikos AG, Harrington DA, Navone NM, Farach-Carson MC: A 3D in vitro model of patient-derived prostate cancer xenograft for controlled interrogation of in vivo tumor-stromal interactions. *Biomaterials* 77: 164-172, 2016
52. Fong EL, Martinez M, Yang J, Mikos AG, Navone NM, Harrington DA, Farach-Carson MC: Hydrogel-based 3D model of patient-derived prostate xenograft tumors suitable for drug screening. *Mol Pharm* 11(7): 2040-2050, 2014
53. Sachs N, Clevers H: Organoid cultures for the analysis of cancer phenotypes. *Current opinion in genetics & development* 24: 68-73, 2014
54. van de Wetering M, Francies HE, Francis JM, Bounova G, Iorio F, Pronk A, van Houdt W, van Gorp J, Taylor-Weiner A, Kester L, McLaren-Douglas A, Blokker J, Jaksani S, Bartfeld S, Volckman R, van Sluis P, Li VS, Seepo S, Sekhar P, Peadarallu C, Cibulskis K, Carter SL, McKenna A, Lawrence MS, Lichtenstein L, Stewart C, Koster J, Versteeg R, van Oudenaarden A, Saez-Rodriguez J, Vries RG, Getz G, Wessels L, Stratton MR, McDermott U, Meyerson M, Garnett MJ, Clevers H: Prospective derivation of a living organoid biobank of colorectal cancer patients. *Cell* 161(4): 933-945, 2015
55. Krausz E, de Hoogt R, Gustin E, Cornelissen F, Grand-Perret T, Janssen L, Vloemans N, Wuyts D, Frans S, Axel A, Peeters PJ, Hall B, Cik M: Translation of a tumor microenvironment mimicking 3D tumor growth co-culture assay platform to high-content screening. *Journal of biomolecular screening* 18(1): 54-66, 2013
56. Kunz-Schughart LA, Freyer JP, Hofstaedter F, Ebner R: The use of 3-D cultures for high-throughput screening: the multicellular spheroid model. *Journal of biomolecular screening* 9(4): 273-285, 2004

57. Kelm JM, Timmins NE, Brown CJ, Fussenegger M, Nielsen LK: Method for generation of homogeneous multicellular tumor spheroids applicable to a wide variety of cell types. *Biotechnology and bioengineering* 83(2): 173-180, 2003
58. Baker BM, Chen CS: Deconstructing the third dimension – how 3D culture microenvironments alter cellular cues. *Journal of cell science* 125(13): 3015-3024, 2012
59. DeVolder R, Kong HJ: Hydrogels for in vivo-like three-dimensional cellular studies. *Wiley interdisciplinary reviews Systems biology and medicine* 4(4): 351-365, 2012
60. Tibbitt MW, Anseth KS: Hydrogels as extracellular matrix mimics for 3D cell culture. *Biotechnology and bioengineering* 103(4): 655-663, 2009
61. Guan X, Avci-Adali M, Alarcin E, Cheng H, Kashaf SS, Li Y, Chawla A, Jang HL, Khademhosseini A: Development of hydrogels for regenerative engineering. *Biotechnology journal* 12(5), 2017
62. Barnes AL, Genever PG, Rimmer S, Coles MC: Collagen–Poly(N-isopropylacrylamide) Hydrogels with Tunable Properties. *Biomacromolecules* 17(3): 723-734, 2016
63. Kleinman HK, McGarvey ML, Hassell JR, Star VL, Cannon FB, Laurie GW, Martin GR: Basement membrane complexes with biological activity. *Biochemistry* 25(2): 312-318, 1986
64. Cushing MC, Anseth KS: Materials science. Hydrogel cell cultures. *Science (New York, NY)* 316(5828): 1133-1134, 2007
65. Cruz-Acuna R, Garcia AJ: Synthetic hydrogels mimicking basement membrane matrices to promote cell-matrix interactions. *Matrix Biol* 57-58 324-333, 2017
66. Yamada M, Sekiguchi K: Molecular Basis of Laminin-Integrin Interactions. *Curr Top Membr* 76 197-229, 2015
67. Streuli CH, Bailey N, Bissell MJ: Control of mammary epithelial differentiation: basement membrane induces tissue-specific gene expression in the absence of cell-cell interaction and morphological polarity. *J Cell Biol* 115(5): 1383-1395, 1991
68. Ruel-Gariepy E, Leroux JC: In situ-forming hydrogels-review of temperature-sensitive systems. *European journal of pharmaceutics and biopharmaceutics : official journal of Arbeitsgemeinschaft fur Pharmazeutische Verfahrenstechnik eV* 58(2): 409-426, 2004
69. Ryan SL, Baird AM, Vaz G, Urquhart AJ, Senge M, Richard DJ, O'Byrne KJ, Davies AM: Drug Discovery Approaches Utilizing Three-Dimensional Cell Culture. *Assay and drug development technologies* 14(1): 19-28, 2016
70. Bilgin CC, Fontenay G, Cheng Q, Chang H, Han J, Parvin B: BioSig3D: High Content Screening of Three-Dimensional Cell Culture Models. *PloS one* 11(3): e0148379, 2016
71. Paulose T, Montevil M, Speroni L, Cerruti F, Sonnenschein C, Soto AM: SAMA: A Method for 3D Morphological Analysis. *PloS one* 11(4): e0153022, 2016
72. Abraham VC, Towne DL, Waring JF, Warrior U, Burns DJ: Application of a high-content multiparameter cytotoxicity assay to prioritize compounds based on toxicity potential in humans. *Journal of biomolecular screening* 13(6): 527-537, 2008

73. Ljosa V, Caie PD, Ter Horst R, Sokolnicki KL, Jenkins EL, Daya S, Roberts ME, Jones TR, Singh S, Genovesio A, Clemons PA, Carragher NO, Carpenter AE: Comparison of methods for image-based profiling of cellular morphological responses to small-molecule treatment. *Journal of biomolecular screening* 18(10): 1321-1329, 2013
74. Horvath P, Aulner N, Bickle M, Davies AM, Nery ED, Ebner D, Montoya MC, Ostling P, Pietiainen V, Price LS, Shorte SL, Turcatti G, von Schantz C, Carragher NO: Screening out irrelevant cell-based models of disease. *Nature reviews Drug discovery* 15(11): 751-769, 2016
75. Booij TH, Klop MJ, Yan K, Szantai-Kis C, Szokol B, Orfi L, van de Water B, Keri G, Price LS: Development of a 3D Tissue Culture-Based High-Content Screening Platform That Uses Phenotypic Profiling to Discriminate Selective Inhibitors of Receptor Tyrosine Kinases. *Journal of biomolecular screening*, 2016
76. Schneider CA, Rasband WS, Eliceiri KW: NIH Image to ImageJ: 25 years of image analysis. *Nature methods* 9(7): 671-675, 2012
77. Carpenter AE, Jones TR, Lamprecht MR, Clarke C, Kang IH, Friman O, Guertin DA, Chang JH, Lindquist RA, Moffat J, Golland P, Sabatini DM: CellProfiler: image analysis software for identifying and quantifying cell phenotypes. *Genome biology* 7(10): R100, 2006
78. Sandercock AM, Rust S, Guillard S, Sachsenmeier KF, Holoweckyj N, Hay C, Flynn M, Huang Q, Yan K, Herpers B, Price LS, Soden J, Freeth J, Jermutus L, Hollingsworth R, Minter R: Identification of anti-tumour biologics using primary tumour models, 3-D phenotypic screening and image-based multi-parametric profiling. *Molecular cancer* 14 147, 2015
79. Di Z, Klop MJ, Rogkoti VM, Le Devedec SE, van de Water B, Verbeek FJ, Price LS, Meerman JH: Ultra high content image analysis and phenotype profiling of 3D cultured micro-tissues. *PloS one* 9(10): e109688, 2014
80. Sameni M, Anbalagan A, Olive MB, Moin K, Mattingly RR, Sloane BF: MAME models for 4D live-cell imaging of tumor: microenvironment interactions that impact malignant progression. *Journal of visualized experiments : JoVE* (60), 2012
81. Bray MA, Carpenter A, Imaging Platform BloMIT, Harvard: Advanced Assay Development Guidelines for Image-Based High Content Screening and Analysis. In: edited by Sittampalam GS, NP Coussens, K Brimacombe, A Grossman, M Arkin, D Auld, C Austin, J Baell, B Bejcek, TDY Chung, JL Dahlin, V Devanaryan, TL Foley, M Glicksman, MD Hall, JV Hass, J Inglese, PW Iversen, SD Kahl, SC Kales, M Lal-Nag, Z Li, J McGee, O McManus, T Riss, OJ Trask, Jr., JR Weidner, M Xia and X Xu, Bethesda (MD), Eli Lilly & Company and the National Center for Advancing Translational Sciences, 2004,
82. Booij TH, Bange H, Leonhard WN, Yan K, Fokkelman M, Kunnen SJ, Dauwerse JG, Qin Y, van de Water B, van Westen GJP, Peters DJM, Price LS: High-Throughput Phenotypic Screening of Kinase Inhibitors to Identify Drug Targets for Polycystic Kidney Disease. *SLAS Discov* 2472555217716056, 2017

chapter 3

Development of a 3D tissue culture-based high-content screening platform that uses phenotypic profiling to discriminate selective inhibitors of receptor tyrosine kinases

Tijmen H. Booij^{1#}; Maarten J.D. Klop^{2#}; Kuan Yan², Csaba Szántai-Kis³, Balint Szokol³, Laszlo Orfi^{3,4}, Bob van de Water¹; Gyorgy Keri^{3,5}, Leo S. Price^{1,2}

- 1 Division of Toxicology, Leiden Academic Centre for Drug Research, Leiden University, Leiden The Netherlands.
- 2 Ocello B.V., Leiden, The Netherlands.
- 3 Vichem Chemie Research Ltd., 1022 Budapest, Hungary
- 4 Department of Pharmaceutical Chemistry, Semmelweis University, 1085 Budapest, Hungary
- 5 MTA-SE Pathobiochemistry Research Group, Department of Medical Chemistry, Semmelweis University, 1085 Budapest, Hungary
- # Authors contributed equally to this work.

Based on: Booij TH, Klop MJ, Yan K, Szantai-Kis C, Szokol B, Orfi L, van de Water B, Keri G, Price LS: Development of a 3D Tissue Culture-Based High-Content Screening Platform That Uses Phenotypic Profiling to Discriminate Selective Inhibitors of Receptor Tyrosine Kinases. *J Biomol Screen*, 2016

Abstract

3D tissue cultures provide a more physiologically relevant context for the screening of compounds, compared to 2D cell cultures. Cells cultured in 3D hydrogels also show complex phenotypes, increasing the scope for phenotypic profiling.

Here we describe a high-content screening platform that uses invasive human prostate cancer cells cultured in 3D in standard 384-well assay plates to study the activity of potential therapeutic small molecules and antibody biologics. Image analysis tools were developed to process 3D image data to measure over 800 phenotypic parameters. Multi-parametric analysis was used to evaluate the effect of compounds on tissue morphology.

We applied this screening platform to measure the activity and selectivity of inhibitors of the c-Met and EGF receptor (EGFR) tyrosine kinases in 3D cultured prostate carcinoma cells. c-Met and EGFR activity was quantified based on the phenotypic profiles induced by their respective ligands, HGF and EGF. The screening method was applied to a novel collection of 80 putative inhibitors of c-Met and EGFR. Compounds were identified that induced phenotypic profiles indicative of selective inhibition of either c-Met, EGFR or bispecific inhibition of both targets.

In conclusion, we describe a fully scalable high-content screening platform that uses phenotypic profiling to discriminate selective and non-selective (off-target) inhibitors in a physiologically relevant 3D cell culture setting.

Introduction

While offering many practical advantages for cell based screening, cells grown on tissue culture plastic lack normal cell-cell and cell-matrix interactions, resulting in deregulated growth, dedifferentiation, disruption of other processes and a poor simulation of the *in vivo* (patho-)physiology.¹ 3D cell culture methods have been developed that enable a more *in vivo* like tissue architecture and are therefore expected to represent a more physiologically relevant context for the evaluation of bioactive molecules.²⁻⁴ Although gaining in popularity for small-scale analyses, 3D cultures have yet to be widely adopted for screening. A number of factors account for this, although high throughput 3D imaging and the analysis of large and complex image data sets can represent the most significant barrier to the implementation of high content 3D culture based screening.⁵ As a result, where 3D assays are used for screening, the most common end-point measurements tend to be biochemical determinations of cell viability, with the loss of potentially valuable phenotypic information.

Cells cultured in extracellular matrix (ECM) -containing hydrogels can generate complex multicellular tissues, supporting a higher level of tissue organisation, such as formation of ductal structures by epithelial cells and complex networks of invasive tumour cells.⁶⁻¹⁰ These features may be relevant to the pathology of the disease being studied and offer a context for screening for therapeutic molecules. Complex phenotypes can also be exploited for compound profiling, allowing compounds that affect different targets and therefore induce different phenotypes to be discriminated, potentially providing additional information on the biological effects of compounds that cannot be obtained from single end point measurements.

In many cultured cells, activation of receptor tyrosine kinases results in increased proliferation and motility.¹¹ Cell motility has previously been used as a readout for high throughput small molecule and siRNA screens for inhibitors of c-Met signalling.¹²⁻¹⁴ In 3D culture, activation of c-Met can result in invasion of tumour cells into the surrounding micro-environment,¹⁵ a process which closely resembles the *in vivo* pathophysiology. Similarly, activation of the EGF receptor is known to induce EMT and invasion in various cancer types.¹⁶⁻¹⁷ As expected, selective inhibition of the receptor tyrosine kinases inhibits the ligand induced effects. However, compounds that inhibit multiple targets or are toxic may also inhibit ligand-induced effects. Here, we describe a 384-well screening assay that uses automated high content analysis and profiling of 3D cultures of invasive prostate cancer tumour cells to identify selective inhibitors of the c-Met and EGFR receptor tyrosine kinases.

MATERIALS AND METHODS

Cell lines

The human prostate adenocarcinoma cell line PC-3 was cultured in DMEM-F12 (Ham's) growth medium (Gibco™ Fisher Scientific, Landsmeer, Netherlands), supplemented with 10% FBS (Gibco™ Fisher Scientific, Landsmeer, Netherlands), 1mM sodium

pyruvate (Gibco™ Fisher Scientific, Landsmeer), 1.5g/L NaHCO₃ (Merck, Schiphol-Rijk, Netherlands), 0.1mM non-essential amino acids (Gibco™ Fisher Scientific, Landsmeer, Netherlands) and 50µg/mL gentamycin (Sigma Aldrich, Zwijndrecht, Netherlands). PC-3 cells were grown in 175cm² tissue culture flasks (Corning, Amsterdam, Netherlands) in culture medium as described above. Before reaching maximal density, cells were washed with 1x PBS (Sigma Aldrich, Zwijndrecht, Netherlands) and trypsinized with 1x Trypsin (Gibco™ Fisher Scientific, Landsmeer, Netherlands). Subsequently, medium was added and cells were pelleted by centrifugation and resuspended in FBS with 10% DMSO (Biosolve B.V., Netherlands) and stored in aliquots at -150°C.

3D invasion assay

PC-3 cells were cultured in 384-well plates (Greiner Bio-One B.V., Alphen aan den Rijn, Netherlands) in 60%v/v growth factor-reduced Matrigel (>9mg/mL) (Corning, Amsterdam, Netherlands) which supported spheroid formation of the highly transformed PC-3 cells and invasion upon addition of motogenic cytokines. To generate gels, thawed cells were mixed with culture medium and growth factor-reduced Matrigel. 14.5µL of cell-gel mix was added to each well of a 384-well plate using a CyBi Selma 96/60 robotic liquid handler (Analytik Jena AG, Jena, Germany), at a final cell density of 2000 cells per well. After polymerization at 37°C for 30 minutes, DMEM-F12 (Ham's) growth medium containing growth factors (HGF or EGF) and compounds were added to the gel. The plate(s) were subsequently covered with a gas permeable adhesive membrane (Thermo Scientific, Zwijndrecht, Netherlands). Compound exposures were performed for 96 hours, after which gels were fixed with 3% formaldehyde (Sigma Aldrich, Zwijndrecht, Netherlands), permeabilised with 0.2% Triton-X100 (Sigma Aldrich, Zwijndrecht, Netherlands) and stained with 0.25µM rhodamine-phalloidin (Sigma Aldrich, Zwijndrecht, Netherlands) and 0.1% Hoechst 33258 (Sigma Aldrich, Zwijndrecht, Netherlands) in PBS at 4°C for 16 hours. After staining, plates were washed in PBS and covered with a Greiner SilverSeal (Greiner Bio-One B.V., Alphen aan den Rijn, Netherlands).

Compounds

Anti c-Met and non-targeting control Fab antibodies were generously provided by Merus Biopharmaceuticals B.V. (Utrecht, The Netherlands). c-Met inhibitor ArQ-197 (Tivantinib) was synthesized by Janssen Pharmaceutica NV (Beerse, Belgium), following the synthesis method published from ArQule, and subsequently sent to the authors as a gift from Souichi Ogata (Janssen Oncology R&D). Results were confirmed using a second source of ArQ-197 (SelleckChem/Bio-Connect B.V. Huissen, Netherlands). EGFR inhibitor AG1478 was obtained from Santa Cruz (SC-200613, Bio-Connect B.V. Huissen, Netherlands). PHA-665752 was a gift from Pfizer Inc. A collection of 80 compounds selected to inhibit both EGFR and/or c-Met was generated by Vichem Chemie, Budapest, Hungary (supplemental table 1).

Imaging

A BD Pathway 855 automated inverted fluorescence microscope (BD Biosciences)

was used for automated imaging of 384-well plates (wide-field epifluorescence). This microscope was used to image both Hoechst 33258 and rhodamine-phalloidin staining, using a 4x Olympus objective, at focal planes spaced at intervals of 50µm throughout the gel using Attovision software accompanying the microscope. The gel was imaged through its entire depth (z-axis), requiring 25 images per well. Each image captured approximately 75% of the area of the well.

Data Analysis

Ominer image analysis software (OcellO, Leiden, Netherlands) and KNIME (<https://www.knime.org>) were used to extract in-focus information from the Z-stacks generated by the BD Pathway 855 for both Hoechst 33258 (nuclei) and rhodamine-phalloidin (F-actin) using maximum-intensity projections.¹⁸ For image processing, a monochrome mask was created for both channels to define the regions of interest (ROI's). The in-focus images were used to quantify staining intensities and a set of Hu moments and Gabor wavelet based features describing image intensity and texture. The Hoechst 33258-derived monochrome mask was used to determine number and area of nuclei and tumouroids. Additionally, a detailed set of parameters was calculated to describe the shape of the rhodamine-phalloidin (F-actin) stained objects.¹⁸ First, for principal components analysis, data were Z-score normalized to the negative control treatment median to account for plate-to-plate differences. The features derived from the image analysis and quantification steps were ranked based on their ability to distinguish positive and negative controls (Z-prime) and the features that showed greatest separation between control groups were retained ($Z' > 1.0$). The median of treatment quadruplicates was used for a principal component analysis (PCA) that combined correlated features into (uncorrelated) principal components. This model was applied to all wells and summarized ~95% of all variation into principal components. The distance between treatment and control groups was quantified as a Z-score in principal component 0 (PCo), which retained 60% of the variation of the data set. 2-dimensional density estimations and linear discriminant analysis (LDA) were performed using the MASS package (<http://www.stats.ox.ac.uk/pub/MASS4/>)¹⁹ for R-studio 0.99.878 (<https://www.rstudio.com/products/rstudio2/>) with R 3.2.3 (<https://www.r-project.org/>). PCA was calculated in KNIME and principal component plots were generated using ggplot2 (<http://ggplot2.org/>)²⁰ with the scatterplot3D package for R-Studio 0.99878 (<https://cran.r-project.org/web/packages/scatterplot3d/index.html>).²¹ Other charts were generated using Graphpad Prism 6 software (<http://www.graphpad.com/scientific-software/prism/>). Results are displayed as mean ± standard deviation unless otherwise stated.

Western blot detection of receptor activation

Phosphorylation status of c-Met and EGFR in response to 20ng/mL HGF or 20ng/mL EGF was evaluated by Western blot. Briefly, 10⁵ PC-3 cells were grown per well in 12 well plates. After 24 hours, growth medium was replaced with starvation medium (without serum and antibiotics) containing test compounds. After 24 hours of compound exposure, growth factors (20ng/mL HGF/EGF) were added for 10 minutes. Protein was

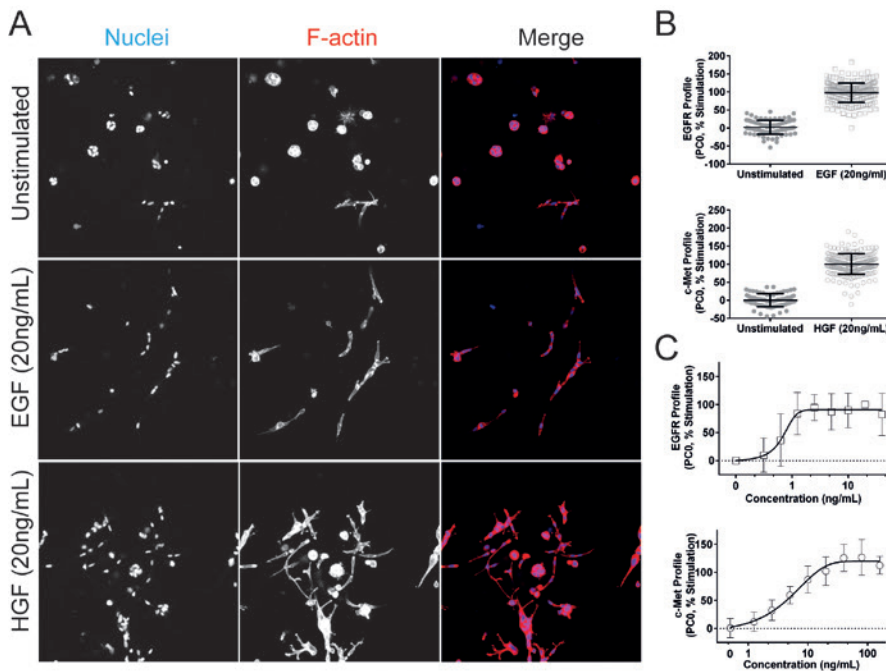


FIGURE 1 Receptor activation induces a quantifiable change in phenotype. **A)** Typical images of unstimulated, HGF- and EGF-stimulated PC-3 cells taken using a Nikon TI Eclipse confocal microscope. Receptor activation induced a change in phenotype characterized by invasion into the surrounding matrix. F-actin stained red, nuclei stained blue. **B)** Phenotypic shift induced by HGF and EGF visualized using supervised (unstimulated-stimulated) principal components analysis (PCA). PCo was scaled between 0% (unstimulated) and 100% (stimulated). Individual data points shown, as well as mean and standard deviations **C)** EGF and HGF cause a dose-dependent change in phenotype. Phenotypic change is derived from PCo and scaled to % response as shown in B. Results are shown as means with standard deviation.

isolated using RIPA lysis buffer (1%w/w deoxycholate, 50mM Tris pH7.5, 0.15M NaCl, 0.1% SDS, 1% NP-40, 2mM EDTA, 1% protease inhibitor cocktail (Sigma Aldrich, Zwijndrecht, Netherlands)) and quantified using the standard BCA method according to manufacturer's instructions (Thermo Scientific, Zwijndrecht, Netherlands). Western blot analysis was performed according to standard protocol using phospho-c-Met (Tyr1234/1235) antibody (Cell Signaling, Cat#3077P) diluted 1:1000 in 5%BSA in TBS-T or phospho-EGFR (Tyr1173) (Cell Signaling, Cat#4407) 1:1000 in 5% BSA in TBS-T. Phospho-c-Met and Phospho-EGFR antibodies were detected using HRP conjugated anti-rabbit IgG secondary antibody (Jackson, 111-035-003) and ECL Plus reagent (GE Healthcare Life Sciences, Eindhoven, The Netherlands, Cat#RPN2132). Detection of antibody was performed using a LAS4000 scanner (GE Healthcare Life Sciences,

Eindhoven, The Netherlands). Tubulin loading control was detected using an anti-Tubulin antibody (Sigma-Aldrich, Zwijndrecht, Netherlands #T-9026) diluted 1:1000 in 5%BSA in TBS-T and an anti-mouse Alexa 647-linked IgG (JacksonImmunoResearch, Suffolk, UK #115-605-006). The Alexa 647 signal was detected directly using the LAS4000.

In vitro kinase activity measurement

EGFR enzyme activity was assayed in 384 microtiter plates (Corning 3676) at 3 compound concentrations, in a total volume of 10 μ L by the Transcreener ADP2 FP method (BellBrook Labs). Assay buffer contained 20mM HEPES pH7.5, 1mM DTT, 10mM MgCl₂, 2mM MnCl₂, 0.01%v/v NP40. The final EGFR concentration was 7nM. Poly Glu-Tyr (4:1) / Poly Glu-Tyr (4:1)/ was used as substrate at final concentration of 0.01mg/mL. The final ATP concentration was at 7.52 μ M. The enzyme reaction was incubated for 60 minutes and stopped by addition of 10 μ L ADP detection mixture (1x). Measurements were performed on a Tecan Infinite M1000Pro reader. c-Met enzyme activity was assayed in 384 microtiter plates (Corning 3676) at 3 compound concentrations, in total volume of 10 μ L by the Transcreener ADP2 FP method (BellBrook Labs). Assay buffer contained 20mM HEPES pH7.5, 1mM DTT, 3mM MgCl₂, 3mM MnCl₂, 0.01%v/v Tween20. The final c-Met concentration was 8nM. Poly Ala-Glu-Lys-Tyr (6:2:5:1) was used as substrate at final concentration of 0.25mg/ml. The final ATP concentration was at 9.6 μ M. The enzyme reaction was incubated for 60 minutes and stopped by addition of 10 μ L ADP detection mixture (1x). Measurements were performed using a Tecan Infinite M1000Pro reader.

RESULTS

Quantification of complex phenotypic changes of prostate cancer cells cultured in 3D in 384 well microplates.

We developed a 3D cell culture screening method for tumour cell invasion driven by c-Met and EGFR. PC-3 cells were cultured in extracellular matrix (ECM) protein-rich hydrogels in 384-well plates in the presence or absence of c-Met/EGFR agonists and antagonists. After fixation and staining with rhodamine-phalloidin to reveal the structure of prostate cancer tumouroids and Hoechst 33258 to label nuclei, gels were imaged in two fluorescence channels using a BD Pathway 855, collecting paired stacks of xy images throughout the z-plane for each well. In-focus information from each image was extracted and a single xy image projection was generated (supplemental figure 1).

In the absence of added c-Met or EGFR agonists, PC3 cells developed into spheroids over a period of 4 days (figure 1A, upper panel). Treatment with the c-Met ligand (HGF) or the EGFR ligand (EGF), induced a highly invasive phenotype (figure 1A, middle and lower panels). To quantify these phenotypic changes in detail, Ominer and KNIME software were used to identify and quantify different morphological features from the 2D projections of the cytoskeleton and nuclei-derived image stacks. To do this, a collection of different image analysis algorithms was applied to derive measurements of the shape and fluorescence intensity of individual tumouroids, and wavelets, Hu and

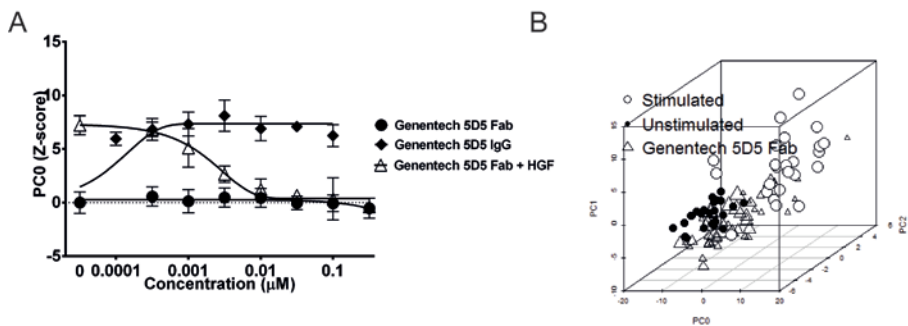


FIGURE 2 c-Met-dependent phenotypic changes. A) Inhibition of HGF-induced invasion in 3D-cultured PC-3 cells by function blocking c-Met Fab antibody 5D5 (Genentech), and stimulation of invasion by the crosslinking and activating bivalent IgG isoform. PCA trained on unstimulated and stimulated control, PCo shown and scaled as Z-score to unstimulated control. Results are shown as means of quadruplicate wells and standard deviations. **B)** 5D5 Fab (triangles) causes a shift in phenotype from stimulated (empty circles) back to unstimulated control (filled circles). Point size of markers for Fab treatment increases with concentration (7 concentrations, range 0.316-316nM). Individual datapoints are shown as a 3D scatterplot with PCo, PC1 and PC2.

Zernike moments as previously described.¹⁸ Supervised principal components analysis (PCA) was used to reduce measurements from approximately 800 phenotypic parameters to principal components (PC). EGF-treated and untreated PC3 cells were used to train a profile to represent active and inactive EGFR inhibitors, respectively, which was subsequently scaled to %-stimulation. Similarly, a separate supervised analysis was performed which was trained with HGF-treated and untreated cells to separate phenotypes representing active c-Met from unstimulated control phenotypes. The primary principal component (PCo) was plotted for both EGF- and HGF-induced phenotypic changes in order to visualise the responses (figure 1B). Both HGF and EGF induced phenotypes of PC-3-derived tumouroids could be clearly discriminated from untreated tissues. Many of the phenotypic features separating HGF- and EGF- induced changes in phenotype from unstimulated controls describe shape, circularity and intensity. The distance in phenotypic space along PCo to the unstimulated controls was presented graphically as a function of EGF or HGF concentration (figure 1C).

Phenotypic profiling can be used to quantify c-Met activation and inactivation.

To test whether HGF-induced phenotypes could report c-Met activation, HGF was added in the presence of the c-Met function blocking Fab antibody, Genentech 5D5 Fab (Genentech). 5D5 antibody effectively inhibited the HGF-induced response (PCo, figure 2A), resulting in phenotypes that projected in a similar location to unstimulated controls in phenotypic space (represented by three principal components), with an inhibition that was dose-dependent (figure 2A and 2B). The c-Met inhibitory antibody had no

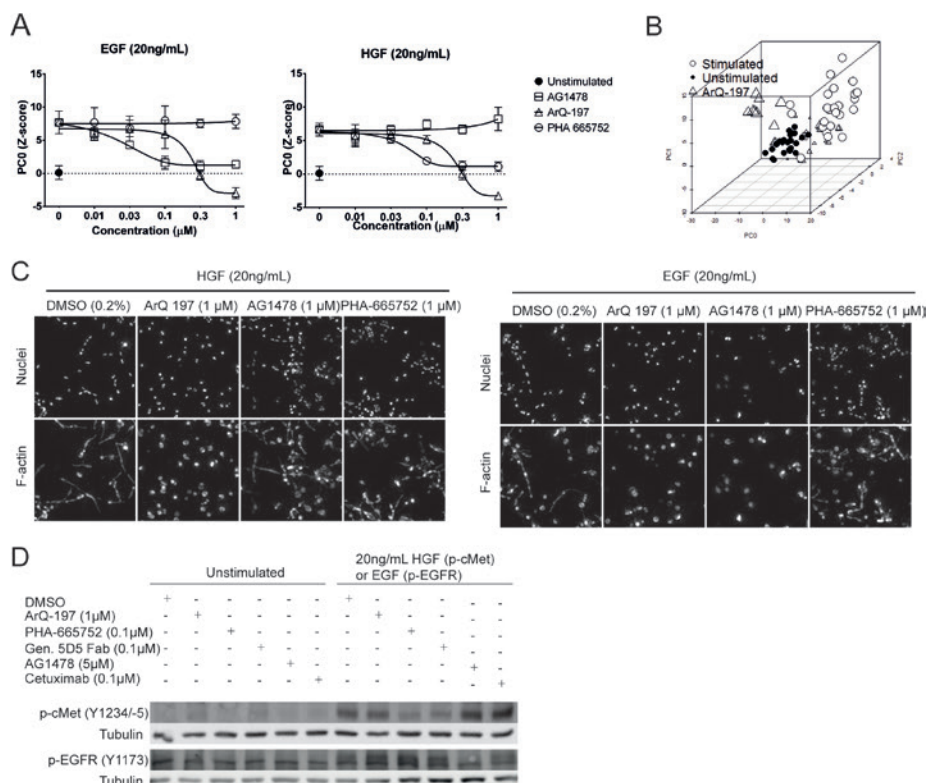


FIGURE 3 Discriminating on-target effects from off-target effects. **A)** HGF- (left panel) and EGF-induced (right panel) phenotypes can be inhibited by small molecules targeting c-Met and EGFR, respectively. Responses are shown as PCo, z-score normalized to unstimulated. Values shown as means of quadruplicate wells with standard deviation. **B)** PCA plot identifies novel phenotype introduced by ArQ-197 (triangles) at high doses. Individual data points are shown as a 3D scatterplot with PCo, PC1 and PC2. Empty circles, stimulated controls; filled circles, unstimulated controls. **C)** Representative images showing HGF and EGF induced invasion and inhibition by small molecules. Maximum intensity projections of both image channels shown. **D)** Western blot of c-Met and EGFR phosphorylation in 2D-cultured PC-3 cells exposed to EGF or HGF and inhibitors.

quantifiable effect on the PC-3 phenotype in the absence of HGF (figure 2A). In contrast, treatment of PC-3 cells with a c-Met activating antibody, the bivalent IgG form of 5D5, which crosslinks c-Met, induced a phenotype which was indistinguishable from that induced by HGF. Together these results confirm the c-Met dependency of the HGF-induced phenotype and demonstrate that principal components can be used to quantify HGF-induced phenotypic changes correlating with c-Met activation and inhibition.

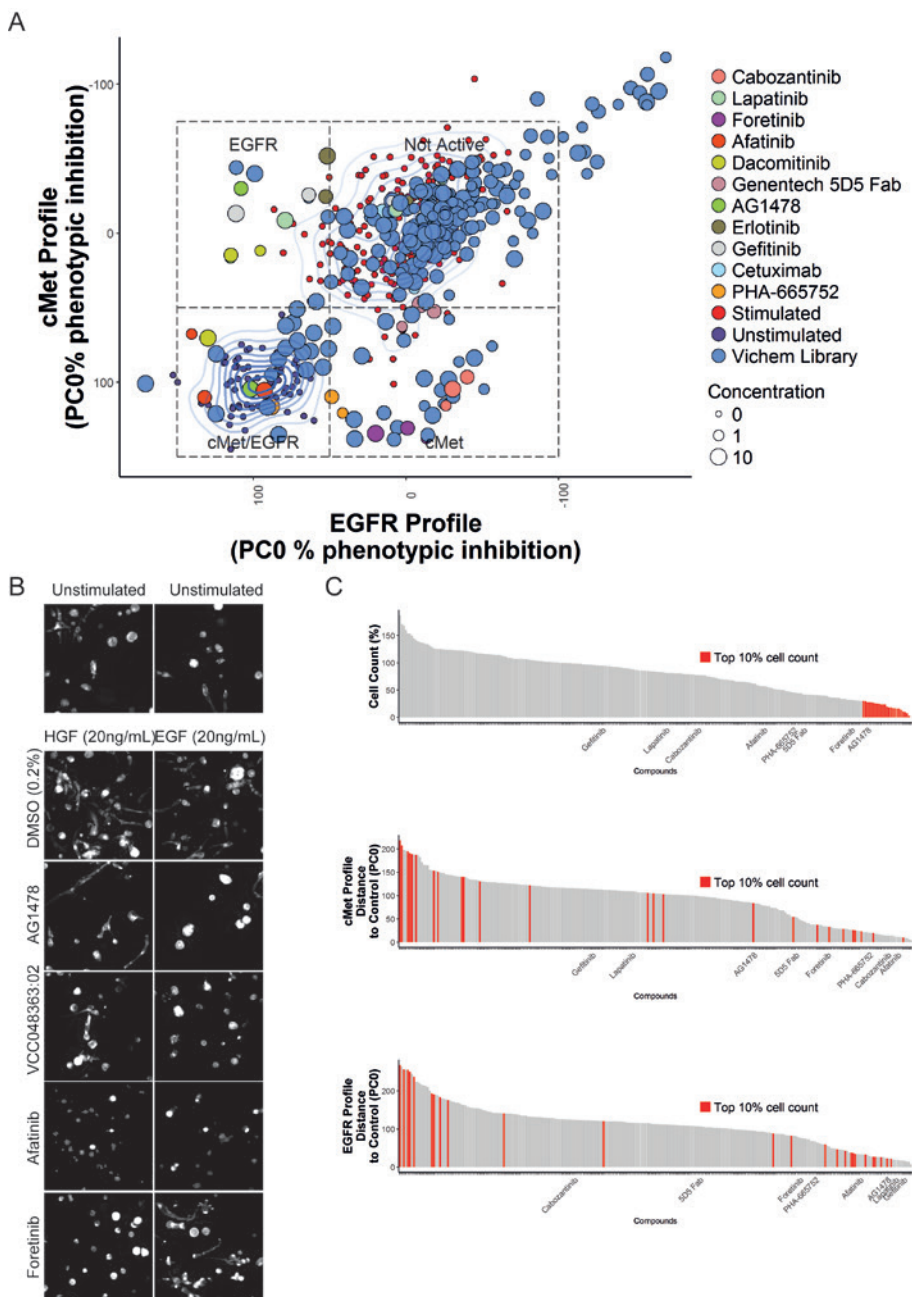


FIGURE 4 Identification of selective c-Met/EGFR inhibitors in a Vichem EGFR/c-Met inhibiting compound library. **A)** Compound screen of 80 Vichem compounds tested at 10, 3.16 and $1\mu\text{M}$. Compounds were divided over triplicate plates and co-exposed with either HGF (20ng/mL) or EGF (20ng/mL). PCA was trained on unstimulated and stimulated controls separately for plates exposed to HGF or EGF, respectively, to obtain (legend continues on next page)

a principal component that could separate c-Met and EGFR responses. Data points represent mean determinations from 3 wells. Controls are color-coded as indicated in the legend. For stimulated (top middle) and unstimulated controls (bottom left), a 2D-density estimation (contour lines) is shown. **B)** Representative 2D projected images derived from the F-actin staining after 96 hours of compound treatment. Except for AG1478, which was 3.16 μ M, shown treatment concentrations were 10 μ M. Pictures were obtained using a BD Pathway 855 microscope (images trimmed to 300x300 pixels for presentation purposes). **C)** Cell count (viability) is a poor criterion for selecting c-Met and EGFR inhibitors. Number of nuclei per well was %-normalized to stimulated control (100%) and lowest detected cell count and 0%, top panel. The top ranking 10% of compounds affecting cell count are colour-coded in red. Middle and lower panel shows the same compounds ranked on efficacy on c-Met and EGFR profiles (distance to unstimulated control). Mean values shown; each chart contains compounds at three different concentrations.

Using phenotype to discriminate compounds based on target selectivity.

To determine whether the phenotypic assay can discriminate between selective c-Met and EGF inhibitors, PC-3 cells were cultured in the presence of either HGF or EGF, together with established small molecule and antibody inhibitors of their cognate receptors. As expected, the small molecule c-Met inhibitor PHA-665752²²⁻²³ selectively inhibited the phenotype induced by HGF. In contrast, the EGFR inhibitor AG1478²⁴ had no significant effect on the HGF-induced phenotype up to a concentration of 1 μ M (figure 3A and 3C, right panel). Conversely, AG1478 but not PHA-665752 inhibited the EGF-induced phenotype (figure 3A and 3C, left panel). These findings suggest that residual c-Met and EGFR activity does not contribute to the 3D phenotype under the conditions used and that c-Met does not require EGFR for the ligand induced response and vice versa. Interestingly, ArQ-197, which is reported to be a selective inhibitor of c-Met,²⁵⁻²⁶ inhibited both the HGF and EGF-induced responses with a similar IC_{50} , suggesting a more complex mechanism of action. At higher concentrations (>1 μ M), this compound introduced a novel phenotype, shown by a shift away from the controls in a representation of phenotypic space (figure 3B).

To confirm that the interpretations based on phenotypic changes correlated with inhibition of receptor kinase activity, we performed Western blot analysis for phosphorylated c-Met (Y1234/-5) and phosphorylated EGFR (Y1173) (figure 3D). Results showed that PHA-665752 and the Genentech 5D5 Fab potently inhibited phosphorylation of c-Met, but not EGFR phosphorylation. Conversely, AG1478 and cetuximab treatment inhibited phosphorylation of EGFR, but not of c-Met. ArQ-197 did not show detectable inhibition of EGFR (Y1173) or c-Met (Y1234/-5) phosphorylation under these conditions (figure 3D). Therefore, inhibition of phenotypes in 3D culture by c-Met and EGFR inhibitors correlates with inhibition of the respective kinases.

TABLE 1 Hit selection phenotypic screen

Vichem Compound-ID	1 μ M	3.16 μ M	10 μ M
VCC030450:22	EGFR	EGFR	EGFR
VCC048363:02	EGFR	EGFR	EGFR/cMet
VCC055393:01	EGFR/cMet	EGFR/cMet	EGFR/cMet
VCC109756:01	cMet	cMet	cMet
VCC155409:01	None	None	EGFR/cMet
VCC228833:01	None	None	Top 10% cell count
VCC285946:01	None	cMet	cMet
VCC376189:01	cMet	cMet	EGFR/cMet
VCC378728:01	None	EGFR	None
VCC407451:10	None	EGFR	EGFR
VCC415997:02	cMet	cMet	cMet
VCC429285:02	None	None	EGFR/cMet
VCC444414:01	cMet	cMet	cMet
VCC450892:17	cMet	cMet	cMet
VCC497510:01	cMet	cMet	EGFR/cMet
VCC502987:01	None	None	EGFR/cMet
VCC528301:01	None	None	EGFR/cMet
VCC656576:02	None	None	None
VCC716837:01	None	None	Top 10% cell count
VCC740005:11	None	EGFR	EGFR
VCC744093:03	None	None	None
VCC833029:24	None	None	EGFR
VCC868449:01	None	None	EGFR/cMet
VCC960450:01	cMet	cMet	cMet

TABLE 2 Enzyme activity measurement (percent inhibition)

Vichem Compound-ID	EGFR Inh (%) 10 μ M	EGFR Inh (%) 1 μ M	EGFR Inh (%) 0.1 μ M	c-Met Inh (%) 10 μ M	c-Met Inh (%) 1 μ M	c-Met Inh (%) 0.1 μ M
VCC030450:22	101	99	97	4	2	0
VCC048363:02	101	100	97	1	-2	-1
VCC055393:01	99	100	100	3	3	-4
VCC109756:01	43	7	2	93	61	7
VCC155409:01	76	34	10	25	2	-2
VCC228833:01	16	1	0	4	0	-2
VCC285946:01	32	0	9	84	49	8
VCC376189:01	12	2	-2	83	56	9
VCC378728:01	85	41	8	72	16	0
VCC407451:10	93	92	73	7	0	-4
VCC415997:02	-11	-11	-7	95	77	14
VCC429285:02	3	2	0	6	-2	2
VCC444414:01	7	-4	-6	90	47	3
VCC450892:17	32	10	5	85	39	4
VCC497510:01	20	10	2	90	54	9
VCC502987:01	19	9	1	4	1	0
VCC528301:01	94	82	29	37	7	1
VCC656576:02	-2	-7	-13	0	-4	-4
VCC716837:01	48	10	1	41	6	0
VCC740005:11	105	102	93	11	1	3
VCC744093:03	77	25	3	27	-1	-1
VCC833029:24	97	90	37	-3	0	0
VCC868449:01	95	89	37	56	14	3
VCC960450:01	-11	-7	-10	87	50	11

Taken together, these results show that measurement of ligand-induced phenotypic changes can be used to discriminate and measure inhibition of c-Met and EGFR.

Using phenotypic profiles to identify novel selective c-Met and EGFR inhibitors

Using data obtained from c-Met and EGFR in vitro kinase assays, a collection of 80 putative single and dual specificity EGFR and c-Met inhibitors was compiled (supplemental table 1), which included several well-characterized reference compounds. These were screened in 3D-cultured PC-3 cells together with several published reference inhibitors of c-Met and EGFR. All compounds were screened in 384-well plates at three concentrations (10 μ M, 3.16 μ M and 1 μ M) in triplicate plates in both EGF- and HGF-stimulated conditions. Multiparametric analysis was performed as before, followed by Z-score normalisation of each parameter to the plate median. Supervised principal components analysis was used to condense phenotypic measurements to one phenotypic descriptor (PCo), which was scaled to %-inhibition. PCA was found to perform superior to individual features in separating out stimulated and unstimulated controls (supplemental figure 2).

Figure 4A depicts the screening results combining the first principal component, PCo, for both EGF- and HGF-induced phenotypic changes in a single plot. Inhibition of c-Met is therefore represented by a decrease in the c-Met PCo value, from the growth factor-treated to growth factor-untreated controls. Compounds that induced such a shift in the c-Met PCo included various established c-Met reference inhibitors that were included in the screen, including the Genentech 5D5 Fab antibody, foretinib and lower doses of PHA-665752. This confirmed that the phenotypic training using HGF treated and untreated samples discriminated c-Met active and inactive conditions and was able to select compounds that induced a c-Met inhibitory phenotypic profile. Selective inhibition of the EGFR could be characterized by a horizontal shift to the left, from a profile associated with EGF-stimulated phenotype to one associated with an unstimulated phenotype. This region contained several EGFR reference inhibitors, including erlotinib, gefitinib and AG1478 (at 1 and 3.16 μ M), which were included in the screen alongside test compounds. Compounds that clustered together with the unstimulated controls (figure 4A, bottom left quadrant) were predicted to have a dual inhibitory activity for both c-Met and EGFR. The compounds clustering in this area included afatinib, and also a number of previously untested compounds of the Vichem library. The class to which each compound was attributed using this approach is shown in table 1 and supplemental table 2. By using another form of supervised clustering, linear discriminant analysis (LDA), we could separate the highly similar EGF- and HGF-induced phenotypes into a multidimensional plot (supplemental figure 3). However, this approach did not improve classification of reference c-Met and EGFR inhibitor compounds.

Representative images of 3D-cultured PC-3 cells treated with EGFR and c-Met inhibitors are presented in figure 4B and show a consistency between the automated classification of compounds to a specific inhibitory class and the phenotype which is induced in the presence of a specific growth factor. We compared the pheno-

typic classification of compounds with measurements of EGFR or c-Met enzyme inhibitory activity (table 2 and supplemental table 3). Phenotypic classification was found to frequently overlap with biochemical measurements. Inhibition of c-Met activity in enzymatic and phenotypic assays was closely correlated, with all compounds showing greater than 40% inhibition in an enzymatic assay being inhibitory in the phenotypic assay at the equivalent concentration. However, approximately half of the compounds that were active in EGFR enzymatic assays were inactive in the cell based phenotypic assays. Furthermore, several of the compounds that were inhibitory at the lowest doses in the EGFR enzymatic assay, only showed activity in the corresponding phenotypic assay at higher concentrations (e.g. VCC833029:24, VCC740005:11 and VCC407451:10), indicating lower sensitivity of the phenotypic assay compared to the enzymatic assay. Not all compounds that induced enzymatic inhibition of EGFR and/or c-Met could be identified as inhibitors from our screening results, suggesting that enzymatic inhibition does not directly translate to a phenotypic change under all conditions.

We then compared ranking of compounds based on phenotypic profiling with ranking based on cell count. Cell count was determined by the number of nuclei counted per well (one of the many features scored by the multiparametric analysis) and is a feature that correlates closely with biochemical measurements of cell proliferation (not shown). Using a ranking based on cell proliferation, inhibitors which were shown to potently inhibit the c-Met phenotype, including Genentech 5D5 Fab, did not score in the top 10% inhibitors of proliferation (Figure 4C and supplemental figure 4). Consistent with the profiling results in figure 4A, when compounds were ranked based on the difference of their phenotypic profiles to unstimulated controls (measured along PCo), a strong enrichment of c-Met and EGFR inhibitors was observed in the top 10% of ranked compounds in the presence of HGF and EGF respectively (supplemental figure 4). The most potent inhibitors of proliferation were found to perform poorly when ranked based on their phenotypic profiles (figure 4C). An analysis of the images from 3D cultures treated with these compounds showed that spheroid formation was disrupted, consistent with cytotoxicity of these compounds.

Discussion

Because tumour cells exist in a 3D extracellular matrix-rich environment, 3D matrix-embedded cell cultures provide a more physiologically relevant context in which to perform compound screening.²⁻⁴ The increased complexity of 3D cultures also offers increased potential for phenotypic profiling.²⁷⁻²⁹ We developed a fully scalable 3D tissue culture-based high-content screening platform that uses phenotypic profiling of cultured tumouroids derived from a prostate cancer cell line. This screening platform was used to identify several selective inhibitors for c-Met and EGFR, which represent important targets in many cancers and are known to be able to stimulate survival and invasive growth of tumours.¹⁵⁻¹⁷ We show that activation of c-Met with its ligand, HGF, induced a dose-dependent reorganisation of PC-3 spheroids characterized by invasion of cells into the surrounding matrix. A similar change in phenotype was induced by the addition of EGF to the PC-3 cells. These phenotypic changes were not observed in 2D

monolayers. Ultra-high content multiparametric analysis allowed a clear discrimination of the phenotypes associated with active and inactive c-Met and EGFR, which could be quantified using a single PCA measurement. This approach allowed us to discriminate inhibitors of c-Met and EGFR and also putative bi-selective inhibitors of these receptor tyrosine kinases. The method also enabled non-selective compounds to be discriminated since they induced phenotypes that failed to match those induced by selective inhibition of c-Met or EGFR. The screening results were cross-validated with an *in vitro* measurement of enzyme activity, and were found to largely correlate. Some compounds that inhibited EGFR or c-Met in the biochemical measurement were not identified by our phenotypic screen as inhibitors for these pathways, indicating that inhibition of purified enzyme does not always correlate with inhibition of the target enzyme in cells. These differences may be explained by poor compound stability over multiple days in aqueous solution (medium) or poor membrane permeability, resulting in lower cytoplasmic concentrations. It is also possible that these compounds induce mild phenotypic changes that are below the threshold of the phenotypic assay. A number of compounds were found to induce phenotypic changes in the EGFR and/or c-Met profiles, even though these failed to induce inhibition of either EGFR or c-Met activity. A possible explanation for this finding is that these molecules induced off-target phenotypic effects that could not be discriminated from inhibition of c-Met and EGFR.

Improvements in 3D cell culture reagents, methods and automated microscopes that can capture 3D image data is making screening in 3D more accessible, including more complex models such as co-cultures.^{5, 30} Here we describe how high content analysis can maximise the information that can be extracted from the more complex phenotypes obtained in 3D cell culture. These include disease-relevant features, such as tumour cell invasion, but also a multitude of other features that can be exploited for profiling purposes. Thus, in addition to screening for inhibition of a disease phenotype, target based screening can be performed. Traditionally, receptor activation has been measured using biochemical methods. While sensitive, these methods do not discriminate non-selective inhibition of the target. An advantage of the multiparametric profiling approach described here is that in addition to detecting inhibition of the c-Met and EGFR, off-target effects can also be detected if the off-targets have an impact on tissue phenotype.

Our method was used to determine inhibitory activity of both small molecules and antibodies. We applied the method to both c-Met and EGFR but, in principle, it can be applied to any target if a cell line can be identified in which the activity of the target influences cell phenotype. Combining the advantages of physiological relevance and phenotypic complexity, phenotypic screening and profiling with 3D cell cultures has the potential to improve the quality of hits from screens and make previously challenging targets more accessible, potentially leading to a higher success rate of molecules in clinical trials.

Acknowledgments

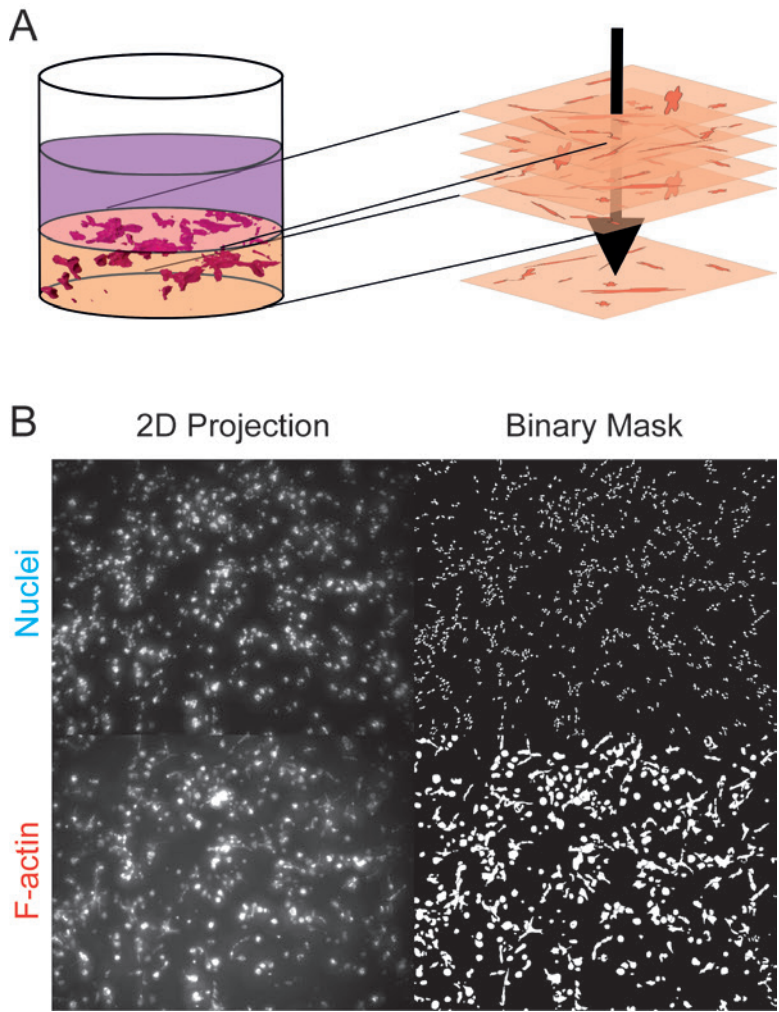
The authors would like to thank Souichi Ogata (Janssen Oncology R&D) for kindly providing ArQ-197 and Rob Roovers (Merus) for providing the Genentech 5D5 Fab and IgG. Furthermore, we thank Dr Marc Bickle, Max Planck, Dresden, for introducing us to the KNIME software.

References

1. Mishra DK, Sakamoto JH, Thrall MJ, Baird BN, Blackmon SH, Ferrari M, Kurie JM, Kim MP: Human lung cancer cells grown in an ex vivo 3D lung model produce matrix metalloproteinases not produced in 2D culture. *PLoS One* 7(9): e45308, 2012
2. Bradbury P, Fabry B, O'Neill GM: Occupy tissue: the movement in cancer metastasis. *Cell Adh Migr* 6(5): 424-432, 2012
3. Smalley KS, Lioni M, Herlyn M: Life isn't flat: taking cancer biology to the next dimension. *In Vitro Cell Dev Biol Anim* 42(8-9): 242-247, 2006
4. Breslin S, O'Driscoll L: Three-dimensional cell culture: the missing link in drug discovery. *Drug Discov Today* 18(5-6): 240-249, 2013
5. Li L, Zhou Q, Voss TC, Quick KL, LaBarbera DV: High-throughput imaging: Focusing in on drug discovery in 3D. *Methods* 96 97-102, 2016
6. Taubenberger AV, Bray LJ, Haller B, Shaposhnykov A, Binner M, Freudenberg U, Guck J, Werner C: 3D extracellular matrix interactions modulate tumour cell growth, invasion and angiogenesis in engineered tumour microenvironments. *Acta Biomater* 36 73-85, 2016
7. Debnath J, Brugge JS: Modelling glandular epithelial cancers in three-dimensional cultures. *Nat Rev Cancer* 5(9): 675-688, 2005
8. Schmeichel KL, Bissell MJ: Modeling tissue-specific signaling and organ function in three dimensions. *J Cell Sci* 116(Pt 12): 2377-2388, 2003
9. O'Brien LE, Zegers MM, Mostov KE: Opinion: Building epithelial architecture: insights from three-dimensional culture models. *Nat Rev Mol Cell Biol* 3(7): 531-537, 2002
10. Harma V, Knuutila M, Virtanen J, Mirtti T, Kohonen P, Kovanen P, Happonen A, Kaewphan S, Ahonen I, Kallioniemi O, Grafstrom R, Lotjonen J, Nees M: Lysophosphatidic acid and sphingosine-1-phosphate promote morphogenesis and block invasion of prostate cancer cells in three-dimensional organotypic models. *Oncogene* 31(16): 2075-2089, 2012
11. Ren Y, Cao B, Law S, Xie Y, Lee PY, Cheung L, Chen Y, Huang X, Chan HM, Zhao P, Luk J, Vande Woude G, Wong J: Hepatocyte growth factor promotes cancer cell migration and angiogenic factors expression: a prognostic marker of human esophageal squamous cell carcinomas. *Clin Cancer Res* 11(17): 6190-6197, 2005
12. Chan GK, Lutterbach BA, Pan BS, Kariv I, Szewczak AA: High-throughput analysis of HGF-stimulated cell scattering. *J Biomol Screen* 13(9): 847-854, 2008
13. Radtke S, Milanovic M, Rosse C, De Rycker M, Lachmann S, Hibbert A, Kermorgant S, Parker PJ: ERK2 but not ERK1 mediates HGF-induced motility in non-small cell lung carcinoma cell lines. *J Cell Sci* 126(Pt 11): 2381-2391, 2013

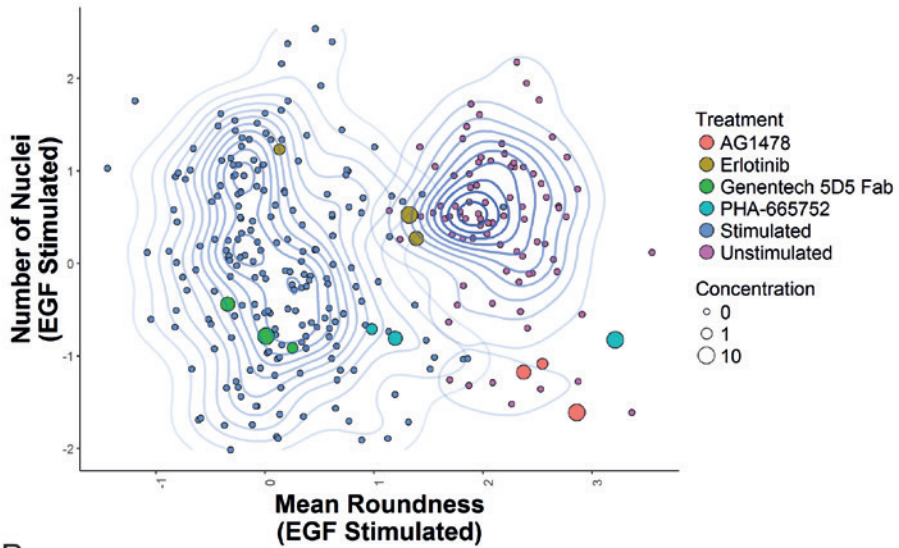
14. Zaritsky A, Natan S, Ben-Jacob E, Tsarfaty I: Emergence of HGF/SF-induced coordinated cellular motility. *PLoS One* 7(9): e44671, 2012
15. Comoglio PM, Trusolino L: Invasive growth: from development to metastasis. *J Clin Invest* 109(7): 857-862, 2002
16. Hardy KM, Booth BW, Hendrix MJ, Salomon DS, Strizzi L: ErbB/EGF signaling and EMT in mammary development and breast cancer. *J Mammary Gland Biol Neoplasia* 15(2): 191-199, 2010
17. Appert-Collin A, Hubert P, Cremel G, Bennasroune A: Role of ErbB Receptors in Cancer Cell Migration and Invasion. *Front Pharmacol* 6 283, 2015
18. Di Z, Klop MJ, Rogkoti VM, Le Devedec SE, van de Water B, Verbeek FJ, Price LS, Meerman JH: Ultra high content image analysis and phenotype profiling of 3D cultured micro-tissues. *PLoS One* 9(10): e109688, 2014
19. Venables WNR, B.D.: Modern Applied Statistics with S. In: edited by Springer-Verlag New York, 2002,
20. Wickham H: ggplot2: Elegant Graphics for Data Analysis. In: edited by Springer Publishing Company, Incorporated, 2009,
21. Ligges UM, M.: Scatterplot3d - An R Package for Visualizing Multivariate Data. *Journal of Statistical Software* 008(i11): 20, 2003
22. Tu WH, Zhu C, Clark C, Christensen JG, Sun Z: Efficacy of c-Met inhibitor for advanced prostate cancer. *BMC Cancer* 10 556, 2010
23. Yang Y, Wislez M, Fujimoto N, Prudkin L, Izzo JG, Uno F, Ji L, Hanna AE, Langley RR, Liu D, Johnson FM, Wistuba I, Kurie JM: A selective small molecule inhibitor of c-Met, PHA-665752, reverses lung premalignancy induced by mutant K-ras. *Mol Cancer Ther* 7(4): 952-960, 2008
24. Caja L, Sancho P, Bertran E, Ortiz C, Campbell JS, Fausto N, Fabregat I: The tyrphostin AG1478 inhibits proliferation and induces death of liver tumor cells through EGF receptor-dependent and independent mechanisms. *Biochem Pharmacol* 82(11): 1583-1592, 2011
25. Adjei AA, Schwartz B, Garmey E: Early clinical development of ARQ 197, a selective, non-ATP-competitive inhibitor targeting MET tyrosine kinase for the treatment of advanced cancers. *Oncologist* 16(6): 788-799, 2011
26. Feldman DR, Einhorn LH, Quinn DI, Lorient Y, Joffe JK, Vaughn DJ, Flechon A, Hajdenberg J, Halim AB, Zahir H, Motzer RJ: A phase 2 multicenter study of tivantinib (ARQ 197) monotherapy in patients with relapsed or refractory germ cell tumors. *Invest New Drugs* 31(4): 1016-1022, 2013
27. Sirenko O, Mitlo T, Hesley J, Luke S, Owens W, Cromwell EF: High-content assays for characterizing the viability and morphology of 3D cancer spheroid cultures. *Assay Drug Dev Technol* 13(7): 402-414, 2015
28. Harma V, Schukov HP, Happonen A, Ahonen I, Virtanen J, Siitari H, Akerfelt M, Lotjonen J, Nees M: Quantification of dynamic morphological drug responses in 3D organotypic cell cultures by automated image analysis. *PLoS One* 9(5): e96426, 2014

29. Robinson S, Guyon L, Nevalainen J, Toriseva M, Akerfelt M, Nees M: Segmentation of Image Data from Complex Organotypic 3D Models of Cancer Tissues with Markov Random Fields. *PLoS One* 10(12): e0143798, 2015
30. Krausz E, de Hoogt R, Gustin E, Cornelissen F, Grand-Perret T, Janssen L, Vloemans N, Wuyts D, Frans S, Axel A, Peeters PJ, Hall B, Cik M: Translation of a tumor microenvironment mimicking 3D tumor growth co-culture assay platform to high-content screening. *J Biomol Screen* 18(1): 54-66, 2013

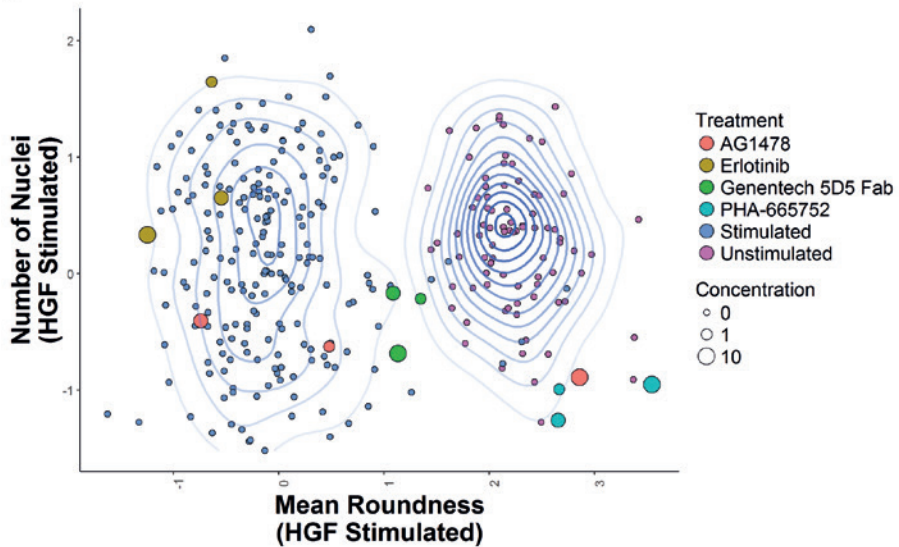


SUPPLEMENTAL FIGURE 1 3D cell culture based screening platform pipeline. **A)** PC-3 cells were cultured in 384 well plate format embedded in ECM-protein hydrogels. Compound treatment was performed for 96 hours, after which the 3D cultures were stained for F-actin and nuclei. Images were obtained for both channels at different z-planes in the gel using a BD Pathway 855 imager. In-focus information of all Z-stacks was extracted by means of a 2D maximum intensity projection. **B)** Binary black and white masks were generated to define the segmented objects and were used for shape measurements. Fluorescence intensity parameters were obtained from the segmented regions of the original micrograph projection.

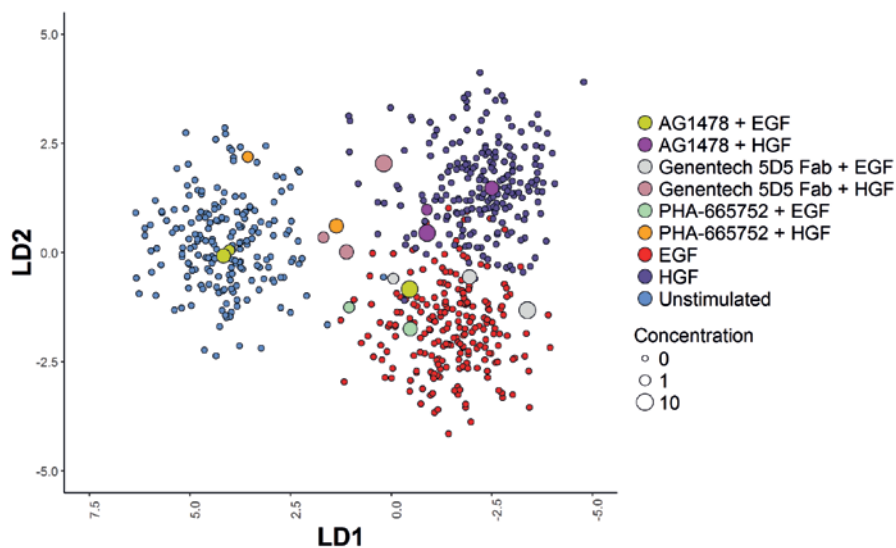
A



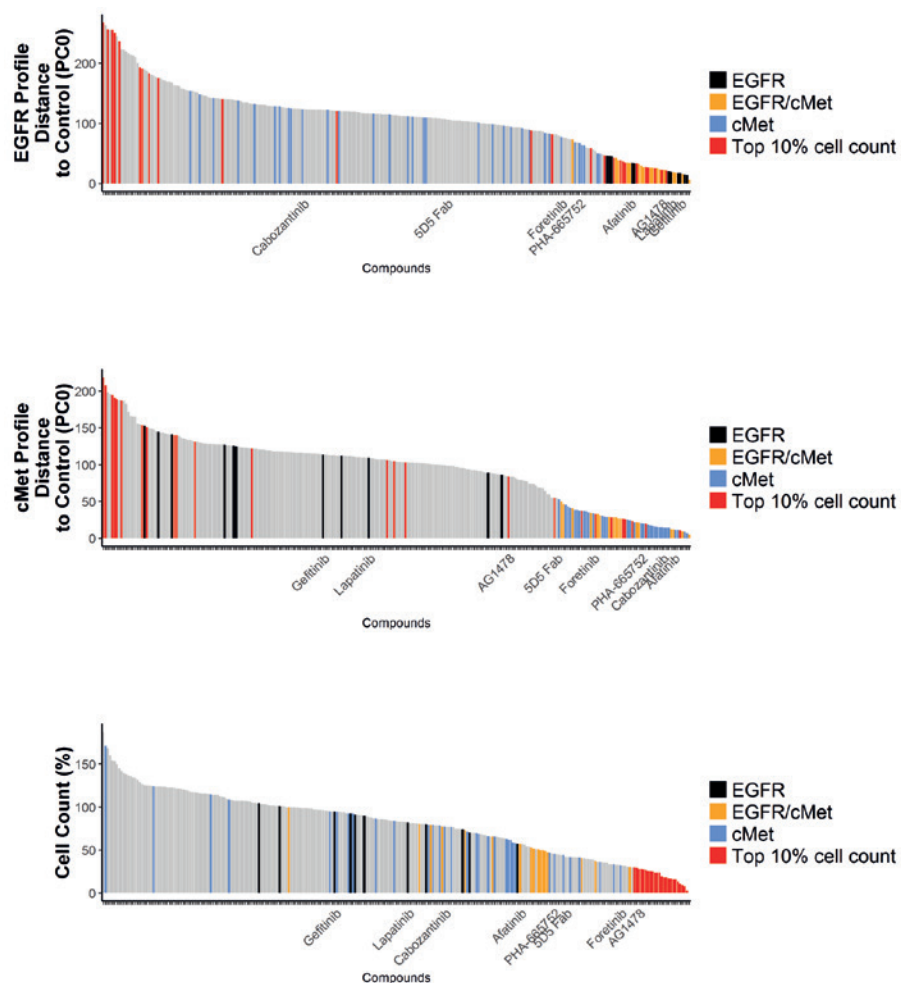
B



SUPPLEMENTAL FIGURE 2 Performance of individual phenotypic parameters to identify selective c-Met or EGFR inhibitors. **A)** Z-score normalized roundness and number of nuclei of tumouroids shown for EGF stimulated condition. **B)** Z-score normalized roundness and number of nuclei of tumouroids shown for HGF stimulated condition.



SUPPLEMENTAL FIGURE 3 EGF-and HGF-induced phenotypes are both characterized by invasion into the ECM, but can be differentiated using linear discriminant analysis (LDA). LDA training was performed using KNIME and RStudio (MASS package). Linear correlation filter was applied to all parameters ($R^2 < 0.85$) prior to training LDA on EGF, HGF and unstimulated groups, in order to filter out the most highly collinear variables. Approximately 250 phenotypic descriptors are required to separate both phenotypes. LDA was subsequently applied to the complete dataset. Individual data points for EGF, HGF and unstimulated shown. Mean data shown for AG1478, Genentech 5D5 Fab and PHA-665752.



SUPPLEMENTAL FIGURE 4 Hit selection based on cell count does not identify selective c-Met and EGFR inhibitors. Ranking performed on cell count and on c-Met and EGFR profile, as in figure 4C, show different results.

SUPPLEMENTAL TABLE 1 Vichem compound information

Compound ID	References	Core structure
VCC030450:22	D.W.Fry et al. 1994 Science 265, 1093-95.	quinazoline
VCC613596:10	WO 2009104027 A1	benzothieno[2,3-d]pyrimidine
VCC912492:07	WO 2012080727 A2	benzothieno[2,3-d]pyrimidine
VCC740005:11	Cancer Res, Vol.65 Nr., 379-382, 2005.	quinazoline
VCC407451:10	Bioorg Med Chem Lett, Vol.14 Nr.1, 111-114, 2004.	quinazoline
VCC075648:03	J. Med. Chem., 1999, 42, 5120-5130, Cancer Research (2003), 63(17), 5462-5469	indol-2-one
VCC475979:01	unpublished	indol-2-one
VCC884444:01	unpublished	indol-2-one
VCC833029:24	Bioorg Med Chem Lett, Vol.16 Nr.17, 4686-4691, 2006.	quinazoline
VCC502987:01	unpublished	indol-2-one
VCC370686:02	unpublished	indol-2-one
VCC703724:02	unpublished	indol-2-one
VCC260084:01	unpublished	indol-2-one
VCC458127:03	Bioorg. Med. Chem.Lett. 2001,11,2867-2870	4-(1H-imidazol-5-yl)pyrimidine
VCC930986:01	Tetrahedron Letters (2008), 49(7), 1269-1273.	quinazoline
VCC996608:06	Current Medicinal Chemistry (2014), 21(17), 1938-1955.	quinoline
VCC398520:05	Preparation of quinoline derivatives as AXL kinase inhibitors WO 2009127417 A1	quinoline
VCC285946:01	Molecular Cancer Therapeutics (2009), 8(12), 3181-3190.	[1,2,4]triazolo[4,3-b]pyridazine
VCC055393:01	2008 Oncogene 27 (34), pp. 4702-4711	quinazoline
VCC131028:02	unpublished	quinoline
VCC098211:02	unpublished	quinoline
VCC999628:01	unpublished	quinoline
VCC376189:01	ACS Medicinal Chemistry Letters (2014), 5(4), 298-303.	quinoline
VCC967844:01	ACS Medicinal Chemistry Letters (2014), 5(4), 298-303.	quinoline
VCC617235:01	unpublished	quinoline
VCC395122:01	ACS Medicinal Chemistry Letters (2014), 5(4), 298-303.	quinoline
VCC883733:01	ACS Medicinal Chemistry Letters (2014), 5(4), 298-303.	quinoline
VCC868449:01	ACS Medicinal Chemistry Letters (2014), 5(4), 298-303.	quinoline
VCC155409:01	ACS Medicinal Chemistry Letters (2014), 5(4), 298-303.	quinoline
VCC048363:02	Clinical Cancer Research 2009, 15, 5040, Cancer Res 2007;67(24):11924-32	quinazoline
VCC957400:02	ACS Medicinal Chemistry Letters (2014), 5(4), 298-303.	quinoline
VCC716837:01	ACS Medicinal Chemistry Letters (2014), 5(4), 298-303.	quinoline
VCC656237:01	unpublished	quinoline
VCC378728:01	ACS Medicinal Chemistry Letters (2014), 5(4), 298-303.	quinoline
VCC461663:01	unpublished	quinoline
VCC325112:01	ACS Medicinal Chemistry Letters (2014), 5(4), 298-303.	quinoline
VCC109756:01	ACS Medicinal Chemistry Letters (2014), 5(4), 298-303.	quinoline
VCC497510:01	ACS Medicinal Chemistry Letters (2014), 5(4), 298-303.	quinoline
VCC444414:01	ACS Medicinal Chemistry Letters (2014), 5(4), 298-303.	quinoline
VCC960450:01	Clin Cancer Res. 2010 Dec 15;16(24):5936-41.	quinoline
VCC450892:17	Cancer Res. 2009 Oct 15;69(20):8009-16.	quinoline
VCC528301:01	ACS Medicinal Chemistry Letters (2014), 5(4), 298-303.	quinoline
VCC778672:01	ACS Medicinal Chemistry Letters (2014), 5(4), 298-303.	quinoline
VCC466812:01	ACS Medicinal Chemistry Letters (2014), 5(4), 298-303.	quinoline
VCC444508:05	ACS Medicinal Chemistry Letters (2014), 5(4), 298-303.	quinoline
VCC590177:01	unpublished	quinoline
VCC221701:01	Preparation of benzopyrrolidone derivatives for use as GRK5 modulators WO 2015022437 A1	indol-2-one
VCC979277:01	Preparation of benzopyrrolidone derivatives for use as GRK5 modulators WO 2015022437 A1	indol-2-one

(table continues on next page)

VCC935482:01	Preparation of benzopyrrolidone derivatives for use as GRK5 modulators	WO	indol-2-one
VCC443915:01	2015022437 A1 Preparation of benzopyrrolidone derivatives for use as GRK5 modulators	WO	indol-2-one
VCC051013:02	2015022437 A1 Preparation of benzopyrrolidone derivatives for use as GRK5 modulators	WO	indol-2-one
VCC228833:01	2015022437 A1 Preparation of benzopyrrolidone derivatives for use as GRK5 modulators	WO	indol-2-one
VCC685240:01	2015022437 A1 Preparation of benzopyrrolidone derivatives for use as GRK5 modulators	WO	indol-2-one
VCC804481:01	2015022437 A1 Preparation of benzopyrrolidone derivatives for use as GRK5 modulators	WO	indol-2-one
VCC365775:01	2015022437 A1 Preparation of benzopyrrolidone derivatives for use as GRK5 modulators	WO	indol-2-one
VCC744093:03	2015022437 A1 Preparation of benzopyrrolidone derivatives for use as GRK5 modulators	WO	indol-2-one
VCC323972:01	WO 2014022116 A2 20140206		4-phenoxy pyridine
VCC353749:01	2015022437 A1 Preparation of benzopyrrolidone derivatives for use as GRK5 modulators	WO	indol-2-one
VCC317779:01	WO 2014022116 A2 20140206		4-phenoxy pyridine
VCC415997:02	WO 2008102870 A1		4-phenoxy pyridine
VCC055876:02	2015022437 A1 Preparation of benzopyrrolidone derivatives for use as GRK5 modulators	WO	4-phenoxy pyridine
VCC429285:02	2015022437 A1 Preparation of benzopyrrolidone derivatives for use as GRK5 modulators	WO	indol-2-one
VCC372550:01	2015022437 A1 Preparation of benzopyrrolidone derivatives for use as GRK5 modulators	WO	indol-2-one
VCC290183:01	2015022437 A1 Preparation of benzopyrrolidone derivatives for use as GRK5 modulators	WO	indol-2-one
VCC031393:01	2015022437 A1 Preparation of benzopyrrolidone derivatives for use as GRK5 modulators	WO	indol-2-one
VCC346202:02	2015022437 A1 Preparation of benzopyrrolidone derivatives for use as GRK5 modulators	WO	indol-2-one
VCC563740:02	2015022437 A1 Preparation of benzopyrrolidone derivatives for use as GRK5 modulators	WO	indol-2-one
VCC180368:02	unpublished		quinoline
VCC239215:01	unpublished		4-phenoxy pyridine
VCC898902:01	unpublished		4-phenoxy pyridine
VCC733981:01	unpublished		4-phenoxy pyridine
VCC656576:02	unpublished		4-phenoxy pyridine
VCC034014:01	unpublished		4-phenoxy pyridine
VCC132459:01	unpublished		4-phenoxy pyridine
VCC692601:01	unpublished		4-phenoxy pyridine
VCC581800:03	unpublished		quinoline
VCC232089:02	2015022437 A1 Preparation of benzopyrrolidone derivatives for use as GRK5 modulators	WO	indol-2-one
VCC650454:03	2015022437 A1 Preparation of benzopyrrolidone derivatives for use as GRK5 modulators	WO	indol-2-one
VCC227946:01	2015022437 A1 Preparation of benzopyrrolidone derivatives for use as GRK5 modulators	WO	indol-2-one

SUPPLEMENTAL TABLE 2 Hit selection phenotypic screen

3

Vichem ID	1 μ M	3.16 μ M	10 μ M
VCC030450:22	EGFR	EGFR	EGFR
VCC031393:01	Top 10% cell count	None	cMet
VCC034014:01	None	None	None
VCC048363:02	EGFR	EGFR	EGFR/cMet
VCC051013:02	Top 10% cell count	Top 10% cell count	None
VCC055393:01	EGFR/cMet	EGFR/cMet	EGFR/cMet
VCC055876:02	None	None	None
VCC075648:03	None	None	None
VCC098211:02	None	None	None
VCC109756:01	cMet	cMet	cMet
VCC131028:02	None	None	None
VCC132459:01	None	None	None
VCC155409:01	None	None	EGFR/cMet
VCC180368:02	None	None	None
VCC221701:01	None	None	None
VCC227946:01	None	None	EGFR/cMet
VCC228833:01	None	None	Top 10% cell count
VCC232089:02	None	None	Top 10% cell count
VCC239215:01	None	None	None
VCC260084:01	None	None	None
VCC285946:01	None	cMet	cMet
VCC290183:01	None	None	None
VCC317779:01	None	None	None
VCC323972:01	None	None	None
VCC325112:01	None	None	None
VCC346202:02	Top 10% cell count	Top 10% cell count	Top 10% cell count
VCC353749:01	None	None	None
VCC365775:01	None	None	cMet
VCC370686:02	None	None	None
VCC372550:01	None	None	None
VCC376189:01	cMet	cMet	EGFR/cMet
VCC378728:01	None	EGFR	None
VCC395122:01	None	None	cMet
VCC398520:05	None	None	None
VCC407451:10	None	EGFR	EGFR
VCC415997:02	cMet	cMet	cMet
VCC429285:02	None	None	EGFR/cMet
VCC443915:01	Top 10% cell count	None	cMet
VCC444414:01	cMet	cMet	cMet
VCC444508:05	None	None	Top 10% cell count
VCC450892:17	cMet	cMet	cMet
VCC458127:03	None	None	EGFR/cMet
VCC461663:01	None	None	None
VCC466812:01	None	None	None
VCC475979:01	None	None	Top 10% cell count
VCC497510:01	cMet	cMet	EGFR/cMet
VCC502987:01	None	None	EGFR/cMet
VCC528301:01	None	None	EGFR/cMet
VCC563740:02	None	Top 10% cell count	None
VCC581800:03	cMet	cMet	cMet
VCC590177:01	None	None	None
VCC613596:10	None	None	None
VCC617235:01	None	None	None
VCC650454:03	Top 10% cell count	Top 10% cell count	Top 10% cell count
VCC656237:01	None	None	None
VCC656576:02	None	None	None
VCC685240:01	None	None	cMet
VCC692601:01	None	None	None
VCC703724:02	None	None	None
VCC716837:01	None	None	Top 10% cell count
VCC733981:01	None	None	None
VCC740005:11	None	EGFR	EGFR
VCC744093:01	None	None	None
VCC744093:03	None	Top 10% cell count	EGFR/cMet
VCC778672:01	None	None	None
VCC804481:01	None	None	Top 10% cell count
VCC833029:24	None	None	EGFR
VCC868449:01	None	None	EGFR/cMet
VCC883733:01	None	None	None
VCC884444:01	None	None	Top 10% cell count
VCC898902:01	None	None	None
VCC912492:07	None	None	None
VCC930986:01	None	None	None
VCC935482:01	None	None	None
VCC957400:02	None	None	Top 10% cell count
VCC960450:01	cMet	cMet	cMet
VCC967844:01	None	None	None
VCC979277:01	None	None	EGFR/cMet
VCC996608:06	None	None	Top 10% cell count
VCC999628:01	None	None	None

SUPPLEMENTAL TABLE 3 Enzyme activity measurement (% inhibition)

Vicheck Compound-ID	EGFR Inh (%) 10µM	EGFR Inh (%) 1µM	EGFR Inh (%) 0.1µM	c-Met Inh (%) 10µM	c-Met Inh (%) 1µM	c-Met Inh (%) 0.1µM
VCC030450.22	101	99	97	4	2	0
VCC031393.01	11	2		16	0	
VCC034014.01	18	3		2	5	
VCC048363.02	101	100	97	1	-2	-1
VCC051013.02	16	0		41	6	
VCC055393.01	99	100	100	3	3	-4
VCC055876.02	-2	-9		22	-1	
VCC075648.03	66	13		41	6	
VCC098211.02	47	7		26	1	
VCC109756.01	43	7	2	93	61	7
VCC131028.02	30	-2		12	-4	
VCC132459.01	6	0		7	0	
VCC155409.01	76	34	10	25	2	-2
VCC180368.02	92	83		35	7	
VCC221701.01	22	4		22	1	
VCC227946.01	8					
VCC228833.01	16	1	0	4	0	-2
VCC232089.02	69					
VCC239215.01	17	4		16	4	
VCC260084.01	8	3		2	1	
VCC285946.01	32	0	9	84	49	8
VCC290183.01	16	4		27	3	
VCC317779.01	3	-1		82	18	
VCC323972.01	-2	-8		19	4	
VCC325112.01	59	16		44	5	
VCC346202.02	3	1		25	2	
VCC353749.01	5	1		26	1	
VCC365775.01	13	4		36	5	
VCC370686.02	-4	-8		2	-3	
VCC372550.01	-12	-9		2	-2	
VCC376189.01	12	2	-2	83	56	9
VCC378728.01	85	41	8	72	16	0
VCC395122.01	93	69	10	52	2	-3
VCC398520.05	98	55		87	30	
VCC407451.10	93	92	73	7	0	-4
VCC415997.02	-11	-11	-7	95	77	14
VCC429285.02	3	2	0	6	-2	2
VCC443915.01	23	3		27	1	
VCC444414.01	7	-4	-6	90	47	3
VCC444508.05	100	93		41	8	
VCC450892.17	32	10	5	85	39	4
VCC458127.03	95	62		3	0	
VCC461663.01	88	43		51	7	
VCC466812.01	102	84		67	13	
VCC475979.01	20	10		14	1	
VCC497510.01	20	10	2	90	54	9
VCC502987.01	19	9	1	4	1	0
VCC528301.01	94	82	29	37	7	1
VCC563740.02	15	10		25	5	
VCC581800.03	50			100		
VCC590177.01	94	67		56	3	
VCC613596.10	91	55		0	-1	
VCC617235.01	80	25		37	4	
VCC650454.03	39					
VCC656237.01	81	43		43	8	
VCC656576.02	-2	-7	-13	0	-4	-4
VCC685240.01	10	-6		4	1	
VCC692601.01	5	4		20	7	
VCC703724.02	9	9		7	4	
VCC716837.01	48	10	1	41	6	0
VCC733981.01	9	5		8	1	
VCC740005.11	105	102	93	11	1	3
VCC744093.03	77	25	3	27	-1	-1
VCC778672.01	101	85		56	9	
VCC804481.01	3	5		12	0	
VCC833029.24	97	90	37	-3	0	0
VCC868449.01	95	89	37	56	14	3
VCC883733.01	81	40		42	12	
VCC884444.01	2	-9		3	-2	
VCC898902.01	7	4		5	0	
VCC912492.07	87	47		2	-1	
VCC930986.01	92	49		0	-2	
VCC935482.01	-3	-2		-1	-3	
VCC957400.02	83	37		25	0	
VCC960450.01	-11	-7	-10	87	50	11
VCC967844.01	87	33		39	6	
VCC979727.01	12	5		17	3	
VCC996608.06	96	58		81	26	
VCC999628.01	26	0		14	1	

chapter 4

High-throughput phenotypic screening of kinase inhibitors to identify drug targets for polycystic kidney disease

Tijmen H. Booij¹, Hester Bange¹, Wouter N. Leonhard²,
Kuan Yan³, Michiel Fokkelman¹, Steven J. Kunnen²,
Johannes G. Dauwerse², Yu Qin¹, Bob van de Water¹,
Gerard J.P. van Westen⁴, Dorien J.M. Peters², Leo S. Price^{1,3}

- 1 Division of Toxicology, Leiden Academic Centre for Drug Research, Leiden, The Netherlands
- 2 Human Genetics, Leiden University Medical Center, Leiden, The Netherlands
- 3 Ocello B.V., Leiden, The Netherlands
- 4 Division of Medicinal Chemistry, Leiden Academic Centre for Drug Research, Leiden, The Netherlands

Based on: Booij TH, Bange H, Leonhard WN, Yan K, Fokkelman M, Kunnen SJ, Dauwerse J, Qin Y, van de Water B, van Westen GJP, Peters DJM, Price LS: High-throughput phenotypic screening of kinase inhibitors to identify drug targets for polycystic kidney disease. *SLAS Discov*, 2017

Abstract

Polycystic kidney disease (PKD) is a prevalent disorder characterized by renal cysts that lead to kidney failure. Various signaling pathways have been targeted to stop disease progression, but most interventions still focus on alleviating PKD associated symptoms. The mechanistic complexity of the disease, as well as the lack of functional *in vitro* assays for compound testing, has made drug discovery for PKD challenging.

To identify modulators of polycystic kidney disease, *Pkd1*^{-/-} kidney tubule epithelial cells were applied to a scalable and automated 3D cyst culture model for compound screening, followed by phenotypic profiling to determine compound efficacy. We used this screening platform to screen a library of 273 kinase inhibitors to probe various signaling pathways involved in cyst growth. We show that inhibition of several targets, including aurora kinase, CDK, Chk, IGF-1R, Syk, mTOR, but, surprisingly, not PI3K, prevented forskolin-induced cyst swelling. Additionally, we show that multiparametric phenotypic classification discriminated potentially undesirable (i.e. cytotoxic) compounds from molecules inducing the desired phenotypic change, greatly facilitating hit selection and validation.

Our findings show that a pathophysiological relevant 3D cyst-culture model of PKD coupled to phenotypic profiling can be used to identify potentially therapeutic compounds and predict and validate molecular targets for PKD.

Introduction

Polycystic kidney disease (PKD) is an inherited genetic disorder that is characterized by the formation of renal cysts that block normal tubular function and thereby cause a progressive decline in kidney function with age, typically leading to end-stage renal disease (ESRD) by the 6th decade of life. This prevalent disorder occurs in approximately 1:2500 people¹ and, in addition to its detrimental effects on kidney function, also affects other organs such as the liver.²

The most prevalent form of PKD, autosomal dominant polycystic kidney disease (ADPKD) is in most cases caused by mutations in the *PKD1* gene or, less commonly, in *PKD2*. *PKD1* encodes polycystin-1, which is a receptor-like protein thought to be a receptor for various WNT ligands³. *PKD2* encodes polycystin-2, which is a known ion-channel with some selectivity for calcium ions. Together polycystin-1 and polycystin-2 can function as a complex which is thought to be involved in mechanotransduction of urine flow⁴ due to its localization in the cells' primary cilium.⁵ The polycystin proteins also localize to other areas of the cell, including the plasma membrane^{4,6} and the endoplasmic reticulum (ER).⁴

Loss-of-function mutations in either *PKD1* or *PKD2* or reduced levels of functional protein are causative for cyst formation,⁷ but the mechanisms behind this process are still poorly understood. Dysfunction of the polycystin proteins leads to a reduction in intracellular calcium levels and a consequent rise in intracellular cyclic adenosine monophosphate (cAMP) levels due to the activation of calcium-inhibitable adenylyl cyclase 6 (AC6) and reduced activity of the calcium-dependent cAMP-dependent phosphodiesterases (PDE1/4c)⁸. This increase in cAMP, in turn, leads to alterations in cell proliferation, apoptosis, cell-cell and cell-matrix interactions and cell polarity.⁸ These events are known contributors to cyst initiation and cyst growth progression.

The mechanistic complexity of this disease has made it particularly difficult to develop effective medicines. As of yet, the only EMA-approved therapy in Europe for ADPKD is Jinarc (Tolvaptan), which is a vasopressin-2 receptor antagonist, consequently requiring the patients to consume large quantities of water due to increased urine production.⁹

In addition to the complexity of the disease, the lack of appropriate *in vitro* assays to determine drug efficacy is a likely factor underlying the limited choice of therapies available. Traditionally, cells cultured as monolayers have been used to determine drug efficacy and toxicity, but such *in vitro* systems cannot be used to adequately recapitulate the pathophysiology of ADPKD, since cysts cannot form in a two-dimensional environment. In contrast, three-dimensional (3D) culture techniques have been developed over the past decade to address these issues and to bridge the gap between 2D monolayers and animal models. Traditionally these techniques have been generally associated with high costs and low reproducibility and scalability, but due to their physiological relevance 3D phenotypic screening techniques have become a fundamental research tool in many fields,¹⁰ including cancer research.¹¹

In order to identify effective molecules and therapeutic targets in a more physiologically relevant model, we have developed a high-content and high-throughput screening platform that uses 3D-cultured cysts and used this to screen a kinase inhibitor library with known molecular targets. This allowed us to relate compound efficacy to molecular targets potentially involved in cyst growth.

MATERIALS AND METHODS

Generation and Cloning of Cell Lines

To generate cells with reduced *Pkd1* gene expression, wild-type mouse inner medullary collecting duct (mIMCD3, ATCC® CRL-2123™) cells were transduced with a lentivirus containing a short-hairpin against *Pkd1*. Lentiviral constructs expressing shRNAs targeting *Pkd1* (TRCN0000072084, o85, o86 and o87) and a non-targeting control construct (SHC002) were obtained from the Sigma MISSION shRNA library (Sigma-Aldrich, Zwijndrecht, Netherlands). Production of lentiviruses by transfection into 293T cells has been described earlier.¹² Cells were selected using puromycin. Reduced *Pkd1* expression, approximately 60%, was confirmed by qPCR (supplemental figure 1A, mIMCD3 sh*Pkd1*) and cell line transduced with construct TRCN0000072084 was selected for our studies. This cell line was used for the majority of the experiments described here. In addition, *Pkd1* knockout mIMCD3 cell lines were generated (supplemental figure 2) using the dimeric CRISPR RNA-guided FokI nucleases (RFN) method¹³ in mIMCD3 cells. In short, the RFNs for *Pkd1* exon 15 were selected using ZiFiT (<http://zifit.partners.org/ZiFiT/Disclaimer.aspx>) and cloned into vector pSQT1313neo as described previously (http://zifit.partners.org/ZiFiT/Program_use.aspx#_CRISPR_RFNs) (supplemental table 1). In the pSQT1313neo construct we replaced the ampicillin gene of pSQT1313, by the kanamycin/neomycin resistance cassette of pEGFP-N1 (Clontech) in this construct, to facilitate G418 selection of clones that have taken up pSQT1313neoRFN and enrich for clones that carry a *Pkd1* exon15 deletion (pSQT1313 obtained from Addgene). One clone with the correct sequence was selected and co-transfected with pSQT1601 (Addgene) the plasmid expressing the Csy4 and dCas9-FokI fusion proteins. mIMCD3 cells were grown to 80% confluency in a 9cm petri dish and transfected with 2µg Pkd1ex15RFN and 8µg pSQT1601 DNA using Lipofectamin 2000 (Invitrogen). G418 (0.5mg/ml) selection was applied after 48 hours. After 7 days, cells were re-plated at a density of ~50 cells per 9cm plate. Single colonies were picked and analyzed using PCR with primers flanking the RFN target sites (supplemental table 2). PCR products were digested with restriction-endonuclease *PvuII*, which cuts between the Pkd1ex15RFN target sites. From clones that showed undigested PCR products, demonstrating a deletion of the *PvuII* restriction site on both alleles, the PCR products were subcloned using the TOPO® cloning kit (Invitrogen). Fifteen subclones were analyzed by Sanger sequencing. The sequences for clone 5E4 revealed a 25bp out of frame deletion on one allele and an 295bp out of frame deletion for the other allele. These cells will be denoted as mIMRFNPKD 5E4 throughout this publication.

Maintenance of Cell Lines

All mIMCD3 cell lines were cultured in 175-cm² culture flasks at 37°C in an environment of 5% CO₂ in DMEM/F12 (Ham's) culture medium (D8062, Sigma Aldrich, Zwijndrecht, Netherlands), supplemented with 10% fetal bovine serum (FBS, Gibco Fisher Scientific, Landsmeer, Netherlands), Glutamax and penicillin/streptomycin. Before maximal cell density was reached, cells were washed with 1x PBS (Sigma Aldrich, Zwijndrecht, Netherlands) and trypsinized with 1x Trypsin (Gibco Fisher Scientific, Landsmeer, Netherlands). Medium was subsequently added and cells were pelleted by centrifugation for 5 minutes at 1500rpm. The cell pellet was resuspended in FBS with 10% DMSO (Biosolve B.V., Valkenswaard, Netherlands) and frozen in aliquots to -150°C.

3D Cyst Assay

For the primary screen of the SelleckChem library (Munich, Germany), cryopreserved mIMCD3 cells were quick-thawed using a 37°C water bath and immediately added to Cyst-Gel (OcellO, Leiden, The Netherlands). For all subsequent experiments, including the validation screen, we modified this procedure to allow cryopreserved cells to recover in 2D culture for 72 hours prior to use in the 3D assay, which resulted in improved cyst homogeneity and overall assay performance. For all subsequent experiments therefore, cryopreserved mIMCD3 cells were quick-thawed in a 37°C water bath and added to 175cm² culture flasks and cultured for 72 hours at 37°C in an environment of 5% CO₂ prior to initiation of the cyst assay. After 24 hours, medium was refreshed and after 72 hours the monolayer was washed with 1x PBS (Sigma Aldrich, Zwijndrecht, Netherlands) and cells were trypsinized using 1x Trypsin (Gibco Fisher Scientific, Landsmeer, Netherlands) and mixed with Cyst-Gel (OcellO, Leiden, The Netherlands). 14.5mL of cell-gel mix was pipetted to 384-well plates (Greiner mClear, Greiner Bio-One B.V., Alphen aan den Rijn, Netherlands) using a CyBi Selma 96/60 robotic liquid dispenser (Analytik Jena AG, Jena, Germany). Gel-cell mix was plated at a final cell density of 2175 cells per well. After gel polymerization at 37°C for 30 minutes, 33.5mL medium was added to each well. Cells were grown in gel for 72 hours (in order to initiate lumen formation prior to compound exposures), after which the cells were co-exposed with forskolin (*Coleus Forskohlii*, Calbiochem, Millipore BV, Amsterdam, Netherlands) and molecules to be tested alongside positive controls using the CyBi Selma 96/60 or a BioMek FXP (Beckman Coulter B.V., Woerden, Netherlands). After 72 hours, cultures were fixed with 4% formaldehyde (Sigma Aldrich, Zwijndrecht, Netherlands) and simultaneously permeabilized with 0.2% Triton-X100 (Sigma Aldrich, Zwijndrecht, Netherlands) and stained with 0.25mM rhodamine-phalloidin (Sigma Aldrich, Zwijndrecht, Netherlands) and 0.1% Hoechst 33258 (Sigma Aldrich, Zwijndrecht, Netherlands) in 1x PBS for 12 hours at 4°C, protected from light. After fixation and staining, plates were washed in 1x PBS for 12-24 hours, after which plates were sealed with a Greiner SilverSeal (Greiner Bio-One B.V., Alphen aan den Rijn, Netherlands) and stored at 4°C prior to imaging (screening procedure illustrated in figure 1).

Compounds

A kinase inhibitor library containing 273 compounds (L1200) was obtained from

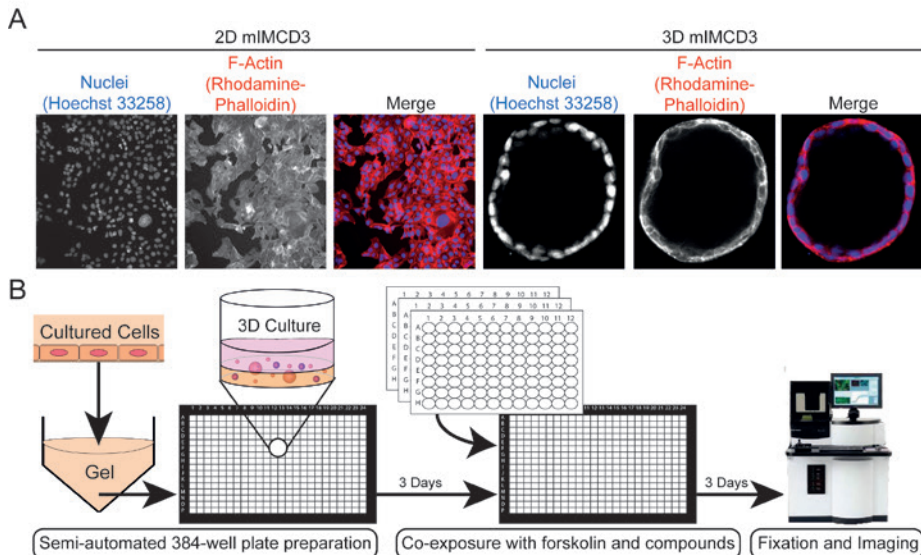


FIGURE 1 3D high-content screening platform that uses mIMCD3 cysts grown in hydrogels as an *in vitro* model for polycystic kidney disease. **A**) mIMCD3 *shPkd1* cells grown on culture plastic cannot recapitulate cystic structures (left panel); in contrast, mIMCD3 *shPkd1* cells can form cysts when grown in a 3D microenvironment (right panel). **B**) 3D high-content screening platform that uses mIMCD3 *shPkd1* or mIMRFPKD 5E4 cysts to determine compound efficacy.

SelleckChem (Munich, Germany), with compounds pre-dissolved to 10mM in DMSO. Analytical grade DMSO was obtained from Biosolve B.V. (Valkenswaard, Netherlands). Rapamycin, roscovitine, sorafenib tosylate, torin 1 and buparlisib (NVP-BKM-120) were purchased from SelleckChem (Munich, Germany) through distributor Bio-Connect B.V. (Huissen, Netherlands). Metformin HCl was obtained from Sigma Aldrich (Zwijndrecht, Netherlands).

Fluorescence Microscopy

Hoechst 33258 and rhodamine-phalloidin – stained cysts in 384-well plates were imaged using a BD Pathway 855 (BD Biosciences, Breda, Netherlands) automated inverted wide-field microscope using a 4x Olympus objective. Images were obtained using BD Attovision software (BD Biosciences, Breda, Netherlands) accompanying the microscope, which was used to image focal planes throughout the gel at intervals of 50µm. The gel was imaged through its entire depth (z-axis), requiring around 25 images per well; each image captured approximately 75% of the well area (supplemental figure 3A). High-resolution confocal images were made using a 20x objective on a Nikon Ti Eclipse confocal laser microscope (lasers 561 and 408nm). Confocal images were exported using NIS Elements Viewer (Nikon Instruments Europe B.V., Amsterdam, Netherlands).

Image – and Data Analysis

Images obtained with the BD Pathway 855 imager were processed through Ominer software (OcellO B.V., Leiden, Netherlands) integrated in KNIME Analytics Platform (Konstanz, Germany, <http://www.knime.org/>). This software allowed the quantification of images derived from both rhodamine-phalloidin (F-actin) and Hoechst 33258 (nuclei) image channels. This procedure is schematically represented in supplemental figure 3B. For the rhodamine-phalloidin image channel, a monochrome mask was generated for all of the individual images taken along the z-axis of the gel to define regions of interest (ROIs). This approach allowed us to quantify individual cysts – even those vertically overlapping that would otherwise have been detected as one object. These monochrome masks were used to derive shape- and size- related phenotypic descriptors of each cyst. Cyst size was derived from these monochrome masks as an area measurement of the number of pixels occupied per cyst (with approximately 100-150 cysts in each well, supplemental figure 4). The actin-dense region at the boundary of all cysts was quantified separately, so that the thickness- and shape of the cyst wall could be related to the total cyst size. Finally, to derive staining intensity-related quantifications, a maximum intensity projection of the original image stack was generated. For the Hoechst 33258 image channel, the spatial resolution upon imaging with the BD Pathway 855 was not high enough to accurately measure the shape of individual nuclei. Therefore, nuclei image stacks were immediately processed to a maximum intensity projection and processed as described earlier.¹⁴⁻¹⁵ All phenotypic descriptors were subsequently z-score normalized to plate medians and thereafter z-scored to unstimulated control median or scaled to percent inhibition (unstimulated control median to 100%, forskolin-stimulated control median to 0%) using KNIME. For multiparametric phenotypic analysis, phenotypic descriptors were ranked based on Z-prime values >1.0 between stimulated (2.5µM forskolin) and 10nM rapamycin-treated, forskolin-exposed control conditions for all cysts. Supplemental table 3 provides an overview of included phenotypic features. Selected phenotypic features were used for principal components analysis to condense phenotypic information to three principal components (PCo, PC1 and PC2), together comprising 84% of the variation in the dataset. Principal components were exported from KNIME and visualized as a 3D scatterplot generated using the Scatterplot3D package (<https://CRAN.R-project.org/package=scatterplot3d>) for Rstudio 0.99.878 (<https://www.rstudio.com/products/rstudio2>) with R3.2.3 (<https://www.r-project.org/>). Other charts were made using the ggplot2 (<http://ggplot2.org>) package for R-Studio 0.99.878 with R3.2.3 or with Graphpad Prism 7 (Graphpad Software, La Jolla, California, USA).

Assessment of Synergy

The Bliss-independence model¹⁶ was used to assess potential synergistic effects. This model assumes that the effects of a certain drug are independent of those of the other drug. To apply this method, inhibition of cyst growth was scaled between 0 (no inhibition) and 1 (maximum effect). The model is given in the formula $E = E_A + E_B - E_A E_B$, where E is the predicted combined compound response based on the individual effect

of two compounds (E_A -torin 1 and E_B -buparlisib). This method compares the observed combination response with the predicted combined compound response E into a combination index ($CI=(E_A+E_B-E_{AB})/E_{AB}$). The combination is declared synergistic if the observed effect is larger than the predicted combined response, or antagonistic if the observed response is smaller than the predicted response.

Statistical Calculations

Unless otherwise stated in figure legends, figures represent mean and standard deviations (SD). All statistical calculations were performed in Graphpad Prism 7. Z'-factor calculations were performed after correction for number of replicates to reflect assay robustness:¹⁷

$$Z'factor = \frac{\left(AVG_{max} - \frac{3SD_{max}}{\sqrt{n}} \right) - \left(AVG_{min} + \frac{3SD_{min}}{\sqrt{n}} \right)}{AVG_{max} - AVG_{min}} \quad \text{(EQUATION 1)}^{17}$$

In equation 1, AVG is mean and SD standard deviation of stimulated (max) or unstimulated (min) control groups, and n is the number of technical replicates.

RESULTS

mIMCD3 cells form cysts in 3D hydrogels and addition of forskolin induced cyst swelling

To identify modulators of cyst growth, we developed an automation-compatible 3D cyst growth assay, in which cyst swelling is driven by forskolin over a period of 72 hours. mIMCD3 cells with a short hairpin-mediated knockdown of *Pkd1* were cultured in extracellular matrix-based hydrogels in 384-well plates and formed cystic structures by day 3, whereas cysts could not form in 2D monolayer cultures (figure 1A). Cysts were exposed to solvent (0.2% DMSO, unstimulated) in culture medium or 2.5mM forskolin (stimulated) and responded to exposure to forskolin by increased cyst swelling (figure 1B and 2A). Cyst size was measured by quantifying object area from all individual cysts. Mean cyst area and standard deviation of 8 replicates is shown as a function of forskolin concentration and presented as z-score relative to unstimulated control median (figure 2B). It should be noted that this forskolin-driven cyst growth is an intrinsic characteristic of mIMCD3 cells, and is not dependent on the presence of polycystin-1 (supplemental figure 1B-C). Co-exposure with forskolin and rapamycin (inhibitor of mammalian target of rapamycin, mTOR), roscovitine (inhibitor of cyclin-dependent kinases; Cdc2, CDK2, CDK5¹⁸), NVP-BEZ-235 (a dual inhibitor of mTOR/PI3K¹⁹ that potentially also inhibits ATM and ATR at high concentrations²⁰) or sorafenib (sorafenib tosylate, a multikinase inhibitor targeting B-Raf and Raf-1²¹) prevented the increase of cyst swelling induced by forskolin (figure 2C and 2D). The increase in cyst growth by forskolin and consequent blockade of this increase by control compounds was also observed in *Pkd1* knock-out cells (mIMRFNPKD 5E4), as illustrated by three independent experiments presented in supplemental figure 5.

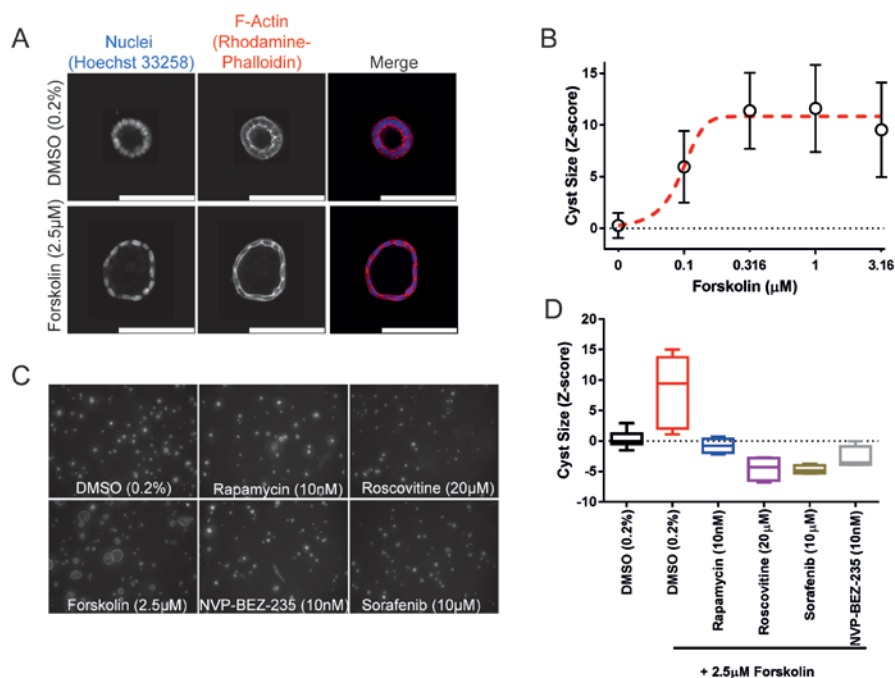


FIGURE 2 mIMCD3 *shPkd1* cyst growth can be enhanced with forskolin and this increase can be prevented with positive control compounds rapamycin, sorafenib, roscovitine and NVP-BEZ-235. **A)** high-resolution images obtained from an unexposed (DMSO 0.2%, top panel) and a forskolin-treated (bottom panel) cyst. **B)** Using Ominer analysis tools, cyst size could be expressed as a function of forskolin concentration. Data points represent means \pm SD of 8 replicate wells (technical replicates). **C)** Representative images of control compounds after co-exposure with forskolin, including unstimulated (DMSO 0.2%) control. **D)** Quantification of average cyst size from C. Whiskers represent min to max. Rapamycin, roscovitine, sorafenib and NVP-BEZ-235 tested in quadruplicate (technical replicates), unstimulated (n=16 replicate wells) and stimulated (n=8 replicate wells). These experiments have been performed independently more than three times (supplemental figures 1B-C and 5A-C also show the performance of control molecules in biological replicates).

Identification of modulators of cyst growth

Having established that inhibitors targeting pathways known to be important in cyst growth can also prevent cyst swelling in our model, we screened a library of 273 kinase inhibitors (SelleckChem-L1200) with described molecular targets. Therefore, in addition to potentially providing therapeutically interesting molecules, the selected hits could also be used to relate compound efficacy to the cellular signaling pathways that may be involved. mIMCD3 *shPkd1* cells were cultured in 3D hydrogels in 384-well plates in which they formed cysts over a period of 72 hours. Subsequently, we co-exposed cysts with 2.5mM forskolin and kinase inhibitors from the SelleckChem compound

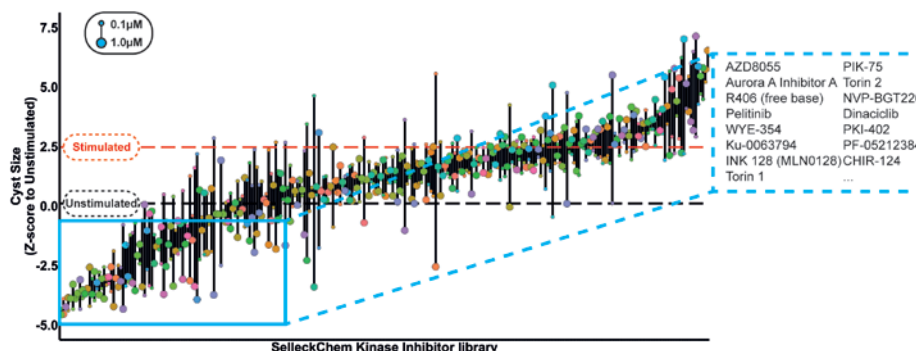


FIGURE 3 SelleckChem kinase inhibitor library screen. Kinase inhibitors were screened in quadruplicate (technical replicates) at 1 μ M and 0.1 μ M, in the presence of 2.5 μ M forskolin to stimulate cyst growth (procedure shown in figure 1). Data were z-score normalized to the plate median and subsequently to the unstimulated control median (unstimulated control, black striped line). Cyst growth induction by forskolin is presented by a red striped line. Compound effects are represented by means of quadruplicate wells of two tested concentrations. Top 15 hit molecules presented in right cutout. The replicate-adjusted Z'-factor for this primary screen reached -0.93 between stimulated- and unstimulated control conditions.

library in quadruplicate wells at 0.1 and 1mM for 72 hours, as illustrated in figure 1B. Cysts were then fixed and stained and imaged using the BD pathway 855 imager. Image data was processed and quantified with Ominer software and cyst size was z-score normalized to the unstimulated control median. Screening results are presented in figure 3. Forskolin induced cyst swelling and various kinase inhibitors inhibited this effect at 0.1 and/or 1mM (figure 3). In this initial screen, we calculated an average Z'-factor of -0.93 between unstimulated and stimulated controls. This weak Z'-factor appeared to be largely due to high variation between technical replicates within the stimulated control group, associated with a variable proportion of poorly expanding cysts in each well. We attributed this to sub-optimal cell health as a result of the use of cryopreserved cells in the assay, since introducing a 3-day recovery period after thawing of cryopreserved cells, improved the Z'-factor to +0.36 in the validation screen. In the primary screen, active molecules were selected based on a reduction of cyst size relative to the stimulated control (red striped line) to a z-score for cyst size ≤ 0 (equal to or smaller than unstimulated control median) at either 0.1 or 1 μ M. Inhibitors selected using this threshold included many inhibitors targeting mTOR, Aurora A Kinase, CDK, IGF-1R, and dual mTOR/PI3K inhibitors. For identified active molecules we obtained their respective molecular target and we validated the efficacy only of compounds with the highest affinity for these targets (shown in supplemental table 4), at six concentrations, decreasing from 1 or 0.1mM (depending on the efficacy of the molecule in the primary screen) (figure 4A). For visualization of compound effects as a function of dose, mean cyst size of quadruplicate wells was scaled to percent inhibition of forskolin-induced cyst swell-

ing and this inhibition was presented graphically as a heat map from yellow (no inhibition) to dark blue (potent inhibition) (figure 4A). Our validation screen showed that the activity of most of the active compounds identified in the primary compound screen could be confirmed. Statistical significance was calculated using one-way ANOVA and correlated with statistical significance of the primary screen. Statistical significance was found to overlap for 58% of selected molecules (supplemental table 5). Dose-response curves for several of the compounds presented in figure 4A have been included in supplemental figure 6A-H to illustrate variation in efficacy between technical replicates. Multiparametric phenotypic analysis using principal components revealed that different compounds with different molecular targets induced novel phenotypes (figure 4B). Forskolin (empty circles) induced a phenotypic change characterized by an increase in cyst swelling, which, after principal components analysis revealed a shift in PCo and PC2. Co-exposure with either rapamycin (green) or metformin (blue) induced a phenotype indistinguishable from unstimulated controls (black). In contrast, exposure of forskolin-stimulated cysts to CDK inhibitor roscovitine (red) or B-Raf/Raf-1 inhibitor sorafenib (orange) caused this phenotypic change to overshoot, causing a novel phenotype (figures 4B, 4D). We further observed that, while roscovitine and sorafenib inhibited cyst growth similarly to rapamycin and metformin, they also appeared to have an effect on nuclei counts (supplemental figure 7), which potentially is an indication of growth inhibition or cytotoxicity related to the concentration of these inhibitors and/or due to their mechanism of action. Using this same projection model that identified the novel phenotypes of roscovitine and sorafenib, we plotted compounds targeting different kinases in the same chart (figure 4C). Indeed, other CDK inhibitors (green) such as dinaciclib were found to cluster in the same region of the PCA plot with roscovitine (figure 4B and 4C compared). In addition to the phenotype induced by dinaciclib, DNA-PK inhibitor PIK-75 (red) also induced a novel phenotype characterized by low cell count (figure 4C and 4D). Although this inhibitor would classify as a potent inhibitor of cyst growth based on cyst size (figure 4A), this molecule induced a phenotypic change that was very different to that of the unstimulated control (black). The novel phenotypes induced by dinaciclib and PIK-75 may be potentially undesirable and appear to be characterized by lower number of viable cells as shown in figure 4D.

mTOR inhibitors, but not PI3K inhibitors, block forskolin-induced cyst swelling

Based on our kinase inhibitor screen described in figure 3, we discovered that almost all mTOR inhibitors showed inhibitory activity on cyst growth, but most PI3K inhibitors showed at most only mild inhibition, which was unexpected in view of the expected role of PI3K in PKD²²⁻²⁴. This was confirmed using PCA based visualization and showed that mTOR inhibitors blocked the forskolin-induced phenotype, whereas PI3K inhibitors had no effect (figure 5A). We therefore re-tested a collection of 40 inhibitors that were annotated as mTOR and PI3K inhibitors from the SelleckChem library, and also tested a panel of 7 dual PI3K/mTOR inhibitors at concentrations up to 0.1 μ M (figure 5B-D). Cyst size was measured and scaled to percent inhibition, denoted by a color scale from yellow (inactive) to dark blue (potent inhibition). Most mTOR inhibitors, and most notably torin 1 and -2, showed potent inhibitory activity (figure 5B), whereas most PI3K

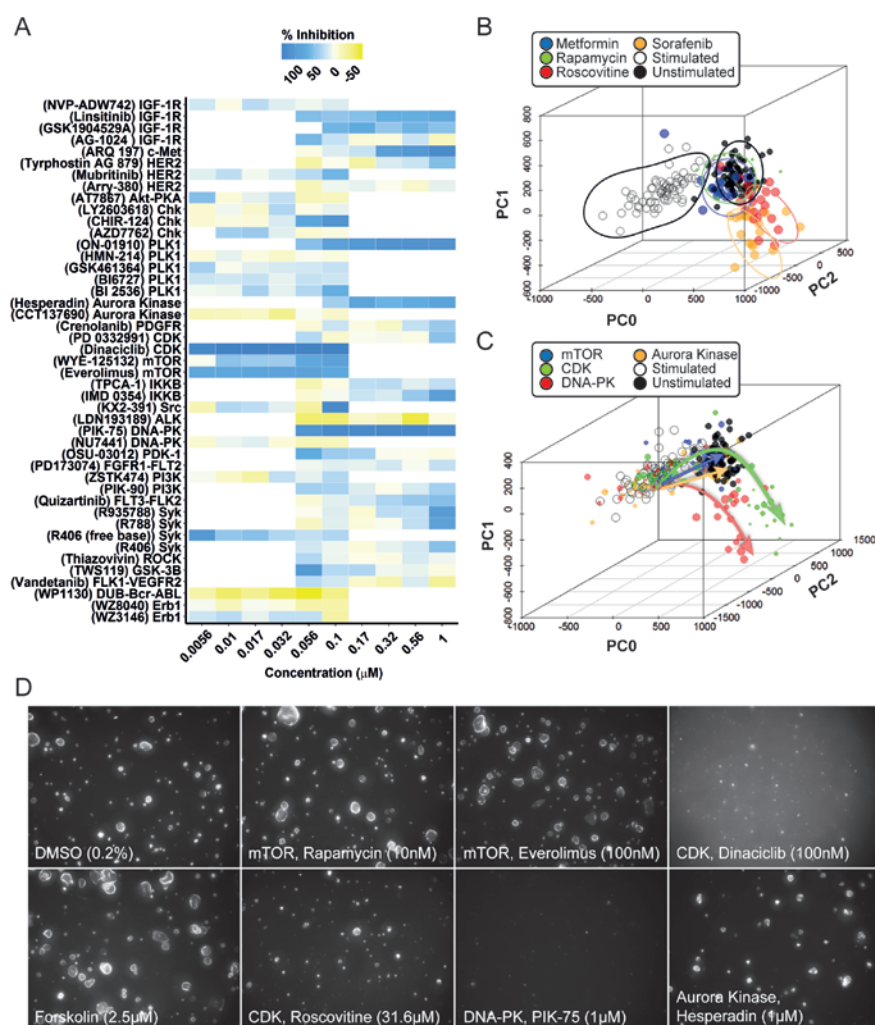


FIGURE 4 Phenotypic analysis discriminates potentially undesirable compound effects. **A**) Validation of compounds from each target identified in figure 3. Mean percent inhibition (technical replicates representing triplicate wells) of cyst growth is depicted by a color scale from yellow (no inhibition of forskolin-induced cyst growth) to blue (complete inhibition of forskolin-induced cyst growth). Standard deviations are not included in this plot; for reference purposes several dose curves are included in supplemental figure 6. A mean Z^2 -factor of +0.36 between stimulated- and unstimulated control conditions was calculated over 6 plates. **B, C**) Multiparametric (PCA) analysis (PCA plot summarizes 84% of variation in the entire dataset) identifies different compound clusters as shown by the contour plots. Forskolin-stimulated controls (large cysts) represented as empty circles, unstimulated controls (small cysts) represented as black dots. Data points represent single wells. **C**) PCA plot summarizing 84% of variation in the entire dataset. Trajectories of different compound (legend continues on next page)

types are indicated by arrows (mTOR inhibitors – blue, CDK inhibitors – green, DNA-PK inhibitors – red, aurora kinase inhibitors – orange). Data points represent single wells, point size correlates with molecule concentration (legend omitted for presentation purposes). **D)** Representative images from conditions shown as in A-C. Novel phenotypes identified in figure B and C are illustrated by images of 100nM dinaciclib and 1 μ M PIK-75.

inhibitors had low efficacy (figure 5C). We noted that the very few PI3K inhibitors that were effective at inhibiting cyst growth, may also have activity against mTOR (e.g. NVP-BGT226²⁵). Most of the dual PI3K/mTOR inhibitors tested, showed potent inhibition of forskolin-induced cyst growth (figure 5D). We therefore considered whether PI3K, which is aberrantly active in PKD,²²⁻²³ was not involved in cyst growth in our model, or whether the PI3K inhibition could exert synergistic effects together with mTOR inhibitors. To test this, we selected one mTOR inhibitor, torin 1²⁶ that displayed potent activity in our previous screens and has a 1000-fold selectivity for mTOR over PI3K²⁷ (supplemental table 4). Similarly, we selected a PI3K inhibitor, NVP-BKM120 (buparlisib), with reduced potency against mTOR²⁸ (supplemental table 4). Figure 5E shows that while both molecules show inhibition of cyst growth at high concentrations, torin 1 is a potent inhibitor at its IC₅₀ concentration, whereas buparlisib shows little activity, except at higher concentrations when it may also inhibit mTOR signaling.²⁹ Furthermore, when combined, these mTOR and PI3K inhibitors did not cause synergistic potentiation of cyst growth inhibition, as illustrated in figure 5E and supplemental figure 8, upon comparison with the predicted combined response. Based on the performed separate experiments with buparlisib and torin 1, an expected additive effect could be derived (supplemental figure 8B). Subsequently, the observed combined effect under combined exposure (e.g. 0.00316 μ M torin 1 and 0.1 μ M buparlisib) was less than this predicted effect (supplemental figure 8C). This discrepancy is reflected by a combination index (CI)>1 (supplemental figure 8D). Together, these findings indicate that mTOR, but not PI3K plays a role in driving forskolin-induced cyst swelling in this model.

Discussion

To evaluate potential targets and therapeutic modulators of polycystic kidney disease, we developed a fully-scalable high-content screening platform that uses 3D cultured cysts to quantify the effects of compounds on cyst growth. We applied this model to screen a kinase inhibitor library (SelleckChem L1200) with pre-described targets. While many small molecule kinase inhibitors often do not have one single molecular target, but rather target a range of kinases, we used this information to investigate the importance of several signaling cascades in our assay. For example, we identified many mTOR inhibitors amongst the most active compounds. The importance of mTOR in PKD has been extensively described,³⁰⁻³¹ so identification of mTOR inhibitors in our selected hits was therefore unsurprising, but confirmative of the validity of the screen. Additionally, we also identified several molecules that targeted CDK, Chk and Aurora A kinase. Since these molecules all target kinases that are important in cell cycle

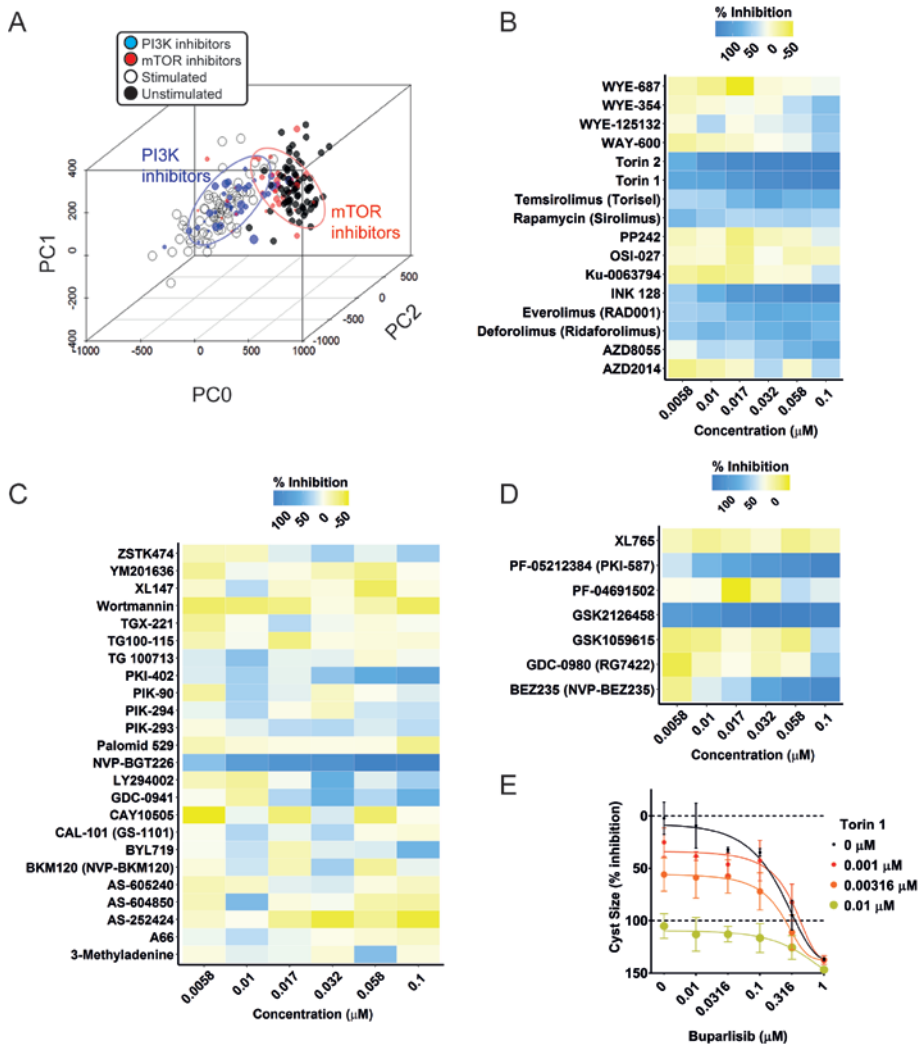


FIGURE 5 mTOR inhibitors but not PI3K inhibitors prevent forskolin-induced cyst swelling. **A)** PCA plot comprising 84% of variation in the entire dataset. mTOR inhibitors (red circles) cluster together with unstimulated control (black dots) whereas PI3K inhibitors (blue circles) cluster with the stimulated condition (empty circles). Data points represent single wells, inhibitor point size correlates with molecule concentration (legend omitted for presentation purposes). **B)** Validation of mTOR inhibitors at concentrations 6nM to 100nM. Cyst growth inhibition displayed by a color gradient ranging from yellow (no inhibition) to blue (inhibition). The color represents the mean value of triplicate wells (technical replicates; mean Z'-factor over 8 plates of 0.28 between stimulated- and unstimulated control conditions, also for figures C and D). **C)** Validation of PI3K inhibitors; color scale as in B. **D)** Validation of dual (legend continues on next page)

PI3K/mTOR inhibitors; color scale as in B. **E)** Combination of mTOR inhibitor torin 1 with PI3K inhibitor buparlisib (NVP-BKM120) to assess synergy, in mIMRFPKD 5E4 cells. Values represent mean \pm SD of quadruplicate wells (technical replicates; Z'-factor of +0.64 between stimulated- and unstimulated control conditions)

progression, it is possible that these molecules block forskolin-induced cyst swelling by limiting proliferation or other growth-limiting effects that are potentially undesirable from a treatment perspective. Indeed, phenotypic analysis showed that especially CDK (e.g. CDK 1, -2, -5 and -9 inhibitor dinaciclib) and DNA-PK (e.g. DNA-PK and PI3K inhibitor PIK-75) inhibitors induced a novel phenotypic change, characterized by cyst sizes smaller than unstimulated control cysts and loss of cyst integrity, that could indicate a toxic effect, rather than only affecting the size of the cysts. Due to the function of CDKs in regulating the cell cycle and the function of DNA-PK in DNA-damage repair,³² the identification of these growth-inhibitory effects is unsurprising. Hence, these molecules are probably not desirable for prolonged therapeutic use in asymptomatic patients.

Consistent with previous reports,³³ we identified several inhibitors for IGF-1R with potent inhibitory effects on cyst swelling. Some of these are also reported to have activity against the insulin receptor at the concentrations that we used, such as linsitinib, which inhibits IGF-1R with an IC₅₀ of 35nM³⁴ and the insulin receptor (IR) at 75nM. Additional studies, for example using function-blocking antibodies, are required to determine whether combined action on IGF-1R and IR are responsible for the observed effect, rather than sole inhibition of IGF-1R.

The c-Met inhibitor ArQ-197 also showed potent inhibitory activity in our assay, although other c-Met inhibitors, such as PHA-665752 and SGX-523 were inactive in the assay. This suggests that ArQ-197 may induce growth inhibitory effects independently of its effects on the c-Met receptor tyrosine kinase, which is consistent with our previous observations.¹⁵ Our observation that cyst growth was reduced by IKK- α/β inhibitors suggests an involvement of the NF κ B pathway, as previously described.³⁵ Additionally, our results hint at the involvement of spleen tyrosine kinase (Syk), which, to our knowledge, has not previously been linked to PKD. Syk may represent an interesting target for various renal diseases.³⁶ However, R788 (fostamatinib) and its active metabolite R406 may also inhibit fms-like tyrosine kinase 3 (Flt3) at the tested concentrations, so their inhibitory activity may not be solely due to inhibition of Syk (supplemental table 4, also quizartinib, an inhibitor of Flt3 displays inhibitory activity as shown in figure 4A). Interestingly, EGFR (epidermal growth factor receptor, ErbB-1) has previously been described for its involvement in cyst growth³⁷, however, inhibitors for EGFR were not identified as hits in our screen. This may be due to the absence of added EGFR-ligands in the 3D cyst cultures. Interestingly, our screen did identify several HER2 (ErbB-2) inhibitors that reduced cyst swelling. HER2 was identified as a potential target in PKD over 10 years ago, but has received little attention since.³⁸

Many mTOR inhibitors were selected as hits but, to our surprise, PI3K inhibitors were not, even though this has been described as a pathway involved in cyst growth.²³⁻²⁴ We therefore tested a larger panel of inhibitors for both protein targets and found that indeed, while mTOR inhibitors showed potent efficacy, PI3K inhibitors generally lacked inhibitory activity. We also showed a lack of synergy between PI3K and mTOR inhibitors buparlisib and torin 1, indicating that PI3K does not play a role in cyst growth in this *in vitro* assay for cyst growth. However, our results do not exclude a role for PI3K in PKD patients, where cyst growth is driven by mutations in the *PKD1* or *PKD2* gene. For instance, PI3K could play a role in different phases of the disease. Furthermore, PI3K may play a more important role in the *PKHD1*-mediated recessive form of PKD.²²

In conclusion, we have developed a high throughput-compatible 3D cell culture-based screening platform to identify molecules that affect cystogenesis. We have used this platform to identify molecular targets involved in cyst swelling and have identified several known- and novel pathways to be involved in cyst growth in our model. Additionally, we used multiparametric analysis to discriminate compounds that effectively inhibited cyst growth from compounds that inhibited through potentially toxic effects.

Declaration of Conflicting Interests

The authors declared the following potential conflicts of interest with respect to the research, authorship, and/or publication of this article: L. S. Price is a founder and major shareholder of Ocello B.V. The other authors declared no potential conflicts of interest with respect to the research, authorship, and/or publication of this article.

Funding

The authors disclosed receipt of the following financial support for the research, authorship, and/or publication of this article: T. H. Booij, W. N. Leonhard, and Y. Qin were supported by the Dutch Technology Foundation STW (Project 11823), which is part of the Netherlands Organization for Scientific Research (NWO). S. J. Kunnen was supported by NWO, Earth and Life Sciences grant 820.02.016. M. Fokkelman was supported by the EU-FP7—Systems Microscopy NoE (grant no. 258068 to B. van de Water). The other authors received no financial support for the research, authorship, and/or publication of this article.

References

1. Willey CJ, Blais JD, Hall AK, Krasa HB, Makin AJ, Czerwiec FS: Prevalence of autosomal dominant polycystic kidney disease in the European Union. *Nephrol Dial Transplant*, 2016
2. Torres VE, Harris PC, Pirson Y: Autosomal dominant polycystic kidney disease. *Lancet* 369(9569): 1287-1301, 2007
3. Kim S, Nie H, Nesin V, Tran U, Outeda P, Bai CX, Keeling J, Maskey D, Watnick T, Wessely O, Tsiokas L: The polycystin complex mediates Wnt/Ca(2+) signalling. *Nat Cell Biol* 18(7): 752-764, 2016

4. Retailliau K, Duprat F: Polycystins and partners: proposed role in mechanosensitivity. *J Physiol* 592(12): 2453-2471, 2014
5. Kotsis F, Boehlke C, Kuehn EW: The ciliary flow sensor and polycystic kidney disease. *Nephrol Dial Transplant* 28(3): 518-526, 2013
6. Ibraghimov-Beskrovnaya O, Dackowski WR, Foggensteiner L, Coleman N, Thiru S, Petry LR, Burn TC, Connors TD, Van Raay T, Bradley J, Qian F, Onuchic LF, Watnick TJ, Piontek K, Hakim RM, Landes GM, Germino GG, Sandford R, Klinger KW: Polycystin: in vitro synthesis, in vivo tissue expression, and subcellular localization identifies a large membrane-associated protein. *Proc Natl Acad Sci U S A* 94(12): 6397-6402, 1997
7. Ong AC, Harris PC: A polycystin-centric view of cyst formation and disease: the polycystins revisited. *Kidney Int* 88(4): 699-710, 2015
8. Torres VE, Harris PC: Strategies targeting cAMP signaling in the treatment of polycystic kidney disease. *J Am Soc Nephrol* 25(1): 18-32, 2014
9. Blair HA, Keating GM: Tolvaptan: A Review in Autosomal Dominant Polycystic Kidney Disease. *Drugs* 75(15): 1797-1806, 2015
10. Pampaloni F, Reynaud EG, Stelzer EH: The third dimension bridges the gap between cell culture and live tissue. *Nat Rev Mol Cell Biol* 8(10): 839-845, 2007
11. Debnath J, Brugge JS: Modelling glandular epithelial cancers in three-dimensional cultures. *Nat Rev Cancer* 5(9): 675-688, 2005
12. Carlotti F, Bazuine M, Kekalainen T, Seppen J, Pognonec P, Maassen JA, Hoebe RC: Lentiviral vectors efficiently transduce quiescent mature 3T3-L1 adipocytes. *Mol Ther* 9(2): 209-217, 2004
13. Tsai SQ, Wyvekens N, Khayter C, Foden JA, Thapar V, Reyon D, Goodwin MJ, Aryee MJ, Joung JK: Dimeric CRISPR RNA-guided FokI nucleases for highly specific genome editing. *Nat Biotechnol* 32(6): 569-576, 2014
14. Di Z, Klop MJ, Rogkoti VM, Le Devedec SE, van de Water B, Verbeek FJ, Price LS, Meerman JH: Ultra high content image analysis and phenotype profiling of 3D cultured micro-tissues. *PLoS One* 9(10): e109688, 2014
15. Booij TH, Klop MJ, Yan K, Szantai-Kis C, Szokol B, Orfi L, van de Water B, Keri G, Price LS: Development of a 3D Tissue Culture-Based High-Content Screening Platform That Uses Phenotypic Profiling to Discriminate Selective Inhibitors of Receptor Tyrosine Kinases. *J Biomol Screen*, 2016
16. Bliss CI: The toxicity of poisons applied jointly. *Ann Appl Biol* 26(3): 585-615, 1939
17. Iversen PW, Beck B, Chen YF, Dere W, Devanarayan V, Eastwood BJ, Farmen MW, Iturria SJ, Montrose C, Moore RA, Weidner JR, Sittampalam GS: HTS Assay Validation. In: edited by Bethesda (MD), Eli Lilly & Company and the National Center for Advancing Translational Sciences, 2012,
18. Meijer L, Borgne A, Mulner O, Chong JP, Blow JJ, Inagaki N, Inagaki M, Delcros JG, Moulinoux JP: Biochemical and cellular effects of roscovitine, a potent and selective inhibitor of the cyclin-dependent kinases cdc2, cdk2 and cdk5. *Eur J Biochem* 243(1-2): 527-536, 1997

19. Maira SM, Stauffer F, Brueggen J, Furet P, Schnell C, Fritsch C, Brachmann S, Chene P, De Pover A, Schoemaker K, Fabbro D, Gabriel D, Simonen M, Murphy L, Finan P, Sellers W, Garcia-Echeverria C: Identification and characterization of NVP-BEZ235, a new orally available dual phosphatidylinositol 3-kinase/mammalian target of rapamycin inhibitor with potent in vivo antitumor activity. *Mol Cancer Ther* 7(7): 1851-1863, 2008
20. Toledo LI, Murga M, Zur R, Soria R, Rodriguez A, Martinez S, Oyarzabal J, Pastor J, Bischoff JR, Fernandez-Capetillo O: A cell-based screen identifies ATR inhibitors with synthetic lethal properties for cancer-associated mutations. *Nat Struct Mol Biol* 18(6): 721-727, 2011
21. Wilhelm SM, Carter C, Tang L, Wilkie D, McNabola A, Rong H, Chen C, Zhang X, Vincent P, McHugh M, Cao Y, Shujath J, Gawlak S, Eveleigh D, Rowley B, Liu L, Adnane L, Lynch M, Auclair D, Taylor I, Gedrich R, Voznesensky A, Riedl B, Post LE, Bollag G, Trail PA: BAY 43-9006 exhibits broad spectrum oral antitumor activity and targets the RAF/MEK/ERK pathway and receptor tyrosine kinases involved in tumor progression and angiogenesis. *Cancer Res* 64(19): 7099-7109, 2004
22. Ren XS, Sato Y, Harada K, Sasaki M, Furubo S, Song JY, Nakanuma Y: Activation of the PI3K/mTOR pathway is involved in cystic proliferation of cholangiocytes of the PCK rat. *PLoS One* 9(1): e87660, 2014
23. Santoso NG, Cebotaru L, Guggino WB: Polycystin-1, 2, and STIM1 interact with IP(3) R to modulate ER Ca release through the PI3K/Akt pathway. *Cell Physiol Biochem* 27(6): 715-726, 2011
24. Franco I, Margaria JP, De Santis MC, Ranghino A, Monteyne D, Chiaravalli M, Pema M, Campa CC, Ratto E, Gulluni F, Perez-Morga D, Somlo S, Merlo GR, Boletta A, Hirsch E: Phosphoinositide 3-Kinase-C2alpha Regulates Polycystin-2 Ciliary Entry and Protects against Kidney Cyst Formation. *J Am Soc Nephrol* 27(4): 1135-1144, 2016
25. Kampa-Schittenhelm KM, Heinrich MC, Akmut F, Rasp KH, Illing B, Dohner H, Dohner K, Schittenhelm MM: Cell cycle-dependent activity of the novel dual PI3K-MTORC1/2 inhibitor NVP-BGT226 in acute leukemia. *Mol Cancer* 12 46, 2013
26. Liu Q, Chang JW, Wang J, Kang SA, Thoreen CC, Markhard A, Hur W, Zhang J, Sim T, Sabatini DM, Gray NS: Discovery of 1-(4-(4-propionylpiperazin-1-yl)-3-(trifluoromethyl)phenyl)-9-(quinolin-3-yl)benz o[h][1,6]naphthyridin-2(1H)-one as a highly potent, selective mammalian target of rapamycin (mTOR) inhibitor for the treatment of cancer. *J Med Chem* 53(19): 7146-7155, 2010
27. Thoreen CC, Kang SA, Chang JW, Liu Q, Zhang J, Gao Y, Reichling LJ, Sim T, Sabatini DM, Gray NS: An ATP-competitive mammalian target of rapamycin inhibitor reveals rapamycin-resistant functions of mTORC1. *J Biol Chem* 284(12): 8023-8032, 2009
28. Burger MT, Pecchi S, Wagman A, Ni ZJ, Knapp M, Hendrickson T, Atallah G, Pfister K, Zhang Y, Bartulis S, Frazier K, Ng S, Smith A, Verhagen J, Haznedar J, Huh K, Iwanowicz E, Xin X, Menezes D, Merritt H, Lee I, Wiesmann M, Kaufman S, Crawford K, Chin M, Bussiere D, Shoemaker K, Zaror I, Maira SM, Voliva CF: Identification of NVP-BKM120 as a Potent, Selective, Orally Bioavailable Class I PI3 Kinase Inhibitor for Treating Cancer. *ACS Med Chem Lett* 2(10): 774-779, 2011

29. Anderson JL, Park A, Akiyama R, Tap WD, Denny CT, Federman N: Evaluation of In Vitro Activity of the Class I PI3K Inhibitor Buparlisib (BKM120) in Pediatric Bone and Soft Tissue Sarcomas. *PLoS One* 10(9): e0133610, 2015
30. Novalic Z, van der Wal AM, Leonhard WN, Koehl G, Breuning MH, Geissler EK, de Heer E, Peters DJ: Dose-dependent effects of sirolimus on mTOR signaling and polycystic kidney disease. *J Am Soc Nephrol* 23(5): 842-853, 2012
31. Shillingford JM, Murcia NS, Larson CH, Low SH, Hedgepeth R, Brown N, Flask CA, Novick AC, Goldfarb DA, Kramer-Zucker A, Walz G, Piontek KB, Germino GG, Weimbs T: The mTOR pathway is regulated by polycystin-1, and its inhibition reverses renal cystogenesis in polycystic kidney disease. *Proc Natl Acad Sci U S A* 103(14): 5466-5471, 2006
32. Robert F, Barbeau M, Ethier S, Dostie J, Pelletier J: Pharmacological inhibition of DNA-PK stimulates Cas9-mediated genome editing. *Genome Med* 7 93, 2015
33. Parker E, Newby LJ, Sharpe CC, Rossetti S, Streets AJ, Harris PC, O'Hare MJ, Ong AC: Hyperproliferation of PKD1 cystic cells is induced by insulin-like growth factor-1 activation of the Ras/Raf signalling system. *Kidney Int* 72(2): 157-165, 2007
34. Mulvihill MJ, Cooke A, Rosenfeld-Franklin M, Buck E, Foreman K, Landfair D, O'Connor M, Pirritt C, Sun Y, Yao Y, Arnold LD, Gibson NW, Ji QS: Discovery of OSI-906: a selective and orally efficacious dual inhibitor of the IGF-1 receptor and insulin receptor. *Future Med Chem* 1(6): 1153-1171, 2009
35. Zhou JX, Fan LX, Li X, Calvet JP, Li X: TNFalpha signaling regulates cystic epithelial cell proliferation through Akt/mTOR and ERK/MAPK/Cdk2 mediated Id2 signaling. *PLoS One* 10(6): e0131043, 2015
36. Ma TK, McAdoo SP, Tam FW: Spleen Tyrosine Kinase: A Crucial Player and Potential Therapeutic Target in Renal Disease. *Nephron* 133(4): 261-269, 2016
37. Torres VE, Sweeney WE, Jr., Wang X, Qian Q, Harris PC, Frost P, Avner ED: EGF receptor tyrosine kinase inhibition attenuates the development of PKD in Han:SPRD rats. *Kidney Int* 64(5): 1573-1579, 2003
38. Wilson SJ, Amsler K, Hyink DP, Li X, Lu W, Zhou J, Burrow CR, Wilson PD: Inhibition of HER-2(neu/ErbB2) restores normal function and structure to polycystic kidney disease (PKD) epithelia. *Biochim Biophys Acta* 1762(7): 647-655, 2006

SUPPLEMENTAL MATERIALS

SUPPLEMENTAL TABLE 1 RFNs for *Pkd1* exon 15

<i>Sequence Name</i>	<i>Target site 1</i>	<i>Target site 2</i>
<i>RFNmPKD1ex15g</i>	AGCAGGATTTCAAAGTGGAC	CTTACTTTCGGACTTCAGGT

SUPPLEMENTAL TABLE 2 Primers flanking RFN target sites

<i>Primer name</i>	<i>Primer sequence</i>
PKD1ex15F2	CACAGTAGAGGAACCCATTGTGA
PKD1ex15R2	CACACCACCCAGTTCATTAAAGG

SUPPLEMENTAL TABLE 3 Phenotypic features incorporated in the PCA

<i>Feature</i>	<i>Image Channel</i>
area (Rhodamine)	Cytoskeleton
average_length_of_branches (Rhodamine)	Cytoskeleton
avg_wall_to_outline_center_dist (Rhodamine)	Cytoskeleton
equivdiameter (Rhodamine)	Cytoskeleton
feret (Rhodamine)	Cytoskeleton
major_Axis (Rhodamine)	Cytoskeleton
maximum_length_of_branches (Rhodamine)	Cytoskeleton
minFeret (Rhodamine)	Cytoskeleton
minor_Axis (Rhodamine)	Cytoskeleton
nNumber_of_connection_points (Rhodamine)	Cytoskeleton
number_of_branches (Rhodamine)	Cytoskeleton
number_of_end_points (Rhodamine)	Cytoskeleton
perimeter (Rhodamine)	Cytoskeleton
ratio_Area_BoundingBox_Area (Rhodamine)	Cytoskeleton
wall_count (Rhodamine)	Cytoskeleton
zernike_order_0_0 (Rhodamine)	Cytoskeleton
zernike_order_1_1 (Rhodamine)	Cytoskeleton
zernike_order_2_0 (Rhodamine)	Cytoskeleton
zernike_order_2_2 (Rhodamine)	Cytoskeleton
zernike_order_3_3 (Rhodamine)	Cytoskeleton
zernike_order_4_2 (Rhodamine)	Cytoskeleton
zernike_order_5_1 (Rhodamine)	Cytoskeleton
zernike_order_5_3 (Rhodamine)	Cytoskeleton
zernike_order_5_5 (Rhodamine)	Cytoskeleton
zernike_order_6_0 (Rhodamine)	Cytoskeleton
zernike_order_6_2 (Rhodamine)	Cytoskeleton
zernike_order_6_4 (Rhodamine)	Cytoskeleton
zernike_order_6_6 (Rhodamine)	Cytoskeleton
zernike_order_7_1 (Rhodamine)	Cytoskeleton
zernike_order_7_7 (Rhodamine)	Cytoskeleton
zernike_order_8_0 (Rhodamine)	Cytoskeleton
zernike_order_8_2 (Rhodamine)	Cytoskeleton
zernike_order_8_4 (Rhodamine)	Cytoskeleton
zernike_order_8_6 (Rhodamine)	Cytoskeleton
zernike_order_8_8 (Rhodamine)	Cytoskeleton
zernike_order_9_1 (Rhodamine)	Cytoskeleton
zernike_order_9_7 (Rhodamine)	Cytoskeleton
zernike_order_9_9 (Rhodamine)	Cytoskeleton
avg_child_to_par_center_dist (Hoechst)	Nucleus
axis_Ratio_Minor_Major (Hoechst)	Nucleus
child_count (Hoechst)	Nucleus
eccentricity (Hoechst)	Nucleus
hu_order_1 (Hoechst)	Nucleus
roundness (Hoechst)	Nucleus
zernike_order_2_2 (Hoechst)	Nucleus
zernike_order_9_3 (Hoechst)	Nucleus
zernike_order_9_5 (Hoechst)	Nucleus

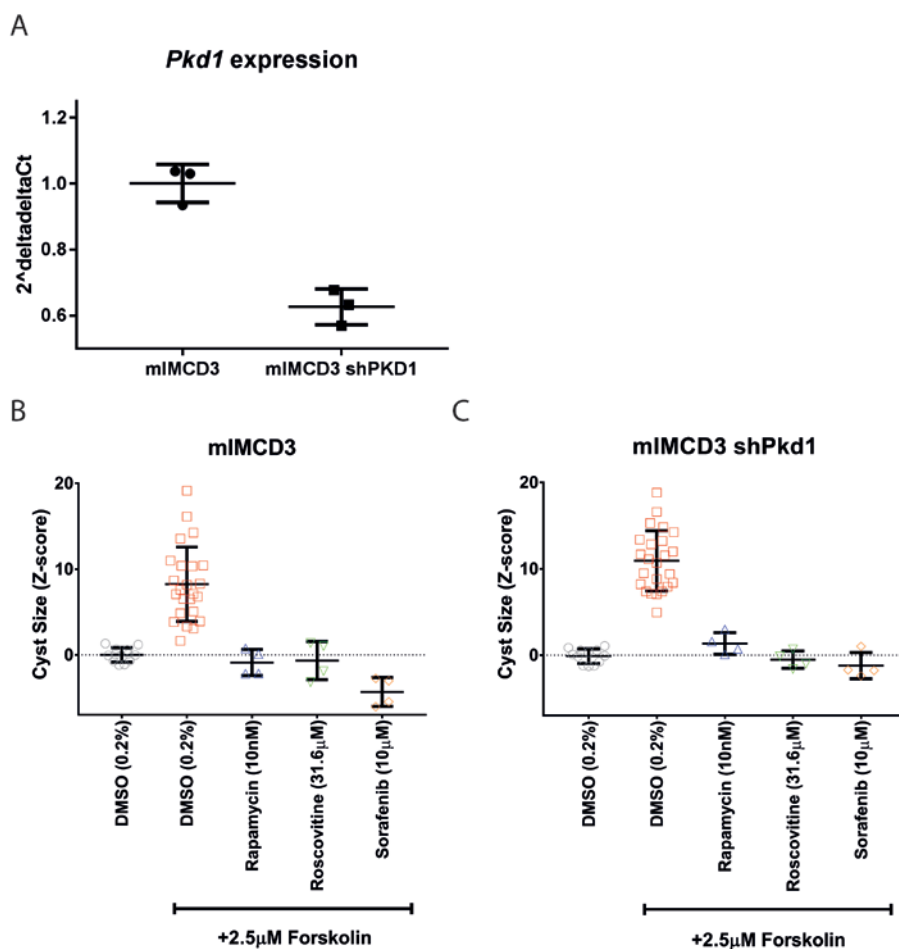
SUPPLEMENTAL TABLE 4 Validation screen molecule information

MOLECULES	TARGET INFORMATION	BRIEF DESCRIPTION (INFORMATION DERIVED FROM WWW.SELLECKCHEM.COM)
AG-1024 ARQ 197 (TIVANTINIB) ARRY-380 AT7867	IGF1R, IR c-Met HER2, EGFR AKT, P70 S6 kinase	Inhibitor of IGF1R/IR autophosphorylation with 7 μ M and 57 μ M, respectively. non-ATP competitive c-Met inhibitor with Ki 0.355 μ M Inhibitor of HER2 (IC50 8nM) and EGFR (IC50 4 μ M) IC50 in cell free assays: Akt2 (17nM), PKA (20nM) Akt1 (32nM), Akt3 (47nM), p70 S6K (85nM), RSK1 (>100nM)
AZD7762	CHK1, CHK2	IC50 in cell free assays: Chk1 (5nM), Chk2 (<10nM). Less potent against CAM, Yes, Fyn, Lyn, Hck and Lck.
BI 2536	PLK1	IC50 in cell free assays: PLK1 (0.83nM), PLK2 (3.5nM), PLK3 (9nM). Molecule also targets PI3K and Met >2 μ M.
BI6727 (VOLASERTIB) BUPARLISIB (NVP-BKM120) CCT137690	PLK1 PI3K (p110 α / β / δ / γ) Aurora A, Aurora B, Aurora C	IC50 in cell free assays: PLK1 (0.87nM) IC50 in cell free assays: p110 α (52nM) p110 β (166nM) p110 δ (116nM) p110 γ (262nM) IC50: Aurora A (15nM), Aurora C (19nM), Aurora B (25nM)
CHIR-124	CHK1	IC50 in cell free assays: Chk1 (0.3nM), FLT3 (5.8nM), PDGFR (6.6nM), GSK-3 (23.3nM), Fyn (98.8nM). Also targets PKA, PKC γ , LCK, CDK2, VEGFR1, Cdc2, VEGFR2, PKC β , PKC α , Chk2 <1 μ M. Kd in CHO cells: PDGFR α (2.1nM), PDGFR β (3.2nM)
CRENOLANIB (CP-868596) DINACICLIB (SCH727965) EVEROLIMUS (RAD001) GSK1904529A	PDGFR- α , PDGFR β CDK2, CDK5, CDK1, CDK9 mTOR IGF1R, IR	IC50 in cell free assays: CDK2 (1nM), CDK5 (1nM), CDK1 (3nM), CDK9 (4nM). Also blocks thymidine DNA incorporation. IC50 in cell free assays: mTOR (FKBP12) (1.6-2.4nM) IC50 in cell free assays: IR (25nM), IGF1R (27nM), B-Raf (>2 μ M) and others at higher concentrations.
GSK461364 HESPERADIN HMN-214	PLK1 Aurora B PLK1	Ki in cell free assay: PLK1 (2.2nM) IC50 in cell free assays TbaUK1 (40nM), Aurora B (250nM) Prodrug of HMN-176. Little in vitro data is available but causes cytotoxic effects in nM-range.
IMD 0354 KX2-391 LDN193189	IKK- β Src ALK2, ALK3	Affects NF κ B nuclear translocation >0.5 μ M. Growth inhibition in cancer cell lines GI 9-60nM. Inhibits transcriptional activity of ALK2 (5nM) and ALK3 (30nM) receptors in cell-based assays.
LINSITINIB (OSI-906) LY2603618 (IC-83) MUBRITINIB (TAK 165) NU7441 (KU-57788) NVP-ADW742 ON-01910 OSU-03012 PD 0332991 (PALBOCIC LIB) HCL PD173074 PIK-75	IGF1R, IR CHK1 HER2 DNA-PK IGF1R PLK1 PDK-1 CDK4, CDK6 FGFR1, VEGFR2 DNA-PK, PI3K (p110 α , β , γ and δ)	Inhibits IR (75nM) and IGR1R (35nM) in cell-free assays. Inhibits CHK1 (IC50 7nM) in vitro. HER2 inhibitor with IC50 of 6nM in BT-474 cells. Inhibits DNA-PK with IC50 14nM, mTOR at 1.7 μ M and PI3K at 5 μ M Inhibits IGF1R with IC50 170nM Inhibits PLK1 with IC50 9nM in cell-free assays. IC50 5 μ M, derivative of celecoxib. IC50 in cell free assays: CDK4/CyclinD3 (9nM), CDK4/CyclinD1 (11nM), CDK6/CyclinD2 (15nM) IC50 in cell free assays: FGFR1 (25nM), VEGFR2 (100-200nM), c-Src (19.8 μ M) IC50 in cell free assays: DNA-PK (2nM), p110 α (5.8nM), p110 β (1.3 μ M), p110 γ (76nM), p110 δ (0.51 μ M)
PIK-90	PI3K (p110 α , β , γ and δ)	IC50 in cell free assays: p110 α (11nM), p110 β (350nM), p110 γ (18nM), p110 δ (58nM)
QUIZARTINIB (AC220) R406 R406(FREE BASE) R788 (FOSTAMATINIB) R935788 (FOSTAMATINIB DISODIUM, R788 DISODIUM) THIAZOVIVIN TORIN-1	FLT3 Syk Syk Syk Syk ROCK mTOR (mTORC1/2)	IC50 in cell lines: FLT3 (IDT) (1.1nM), FLT3 (WT) (4.2nM). Kd for FLT3 1.6nM. Inhibits Syk with IC50 41nM in cell free assays. Also inhibits FLT3. Inhibits Syk with IC50 41nM in cell free assays. Also inhibits FLT3. Prodrug of R406, Syk inhibitor with IC50 of 41nM Prodrug of R406, Syk inhibitor with IC50 of 41nM Inhibits ROCK in low micromolar range. IC50 of 2nM/10nM for mTORC1/2, respectively. 1000-fold selectivity for mTOR over PI3K.
TPCA-1	IKK- β , IKK- α	In a cell free assay, TPCA-1 inhibits IKK- β with an IC50 of 17.9nM, IC50 against IKK- α 400nM, and JNK3 360nM.
TWS119 TYRPHOSTIN AG 879 (AG 879) VANDETANIB (ZACTIMA) WP1130	GSK-3 β HER2 VEGFR, EGFR Deubiquitinase (USP5, UCH-L1, USP9x, USP14, and UCH37) and Bcr/Abl, JAK2, STAT	IC50 in cell free assays: GSK-3 β (30nM) Inhibits HER2 with an IC50 of 1.0 μ M Inhibits VEGFR2 in cell free assays with an IC50 of 40nM. Also inhibits VEGFR3 and EGFR with IC50 110nM and 500nM. Degrasyn is a deubiquitinase that also inhibits Bcr/Abl at 1.8 μ M
WYE-125132 WZ3146	mTOR EGFR	Potent mTOR inhibitor with an IC50 of 0.19nM. Highly selective over PI3Ks. Mutant-selective EGFR inhibitor with IC50 2-14nM. <100-fold less potent against WT EGFR.
WZ8040 ZSTK474	EGFR PI3K (p110 α , β , γ and δ)	Mutant-selective irreversible EGFR inhibitor. <100 fold less potent against WT EGFR IC50 in cell free assays: p110 α (16nM), p110 β (44nM), p110 γ (49nM), p110 δ (4.6nM)

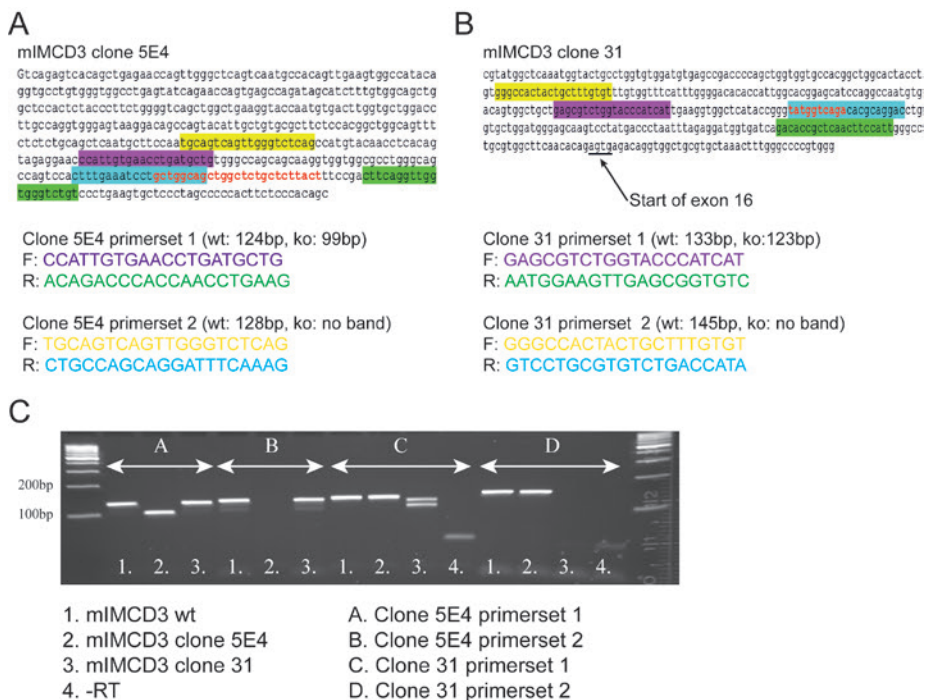
SUPPLEMENTAL TABLE 5 Statistical significance of selected hits

COMPOUND	Conc. (μM)	ONE WAY ANOVA WITH DUNNETT'S MULTIPLE COMPARISON TEST (P<0.05)*		Correlates
		Primary Screen	Validation Screen	
AG-1024	1	0.9995	0.9915	Yes
ARQ 197	1	0.0004	0.0001	Yes
ARRY-380	1	0.999	0.9991	Yes
AT7867	0.1	0.1666	0.9913	Yes
AZD7762	0.1	0.0004	0.9996	No
BI 2536	0.1	0.0001	0.0001	Yes
BI6727	0.1	0.0458	0.9803	No
CCT137690	0.1	0.0001	0.9986	No
CHIR-124	0.1	0.0001	0.0001	Yes
CRENOLANIB	1	0.0008	0.0686	No
DINACICLIB	0.1	0.0001	0.0001	Yes
EVEROLIMUS	0.1	0.0001	0.0001	Yes
GSK1904529A	1	0.4917	0.0147	No
GSK461364	0.1	0.0058	0.898	No
HESPERADIN	1	0.0001	0.0001	Yes
HMN-214	0.1	0.0001	0.9995	No
IMD 0354	1	0.0001	0.0001	Yes
KX2-391	0.1	0.0057	0.0001	Yes
LDN193189	1	0.0001	0.9991	No
LINSITINIB	1	0.0001	0.0001	Yes
LY2603618	0.1	0.0011	0.9991	No
MUBRITINIB	0.1	0.024	0.0007	Yes
NU7441	0.1	0.0002	0.9835	No
NVP-ADW742	0.1	0.0001	0.9985	No
ON-01910	1	0.0001	0.0001	Yes
OSU-03012	1	0.0001	0.9997	No
PD 0332991	1	0.0001	0.0145	Yes
PD173074	1	0.9995	0.87	Yes
PIK-75	1	0.0001	0.0001	Yes
PIK-90	1	0.1057	0.1812	Yes
QUIZARTINIB	1	0.0186	0.0086	Yes
R406	1	0.0067	0.0125	Yes
R406 (FREE BASE)	0.1	0.0001	0.3736	No
R788	1	0.0193	0.0001	Yes
R935788	1	0.3575	0.0001	No
THIAZOVIVIN	1	0.603	0.9994	Yes
TPCA-1	1	0.0002	0.8242	No
TWS119	1	0.9808	0.9996	Yes
TYRPHOSTIN	1	0.9981	0.007	No
AG 879	1	0.1431	0.3565	Yes
VANDETANIB	1	0.0001	0.0943	Yes
WP1130	1	0.0001	0.0001	Yes
WYE-125132	0.1	0.0001	0.592	No
WZ3146	0.1	0.0001	0.6997	No
WZ8040	0.1	0.0001	0.4663	No
ZSTK474	1	0.0001		No

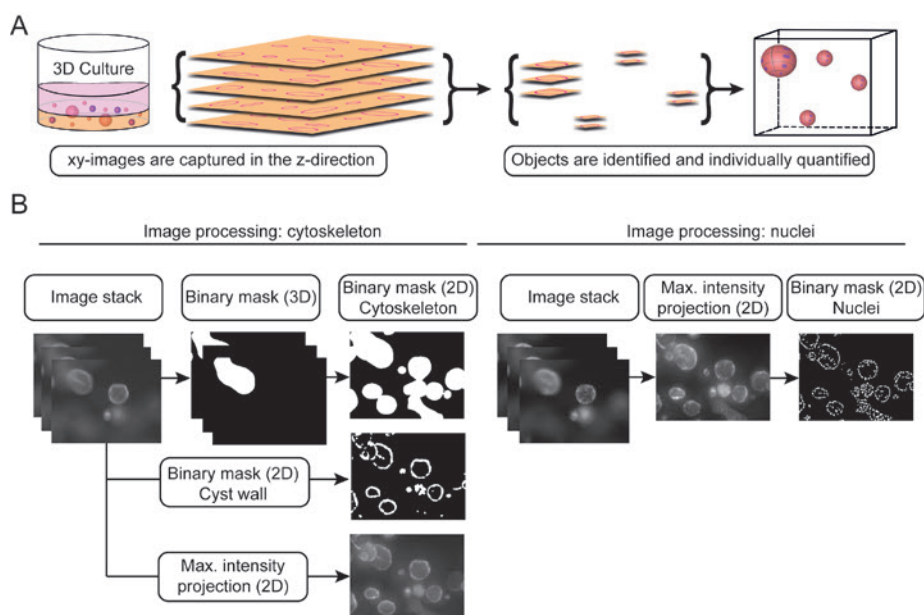
*Statistical significance was assessed compared to forskolin-stimulated controls using ordinary one-way ANOVA with Dunnett's multiple comparison test. Differences were considered significantly different for adjusted P<0.05.



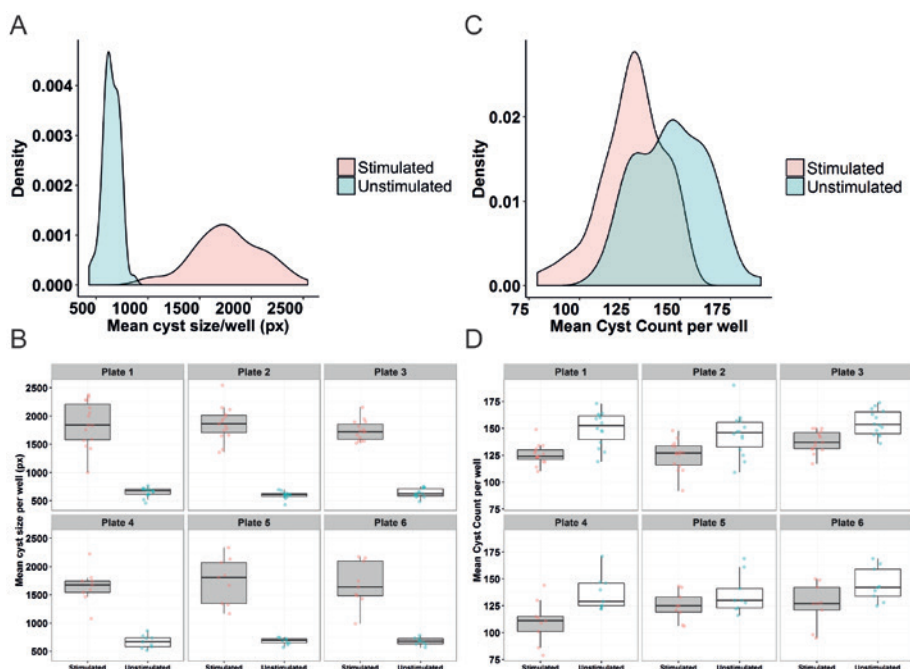
SUPPLEMENTAL FIGURE 1 *Pkd1* expression is reduced in mlMCD3 shPkd1 cells. **A)** qPCR showing reduced expression of *Pkd1* using the $2^{\Delta\Delta Ct}$ method (means ± SD of triplicates). qPCR was performed three times. **B** and **C)** Control conditions in both mlMCD3 wt and mlMCD3 shPkd1 cells. Cyst growth depicted by cyst size z-scored to unstimulated control (DMSO 0.2%, grey circles) median (dotted black line at $y=0$). Induction of cyst growth by forskolin demonstrated by red squares. Individual datapoints and mean ± SD shown.



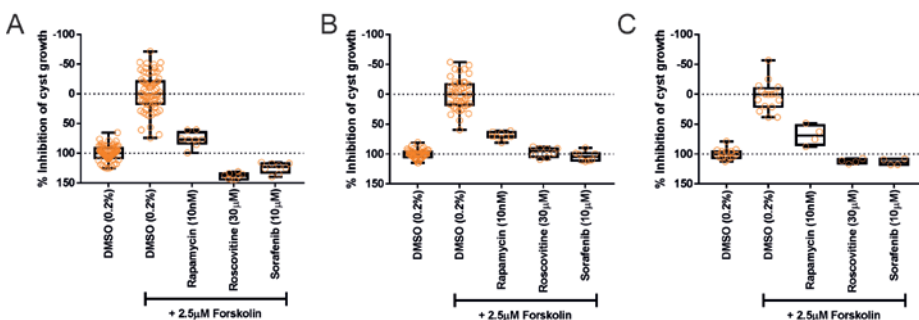
SUPPLEMENTAL FIGURE 2 Generation of *Pkd1* knockout cell lines. **A** and **B**) primer sets for both 5E4 and 31 clones for PCR depicted in **C**. **C**) PCR revealing deletion in *Pkd1* gene in clone 5E4 and clone 31. Clone 5E4 was selected due to improved growth characteristics.



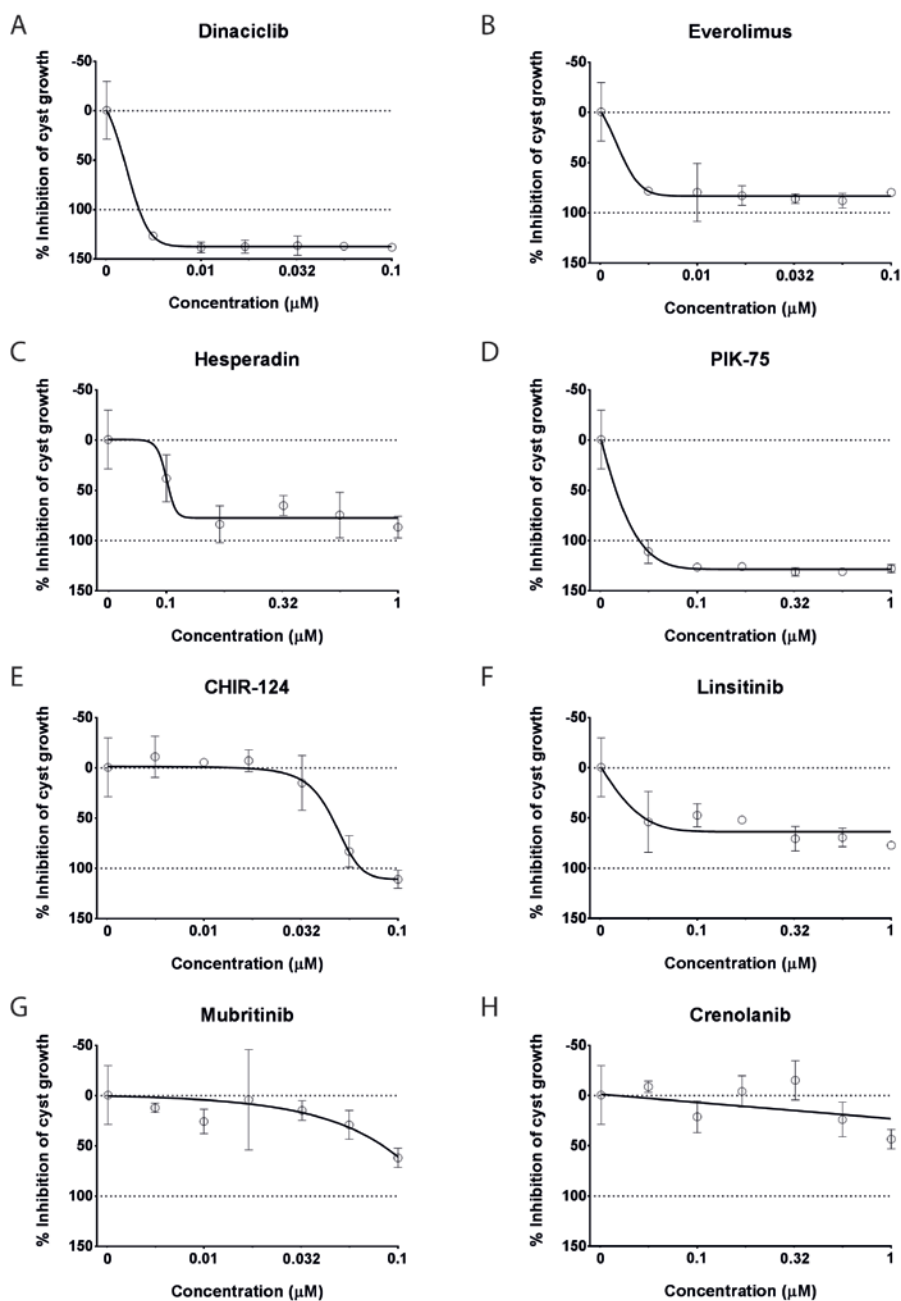
SUPPLEMENTAL FIGURE 3 Schematic representation of image analysis procedure. **A)** Images are captured at 50 μ m intervals throughout the z-axis of the gel and objects are extracted from each image plane and individually quantified. **B)** Image stacks (cutouts shown) of approximately 25 images per well from both cytoskeleton and nucleus image channels are processed to binary masks for quantification of phenotypic descriptors.



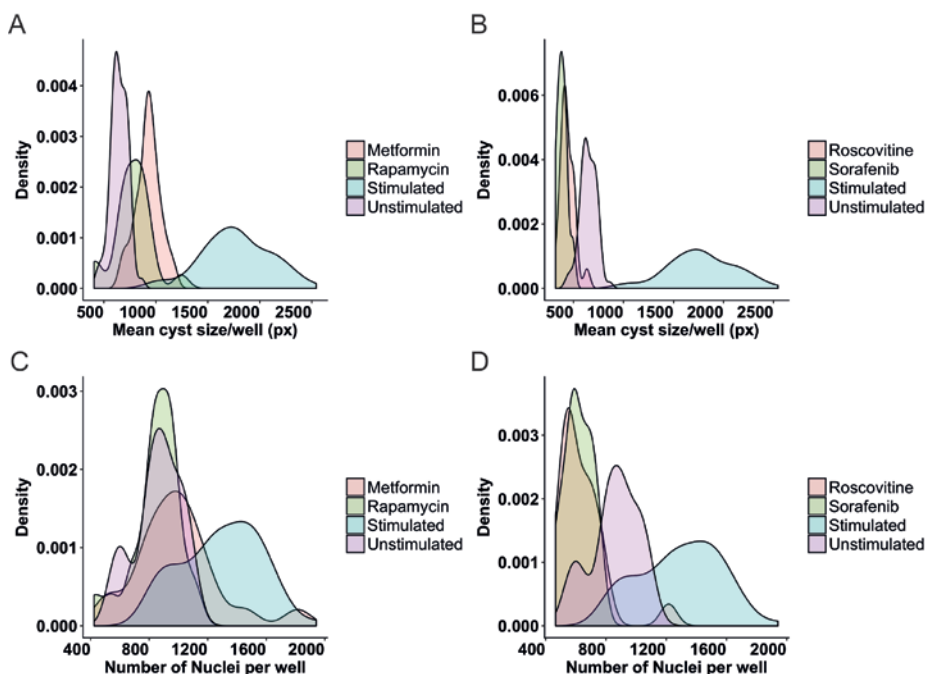
SUPPLEMENTAL FIGURE 4 Forskolin-treatment increases cyst growth. **A)** Density plot of validation screen showing non-normalized cyst size from all six plates in the validation for unstimulated (0.2% DMSO) and stimulated (2.5 μ M forskolin) conditions. **B)** Increased cyst growth after forskolin treatment is highly similar over different plates. **C)** As in A, but showing the number of cysts per well. **D)** As in B, number of cysts per well is similar among the six plates.



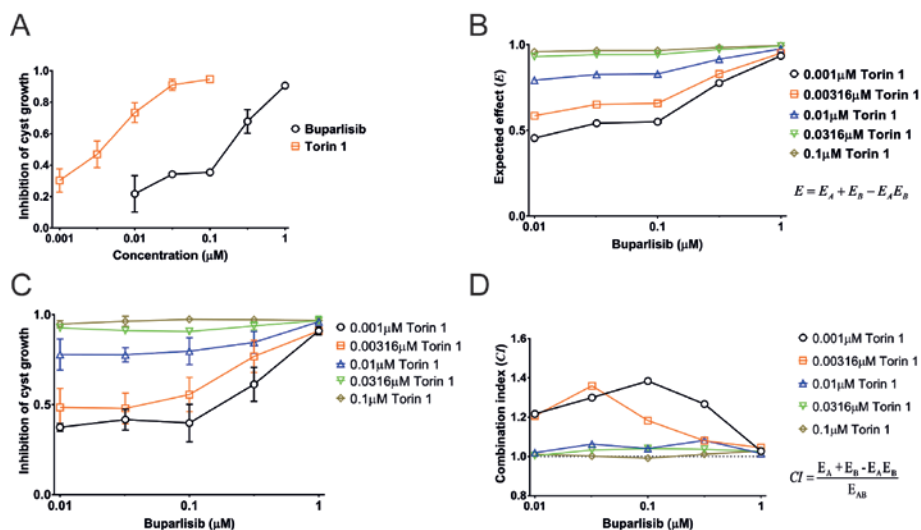
SUPPLEMENTAL FIGURE 5 Forskolin-induced mIMRFNPKD 5E4 cyst growth is inhibited by rapamycin, roscovitine and sorafenib in three independent experiments (A,B,C). Individual wells shown as orange circles. Box plot whiskers represent min to max.



SUPPLEMENTAL FIGURE 6 Concentration- cyst growth inhibition curves of data presented in main figure 4A. Black circles represent mean values of three wells (technical replicates) and error bars represent SD to illustrate intra-experimental variation. In case when error bars are not visible, the SD is smaller than the symbol height. **A)** Dinaciclib, **B)** Everolimus, **C)** Hesperadin, **D)** PIK-75, **E)** CHIR-124, **F)** Linsitinib, **G)** Mubritinib, **H)** Crenolanib.



SUPPLEMENTAL FIGURE 7 Roscovitine and sorafenib may affect cyst phenotype by reducing cell number. This data is derived from the validation screen as depicted in figure 4 and supplemental figure 4. **A)** Density plot as in supplemental figure 4 showing that 5mM metformin and 10nM rapamycin (pink and yellow) slow forskolin-induced cyst growth compared to stimulated (2.5 μ M forskolin, blue) condition. **B)** Roscovitine (31.6 μ M, pink) and sorafenib (10 μ M, yellow) slow forskolin-induced cyst growth compared to stimulated (2.5 μ M forskolin, blue) condition. **C)** Metformin and rapamycin do not cause a reduction in the number of nuclei (as derived from a maximum intensity projection of a 3D image stack) relative to unstimulated (0.2% DMSO vehicle, purple) control. **D)** Roscovitine (pink) and sorafenib (yellow) lower the number of nuclei (as derived from a maximum intensity projection of a 3D image stack) relative to the unstimulated condition (0.2% DMSO vehicle, purple).



SUPPLEMENTAL FIGURE 8 Assessment of synergistic effects of mTOR inhibitor torin 1 and PI3K inhibitor buparlisib (NVP-BKM-120) in mIMRFNPKD 5E4 cells. When combined, these inhibitors do not cause synergistic potentiation of cyst growth inhibition. **A)** Experimental measurement of inhibition of forskolin-induced cyst growth by buparlisib and torin 1 scaled between 0 (no inhibition) and 1 (max inhibition). Data presented represent means \pm SD of four wells (technical replicates). In case when error bars are not visible, the SD is smaller than the symbol height. **B)** Predicted inhibitory activity of combinations of torin 1 and buparlisib, scaled between 0 (no inhibition) and 1 (max inhibition). This prediction used the formula $E = E_A + E_B - E_A E_B$ where E_A is the effect of torin 1 and E_B is the effect of buparlisib. **C)** Experimental measurement of cyst growth inhibition by combinations of buparlisib and torin 1. Response scaled between 0 (no inhibition) and 1 (max inhibition). Data presented represent means \pm SD of four wells (technical replicates). In case when error bars are not visible, the SD is smaller than the symbol height. **D)** Combination index (CI) was defined by dividing the predicted response E with the observed response of combinatory therapy E_{AB} . A $CI < 1$ indicates synergistic effects, a $CI > 1$ indicates antagonistic effects, in contrast to an expected additive effect when $CI = 1$. The observed effect of some conditions (e.g. 0.00316 μM torin 1 and 0.1 μM buparlisib) in C was mildly less potent than the effects predicted in B, causing $CI > 1$. For other combinations, CI was 1, indicating only additive effects.

chapter 5

Phenotypic profiling of 3D-cultured micro-tissues to identify selective inhibitors of cyst growth

Tijmen H. Booij¹, Agnieszka Kaczmarczyk¹, Hester Bange²,
Saskia D. van Asten¹, Kuan Yan², Bob van de Water¹,
Dorien J.M. Peters³, Leo S. Price^{1,2}

- 1 Division of Toxicology, Leiden Academic Centre for Drug Research (LACDR), Leiden University, Leiden, The Netherlands
- 2 Ocello B.V., Leiden, The Netherlands
- 3 Humane Genetica, Leids Universitair Medisch Centrum (LUMC), Leiden, The Netherlands

Manuscript in Preparation

Abstract

Polycystic kidney disease is a relatively frequent monogenetic disorder characterized by the formation of renal cysts that progressively disrupt renal function until the point that patients require dialysis or renal transplantation therapy for survival. Therapeutic options to slow down disease progression are limited, which is partly due to our limited knowledge of the mechanisms contributing to cystogenesis. Additionally, lack of relevant *in vitro* disease models to study cystogenesis has hampered progression in this area.

Here we used a 3D cyst culture screening platform to assess the efficacy of a library of kinase inhibitors with described target specificities. Using phenotypic characterisation, compounds were classified according to phenotypic changes induced by compound intervention, to eliminate potentially cytotoxic compounds. Inhibitor efficacy was related to known molecular targets. Furthermore, to enrich for compounds that specifically inhibited cyst growth, a negative selection was performed in a model for 3D tumour cell invasion.

22 cyst growth inhibitors were retained that could selectively prevent cyst growth without affecting tumour cell morphology. The selected hit compounds targeted, among others, CDK1-9, GSK3, IGF1R/Akt1 and PI3K/Akt1. These results present an opportunity to further investigate therapeutic intervention directed against these targets.

Introduction

Cystogenesis is a process where cells develop into cysts, cell-enclosed cavities, (generally) filled with liquid. While the occurrence of small numbers of individual cysts may not necessarily cause health problems, development and growth of large numbers of cysts can have severe consequences and can be the result of underlying genetic mutations that predispose for cystic disorders. A relatively common cystic disorder is polycystic kidney disease (PKD). This disorder affects approximately 1:2500 people¹ that eventually develop renal failure and require dialysis or a kidney transplant for survival.² This slow-developing disease, caused by mutations in the *PKD1* or *PKD2* gene,³ is notoriously difficult to treat medicinally, due to the plethora of dysregulated cellular signalling pathways.^{3,5} The only currently approved therapy in the EU, tolvaptan, slows down cystogenesis but is also known to have side effects both related⁶⁻⁸ and unrelated⁹⁻¹¹ to its mechanism of action.

A traditional problem associated with this type of disease, where tissue architecture plays a critical role in the pathology, is that conventional two-dimensional (2D) *in vitro* cell monolayers do not provide an adequate context to study drug efficacy. Hence, drugs have generally been tested in animal models that were genetically altered to simulate the pathophysiology.¹²⁻¹⁴ However, while such models have improved relevance to the human disease, they cannot be used to assess the efficacy of large quantities of compounds. To bridge this gap between traditional *in vitro* and *in vivo* disease models, more advanced *in vitro* cell culture techniques, in which cells are cultured as three-dimensional (3D) micro-tissues, have been developed in recent years.¹⁵⁻¹⁹ Unfortunately, despite clear benefits of these 3D cell culture models,^{17, 20} these are still not used routinely for large-scale drug testing.²¹ Another area where these more advanced *in vitro* cell culture models may be essential is the prediction of toxicity of new drugs.²² Unexpected toxicity is a major problem in drug development resulting in a high level of pre-clinical and clinical failure.²²⁻²⁵ Especially for chronic disorders such as PKD, where patients require life-long treatment, it is critical that new drugs have a very favourable safety profile. Screening drugs in more advanced and physiologically relevant biological models will reduce pre-clinical failures and may help introduce safer drugs to the market.²⁶

To find potential new safe therapeutics for PKD and to unravel mechanisms of cyst growth, we screened a library of 428 kinase inhibitors with well-defined target specificity in an *in vitro* assay for cyst development. We subsequently selected drugs that showed a desirable efficacy and safety profile in this *in vitro* model, and counter-screened these compounds using a 3D tumour cell invasion assay in order to select compounds that specifically inhibited cyst growth. Additionally, we investigated the target specificities of the selected compounds, identifying cyclin-dependent kinases (CDKs), glycogen synthase kinase 3 (GSK3)- α/β , insulin-like growth factor 1 receptor (IGF1R), human epidermal growth factor receptor 2 (HER2), and Akt1 as potential targets for therapeutic intervention.

MATERIALS AND METHODS

Cell Lines

For 3D cyst assays and 2D ATPlite viability measurements (discussed below), mouse inner medullary collecting duct (mIMCD3 ATCC® CRL-2123™) cells harbouring a deletion of the *Pkd1* gene were generated using the dimeric CRISPR RNA-guided FokI nucleases (RFN) method²⁷ as previously described.²⁸ These cells are referred to as mIMRFNPKD 5E4 throughout this article. This cell line was maintained in 175cm² culture flasks at 37°C +5% CO₂ in DMEM/F12 Ham's culture medium (D8062, Sigma-Aldrich, Zwijndrecht, Netherlands), supplemented with 10% fetal bovine serum (FBS, Gibco™, ThermoFisher Scientific, Landsmeer, Netherlands), glutamax and penicillin/streptomycin. Before cells reached maximum density, the monolayer was washed with 1x PBS (Sigma-Aldrich, Zwijndrecht, Netherlands) and subsequently trypsinized with 1x Trypsin (Gibco™, ThermoFisher Scientific, Landsmeer, Netherlands). Cells were collected in culture medium and pelleted by centrifugation. Cell pellets were resuspended in FBS containing 10% dimethyl sulfoxide (DMSO, Biosolve B.V., Valkenswaard, Netherlands) for cryopreservation at -150°C.

For tumour cell invasion assays, we used the 4T1 murine breast cancer cell line (ATCC® CRL-2539™). 4T1 cells were maintained in RPMI-1640 culture medium supplemented with 10% FBS and 25µg/mL penicillin and streptomycin (Invitrogen™, ThermoFisher Scientific) according to standard procedure. Cells were cryopreserved at -150°C similarly to mIMRFNPKD 5E4 cells in cryopreservation medium (above).

3D cyst culture assay

The 3D cyst assay was performed as previously described.²⁸ Briefly, frozen mIMRFNPKD 5E4 cells were quick-thawed and cultured in 175cm² flasks 72 hours prior to starting the cyst assay. Growth medium was exchanged after 24 hours and after 72 hours the monolayer was trypsinized according to the procedure described above and the cells were mixed in cold Cyst-Gel (Ocello B.V., Leiden, Netherlands) and plated in 384 well plates, 14.5µL/well, (Greiner µClear, Greiner Bio-One B.V., Alphen aan den Rijn, Netherlands) using a CyBi Selma 96/60 robotic liquid handler (Analytik Jena AG, Jena, Germany). After gel polymerization at 37°C for 30 minutes, 33.5L culture medium was added to each well and small cysts were allowed to develop for a period of 96 hours at 37°C (5% CO₂), after which cells were co-exposed with forskolin (*Coleus Forskohlii*, Calbiochem, Millipore BV, Amsterdam, Netherlands, an activator of adenylyl cyclases to enhance intracellular 3',5'-cyclic adenosine monophosphate (cAMP) levels, which is a known mediator of cyst growth), and test compounds using a CyBi Selma 96/60 liquid handler. After 72 hours of compound exposures, plates were fixed and stained using a solution of 3% formaldehyde (Sigma-Aldrich, Zwijndrecht, Netherlands), 0.2% Triton X-100 (Sigma-Aldrich, Zwijndrecht, Netherlands), 0.25µM rhodamine-phalloidin (Sigma-Aldrich, Zwijndrecht, Netherlands) and 0.1% Hoechst 33258 (Sigma-Aldrich, Zwijndrecht, Netherlands) in 1x PBS for at least 12 hours at 4°C. Subsequently, plates were washed in 1x PBS for 12-24 hours, before sealing with a Greiner SilverSeal (Greiner

Bio-One B.V., Alphen aan den Rijn, Netherlands). The plates were stored at 4°C prior to imaging.

3D 4T1 cell invasion assay

Frozen 4T1 cells were quick-thawed to 37°C and subsequently mixed with a hydrogel mix consisting of Matrigel (BD Biosciences, Breda, Netherlands) and collagen-I (BD Biosciences, Breda, Netherlands) and 14.5 µL was transferred to each well of a 384 well plate (Greiner µClear, Greiner Bio-One B.V., Alphen aan den Rijn, Netherlands), using the CyBi Selma 96/60 robotic liquid handler (Analytik Jena AG, Jena, Germany), as previously described.²⁹ After gel polymerization at 37°C for 30 minutes, 39.5 µL RPMI-1640 culture medium (as described above for 4T1 cell maintenance) was added to all wells. Compound exposures were performed immediately using the CyBi Selma 96/60 robotic liquid handler (Analytik Jena AG, Jena, Germany). Cells were subsequently cultured at 37°C (5% CO₂) or 48 hours, prior to fixing and staining as described above for the 3D cyst culture assay.

ATPlite assay

Measurement of cell viability was performed using PerkinElmer's 1-step ATPlite kit (PerkinElmer Nederland B.V., Groningen, Netherlands) according to manufacturer's instructions in 384 well plates. Briefly, mIMRFNPKD 5E4 cells were seeded in 384 well plates 48 hours prior to compound treatments at a final cell density of 1000c/well. After compound exposure, the total volume in each well was kept at 25 µL. After 48 hours, 25 µL ATPlite reagent was added to all wells and the plates were shaken at 700rpm using an orbital plate shaker. Luminescence readout was performed using a FLUOstar OPTIMA microplate reader (BMG Labtech, Isogen Life Science, De Meern, Netherlands). Luminescence readout was scaled between controls without cells (0%) and solvent condition (100%) using NPI-normalization in KNIME Analytics Platform (KNIME 3.1.2, Konstanz, Germany, <http://www.knime.org/> for Microsoft Windows 7).

Compounds

The kinase inhibitor library (Chemical Validation Library, CVL), with compounds pre-dissolved in DMSO, was developed by Vichem Chemie Research Ltd. (Budapest, Hungary).³⁰⁻³¹ Rapamycin, roscovitine, entinostat, dasatinib and sorafenib tosylate were obtained from SelleckChem (Munich, Germany). IBMX (3-isobutyl-1-methylxanthine) was obtained from Cayman Chemical (Sanbio B.V. Uden, Netherlands). 8-Br-cAMP was obtained from Santa Cruz Biotechnology Inc. (Heidelberg, Germany) and Prostaglandin E1 was obtained from Sigma-Aldrich (Zwijndrecht, Netherlands).

Fluorescence Microscopy

3D micro-tissues were stained with Hoechst 33258 and rhodamine-phalloidin as described above and subsequently imaged using a BD Pathway 855 (BD Biosciences, Breda, Netherlands) automated inverted wide-field microscope using a 4x Olympus objective and accompanying BD Attovision software (BD Biosciences, Breda, Netherlands), or an ImageXpress Micro XLS wide field high-content analysis system

(Molecular Devices, Sunnyvale, CA, USA), equipped with a 4x objective. Images were captured in the z-plane at intervals of 50µm. The gel was imaged through its entire depth (z-axis), requiring around 25 images per well per fluorescence channel.

Image analysis and Image Processing

For mIMRFNPKD 5E4 cyst cultures, image stacks were analysed and phenotypes were quantified using Ominer software (Ocello B.V., Leiden, Netherlands) integrated in KNIME Analytics Platform (KNIME 3.1.2, Konstanz, Germany, <http://www.knime.org/> for Microsoft Windows 7). This software was used to extract 450 phenotypic measurements of cystic structures as described previously.²⁸ The phenotypic measurements were subsequently Z-score normalized (to unstimulated control) or NPI-normalized using KNIME software (between unstimulated control, 100%, and forskolin-stimulated controls, 0%) for presentation purposes. Principal component analysis (PCA) was trained on stimulated and unstimulated control groups, and phenotypic features with $Z^2 > 0.5$ between these groups were retained for PCA training. The trained PCA was subsequently applied over the test data, retaining 3 principal components that preserved 98% of the information. Afterwards, these principal components were used to train clusters based on the K Nearest Neighbour algorithm (k-NN) (3 neighbours to consider) on unstimulated, forskolin-stimulated and staurosporin-treated control groups. The trained classifier was subsequently applied over the test data to classify phenotypic similarities between test compounds and control conditions.

For 4T1 cell tumouroids, Ominer software was used to generate maximum-intensity projections of both Hoechst-33258 and Rhodamine-Phalloidin-derived signals. Phenotypic changes were subsequently quantified using Ominer software as described previously³². The phenotypic measurements were subsequently stored as spreadsheets. Using KNIME Analytics Platform version 3.3.1 for Mac OS X El Capitan, all phenotypic measurements were subsequently Z-score normalized to solvent control (0.1% DMSO). PCA was trained on control conditions (untreated, solvent control, dasatinib, entinostat, excluding several texture- and image moment-related phenotypic parameters: Gabor Wavelets, Zernike Moments and Hu Moments). From the resulting PCA model, 3 principal components (retaining 74% variation) were retained and used for phenotypic classification using k-NN classification integrated in KNIME. The classification algorithm was trained on control conditions (untreated, solvent control, dasatinib, entinostat, sorafenib) using standard settings (3 neighbours to consider) and subsequently applied to classify the test compounds.

Percent-inhibition of cyst growth or viability and classification results are presented using heatmap plots where class or magnitude of inhibition is presented as a colour scale. These plots were generated for presentation purposes of large datasets, using the ggplot2 (<http://ggplot2.org>) package for Rstudio v1.0.136 for Mac OS X El Capitan (<https://www.rstudio.com/products/rstudio>) with R version 3.3.2 for Mac OS X El Capitan (<https://www.r-project.org/>). PCA plots were also made using the ggplot2 package. All other plots were generated using Graphpad Prism 7 (Graphpad Software, La Jolla, California, USA).

RESULTS

Cyst growth can be stimulated by cAMP-enhancing agents and blocked by known cyst growth inhibitors

To identify selective inhibitors of cystogenesis, we followed the workflow presented in supplemental figure 1. First, we further characterized a previously developed model for PKD, to determine whether cyst swelling could be induced by known enhancers and whether this could be inhibited by known inhibitors of cyst growth. We investigated whether cyst growth could be increased by exposure of cysts to forskolin at different concentrations in the absence or presence of an inhibitor of cAMP breakdown, IBMX (3-isobutyl-1-methylxanthine) (figure 1A, left panel). Cyst growth was enhanced relative to solvent control (represented by a dotted line), and was not altered due to the influence of IBMX. Similarly, a membrane-permeable cAMP analogue, 8-Br-cAMP, could enhance cyst swelling on its own, but was much more potent when used in combination with 100 μ M IBMX (figure 1A, middle panel). Prostaglandin E1 can indirectly activate adenylyl cyclases through the prostaglandin receptor, and this also enhanced cyst growth alone and more strongly in combination with IBMX (figure 1A, right panel). For all endpoint conditions, representative images are presented in figure 1B. Cyst swelling induced by forskolin could, in contrast, be inhibited by the actions of compounds that are known to affect pathways involved in cyst growth, such as rapamycin (inhibitor of mammalian target of rapamycin, mTOR³³⁻³⁸), roscovitine (inhibitor of cyclin-dependent kinases; CDK1, CDK2, CDK5, CDK7 and CDK9³⁹⁻⁴²) or sorafenib (sorafenib tosylate, vascular endothelial growth factor receptor (VEGFR)/Raf⁴³⁻⁴⁵) (figure 1C and D).

High-throughput screening of kinase inhibitors identifies inhibitors of forskolin-induced cyst growth

To identify new cyst growth inhibitors and associated molecular targets, we tested a kinase inhibitor library containing 428 kinase inhibitors with varying target specificity for effects on cyst growth. A heat map presenting the known target specificity is included as supplemental figure 2. All compounds were screened at a concentration of 1 μ M, in triplicate wells, in the presence of 2.5 μ M forskolin and subsequently ranked according to their inhibitory potential of cyst growth, as measured by cyst area (figure 2A, 100% inhibition corresponds with unstimulated control and 0% inhibition corresponds with 2.5 μ M forskolin without test compound). Hit compounds were selected that showed $\geq 50\%$ inhibition of cyst growth for the median of triplicate wells, as visualized in figure 2A by the green shade. The selected 99 compounds were re-screened at 1 μ M, 100nM and 10nM in triplicate and cyst growth was scaled between 100% inhibition (unstimulated controls) and 0% inhibition (2.5 μ M forskolin only). DMSO (solvent) was kept at a constant 0.2% throughout all dilutions. The median inhibitory potency of triplicate wells of all compounds is shown in figure 2C as a heatmap, where the colour scale from yellow (no inhibition) to red (strong inhibition of cyst growth) represents the inhibitory potential. Subsequently, 9 of the 99 hits in this secondary screen were rejected as false positives as they failed to inhibit cyst growth by $\geq 50\%$ at 1 μ M (the cut-off in the primary screen, figure 2C, excluded compounds from B shown in red).

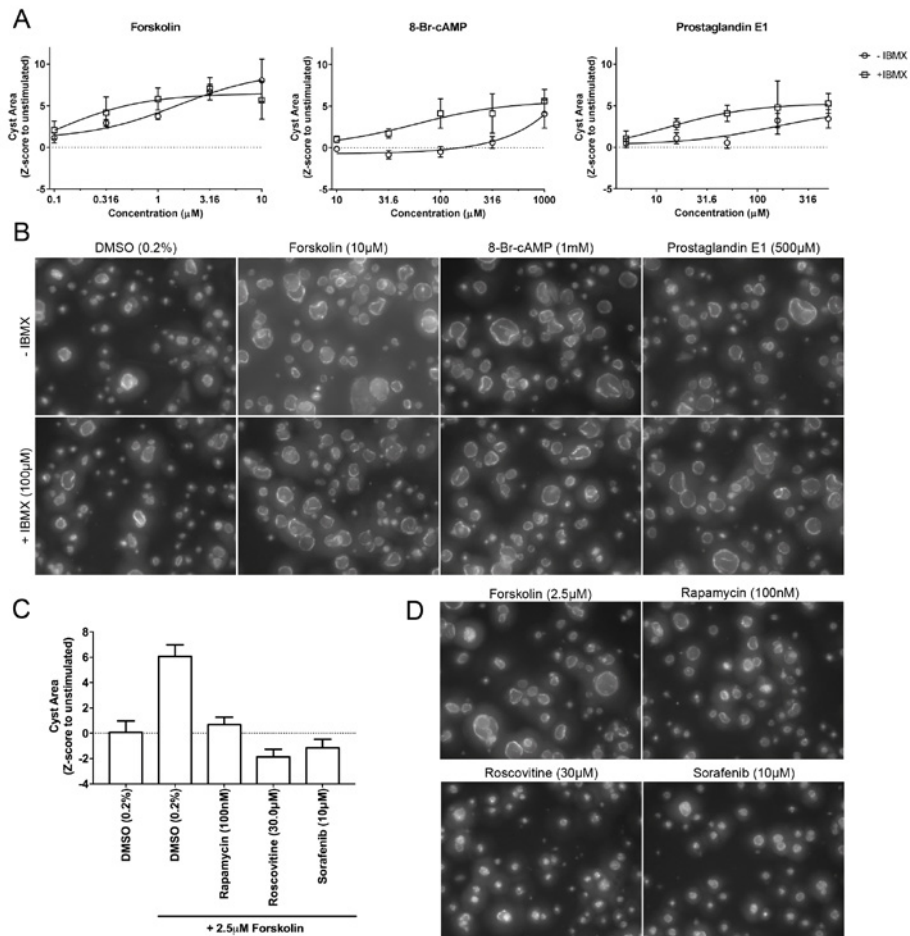


FIGURE 1 Cystogenesis in a 3D-culture assay can be enhanced by cAMP-stimulating agents and inhibited by known inhibitors of cyst growth. **A)** Cystogenesis as measured by cyst size (area) is enhanced as a result of stimulation with forskolin, 8-Br-cAMP or prostaglandin E1 compared to DMSO control, either in the absence of or in the presence of 100 μM IBMX (3-isobutyl-1-methylxanthine). Data points represent mean \pm SD of quadruplicate wells. **B)** Representative images taken with the BD Pathway 855 imager, Filamentous actin (rhodamine-phalloidin) shown. Top panel represents condition without IBMX and bottom panel represents condition with 100 μM IBMX. **C)** Known inhibitors of cyst growth prevent forskolin-induced cyst growth in mIMRFPKD 5E4 cells. Bars represent means \pm SD of ≥ 4 replicate wells. **D)** Representative images taken with the BD Pathway 855 imager from C). Images in B and D are 700x550px cut-out with enhanced contrast and brightness shown for presentation purposes.

Multiparametric phenotypic analysis of cysts can discriminate between effective, ineffective and potentially toxic effects

It is not possible to exclude potentially toxic compounds by solely using a measurement of cyst size. Since phenotypic analysis can visualise diverse phenotypic changes as a result of compound treatment, including those that may be associated with toxicity, a principal components analysis was trained using known control compounds and applied over the validation screen data. Showing the first two principal components, the different control groups can be discriminated clearly (figure 3A). Interestingly, but quite unsurprisingly, 250nM staurosporin (which was included as a positive control for toxicity) induced a phenotypic change different from all other tested control compounds. We subsequently used this information with the K-nearest neighbour algorithm to classify compound effects according to phenotypic similarity with positive- and negative control conditions. We defined three classes: (i) forskolin-stimulated-like compounds, where the phenotype is similar to the condition without compound added; (ii) similar to positive control compounds, where the phenotype is similar to unstimulated controls or rapamycin/roscovitine/sorafenib-treated cysts and where we expect effective and non-toxic compounds; and, (iii) staurosporin-like phenotypes, where we expected most potentially cytotoxic compounds (figure 3B). As all compounds were tested in triplicate, a compound was assigned to a certain class when at least 2/3 replicates were present in that class; this information was subsequently used to generate figure 3C, where the colours represent phenotypic classification. Of interest, compound VCC41 was revealed to be staurosporin, which was included as an internal control compound in the compound library. This internal control was not used to train the classification algorithm, but still classified as ‘staurosporin-like’ at all tested concentrations, illustrating the robustness of this classification.

In order to reveal potential effects on cell viability, the compounds were tested in parallel in 2D-cultured mIMRFNPKD 5E4 cells, and viability was assessed using standard ATPlite assay. This showed that compounds classified as inducing a staurosporin-like phenotypic change also often inhibit viability of 2D cultured cells (figure 3D and supplemental figure 3).

Compounds inducing similar phenotypic changes as staurosporin were considered toxic and excluded from further analysis. Since all compounds may induce toxicity at high doses, compounds that inhibited cyst growth at least two lower concentrations without classifying as ‘staurosporin-like’ were not excluded from further analysis. A few compounds that had previously shown only mild activity at inhibiting cyst growth (<60% inhibition, figure 2B) and also classified as ‘similar to forskolin-treated’ at all tested concentrations in figure 3C (e.g. VCC16, -84), were excluded due to a lack of potency, resulting in 49 compounds remaining (figure 4A-C). While these compounds did not affect phenotypic changes characteristic of cytotoxicity in 3D, cell viability of 2D-cultured mIMRFNPKD 5E4 cells was influenced as measured by ATPlite assay (figure 4B). Because many of the molecules in this kinase library targeted multiple kinases (figure 4C), it is challenging to link 2D cell viability to molecular targets – although some

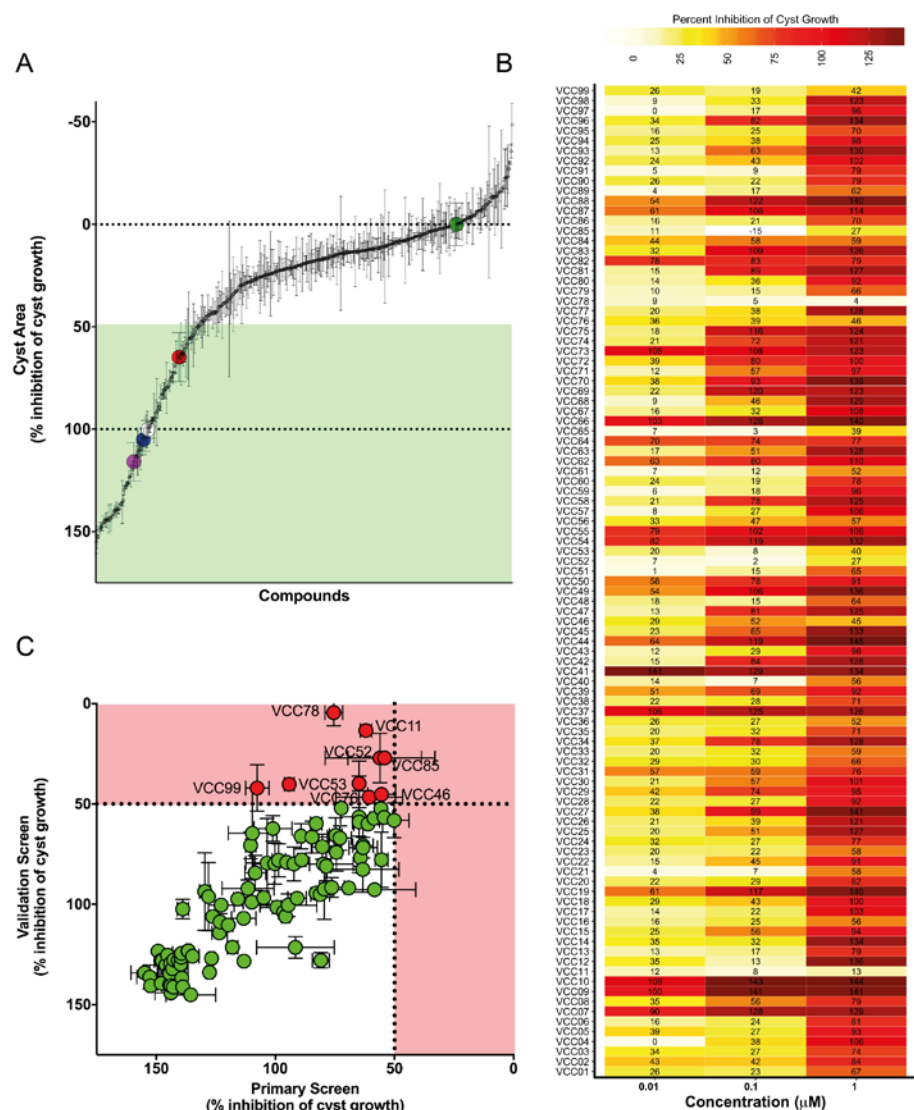


FIGURE 2 Screening a kinase inhibitor library identified inhibitors of cystogenesis. **A)** 428 compounds screened at $1\mu\text{M}$ concentration in triplicate in the presence of $2.5\mu\text{M}$ forskolin, alongside control compounds. Unstimulated control condition (0.2% DMSO, $n=398$) represents 100% cyst growth inhibition and is visualised by a white circle at 100% inhibition. Stimulated controls ($2.5\mu\text{M}$ forskolin, $n=500$) represent 0% inhibition of cyst growth and are visualised by a green circle at 0% inhibition. Positive control compounds that are known to inhibit cyst growth are presented by enlarged circles in purple (roscovitine, $n=24$), blue (sorafenib, $n=24$) and red (rapamycin, $n=24$). All other data points represent median percent inhibition of triplicate wells \pm MAD. Green shaded area contains selected hits (triplicate median $\geq 50\%$ inhibition). (legend continues on next page)

B) 99 selected cyst growth inhibitors rescreened at $1\mu\text{M}$, 100nM and 10nM in triplicate. Median cyst growth inhibitory activity of triplicate wells is presented as a heatmap with colour scale from light yellow (no inhibition) to bright red (strong inhibition). Percent inhibition of cyst growth is included as numeric value in the heatmap plot. **C)** Comparison of compound activity between primary screen and validation screen at $1\mu\text{M}$ concentration. 9 compounds failed to show sufficient activity ($\geq 50\%$ inhibition) and were therefore excluded from further analysis. Data points represent median values of primary- and validation screen. Horizontal error bars represent MAD from primary screen and vertical error bars represent MAD from validation screen. Included compounds shown as green circles; compounds excluded shown as red circles.

molecules (e.g. VCC50) that cause a reduction of cell viability also target a wider range of different kinases. Since the 3D cyst assay did not indicate potential cytotoxic effects of these molecules, we reasoned that these effects may be specific to 2D-cultured cells and therefore decided to use a different 3D assay for the prioritization of compounds.

Counter-screening with 3D-cultured 4T1 breast cancer cells to select selective inhibitors of cystogenesis

To discriminate compounds that have an effect on cyst swelling from more general processes that may affect cyst size, such as proliferation and cell adhesion, we also screened the same kinase inhibitor library on a 3D cancer cell invasion model.²⁹ Compounds that inhibited cyst swelling but did not induce changes in the morphology of 4T1 breast cancer cells cultured in 3D (which do not form cystic structures), were classified as inhibitors of cyst growth independent of more general cellular processes.

Figure 5A shows representative images of 3D-cultured 4T1 cells under control conditions. Consistent with previous results,¹⁴ unstimulated and solvent control conditions revealed small clumps of 4T1 cells expressing ('invasive') branching morphology. In contrast, dasatinib-treated 4T1 cells failed to invade into the surrounding matrix and formed round multicellular spheroids. Sorafenib and entinostat similarly prevented branching morphogenesis, but probably inhibited the growth rate of these spheroidal clumps as judged by reduced structure size.

Analogous to the multiparametric classification approach followed for mIMRFNP-KD 5E4-based analysis, we trained a PCA on 4T1 control phenotypes (first two principal components shown in figure 5B, showing all data points), and subsequently used the K-nearest neighbour algorithm to classify all data points according to the control classes. The trained cluster algorithm was subsequently applied over the Vichem compounds as shown in figure 5C (circles represent median of quadruplicate wells). This showed that a large proportion of the screened compounds affected 4T1 phenotypes. From these compounds, we further analysed those that were previously identified as inhibitors of cystogenesis as shown in figure 4A. The classification of these compounds according to efficacy on 4T1 cells is presented in figure 5D, and the corresponding PCA

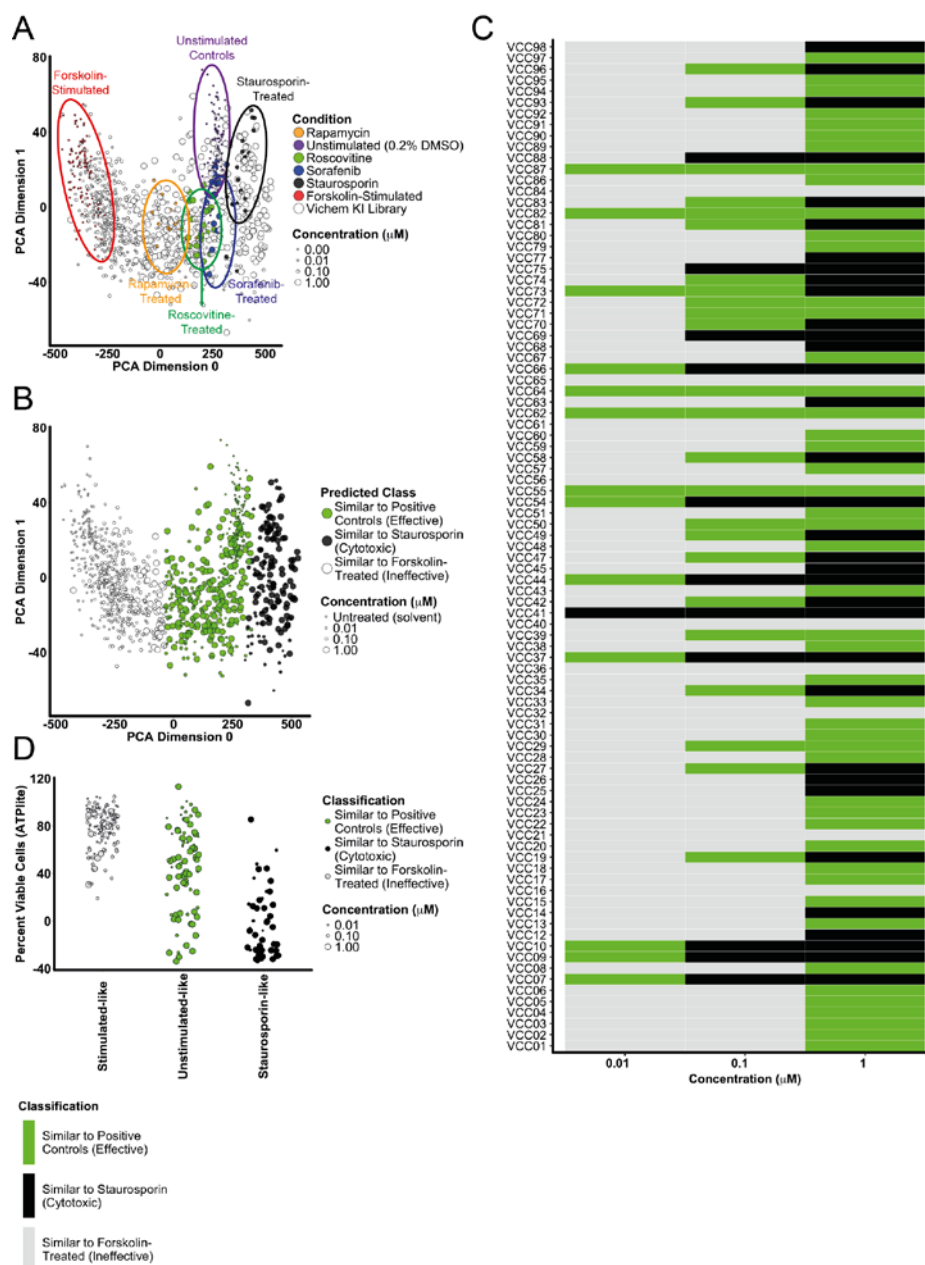


FIGURE 3 Phenotypic classification can be used to identify effective and non-toxic compounds. **A**) PCA was trained on control groups (marked by circles in plot) and subsequently applied to the full dataset. Phenotypic space separates unstimulated (purple) and other positive control compounds (rapamycin, roscovitine, sorafenib) from stimulated (red) controls. Circles represent individual wells. First two principal components shown **B**) K nearest neighbour classification using the first three principal (legend continues on next page)

components discriminates effective (green), ineffective (white), and cytotoxic (black) compounds. Circles represent individual wells. First two principal components shown for presentation purposes. **C)** Heat map showing classification of compounds when $\geq 2/3$ replicates belong to that class. Black colour represents cytotoxic compounds, green represents efficacy and light grey colour represents inactive. **D)** ATPlite measurement of 2D-cultured mIMRFNPKD 5E4 cells after compound classification. Staurosporin-like data points more often inhibit viability.

plot is shown as figure 5E. Several of the inhibitors of cystogenesis that were identified using mIMRFNPKD 5E4 cells also apparently affected 4T1 cell morphology. Therefore, in order to select solely compounds that affected cystogenesis but not 4T1 phenotype, we selected for compounds that could inhibit cystogenesis at concentrations where 4T1 phenotype was unaffected. This stringent selection resulted in 22 compounds that potentially inhibited cyst growth, but did not affect the phenotype of 4T1 cells in 3D. Although many of these compounds did not have targets described with IC₅₀'s below micromolar range, six inhibitors targeted various CDKs, whereas others dual-targeted Akt1/ IGF1R, phosphatidylinositol-4,5-bisphosphate 3-kinase (PI3K)/Akt1 or GSK3-alpha/beta and CDKs (Table 1).

Prioritization of selected compounds using 2D cell viability measurements

Since the compounds that were selected to solely inhibit cyst growth, but not change 4T1 phenotypes may still inhibit 2D cell viability, we plotted dose curves of cyst growth and 2D viability for all selected compounds (supplemental figure 4). Thereafter, we made a selection of compounds for which target information was known and that did not lower 2D cell viability below 50% of control. Figure 6A shows images of mIMRFNPKD 5E4 cysts under control conditions (upper panel) and exposed to test compounds at three concentrations (lower panel). Since these compounds were selected on the condition that 4T1 morphology was not influenced, we provide image data of compound-treated and solvent-treated 4T1 cells in figure 6B. Under solvent conditions, 4T1 cell clumps displayed invasive branching morphology, which was not altered after exposure to VCC03, -18, -23, -55, -73 and -91 at any of the concentrations shown here. VCC55 affected 4T1 morphology at concentrations above 100nM, which was indeed consistent with our phenotypic classification shown in figure 5E. Similarly, VCC73 inhibited cyst growth without affecting 4T1 morphology at 10nM, but affected both 2D cell viability and 4T1 morphology at concentrations ≥ 100 nM.

Discussion and conclusions

To find selective inhibitors of cyst growth and relate compound efficacy to molecular targets, we screened a kinase inhibitor library using a screening platform that uses mIMRFNPKD 5E4 cells as a model of cystogenesis.²⁸ Cyst growth could be enhanced by exposure of these cells to cAMP-enhancing compounds such as forskolin and prostaglandin E1. In addition, cyst growth could be enhanced by membrane permeable 8-Br-cAMP, indicating that the increase in cyst growth is indeed due to increased levels

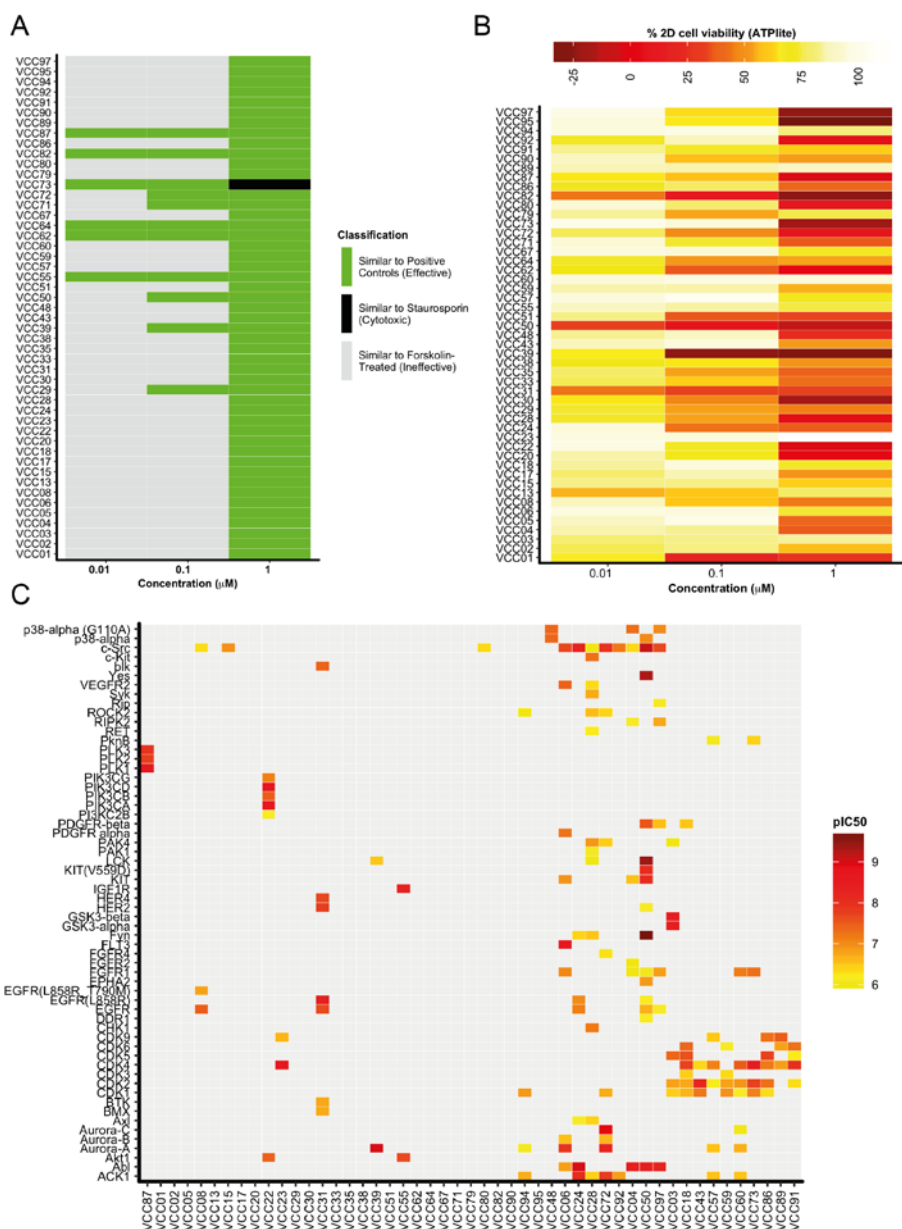


FIGURE 4 Compounds that show low toxicity in 3D cultured mIMRFNPKD 5E4 cells have broad target space. **A)** Selection of compounds from 3C that do not induce staurosporin-like phenotypic changes. Selection criteria: (i) non-staurosporin-like at any concentration or (ii) if at any concentration staurosporin-like, also effective at two lower concentrations ($\geq 2/3$ or replicates for all criteria). **B)** 2D ATPlite on mIMRFNPKD 5E4 represented by yellow to red colour scale. While these compounds do not show toxicity in 3D cysts, they may affect 2D viability. **C)** Target spectrum belonging to (legend continues on next page)

compounds shown in A. pIC₅₀ shown as colour scale from yellow (μ M IC₅₀) to red (\leq nM IC₅₀). Unknown target specificity represented by grey background colour. IC₅₀ values $>1\mu$ M excluded from this list and presented as grey colour.

of intracellular cAMP, in line with previous findings.⁴⁶ As expected, inhibitors that disrupted pathways important in PKD, such as mammalian target of rapamycin (mTOR)³⁴⁻³⁸ (rapamycin), CDKs³⁹⁻⁴¹ (roscovitine) and vascular endothelial growth factor receptor (VEGFR)/Raf⁴³⁻⁴⁵ (sorafenib), also inhibited cyst growth in our model, consistent with our previous observations.²⁸ After assay characterisation, we screened a kinase inhibitor library of 428 compounds to identify cyst growth inhibitors and relate activity to molecular targets. From our screen, we selected 99 cyst growth-inhibiting compounds that were re-screened at three concentrations, confirming the efficacy of 90/99 compounds. The identification of such a large number of effective cyst growth inhibitors was not entirely surprising, since many compounds in the library were either multikinase inhibitors and/or inhibitors of various CDKs at the tested concentrations and had overlapping kinases among their targets.

In order to exclude potentially cytotoxic compounds, we further analysed the phenotypic changes that occurred in mIMRFNPKD 5E4 cysts after compound exposure. Staurosporin is a known inducer of cell death by apoptosis⁴⁷ due to its inhibition of multiple kinases,⁴⁸ and was therefore included as a positive control for cytotoxicity in our screen, since we reasoned that compounds similar to staurosporin are unlikely to become a drug for PKD. We could therefore classify the phenotypic changes as ‘staurosporin-like’, ‘similar to positive control’ or as ‘similar to forskolin-treated’. Many compounds classifying as ‘staurosporin-like’ also lowered cell viability in 2D culture, supporting this toxic classification. Upon prioritisation of compounds that did not induce phenotypic changes associated with staurosporin-like toxicity, we noticed that many of the selected compounds inhibit targets that were previously considered to play a role in cystogenesis. For example, VCC31 inhibited HER2, which was previously implicated in PKD⁴⁹ as well as epidermal growth factor receptor (EGFR)⁵⁰ at the tested concentrations, and VCC55 inhibited the IGF1R, a target previously identified as potential mediator of cyst growth⁵¹⁻⁵² and Akt1. To our surprise, many multikinase inhibitors such as VCCo6, -24, -28, -72, or -50 also showed potent efficacy at inhibiting cyst growth, while not causing detectable cytotoxicity in our 3D cyst assay.

Because we used staurosporin as a model compound for cytotoxicity, our phenotypic classification of cytotoxicity is limited to the morphological characteristics we observed of staurosporin-treated cysts. We cannot exclude the possibility that cellular toxicity is exerted through multiple different phenotypic changes, and it is therefore unclear how this classification would perform in the identification of toxic compounds that have a different mechanism of general toxicity compared to staurosporin (e.g. inhibiting survival signalling). This may explain our observation that some compounds impaired viability of 2D-cultured cells, while no toxicity was observed in 3D-cultured

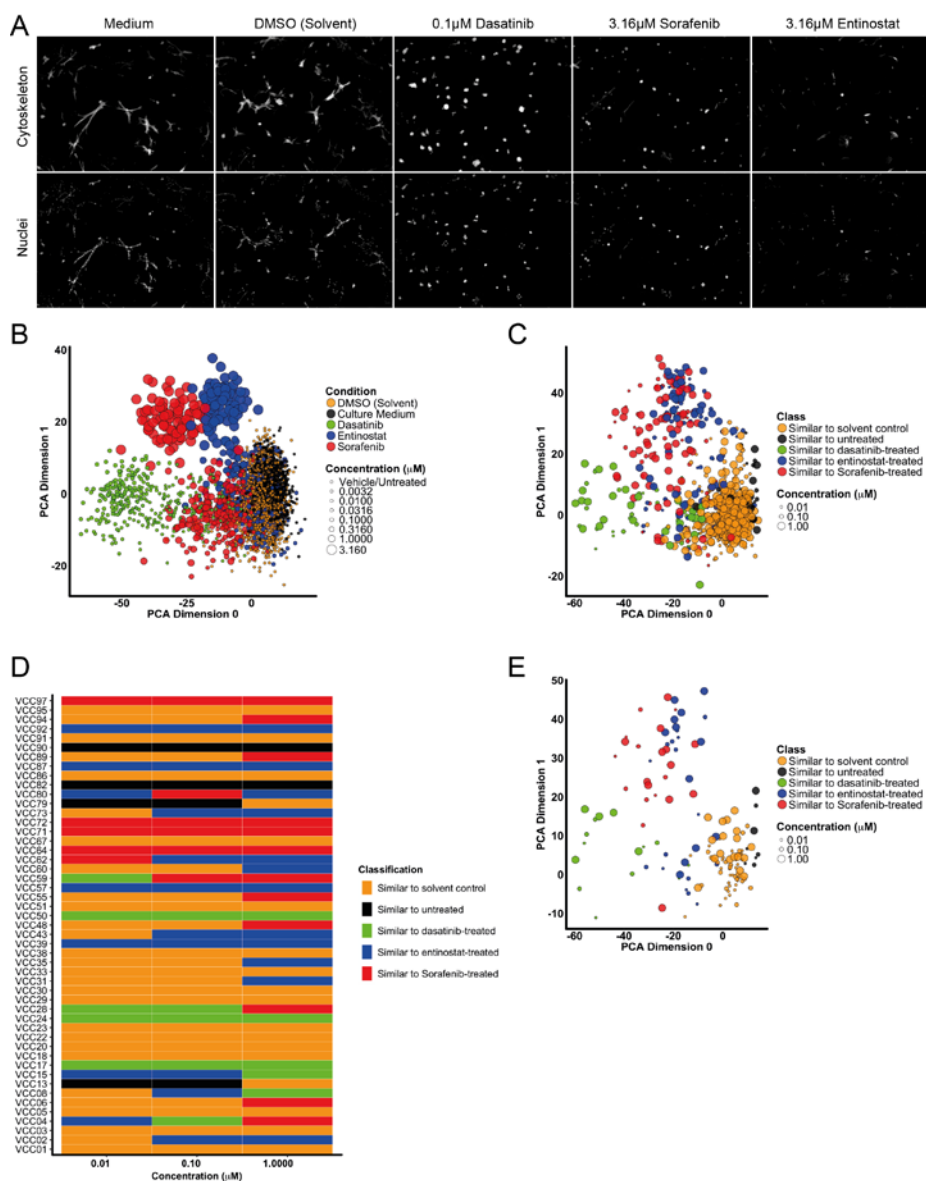


FIGURE 5 Counter screening with 4T1 tumour cells identifies selective inhibitors of cystogenesis. **A)** Representative images of 4T1 under control conditions obtained with the BD Pathway 855 imager. Contrast and brightness were enhanced for presentation purposes. **B)** Control compounds can be discriminated using PCA analysis. Two principal components (67% of variation) shown for presentation purposes. Circles represent individual wells. **C)** 428 Vichem compounds (at 1µM, 100nM and 10nM) classified using K nearest neighbour classification trained on control compounds using PCA. Two principal components (67% of variation) shown for presentation (legend continues on next page)

purposes. Circles represent median values of quadruplicate wells. **D)** Heatmap plot with classification of compounds shown in figure 4A. **E)** PCA plot as in figure C, but showing only molecules presented in figure D (molecules that inhibited cyst growth in our PKD assay). Circles represent median of quadruplicate wells and circle size corresponds to concentration.

TABLE 1 Hit compounds inhibiting cystogenesis but not affecting tumour cell invasion: described targets with $pIC_{50} > 6.0$

<i>VCCID</i>	<i>Target 1</i> (<i>pIC</i> 50)	<i>Target 2</i> (<i>pIC</i> 50)	<i>Target 3</i> (<i>pIC</i> 50)	<i>Target 4</i> (<i>pIC</i> 50)	<i>Target 5</i> (<i>pIC</i> 50)	<i>Target 6</i> (<i>pIC</i> 50)	<i>Target 7</i> (<i>pIC</i> 50)
<i>VCC01</i>	-	-	-	-	-	-	-
<i>VCC03</i>	GSK3- alpha (8.4)	GSK3-beta (8.4)	CDK5 (7.4)	CDK2 (6.8)	CDK1 (6.44)	PAK4 (6.01)	-
<i>VCC05</i>	-	-	-	-	-	-	-
<i>VCC13</i>	-	-	-	-	-	-	-
<i>VCC18</i>	CDK4 (7.73)	CDK5 (7.59)	CDK6 (7.36)	CDK2 (6.73)	CDK1 (6.63)	PDGFR- beta (6.5)	CDK3 (6.44)
<i>VCC20</i>	-	-	-	-	-	-	-
<i>VCC22</i>	PIK3CA (8.52)	PIK3CD (8.52)	PIK3CB (7.48)	Akt1 (7.44)	PIK3CG (7.12)	PI3KC2B (6.17)	-
<i>VCC23</i>	CDK4 (8.62)	CDK9 (6.63)	-	-	-	-	-
<i>VCC29</i>	-	-	-	-	-	-	-
<i>VCC30</i>	-	-	-	-	-	-	-
<i>VCC33</i>	-	-	-	-	-	-	-
<i>VCC38</i>	-	-	-	-	-	-	-
<i>VCC51</i>	-	-	-	-	-	-	-
<i>VCC55</i>	IGF1R (8.3)	Akt1 (7.66)	-	-	-	-	-
<i>VCC67</i>	-	-	-	-	-	-	-
<i>VCC73</i>	CDK4 (8.4)	CDK2 (7.76)	FGFR1 (7.29)	CDK1 (7.1)	PknB (6.4)	-	-
<i>VCC79</i>	-	-	-	-	-	-	-
<i>VCC82</i>	-	-	-	-	-	-	-
<i>VCC86</i>	CDK5 (7.74)	CDK2 (7.28)	CDK9 (7.28)	CDK4 (7.17)	CDK1 (6.31)	-	-
<i>VCC90</i>	-	-	-	-	-	-	-
<i>VCC91</i>	CDK4 (7.96)	CDK6 (7.26)	CDK2 (6.31)	CDK5 (6.21)	-	-	-
<i>VCC95</i>	-	-	-	-	-	-	-

cysts (e.g. VCC50) – although this could also be explained by the large differences between 3D- and 2D cell cultures.^{15, 17} Another limitation associated with the classification of cytotoxicity according to staurosporin-treated cysts, as we performed here, is that we only assessed cytotoxicity on one cell type. Because tissues in the human body are constructed of a tightly regulated functional network of many different cell types and surrounding matrix, it is unclear how our observations relate to the organ toxicity that often causes drug withdrawal. An interesting approach to mapping these phenotypic effects of different toxic chemicals across different cell types, would be to compose a compound library containing compounds with various different mechanisms of cellular toxicity (such as inhibitors of cell cycle progression, inhibitors of survival signalling pathways, DNA-damaging agents or chemicals interfering with energy metabolism). This would enable the classification of the resulting phenotypic changes across multiple cell types (e.g. hepatocytes, cardiomyocytes, endothelial cells, or even co-cultures). Such an effort could potentially alleviate the requirement of performing viability measurements in 2D-cultured cells in parallel. Additionally, mapping the phenotypic alterations that occur from different cytotoxic compounds could contribute to classification of (cytotoxic) compounds in compound libraries other than the screened kinase inhibitor library, and help in the pre-selection of better drugs.

To filter out compounds that may affect other processes than cyst swelling, we therefore performed a counter-screen of the same compound library in a 4T1-cell based tumour invasion assay. This allowed us to prioritise compounds that affected mIMRFNPKD 5E4 cyst growth, but not 4T1 growth and invasion. Importantly, activity of a compound on 4T1 growth and invasion does not necessarily exclude the potential for it to be useful as a treatment against PKD, as cyst growth is also, at least in part, the result of increased proliferation and changes in cell polarity.⁵³ As a result of this stringent prioritization on 4T1 morphology, we selected 22 compounds that interfered solely with forskolin-induced cyst swelling, but not with 4T1 morphology, although potential false-negatives in our 4T1 counter screen were not taken into consideration. Interestingly, this selection caused exclusion of compounds VCCo6, -24, -28, -72 and -50, that were mentioned above as multikinase inhibitors. It is likely that these compounds affected both cystogenesis and 4T1 morphology due to their ability to affect multiple kinases and pathways.

Out of the 22 compounds that were classified as selective cyst growth inhibitors, molecular targets and IC₅₀ values were pre-determined only for 8 compounds (Table 1). An interesting observation is that many of these compounds inhibited various cyclin-dependent kinases (CDKs), such as VCCo3, -18, -23, -73, -86 and VCC91, which is also corresponds with our previous results.²⁸ These compounds generally inhibited CDKs involved in transition through the different phases of the cell-division cycle (CDK1, CDK2, CDK4 and CDK6), or in the case of VCC23 and VCC86, also inhibit CDK9, which can phosphorylate RNA polymerase II, thereby modulating transcription.⁵⁴ Additionally, inhibitory activity towards CDK5 (VCCo3, -18, -86 and -91) may be of particular interest in PKD due to its involvement in regulating ciliary length and cystic

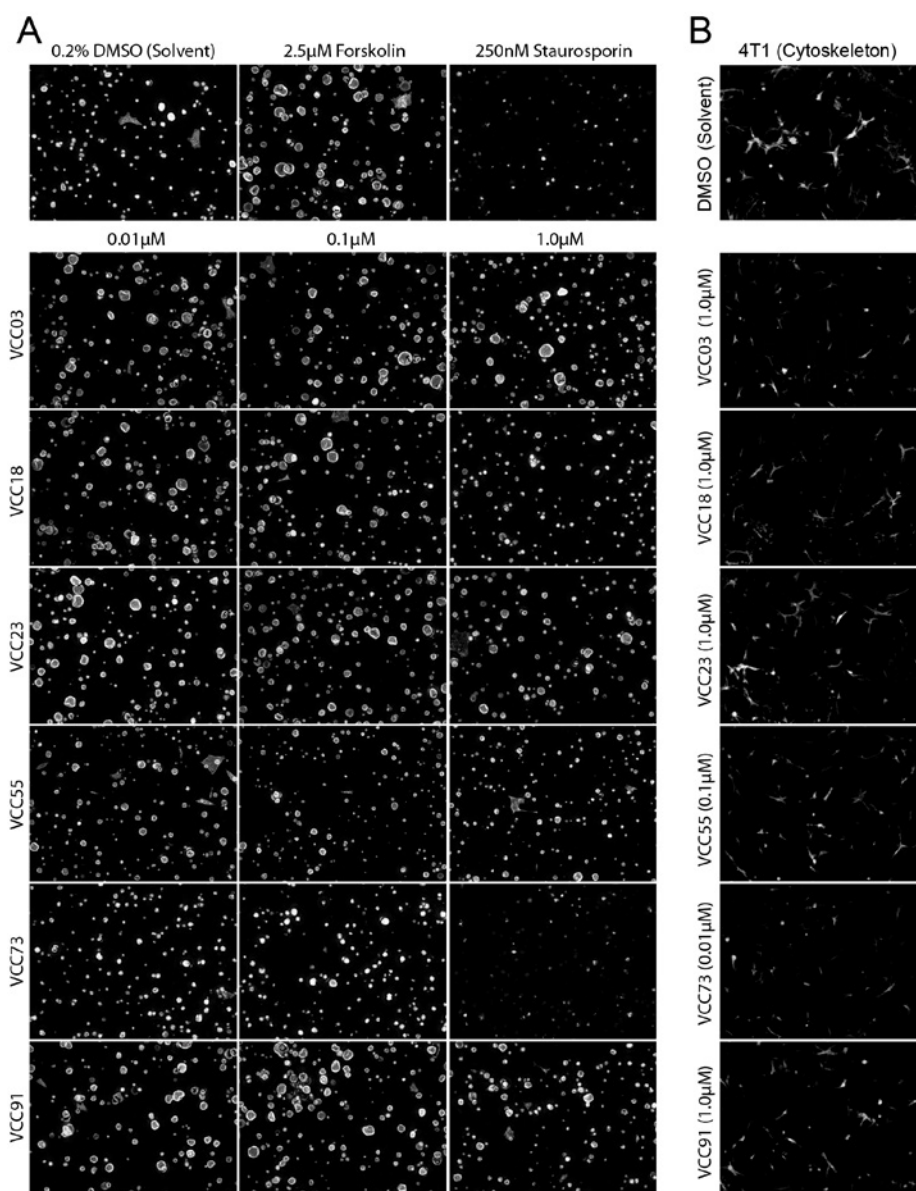


FIGURE 6 Several compounds inhibit cystogenesis without affecting 4T1 phenotype. **A)** Representative images of control conditions (upper panel) and VCC03, VCC18, VCC23, VCC55, VCC73 and VCC91 in three different concentrations (lower panel). Images were taken using an ImageXpress Micro XLS imager. 600x450px cut-out shown of cytoskeleton images. Contrast and brightness are enhanced for presentation purposes. **B)** Representative images of 4T1 phenotype after exposure to compounds from A. Images taken with a BD Pathway 855 imager. Cytoskeleton shown and contrast and brightness increased for presentation purposes.

disease progression.⁵⁵ Likewise, CDK inhibitors such as roscovitine and CR8 have been assessed for efficacy in PKD models on several occasions,⁴⁰⁻⁴¹ these tests have not culminated in clinical trials due to safety with these anticancer drugs for long-term treatment of PKD.⁵⁶⁻⁵⁷ It is also important to note that while many CDK inhibitors were found to be active without causing obvious toxicity in this assay, many other CDK inhibitors were excluded on the basis of toxicity and/or effects on 4T1 cells. Because cell proliferation is an important contributor to cyst growth, inhibition of CDKs for the treatment of PKD may be attractive if, for example, renal targeting can be achieved, if the dosage required to prevent cyst swelling is not associated with side effects, or if more selective CDK inhibitors can be used against CDKs directly implicated in the signalling of polycystin proteins or cystic disease (such as CDK2⁵⁸ or CDK5⁵⁵). In addition to CDKs, some compounds also targeted fibroblast growth factor receptor 1 (FGFR1, VCC73) or platelet-derived growth factor receptor-beta (PDGFR-beta, VCC18) which are potentially involved in deciliation and could therefore have relevance to cyst formation,⁵⁹⁻⁶⁰ although it is currently uncertain if these receptors are expressed in mIMRFNPKD 5E4 cells. However, because these two compounds also potently inhibited various CDKs, it is more likely that the observed effects of these compounds were exerted through CDKs, rather than through FGFR1 or PDGFR-beta. Similarly, VCCo3, in addition to targeting several CDKs, is also known to inhibit GSK3 α/β . GSK3 β has been described to be involved in ciliary maintenance,⁶¹ although GSK3-targeted therapy is also likely to affect multiple tissues and may have side effects in different organs.⁶²

Interestingly, we found one molecule (VCC55) that inhibited both IGF1R and Akt1. The involvement of IGF1R in cystogenesis was previously reported⁶³ and is also in line with our previous findings.³² However, we also observed potent inhibitory activity in the micromolar range of one PI3K/Akt inhibitor, VCC22, which contradicts our previous findings where we screened a panel of PI3K inhibitors and failed to observe a potent effect.²⁸ Because VCC22 has a high affinity for Akt1 (pIC₅₀ of 7.44), a potential explanation for its efficacy is that the observed effects of this compound are mediated through Akt-mTOR, rather than through PI3K. An additional interesting finding was that many compounds inhibiting targets previously implicated in PKD, such as the vascular endothelial growth factor receptor (VEGFR),⁶⁴ EGFR⁵⁰ and Aurora A kinase,⁶⁵⁻⁶⁶ were not selected as selective inhibitors of cyst growth, since these inhibitors often also influenced 4T1 cell morphology or lacked efficacy altogether. While currently the compounds that were identified as selective cyst growth inhibitors in our assays do not reveal new targets to modulate cyst growth, full characterisation of the compounds with undescribed target specificity could elucidate the mechanistic effects that reduced cyst growth.

Because the 22 compounds we described were identified using a PKD assay that uses a murine cell line (mIMRFNPKD 5E4), it is necessary to validate the efficacy of these molecules in a human PKD model. A possibility for this validation is to use a human kidney cell line, although ideally this should be performed using primary human cystic tissue. Such an effort could be used to exclude the possibility that the identified molecules show preferential inhibition in murine cell lines and account for differences

in receptor specificity between murine and human cells.

In conclusion, by testing a kinase inhibitor library using phenotypic screening on 3D-cultured cysts we identified inhibitors of cyst growth, that could be classified according to their predicted toxic effects. Upon counter-selection in a second 3D cell culture model using 4T1 tumour cells, selective inhibitors of cyst growth could be identified based on lack of activity towards 4T1 cells. These compounds are known to target CDKs, IGF1R and others, and future research should focus on the elucidation of the mechanism of action of those compounds where target specificity is currently unknown, in order to potentially identify new modulators of cystogenesis.

Acknowledgments

The authors would like to thank our collaborators at Vichem Chemie Research Ltd, Hungary for providing a small-molecule compound library and target selectivity profiles.

Funding statement

T.H. Booij was supported by the Dutch Technology Foundation STW, project 11823. STW is part of NWO (Netherlands Organization for Scientific Research). The other authors received no financial support for the research or authorship.

Statement of conflicting interests

Leo S. Price is founder and major shareholder of Ocello B.V., a company that provides 3D tissue culture-based screening services. Kuan Yan and Hester Bange are employees of Ocello B.V. The other authors declared no potential conflicts of interest with respect to research or authorship.

References

1. Willey CJ, Blais JD, Hall AK, Krasa HB, Makin AJ, Czerwiec FS: Prevalence of autosomal dominant polycystic kidney disease in the European Union. *Nephrology, dialysis, transplantation : official publication of the European Dialysis and Transplant Association - European Renal Association*, 2016
2. Sommerer C, Zeier M: Clinical Manifestation and Management of ADPKD in Western Countries. *Kidney diseases (Basel, Switzerland)* 2(3): 120-127, 2016
3. Ong AC, Harris PC: A polycystin-centric view of cyst formation and disease: the polycystins revisited. *Kidney international* 88(4): 699-710, 2015
4. Seeger-Nukpezah T, Geynisman DM, Nikonova AS, Benzing T, Golemis EA: The hallmarks of cancer: relevance to the pathogenesis of polycystic kidney disease. *Nature reviews Nephrology* 11(9): 515-534, 2015
5. Saigusa T, Bell PD: Molecular pathways and therapies in autosomal-dominant polycystic kidney disease. *Physiology (Bethesda, Md)* 30(3): 195-207, 2015
6. Baur BP, Meaney CJ: Review of tolvaptan for autosomal dominant polycystic kidney disease. *Pharmacotherapy* 34(6): 605-616, 2014

7. Higashihara E, Torres VE, Chapman AB, Grantham JJ, Bae K, Watnick TJ, Horie S, Nutahara K, Ouyang J, Krasa HB, Czerwiec FS: Tolvaptan in autosomal dominant polycystic kidney disease: three years' experience. *Clinical journal of the American Society of Nephrology : CJASN* 6(10): 2499-2507, 2011
8. Torres VE, Chapman AB, Devuyst O, Gansevoort RT, Grantham JJ, Higashihara E, Perrone RD, Krasa HB, Ouyang J, Czerwiec FS: Tolvaptan in patients with autosomal dominant polycystic kidney disease. *The New England journal of medicine* 367(25): 2407-2418, 2012
9. Woodhead JL, Brock WJ, Roth SE, Shoaf SE, Brouwer KL, Church R, Grammatopoulos TN, Stiles L, Siler SQ, Howell BA, Mosedale M, Watkins PB, Shoda LK: Application of a Mechanistic Model to Evaluate Putative Mechanisms of Tolvaptan Drug-Induced Liver Injury and Identify Patient Susceptibility Factors. *Toxicological sciences : an official journal of the Society of Toxicology* 155(1): 61-74, 2017
10. Watkins PB, Lewis JH, Kaplowitz N, Alpers DH, Blais JD, Smotzer DM, Krasa H, Ouyang J, Torres VE, Czerwiec FS, Zimmer CA: Clinical Pattern of Tolvaptan-Associated Liver Injury in Subjects with Autosomal Dominant Polycystic Kidney Disease: Analysis of Clinical Trials Database. *Drug safety* 38(11): 1103-1113, 2015
11. Fang JL, Wu Y, Gamboa da Costa G, Chen S, Chitranshi P, Beland FA: Human Sulfotransferases Enhance the Cytotoxicity of Tolvaptan. *Toxicological sciences : an official journal of the Society of Toxicology* 150(1): 27-39, 2016
12. Nagao S, Kugita M, Yoshihara D, Yamaguchi T: Animal models for human polycystic kidney disease. *Experimental animals* 61(5): 477-488, 2012
13. Torres VE, Harris PC: Polycystic kidney disease: genes, proteins, animal models, disease mechanisms and therapeutic opportunities. *Journal of internal medicine* 261(1): 17-31, 2007
14. Wilson PD: Mouse models of polycystic kidney disease. *Current topics in developmental biology* 84 311-350, 2008
15. Debnath J, Brugge JS: Modelling glandular epithelial cancers in three-dimensional cultures. *Nature reviews Cancer* 5(9): 675-688, 2005
16. Fischbach C, Chen R, Matsumoto T, Schmelzle T, Brugge JS, Polverini PJ, Mooney DJ: Engineering tumors with 3D scaffolds. *Nature methods* 4(10): 855-860, 2007
17. Birgersdotter A, Sandberg R, Ernberg I: Gene expression perturbation in vitro - a growing case for three-dimensional (3D) culture systems. *Seminars in cancer biology* 15(5): 405-412, 2005
18. Benam KH, Dauth S, Hassell B, Herland A, Jain A, Jang KJ, Karalis K, Kim HJ, MacQueen L, Mahmoodian R, Musah S, Torisawa YS, van der Meer AD, Villenave R, Yadid M, Parker KK, Ingber DE: Engineered in vitro disease models. *Annual review of pathology* 10 195-262, 2015
19. Desrochers TM, Palma E, Kaplan DL: Tissue-engineered kidney disease models. *Advanced drug delivery reviews* 69-70 67-80, 2014
20. Santo VE, Rebelo SP, Estrada MF, Alves PM, Boghaert E, Brito C: Drug screening in 3D in vitro tumor models: overcoming current pitfalls of efficacy read-outs. *Biotechnology journal* 12(1), 2017

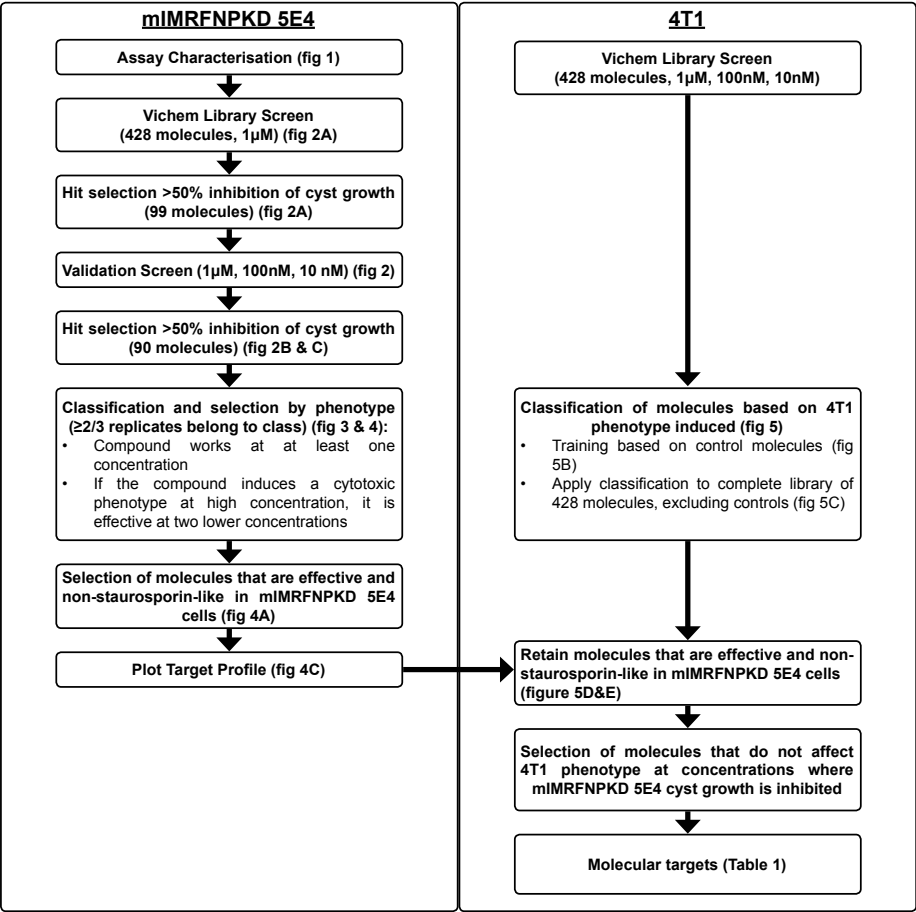
21. Kimlin L, Kassiss J, Virador V: 3D in vitro tissue models and their potential for drug screening. *Expert opinion on drug discovery* 8(12): 1455-1466, 2013
22. DesRochers TM, Suter L, Roth A, Kaplan DL: Bioengineered 3D human kidney tissue, a platform for the determination of nephrotoxicity. *PloS one* 8(3): e59219, 2013
23. Fuchs TC, Hewitt P: Biomarkers for drug-induced renal damage and nephrotoxicity-an overview for applied toxicology. *The AAPS journal* 13(4): 615-631, 2011
24. Lazarou J, Pomeranz BH, Corey PN: Incidence of adverse drug reactions in hospitalized patients: a meta-analysis of prospective studies. *Jama* 279(15): 1200-1205, 1998
25. Uetrecht J, Naisbitt DJ: Idiosyncratic adverse drug reactions: current concepts. *Pharmacological reviews* 65(2): 779-808, 2013
26. Horvath P, Aulner N, Bickle M, Davies AM, Nery ED, Ebner D, Montoya MC, Ostling P, Pietiainen V, Price LS, Shorte SL, Turcatti G, von Schantz C, Carragher NO: Screening out irrelevant cell-based models of disease. *Nature reviews Drug discovery* 15(11): 751-769, 2016
27. Tsai SQ, Wyvekens N, Khayter C, Foden JA, Thapar V, Reyon D, Goodwin MJ, Aryee MJ, Joung JK: Dimeric CRISPR RNA-guided FokI nucleases for highly specific genome editing. *Nature biotechnology* 32(6): 569-576, 2014
28. Booij TH, Bange H, Leonhard WN, Yan K, Fokkelman M, Kunnen SJ, Dauwerse JG, Qin Y, van de Water B, van Westen GJP, Peters DJM, Price LS: High-Throughput Phenotypic Screening of Kinase Inhibitors to Identify Drug Targets for Polycystic Kidney Disease. *SLAS Discov* 2472555217716056, 2017
29. Di Z, Klop MJ, Rogkoti VM, Le Devedec SE, van de Water B, Verbeek FJ, Price LS, Meerman JH: Ultra high content image analysis and phenotype profiling of 3D cultured micro-tissues. *PloS one* 9(10): e109688, 2014
30. Gyorgy K, Laszlo O, Daniel E, Balint H-B, Csaba S-K, Zoltan H, Frigyes W, Jenő M, Istvan S, Janos P, Zoltan G, Doris H, Henrik D, Gerhard M, Bert K, Axel U: Signal Transduction Therapy with Rationally Designed Kinase Inhibitors. *Current Signal Transduction Therapy* 1(1): 67-95, 2006
31. Keri G, Szekelyhidi Z, Banhegyi P, Varga Z, Hegymegi-Barakonyi B, Szantai-Kis C, Hafenbradl D, Klebl B, Muller G, Ullrich A, Eros D, Horvath Z, Greff Z, Marosfalvi J, Pato J, Szabadkai I, Szilagyi I, Szegedi Z, Varga I, Waczek F, Orfi L: Drug discovery in the kinase inhibitory field using the Nested Chemical Library technology. *Assay Drug Dev Technol* 3(5): 543-551, 2005
32. Booij TH, Klop MJ, Yan K, Szantai-Kis C, Szokol B, Orfi L, van de Water B, Keri G, Price LS: Development of a 3D Tissue Culture-Based High-Content Screening Platform That Uses Phenotypic Profiling to Discriminate Selective Inhibitors of Receptor Tyrosine Kinases. *Journal of biomolecular screening* 21(9): 912-922, 2016
33. Edwards SR, Wandless TJ: The rapamycin-binding domain of the protein kinase mammalian target of rapamycin is a destabilizing domain. *J Biol Chem* 282(18): 13395-13401, 2007

34. Shillingford JM, Murcia NS, Larson CH, Low SH, Hedgepeth R, Brown N, Flask CA, Novick AC, Goldfarb DA, Kramer-Zucker A, Walz G, Piontek KB, Germino GG, Weimbs T: The mTOR pathway is regulated by polycystin-1, and its inhibition reverses renal cystogenesis in polycystic kidney disease. *Proc Natl Acad Sci U S A* 103(14): 5466-5471, 2006
35. Novalic Z, van der Wal AM, Leonhard WN, Koehl G, Breuning MH, Geissler EK, de Heer E, Peters DJ: Dose-dependent effects of sirolimus on mTOR signaling and polycystic kidney disease. *Journal of the American Society of Nephrology : JASN* 23(5): 842-853, 2012
36. Kim HJ, Edelstein CL: Mammalian target of rapamycin inhibition in polycystic kidney disease: From bench to bedside. *Kidney research and clinical practice* 31(3): 132-138, 2012
37. Lieberthal W, Levine JS: Mammalian target of rapamycin and the kidney. I. The signaling pathway. *American journal of physiology Renal physiology* 303(1): F1-10, 2012
38. Ren XS, Sato Y, Harada K, Sasaki M, Furubo S, Song JY, Nakanuma Y: Activation of the PI3K/mTOR pathway is involved in cystic proliferation of cholangiocytes of the PCK rat. *PloS one* 9(1): e87660, 2014
39. Meijer L, Borgne A, Mulner O, Chong JP, Blow JJ, Inagaki N, Inagaki M, Delcros JG, Moulinoux JP: Biochemical and cellular effects of roscovitine, a potent and selective inhibitor of the cyclin-dependent kinases cdc2, cdk2 and cdk5. *Eur J Biochem* 243(1-2): 527-536, 1997
40. Bukanov NO, Smith LA, Klinger KW, Ledbetter SR, Ibraghimov-Beskrovnaya O: Long-lasting arrest of murine polycystic kidney disease with CDK inhibitor roscovitine. *Nature* 444(7121): 949-952, 2006
41. Bukanov NO, Moreno SE, Natoli TA, Rogers KA, Smith LA, Ledbetter SR, Oumata N, Galons H, Meijer L, Ibraghimov-Beskrovnaya O: CDK inhibitors R-roscovitine and S-CR8 effectively block renal and hepatic cystogenesis in an orthologous model of ADPKD. *Cell cycle (Georgetown, Tex)* 11(21): 4040-4046, 2012
42. Bach S, Knockaert M, Reinhardt J, Lozach O, Schmitt S, Baratte B, Koken M, Coburn SP, Tang L, Jiang T, Liang DC, Galons H, Dierick JF, Pinna LA, Meggio F, Totzke F, Schachtele C, Lerman AS, Carnero A, Wan Y, Gray N, Meijer L: Roscovitine targets, protein kinases and pyridoxal kinase. *J Biol Chem* 280(35): 31208-31219, 2005
43. Wilhelm SM, Carter C, Tang L, Wilkie D, McNabola A, Rong H, Chen C, Zhang X, Vincent P, McHugh M, Cao Y, Shujath J, Gawlak S, Eveleigh D, Rowley B, Liu L, Adnane L, Lynch M, Auclair D, Taylor I, Gedrich R, Voznesensky A, Riedl B, Post LE, Bollag G, Trail PA: BAY 43-9006 exhibits broad spectrum oral antitumor activity and targets the RAF/MEK/ERK pathway and receptor tyrosine kinases involved in tumor progression and angiogenesis. *Cancer Res* 64(19): 7099-7109, 2004
44. Yamaguchi T, Reif GA, Calvet JP, Wallace DP: Sorafenib inhibits cAMP-dependent ERK activation, cell proliferation, and in vitro cyst growth of human ADPKD cyst epithelial cells. *American journal of physiology Renal physiology* 299(5): F944-951, 2010

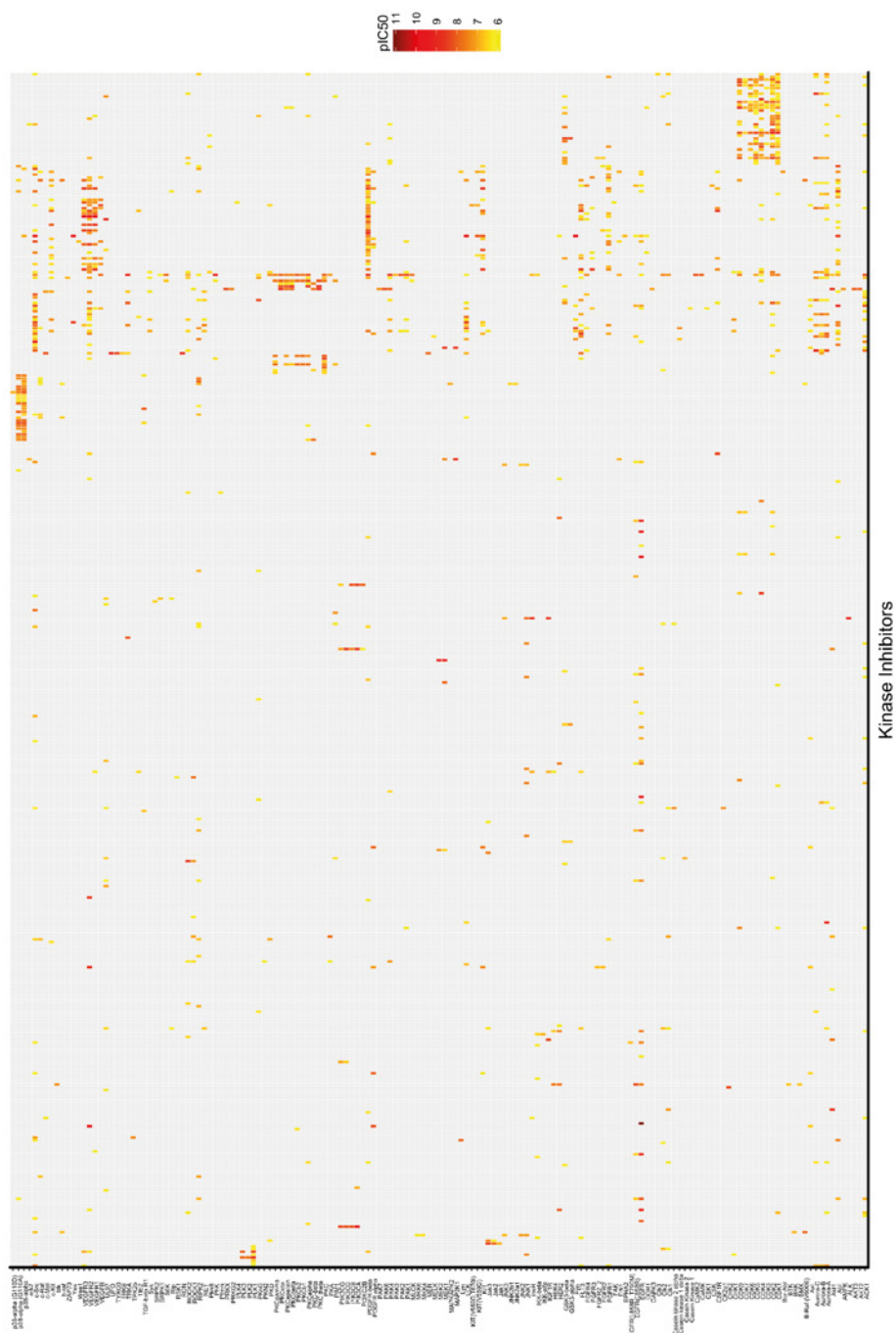
45. Sas KM: Targeting B-Raf as a treatment strategy for polycystic kidney disease. *American journal of physiology Renal physiology* 299(5): F942-943, 2010
46. Neufeld TK, Douglass D, Grant M, Ye M, Silva F, Nadasdy T, Grantham JJ: In vitro formation and expansion of cysts derived from human renal cortex epithelial cells. *Kidney international* 41(5): 1222-1236, 1992
47. Belmokhtar CA, Hillion J, Segal-Bendirdjian E: Staurosporine induces apoptosis through both caspase-dependent and caspase-independent mechanisms. *Oncogene* 20(26): 3354-3362, 2001
48. Karaman MW, Herrgard S, Treiber DK, Gallant P, Atteridge CE, Campbell BT, Chan KW, Ciceri P, Davis MI, Edeen PT, Faraoni R, Floyd M, Hunt JP, Lockhart DJ, Milanov ZV, Morrison MJ, Pallares G, Patel HK, Pritchard S, Wodicka LM, Zarrinkar PP: A quantitative analysis of kinase inhibitor selectivity. *Nature biotechnology* 26(1): 127-132, 2008
49. Wilson SJ, Amsler K, Hyink DP, Li X, Lu W, Zhou J, Burrow CR, Wilson PD: Inhibition of HER-2(neu/ErbB2) restores normal function and structure to polycystic kidney disease (PKD) epithelia. *Biochimica et biophysica acta* 1762(7): 647-655, 2006
50. Torres VE, Sweeney WE, Jr., Wang X, Qian Q, Harris PC, Frost P, Avner ED: EGF receptor tyrosine kinase inhibition attenuates the development of PKD in Han:SPRD rats. *Kidney international* 64(5): 1573-1579, 2003
51. Liu C, Zhang Y, Yuan L, Fu L, Mei C: Rosiglitazone inhibits insulin-like growth factor1-induced polycystic kidney disease cell growth and p70S6 kinase activation. *Molecular medicine reports* 8(3): 861-864, 2013
52. Bach LA, Hale LJ: Insulin-like growth factors and kidney disease. *American journal of kidney diseases : the official journal of the National Kidney Foundation* 65(2): 327-336, 2015
53. Happe H, de Heer E, Peters DJ: Polycystic kidney disease: the complexity of planar cell polarity and signaling during tissue regeneration and cyst formation. *Biochimica et biophysica acta* 1812(10): 1249-1255, 2011
54. Malumbres M: Cyclin-dependent kinases. *Genome Biol* 15(6): 122, 2014
55. Husson H, Moreno S, Smith LA, Smith MM, Russo RJ, Pitstick R, Sergeev M, Ledbetter SR, Bukanov NO, Lane M, Zhang K, Billot K, Carlson G, Shah J, Meijer L, Beier DR, Ibraghimov-Beskrovnaya O: Reduction of ciliary length through pharmacologic or genetic inhibition of CDK5 attenuates polycystic kidney disease in a model of nephronophthisis. *Hum Mol Genet* 25(11): 2245-2255, 2016
56. Cicas J, Kalyan K, Sorokinas A, Stankunas E, Levy J, Meskinyte I, Stankevicius V, Kaupinis A, Valius M: Roscovitine in cancer and other diseases. *Annals of Translational Medicine* 3(10), 2015
57. Song H, Vita M, Sallam H, Tehranchi R, Nilsson C, Siden A, Hassan Z: Effect of the Cdk-inhibitor roscovitine on mouse hematopoietic progenitors in vivo and in vitro. *Cancer chemotherapy and pharmacology* 60(6): 841-849, 2007
58. Bhunia AK, Piontek K, Boletta A, Liu L, Qian F, Xu PN, Germino FJ, Germino GG: PKD1 induces p21(waf1) and regulation of the cell cycle via direct activation of the JAK-STAT signaling pathway in a process requiring PKD2. *Cell* 109(2): 157-168, 2002

59. Pan J, Seeger-Nukpezah T, Golemis EA: The role of the cilium in normal and abnormal cell cycles: emphasis on renal cystic pathologies. *Cellular and molecular life sciences : CMLS* 70(11): 1849-1874, 2013
60. Tucker RW, Scher CD, Stiles CD: Centriole deciliation associated with the early response of 3T3 cells to growth factors but not to SV40. *Cell* 18(4): 1065-1072, 1979
61. Thoma CR, Frew IJ, Hoerner CR, Montani M, Moch H, Krek W: pVHL and GSK3beta are components of a primary cilium-maintenance signalling network. *Nat Cell Biol* 9(5): 588-595, 2007
62. Gray JE, Infante JR, Brail LH, Simon GR, Cooksey JF, Jones SF, Farrington DL, Yeo A, Jackson KA, Chow KH, Zamek-Gliszczynski MJ, Burris HA, 3rd: A first-in-human phase I dose-escalation, pharmacokinetic, and pharmacodynamic evaluation of intravenous LY2090314, a glycogen synthase kinase 3 inhibitor, administered in combination with pemetrexed and carboplatin. *Invest New Drugs* 33(6): 1187-1196, 2015
63. Parker E, Newby LJ, Sharpe CC, Rossetti S, Streets AJ, Harris PC, O'Hare MJ, Ong AC: Hyperproliferation of PKD1 cystic cells is induced by insulin-like growth factor-1 activation of the Ras/Raf signalling system. *Kidney international* 72(2): 157-165, 2007
64. Tao Y, Kim J, Yin Y, Zafar I, Falk S, He Z, Faubel S, Schrier RW, Edelstein CL: VEGF receptor inhibition slows the progression of polycystic kidney disease. *Kidney international* 72(11): 1358-1366, 2007
65. Plotnikova OV, Pugacheva EN, Golemis EA: Aurora A kinase activity influences calcium signaling in kidney cells. *The Journal of cell biology* 193(6): 1021-1032, 2011
66. Nikonova AS, Deneka AY, Eckman L, Kopp MC, Hensley HH, Egleston BL, Golemis EA: Opposing Effects of Inhibitors of Aurora-A and EGFR in Autosomal-Dominant Polycystic Kidney Disease. *Frontiers in oncology* 5 228, 2015

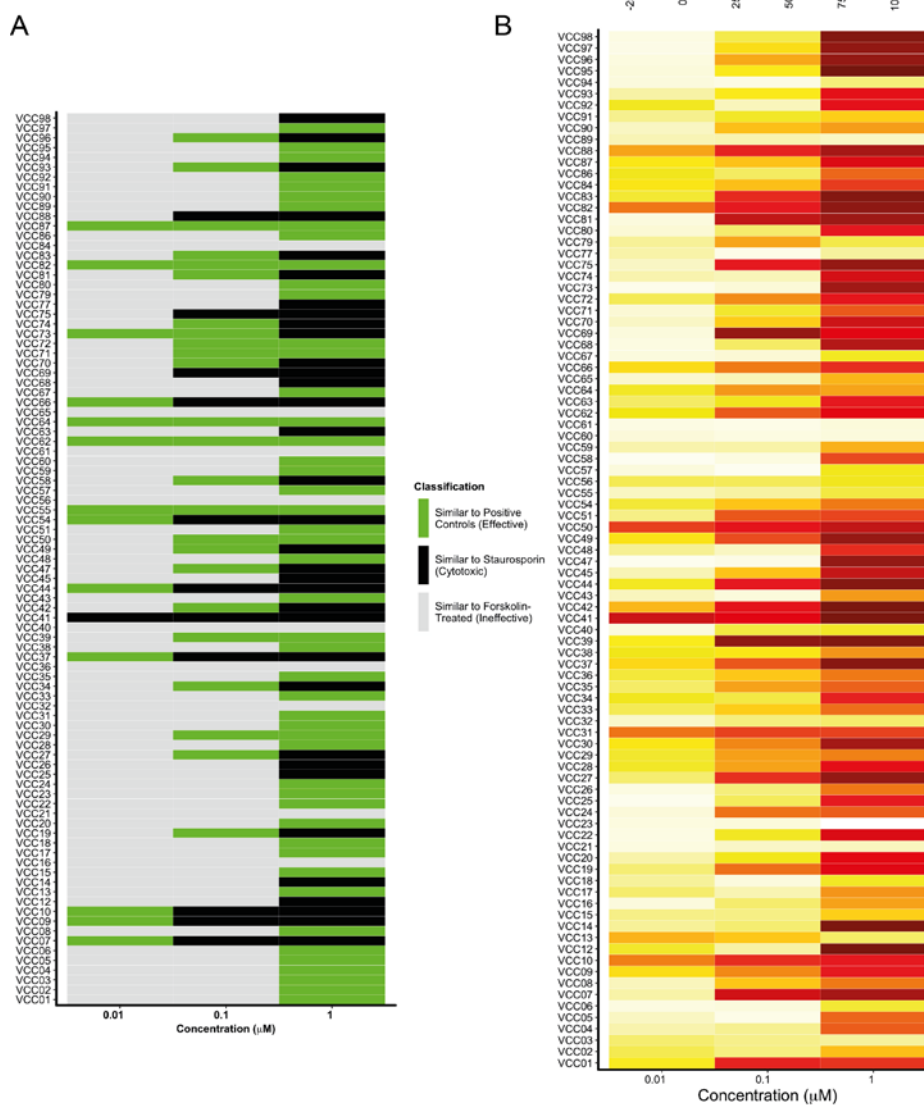
SUPPLEMENTAL MATERIALS



SUPPLEMENTAL FIGURE 1 Data analysis workflow with references to main figures.

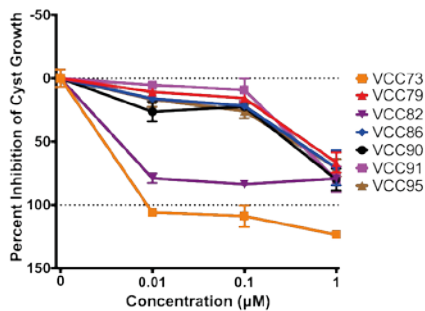
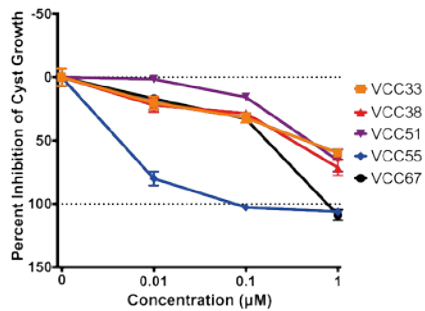
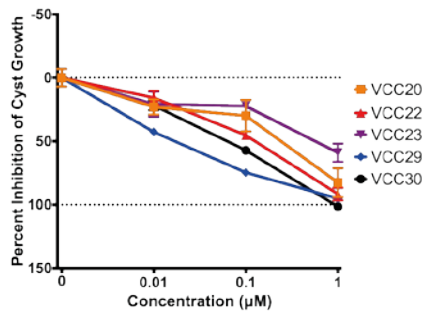
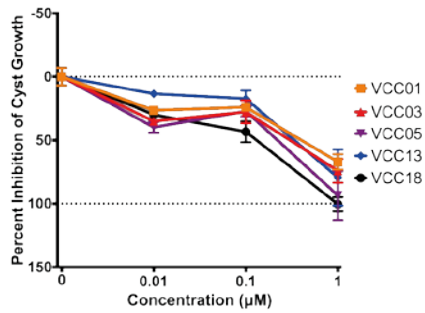


SUPPLEMENTAL FIGURE 2 Target spectrum of all screened compounds with $IC_{50} \leq 1 \mu M$ represented by a yellow to red colour scale.

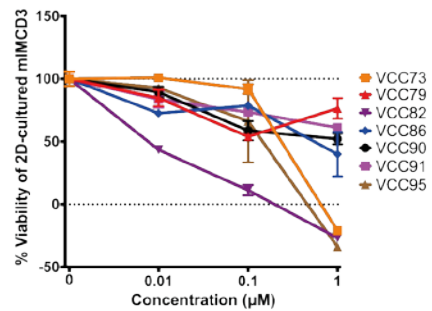
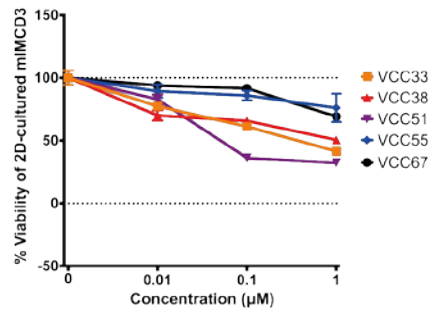
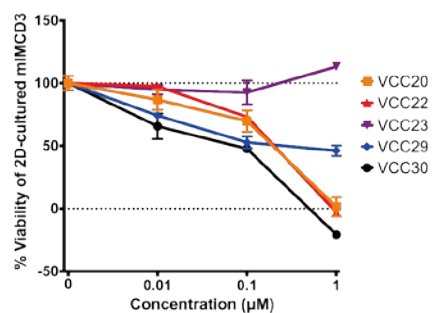
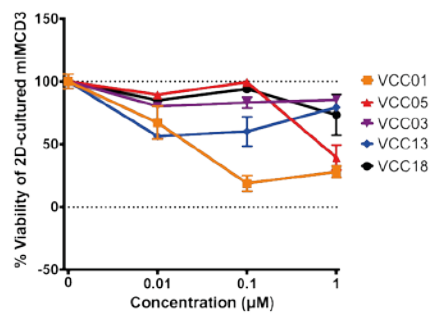


SUPPLEMENTAL FIGURE 3 Correlation of 3D classification using K nearest neighbour classification and 2D cell viability measured by ATPlite. **A)** Heat map showing classification of compounds when $\geq 2/3$ replicates belong to that class. Black colour represents cytotoxic compounds, green represents efficacy and light grey colour represents inactive. **B)** 2D ATPlite on mIMRFPKD 5E4 represented by yellow to red colour scale. While these compounds do not show toxicity in 3D cysts, they may affect 2D viability.

Cyst Growth



2D cell viability



◀ **SUPPLEMENTAL FIGURE 4** Dose curves for inhibition of cyst growth and 2D cell viability for all compounds presented in figure 5G. Data points represent median \pm MAD of triplicate wells. In case error bars are not visible, the MAD is smaller than the point size.

chapter 6

In vitro 3D phenotypic drug screen identifies celastrol as an effective *in vivo* inhibitor of polycystic kidney disease

Tijmen H. Booij^{1#}, Wouter N. Leonhard^{2#}, Kuan Yan³,
Michiel Fokkelman¹, Anna J. Plugge², Kimberley A.M.
Veraar², Johannes G. Dauwerse², Gerard J.P. van Westen⁴,
Bob van de Water¹, Leo S. Price^{1,3¥}, Dorien J.M. Peters^{2¥}.

Authors contributed equally

¥ Authors contributed equally

- 1 Division of Toxicology, Leiden Academic Centre for Drug Research (LACDR), Leiden University, Leiden, The Netherlands
- 2 Department of Human Genetics, Leiden University Medical Center (LUMC), Leiden, The Netherlands
- 3 Ocello B.V., Leiden, The Netherlands
- 4 Division of Medicinal Chemistry, Leiden Academic Centre for Drug Research (LACDR), Leiden, The Netherlands

Manuscript submitted and under revision

Abstract

Polycystic kidney disease (PKD) is a prevalent genetic disorder, characterized by the formation of kidney cysts that progressively lead to kidney failure. The currently available drug tolvaptan is not well tolerated by all patients and there remains a strong need for alternative treatments. The signaling rewiring in PKD that drives cyst formation is highly complex and not fully understood. As a consequence, the effects of drugs are sometimes difficult to predict. We previously established a high throughput microscopy phenotypic screening method for quantitative assessment of renal cyst growth. Here we applied this 3D cyst growth phenotypic assay and screened 2320 small drug-like molecules, including approved drugs. We identified 81 active molecules that inhibit cyst growth. Multi-parametric phenotypic profiling of the effects on 3D cultured cysts discriminated molecules that showed preferred pharmacological effects above genuine toxicological properties. Celastrol, a triterpenoid from *Tripterygium Wilfordii*, was identified as a potent inhibitor of cyst growth *in vitro*. In an *in vivo* iKspCre-*Pkd1*^{lox,lox} mouse model for PKD, celastrol inhibited the growth of renal cysts and maintained kidney function.

Introduction

Autosomal Dominant Polycystic kidney disease (ADPKD) affects approximately 1 in 2500¹ people that will develop renal failure as a result of progressive growth of renal cysts that interfere with normal kidney function. The disease is caused by mutations in the *PKD1*- or *PKD2* genes that encode polycystin-1 or polycystin-2, respectively.² These proteins are expressed in several cellular compartments and form multimeric protein complexes, that modulate several signaling pathways, which in concert control essential cellular functions such as proliferation, apoptosis, cell adhesion and differentiation. However, how mutations in the PKD genes drive the development of renal cysts is still not fully understood. In addition, we know little about how the signaling pathways involved in driving renal cyst growth, are interconnected and how they contribute to this process. As a consequence, it is also poorly understood how certain compounds that are under investigation for their therapeutic potential, exert their ‘cyst-reducing’ properties and why certain therapies become less effective at the more progressive stages. Currently only one drug, tolvaptan (Jinarc), is marketed for the treatment of PKD. This drug has massive diuresis as a side-effect, which may limit compliance of otherwise asymptomatic patients.³ Because PKD patients require therapy for many decades, it is critical to improve the balance between side-effects and preventing cyst growth. A possibility to achieve this goal is by combination therapy with multiple effective drugs, allowing for dose reduction, or the identification of more effective drugs with fewer side effects.

Results and discussion

To identify new drug candidates that prevent cyst growth, we developed a 3D cyst culture-based high-throughput screening platform, which can be used to screen large libraries of molecules for the identification of cyst-inhibiting compounds.⁴ This 3D assay uses phenotypic profiling of cysts as a measure of compound efficacy. Phenotypic screening can enable the identification of effective molecules irrespective of their mechanism of action and without a comprehensive understanding of the pathophysiology and can be effective at identifying first-in-class treatments.⁵ Here, we screened the SPECTRUM library, containing 2320 molecules including kinase inhibitors, natural molecules and FDA-approved drugs. We cultured epithelial cysts from mIMCD3 cells with short hairpin-mediated reduced *Pkd1* expression (mIMCD3 sh*Pkd1*) in 384-well plates in protein hydrogels. Following exposure to forskolin, to induce cyclic adenosine monophosphate (cAMP) production by adenylyl cyclase and subsequent cyst swelling, we co-exposed the cysts to control compounds or test compounds of the SPECTRUM library at 1 μ M (supplemental figure 1). After imaging and calculating cyst size using phenotypic measurement, we ranked the molecules on their potency to inhibit cyst growth as presented in figure 1A, top panel. As criterion for hit selection, molecules were selected that were at least one standard deviation below the stimulated control condition (2.5 μ M forskolin). As a result, 81 cyst-inhibiting hits were identified (figure 1A, bottom panel). All hits were re-screened at six concentrations in triplicate wells using RNA-guided *FokI* nuclease-mediated⁶ *Pkd1*-knockout cells (mIMCD3 *Pkd1*^{-/-}). (Supplemental figure 2A-B), confirming the activity of 66.6% of the molecules (54 molecules with cyst growth inhibition >50% at 1 μ M).

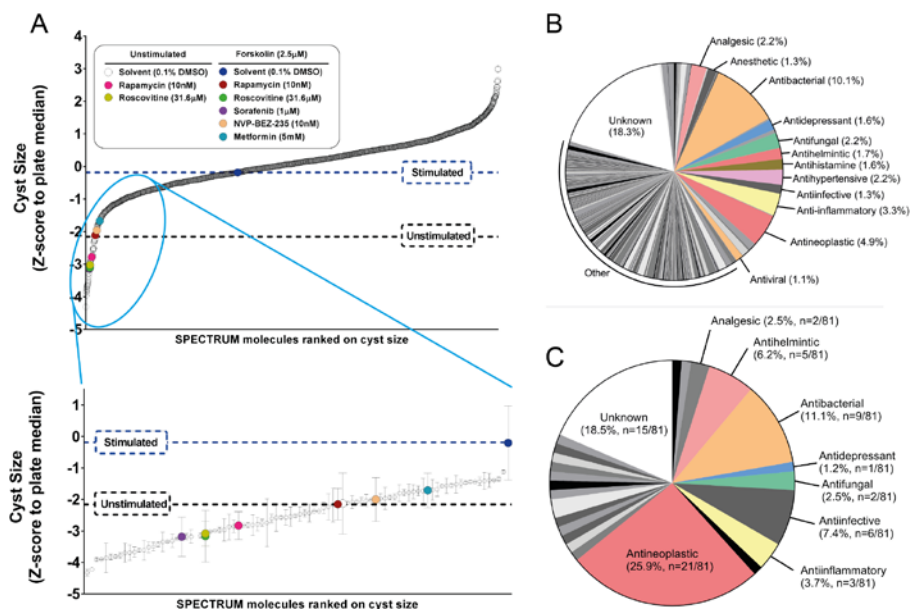


FIGURE 1 Screening a small-molecule library to identify inhibitors of cyst growth.

A) 2320 molecules were ranked according to inhibitory effect on cyst growth on mIMCD3 *shPkd1* cysts (z-score normalized to plate median). Molecules inhibiting cyst growth relative to forskolin-stimulated control (“Stimulated”) included positive control molecules, as indicated by colored circles in the enlarged cut-out. For control molecules, error bars represent standard deviations (SD). For all other molecules, error bars represent $\frac{1}{2}$ *difference between two replicate wells. **B)** Many molecules contained in the library have an antibacterial or antineoplastic mechanism of action. Since for some natural molecules the mechanism of activity is not elucidated, the bioactivity is listed as “unknown”. **C)** The selected 81 cyst growth-inhibiting hits were markedly enriched in antineoplastic, anti-infective and anthelmintic molecules, compared to figure B.

To get more insight into the molecules that were active in our screen, we listed the molecules according to their bioactivities described in the manufacturer’s datasheet. It is important to note that some molecules do not belong exclusively to one class and may have dual bioactivities. An evaluation of the 81 hits revealed that the largest group of selected hits were molecules known to have an antineoplastic mechanism of action (25.9% of our hits compared to 4.9% of the library) (figure 1B-C).

Since most ADPKD patients will need drug treatment for decades, antineoplastic drugs are unlikely to become therapeutic candidates. Therefore, we applied linear discriminant analysis (LDA) on measured phenotypic parameters (with correlation <0.85), to discriminate known toxic molecules from stimulated- and unstimulated controls.

This strategy allowed us to separate most antineoplastic molecules from molecules with a different mode of action. (supplemental figure 3A-B). For all molecules we determined the proximity in feature space to the unstimulated control group as a measure of desirable efficacy. Supplemental figure 3C presents this distance as a color scale from yellow to blue. While most anti-infective and anthelmintic retained their favorable activity (distance <50 at $1\mu\text{M}$), most antineoplastic molecules remained distant from the favorable (and small) control cysts phenotype.

Based on these results, we found that celastrol (figure 2A), a triterpenoid extracted from *Tripterygium Wilfordii*,⁷ and pyrvinium pamoate, an anthelmintic drug⁸ and WNT inhibitor⁹ (supplemental figure 4A), were very potent at inhibiting cyst growth *in vitro*. Celastrol appeared to induce phenotypes associated with toxicity only at high concentrations ($\geq 316\text{nM}$), and potentially inhibited forskolin-induced cyst growth at 100nM (figure 2B-C). Pyrvinium pamoate showed no indication of toxicity even at high concentrations (supplemental figure 4B). Interestingly, we also discovered that several closely-related structural analogues of celastrol displayed a similar activity profile (supplemental figure 5A-B).

To investigate whether the inhibition shown by celastrol was dependent on cAMP induction by forskolin, we assessed whether it could inhibit cyst growth in the absence of forskolin. While more variation within wells was observed within this long-duration assay (attributable to the necessity to refresh compounds and culture media), we observed activity of celastrol at 100nM , but not 10nM , compared to solvent control (figure 2D).

To investigate whether the findings *in vitro* could be translated to a response *in vivo*, we tested both celastrol and pyrvinium pamoate in a $\text{iKspCre-Pkd1}^{\text{lox,lox}}$ mouse model, where tamoxifen was used to inactivate the *Pkd1* gene at postnatal day (P) 10 and P11, to induce rapid cyst formation.¹⁰⁻¹¹ Treatment with pyrvinium pamoate from P13 appeared to be toxic at 1mg/kg/day , and lower dosages did not affect PKD progression in this model (supplemental figure 4C, 4D). We therefore did not further pursue this compound as a possible candidate for PKD treatment. By contrast, celastrol treatment inhibited PKD progression in two separate experiments. The effects of celastrol were first measured at 1mg/kg/day (7 mice) from P13-P27, and, even though changes in bodyweight were observed initially, between P13 and P18, celastrol appeared to be well tolerated. In a subsequent independent experiment, we observed similar effects of celastrol at 0.5mg/kg/day (8 mice) but not at 0.2mg/kg/day (8 mice) (supplemental figure 6A). The reduction in body weight may be related to celastrol's reported role as a leptin sensitizer,¹² and, while this finding may introduce bias (food restriction is known to ameliorate cystogenesis in patients¹³), we consider it unlikely that anti-obesity effects would explain such profound effects *in vivo* and particularly not efficacy *in vitro*. In line with the *in vitro* findings, celastrol strongly protected kidney function, while lowering cyst burden (figure 3A-C and supplemental figure 6B-E) and PKD-associated fibrosis (figure 3D-E) at 0.5 and 1.0mg/kg/day , but not at 0.2mg/kg/day .

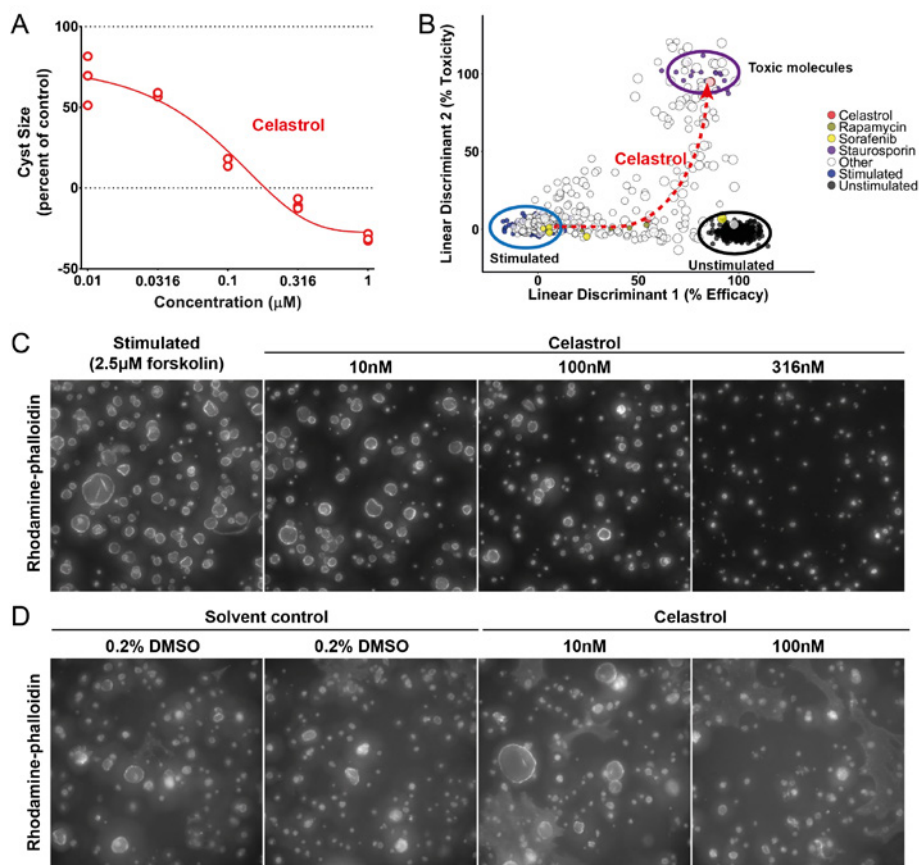


FIGURE 2 Celastrol inhibits cyst growth dose-dependently. **A**) Celastrol inhibits mIMCD3 *Pkd1*^{-/-} cyst growth. At the highest concentrations (316 and 1000nM) cyst size is lower than unstimulated control, possibly corresponding to effects shown in B in linear discriminant 2. These experiments were repeated at least three times. **B**) LDA plot showing efficacy (linear discriminant 1) and toxicity (linear discriminant 2) of celastrol using multiparametric phenotypic measurements on mIMCD3 *Pkd1*^{-/-} cysts. At the left (ringed in blue) the forskolin stimulated large cysts. At the right (ringed in black) the unstimulated small cysts. Larger dot sizes correspond to higher compound concentrations. Celastrol (red dots) is only toxic at the highest concentration. **C**) Representative images of 3D-cultured mIMCD3 *Pkd1*^{-/-} cysts (cytoskeleton, F-actin) co-exposed with 2.5 μ M forskolin and celastrol at different concentrations, or vehicle control (stimulated, 2.5 μ M forskolin). 500x500px cut-out of images taken with the ImageXpress Micro XLS imager shown for presentation purposes. **D**) Long-term exposure with celastrol shows inhibition of spontaneous cyst growth over 13 days. 1000x1000px cutout of (cytoskeleton, F-actin) images taken with the BD Pathway 855 imager. Brightness and contrast of all images were enhanced for presentation purposes.

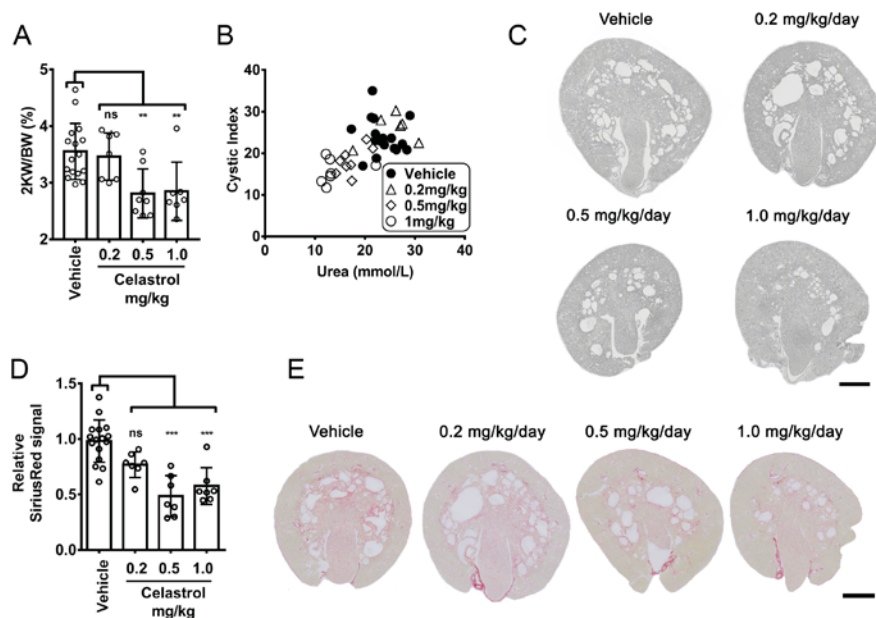


FIGURE 3 Celastrol inhibits cyst growth *in vivo* in iKspCre-*Pkd1*^{lox,lox} mice and prevents decline of kidney function. The results presented here combined two independent experiments, where celastrol was first tested at 1mg/kg/day and later at 0.2 and 0.5mg/kg/day because the vehicle controls were highly similar. **A**) Two-kidney weight as percentage of bodyweight of vehicle-treated or celastrol-treated mice at postnatal day 27. Data shown represent means \pm SD and individual data points for all mice. Vehicle treated (n=16), celastrol 0.2mg/kg (n=7), 0.5mg/kg (n=8) and 1.0mg/kg (n=7). **B**) Blood urea nitrogen (BUN/Urea) given in mmol/L for vehicle- or celastrol-treated mice as a measurement of kidney function plotted against cystic index, indicating *in vivo* cyst size (disease severity) measured in P27 kidneys after vehicle or celastrol treatment. Vehicle treated (n=16), celastrol 0.2mg/kg (n=7), 0.5mg/kg (n=8) and 1.0mg/kg (n=7). **C**) Representative images of renal histology of P27 kidneys showing renal cysts are reduced after celastrol treatment for 0.5 and 1.0mg/kg treatment groups, compared to vehicle. Additional tissue sections are presented in supplemental figure 6 to illustrate experimental variation. **D**) Fibrotic index as measured by intensity of Sirius Red signal (normalized to vehicle control) for vehicle-treated (n=16), 0.2mg/kg/day celastrol-treated (n=7), 0.5mg/kg/day celastrol-treated (n=7) and 1.0mg/kg/day celastrol-treated (n=7) mice. **E**) Representative Sirius Red-stained sections of P27 kidneys of celastrol treated (0.2, 0.5 and 1.0mg/kg/day) compared to vehicle-treated. Statistical significance was assessed with ordinary one-way ANOVA with Dunnett's multiple comparisons test. *p<0.05, **p<0.01, ***p<0.001.

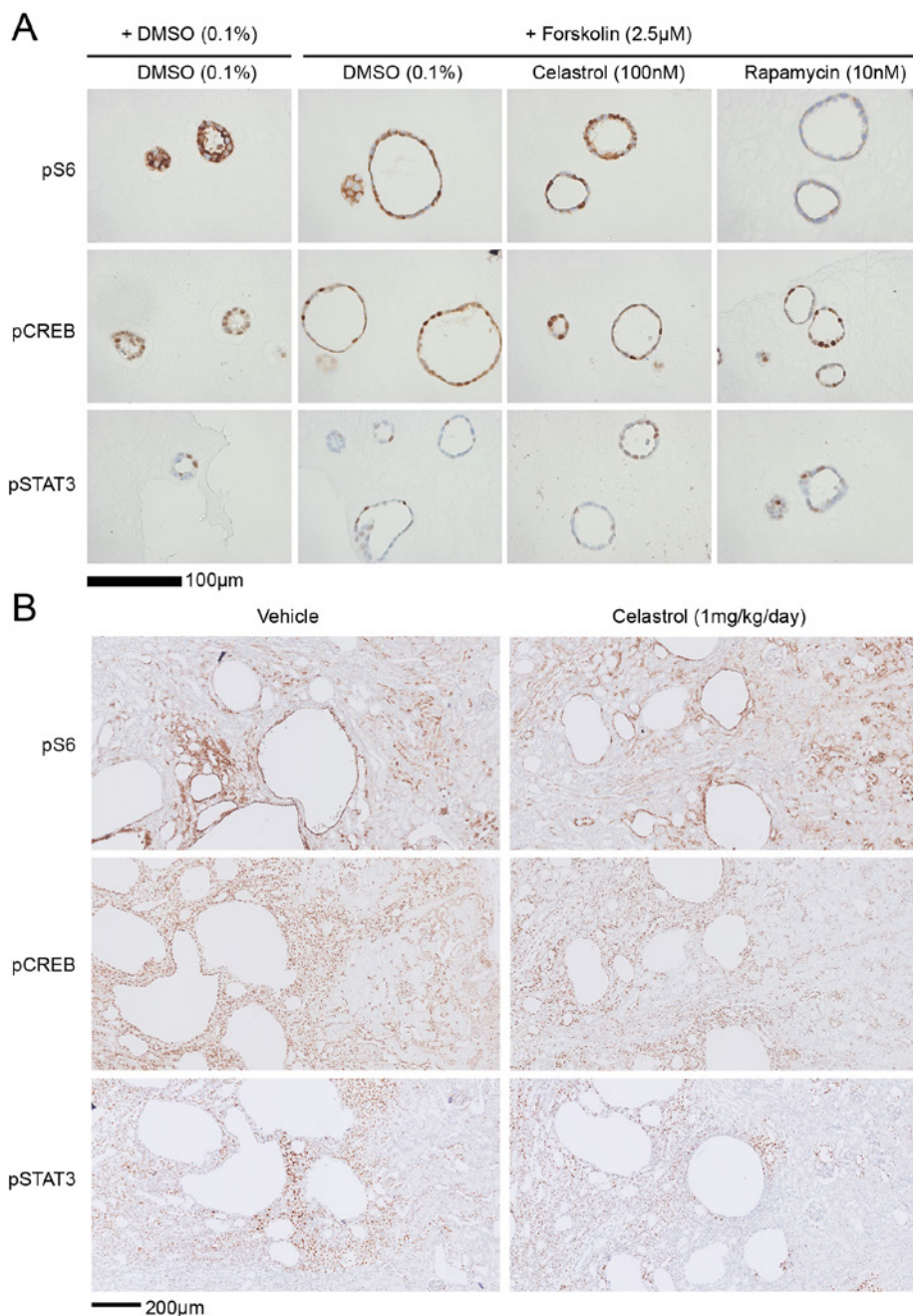


FIGURE 4 Celastrol does not affect known PKD-associated signaling. A selection of PKD-associated pathways has been analyzed. **A)** Representative images of sections of 3D-cultured mIMCD3 *Pkd1*^{-/-} cysts, treated with solvent (DMSO), celastrol or rapamycin and stained for pS6 (mTOR activity), pCREB and pSTAT3 after fixation. (legend continues on next page)

B) Tissue sections after staining for pS6, pCREB and pSTAT3 of vehicle-treated and celastrol-treated mice (1mg/kg/day shown). Images were made in areas where cystic and non-cystic tissue was present, to minimize bias of differential signaling associated with cystic versus non-cystic tissue (not related to celastrol treatment).

Celastrol has been investigated for other indications where it has shown promising responses, such as inflammatory disorders, cancer and obesity.^{12, 14-16} However, the mechanism by which celastrol may affect cyst growth is unclear and we therefore investigated its effects on known PKD-associated signaling (pCREB, pS6, pSTAT3). Both, in 3D cyst cultures (figure 4A) and tissue sections (figure 4B), we found no effects of celastrol treatment on these targets. A variety of studies suggested a large number of signaling pathways that may be affected by celastrol including HSP90/Cdc37¹⁷⁻¹⁸ and NFκB¹⁹ (for a literature overview see supplemental table 2). We therefore consider it likely that celastrol affects cystogenesis by a multi-target mechanism. This idea was further supported by recent research by Zhou et al, where 66 celastrol-binding proteins were identified, which function in various different processes, including (redox-) metabolism and the ubiquitin proteasome pathway.²⁰ This multi-target mechanism may be the result of interactions of celastrol (and other triterpenoids) with thiol groups in many proteins.²⁰⁻²² Interestingly, similar Michael acceptor properties have been reported for curcumin,²³ a molecule that also delays cystogenesis in mice.²⁴ Because these molecules may have different affinity towards different thiol residues, it is possible that they affect other proteins and pathways as a result of concentration changes.²² Celastrol is also known to have antioxidant activity,²⁵ and may therefore reduce kidney damage by induction of cytoprotective genes, as reported for curcumin,²⁶ which can in turn ameliorate cystogenesis.²⁷⁻²⁹

Conclusions

In conclusion, using phenotypic screening, we have identified celastrol as a potent inhibitor of cyst growth. We confirmed the efficacy of celastrol in a juvenile PKD model where it potentially protected kidney function and lowered cyst burden. The phenotypic screening approach allowed for the identification of this molecule without knowing its mechanism of action, which is likely not specific for one target. Celastrol may prove to be an interesting treatment option for PKD, provided that it has a desirable safety- and efficacy profile.

CONCISE METHODS

3D cyst culture procedure

Cyst culture and screening was performed as described previously.⁴ Briefly, cryo-preserved mIMCD3 *shPkd1* or mIMCD3 *Pkd1*^{-/-} cells were quick-thawed and grown in culture medium (DMEM/F12 Ham's, supplemented with FBS and antibiotics) for 72 hours. Cells were trypsinized and mixed with Cyst-Gel (OcellO) and plated in 384 well plates (Greiner Bio-One). After addition of culture medium, cysts were allowed to form

during 72 hours (*shPkd1*) or 96 hours (*Pkd1^{-/-}*) and subsequently exposed to forskolin (Calbiochem) and test compounds for 72 hours. Cysts were thereafter fixed and simultaneously stained for F-actin and nuclei for 12-24 hours at 4°C. After washing in 1x PBS (Sigma Aldrich) for 24 hours, plates were imaged using either a BD Pathway 855 microscope (BD Bioscience) or ImageXpress Micro XLS (Molecular Devices), with a 4x objective.

Image- and data analysis

Image stacks for each well were analyzed and phenotypes were quantified using Ominer software (Ocello) integrated in KNIME Analytics Platform (<http://www.knime.org>) (supplemental figure 1A, C). 450 phenotypic measurements were z-score normalized to plate median or normalized to percent of control. Linear discriminant analysis (LDA) was performed using the 83 least correlating phenotypic parameters (Pearson product-moment correlation coefficient <0.85). LDA was trained on unstimulated (solvent), stimulated (forskolin-treated) and known cytotoxic molecules (daunorubicin, doxorubicin, staurosporin, gambogic acid, epirubicin, at 1µM) and the trained model was applied to all data. The two resulting linear discriminants were scaled and a small absolute distance (<50) to the unstimulated control group was considered as desirable efficacy.

Compounds

A molecule library containing 2320 compounds (SPECTRUM 2320) was obtained from MicroSource Discovery Systems. Compounds were pre-dissolved to 10mM in DMSO (Biosolve) and final DMSO content was kept constant at a well-tolerated 0.2%v/v for all *in vitro* experiments. Celastrol was derived from this library and performed equally well compared to celastrol obtained from another source (Sigma Aldrich).

Animal procedures

The local animal experimental committee of the Leiden University Medical Center (LUMC) and the Commission Biotechnology in Animals of the Dutch Ministry of Agriculture approved all animal experiments performed. Kidney specific, tamoxifen-inducible Cre-*Pkd1*lox mice (iKspCre-*Pkd1*^{lox,lox})^{30, 30} received 15mg/kg Tamoxifen at post-natal day 10 and 11 to inactivate *Pkd1* to cause rapid cyst formation. Mice received i.p. injections of celastrol, pyrinium pamoate or vehicle (5% DMSO + 10% Kolliphor EL in PBS) between P13 and P27. Mice were euthanized at P27 after blood sample collection to measure blood urea levels using Reflotron Technology. Kidneys were halved and snap frozen or embedded in paraffin. Image scans of Periodic acid-Schiff (PAS) stained kidney sections were analyzed by an investigator blinded to the treatment. The fibrotic index was calculated as done previously on the basis of Sirius Red staining.¹¹

Statistical analysis

Statistical analyses were performed in Graphpad Prism 7 software using ANOVA with Dunnett's multiple comparison's test unless otherwise stated. Results were considered statistically significant for p<0.05.

Detailed descriptions of the experimental procedures are included as supplemental methods.

Acknowledgments

T.H. Booij and W.N. Leonhard were supported by the Dutch Technology Foundation STW (Project 11823), which is part of The Netherlands Organization for Scientific Research (NWO). Gerard van Westen is supported by the Dutch technology Foundation STW (Project 14410). Michiel Fokkelman was supported by the EU-FP7 — Systems Microscopy NoE (grant no. 258068) and Anna J. Plugge by a grant from the Dutch Kidney Foundation (4OIP12).

Disclosures

L.S. Price is co-founder and CSO of Ocello B.V., a drug discovery contract research organisation located in Leiden, The Netherlands.

References

1. Willey CJ, Blais JD, Hall AK, Krasa HB, Makin AJ, Czerwiec FS: Prevalence of autosomal dominant polycystic kidney disease in the European Union. *Nephrol Dial Transplant*, 2016
2. Torres VE, Harris PC, Pirson Y: Autosomal dominant polycystic kidney disease. *Lancet* 369(9569): 1287-1301, 2007
3. Torres VE, Chapman AB, Devuyst O, Gansevoort RT, Grantham JJ, Higashihara E, Perrone RD, Krasa HB, Ouyang J, Czerwiec FS: Tolvaptan in patients with autosomal dominant polycystic kidney disease. *N Engl J Med* 367(25): 2407-2418, 2012
4. Booij TH, Bange H, Leonhard WN, Yan K, Fokkelman M, Kunnen SJ, Dauwerse J, Qin Y, van de Water B, van Westen GJP, Peters DJM, Price LS: High-throughput phenotypic screening of kinase inhibitors to identify drug targets for polycystic kidney disease. *SLAS Discov (in press)*
5. Swinney DC: Phenotypic vs. target-based drug discovery for first-in-class medicines. *Clin Pharmacol Ther* 93(4): 299-301, 2013
6. Tsai SQ, Wyvekens N, Khayter C, Foden JA, Thapar V, Reyon D, Goodwin MJ, Aryee MJ, Joung JK: Dimeric CRISPR RNA-guided FokI nucleases for highly specific genome editing. *Nat Biotechnol* 32(6): 569-576, 2014
7. Wong KF, Yuan Y, Luk JM: Tripterygium wilfordii bioactive compounds as anticancer and anti-inflammatory agents. *Clin Exp Pharmacol Physiol* 39(3): 311-320, 2012
8. Jung RC: Treatment of intestinal parasitic disease. *South Med J* 69(6): 799-804, 1976
9. Thorne CA, Hanson AJ, Schneider J, Tahinci E, Orton D, Cselenyi CS, Jernigan KK, Meyers KC, Hang BI, Waterson AG, Kim K, Melancon B, Ghidu VP, Sulikowski GA, LaFleur B, Salic A, Lee LA, Miller DM, 3rd, Lee E: Small-molecule inhibition of Wnt signaling through activation of casein kinase 1alpha. *Nat Chem Biol* 6(11): 829-836, 2010

10. Lantinga-van Leeuwen IS, Leonhard WN, van der Wal A, Breuning MH, de Heer E, Peters DJ: Kidney-specific inactivation of the Pkd1 gene induces rapid cyst formation in developing kidneys and a slow onset of disease in adult mice. *Hum Mol Genet* 16(24): 3188-3196, 2007
11. Leonhard WN, Kunnen SJ, Plugge AJ, Pasternack A, Jianu SB, Veraar K, El Bouazzaoui F, Hoogaars WM, Ten Dijke P, Breuning MH, De Heer E, Ritvos O, Peters DJ: Inhibition of Activin Signaling Slows Progression of Polycystic Kidney Disease. *J Am Soc Nephrol* 27(12): 3589-3599, 2016
12. Liu J, Lee J, Salazar Hernandez MA, Mazitschek R, Ozcan U: Treatment of obesity with celastrol. *Cell* 161(5): 999-1011, 2015
13. Warner G, Hein KZ, Nin V, Edwards M, Chini CC, Hopp K, Harris PC, Torres VE, Chini EN: Food Restriction Ameliorates the Development of Polycystic Kidney Disease. *J Am Soc Nephrol* 27(5): 1437-1447, 2016
14. Venkatesha SH, Dudics S, Astry B, Moudgil KD: Control of autoimmune inflammation by celastrol, a natural triterpenoid. *Pathog Dis* 74(6), 2016
15. Kannaiyan R, Shanmugam MK, Sethi G: Molecular targets of celastrol derived from Thunder of God Vine: potential role in the treatment of inflammatory disorders and cancer. *Cancer Lett* 303(1): 9-20, 2011
16. Liu Z, Ma L, Zhou GB: The main anticancer bullets of the Chinese medicinal herb, thunder god vine. *Molecules* 16(6): 5283-5297, 2011
17. Hieronymus H, Lamb J, Ross KN, Peng XP, Clement C, Rodina A, Nieto M, Du J, Stegmaier K, Raj SM, Maloney KN, Clardy J, Hahn WC, Chiosis G, Golub TR: Gene expression signature-based chemical genomic prediction identifies a novel class of HSP90 pathway modulators. *Cancer Cell* 10(4): 321-330, 2006
18. Dal Piaz F, Terracciano S, De Tommasi N, Braca A: Hsp90 Activity Modulation by Plant Secondary Metabolites. *Planta Med* 81(14): 1223-1239, 2015
19. Lee JH, Koo TH, Yoon H, Jung HS, Jin HZ, Lee K, Hong YS, Lee JJ: Inhibition of NF-kappa B activation through targeting I kappa B kinase by celastrol, a quinone methide triterpenoid. *Biochem Pharmacol* 72(10): 1311-1321, 2006
20. Zhou Y, Li W, Wang M, Zhang X, Zhang H, Tong X, Xiao Y: Competitive profiling of celastrol targets in human cervical cancer HeLa cells via quantitative chemical proteomics. *Mol Biosyst* 13(1): 83-91, 2016
21. Salminen A, Lehtonen M, Paimela T, Kaarniranta K: Celastrol: Molecular targets of Thunder God Vine. *Biochem Biophys Res Commun* 394(3): 439-442, 2010
22. Liby KT, Yore MM, Sporn MB: Triterpenoids and rexinoids as multifunctional agents for the prevention and treatment of cancer. *Nat Rev Cancer* 7(5): 357-369, 2007
23. Na HK, Surh YJ: Transcriptional regulation via cysteine thiol modification: a novel molecular strategy for chemoprevention and cytoprotection. *Mol Carcinog* 45(6): 368-380, 2006
24. Leonhard WN, van der Wal A, Novalic Z, Kunnen SJ, Gansevoort RT, Breuning MH, de Heer E, Peters DJ: Curcumin inhibits cystogenesis by simultaneous interference of multiple signaling pathways: in vivo evidence from a Pkd1-deletion model. *Am J Physiol Renal Physiol* 300(5): F1193-1202, 2011

25. Wang C, Shi C, Yang X, Yang M, Sun H, Wang C: Celastrol suppresses obesity process via increasing antioxidant capacity and improving lipid metabolism. *Eur J Pharmacol* 744 52-58, 2014
26. Balogun E, Hoque M, Gong P, Killeen E, Green CJ, Foresti R, Alam J, Motterlini R: Curcumin activates the haem oxygenase-1 gene via regulation of Nrf2 and the antioxidant-responsive element. *Biochem J* 371(Pt 3): 887-895, 2003
27. Happe H, Leonhard WN, van der Wal A, van de Water B, Lantinga-van Leeuwen IS, Breuning MH, de Heer E, Peters DJ: Toxic tubular injury in kidneys from Pkd1-deletion mice accelerates cystogenesis accompanied by dysregulated planar cell polarity and canonical Wnt signaling pathways. *Hum Mol Genet* 18(14): 2532-2542, 2009
28. Takakura A, Contrino L, Zhou X, Bonventre JV, Sun Y, Humphreys BD, Zhou J: Renal injury is a third hit promoting rapid development of adult polycystic kidney disease. *Hum Mol Genet* 18(14): 2523-2531, 2009
29. Malas TB, Formica C, Leonhard WN, Rao P, Granchi Z, Roos M, Peters DJ, t Hoen PA: Meta-analysis of polycystic kidney disease expression profiles defines strong involvement of injury repair processes. *Am J Physiol Renal Physiol* 312(4): F806-f817, 2017
30. Lantinga-van Leeuwen IS, Leonhard WN, van de Wal A, Breuning MH, Verbeek S, de Heer E, Peters DJ: Transgenic mice expressing tamoxifen-inducible Cre for somatic gene modification in renal epithelial cells. *Genesis* 44(5): 225-232, 2006

SUPPLEMENTAL METHODS

Cell lines and maintenance

mIMCD3 sh*Pkd1* cells, with a short-hairpin mediated knockdown of *Pkd1*, and mIMCD3 *Pkd1*^{-/-}, an RNA-guided FokI nuclease-mediated *Pkd1* knockout cell line (mIMRFNPKD clone 5E4), were generated previously¹ and maintained in DMEM/F12 (Ham's) culture medium (D8062, Sigma Aldrich, Zwijndrecht, Netherlands), supplemented with 10% fetal bovine serum (FBS, obtained from Gibco Fisher Scientific, Landsmeer, Netherlands), glutamax and penicillin/streptomycin in 175cm² culture flasks (Corning). Before reaching maximal confluence, the monolayers were washed with 1x PBS (Sigma Aldrich, Zwijndrecht, Netherlands) and subsequently trypsinized with 1x Trypsin (Gibco Fisher Scientific, Landsmeer, Netherlands) and subsequently passaged to a new culture flask. Cell passage numbers were kept below 20 for all experiments. For cryopreservation, trypsinized cells were pelleted by centrifugation at 1500rpm for 5 minutes and the cell pellet was subsequently mixed with freezing medium consisting of 90% FBS and 10% DMSO (Biosolve B.V., Valkenswaard, Netherlands) at a concentration of 9×10^6 cells per mL and subsequently slow-frozen to -150°C.

3D cyst culture procedure

mIMCD3 sh*Pkd1* or mIMCD3 *Pkd1*^{-/-} cells were quick-thawed and cultured in 175cm² culture flasks 72 hours prior to initiation of the 3D cultures. 3D cyst cultures were prepared as described previously.¹ Briefly, cells were trypsinized and subsequently pelleted by centrifugation. The cell pellet was mixed with Cyst-Gel (Ocello B.V. Leiden, Netherlands) at a cell density of 3×10^6 cells per mL. Using a CyBi Selma 96 automated liquid handler (Analytik Jena AG, Jena, Germany), cell-gel mix was transferred to Greiner µClear 384 well plates (Greiner Bio-One B.V. Alphen aan den Rijn, Netherlands), 14.5µL per well, at a final cell density of 2175 cells per well. After 30 minutes of gel polymerization at 37°C, 33.5µL culture medium was added and cells were grown for 72 hours (mIMCD3 sh*Pkd1* cells) or 96 hours (mIMCD3 *Pkd1*^{-/-}) at 37°C (5% CO₂) to initiate lumen formation, prior to compound exposures. Subsequently, cells were co-exposed with 2.5µM forskolin (*Coleus forskohlii*, Calbiochem, Millipore B.V., Amsterdam, Netherlands), to enhance cyst swelling due to the activation of adenylyl cyclase to produce cAMP, and compounds, using either the CyBi Selma 96 (for smaller scale experiments), or, to screen compound libraries, a BioMek FXP (Beckman Coulter B.V., Woerden, Netherlands) equipped with a 96-tip pipetting head. After 72 hours of compound exposures, plates were fixed with 4% formaldehyde (Sigma Aldrich, Zwijndrecht, Netherlands), permeabilized with Triton X-100 (Sigma Aldrich, Zwijndrecht, Netherlands) and stained with rhodamine-phalloidin (Sigma Aldrich, Zwijndrecht, Netherlands) and Hoechst 33258 (Sigma Aldrich, Zwijndrecht, Netherlands) for cytoskeleton and nuclei, respectively, for 12 to 24 hours at 4°C. After fixation and staining, plates were washed with 1x PBS for 24 hours and sealed with an aluminium plate seal (Greiner Bio-One B.V. Alphen aan den Rijn, Netherlands) and subsequently stored at 4°C prior to imaging (the screening procedure is schematically presented in supplemental figure 1).

Long-term 3D cyst culture procedure without forskolin

3D cyst cultures of mIMCD3 *Pkd1*^{-/-} cells were prepared as described in the previous section. 33.5μL of culture medium was added to the prepared cultures, and cells were allowed to form cysts for 96 hours prior to compound exposures. 3D cultured cysts were exposed to 100nM celastrol or solvent (0.1% DMSO) in a final volume of 60μL. After 96 hours, 30μL medium/compound mix was aspirated using a CyBi Selma 96, and 18μL fresh medium and 2x 6μL fresh compound was added. After 96 hours, the cysts were fixed with 4% formaldehyde and further processed as described above.

Compounds

A (SPECTRUM) compound library with 2320 molecules was obtained from MicroSource (MicroSource Discovery Systems, Inc., Gaylordsville, Connecticut, USA). Compounds were pre-dissolved to 10mM in DMSO. Analytical grade DMSO was obtained from Biosolve B.V. (Valkenswaard, Netherlands). Rapamycin, sorafenib tosylate, roscovitine and NVP-BEZ-235 were obtained from SelleckChem (Munich, Germany). Metformin HCl was obtained from Sigma Aldrich (Zwijndrecht, Netherlands). Celastrol was obtained from two different sources (MicroSource Discovery Systems, Inc., Gaylordsville, Connecticut, USA for the primary screen and Sigma Aldrich, Zwijndrecht, Netherlands for further validation experiments and animal experiments). Both sources performed equally well in terms of cyst growth inhibition *in vitro* (not shown).

Fluorescence microscopy

384 well plates of the SPECTRUM screen were imaged using an automated (wide-field) BD Pathway 855 imager (BD Biosciences, Breda, Netherlands) with a 4x Olympus objective, coupled to a Twister II robotic arm, as described previously². Subsequent experiments were imaged using an ImageXpress Micro XLS wide field high-content analysis system (Molecular Devices, Sunnyvale, CA, USA) with a 4x objective. xy-images were made in the z-direction for each well, requiring approximately 25 images for each well. Images captured with the BD pathway microscope captured approximately 70% of each well, whereas images made with the ImageXpress imager could capture the entire well.

Image- and data analysis

Image stacks for each well were analysed and phenotypes were quantified as described previously,¹ using Ominer software integrated in KNIME Analytics Platform (KNIME version 3.1.2, Konstanz, Germany, <http://www.knime.org/>). 450 phenotypic measurements were z-score normalized to plate median, or normalized to percent of control (100% corresponding with forskolin-stimulated control median and 0% with unstimulated/vehicle control median). For heatmap plots of efficacy, data was scaled between 0% inhibition of cyst growth (forskolin-stimulated control median) and 100% inhibition (unstimulated control median) for presentation purposes. Linear discriminant analysis (LDA) for the validation screen was performed using an R script (<https://www.r-project.org/>) integrated in KNIME. In order to remove most highly correlating phenotypic parameters prior to training the LDA, we applied a correlation filter (Pearson product-moment correlation coefficient <0.85 or >0.85) to all 450

phenotypic parameters to filter out the 367 most highly correlating parameters. The LDA model was subsequently trained based on unstimulated control (solvent, 0.2% DMSO), stimulated control (2.5µM forskolin) and known cytotoxic molecules in the library (epirubicin, doxorubicin, daunorubicin, staurosporin and gambogic acid, at 1µM concentration) and thereafter applied to all data, yielding two linear discriminants, linear discriminant 1 (LD1) and linear discriminant 2 (LD2). Linear discriminants were thereafter scaled from 0 to 100% (labelled % efficacy and % toxicity for LD1 and LD2, respectively, for presentation purposes). The phenotypic descriptors and their coefficients that were included in the linear discriminants are presented in supplemental table 1 (top 10 ranked features only). While LD1 strongly separated unstimulated (0.2% DMSO) controls from stimulated controls (2.5µM forskolin), LD2 exclusively discriminated (un)stimulated conditions from known toxic molecules. The absolute distance to the unstimulated control group for all data points was calculated based on these scaled linear discriminants and presented as a heatmap plot using the ggplot2 package (<http://ggplot2.org>) for Rstudio 0.99.878 (<https://www.rstudio.com/products/rstudio2>) with R3.2.3 (<https://www.r-project.org/>). S-curve plots were made using the ggplot2 package. 3D scatterplots presented in the supplemental figures were generated with the Scatterplot3D package (<https://CRAN.R-project.org/package=scatterplot3d>)³ in R3.2.3. Density plots were generated with ggplot2 for R and other charts were generated with Graphpad Prism 7 (Graphpad Software, La Jolla, California, USA).

Animal procedures

The local animal experimental committee of the Leiden University Medical Center (LUMC) and the Commission Biotechnology in Animals of the Dutch Ministry of Agriculture approved all animal experiments performed.

To assess the efficacy of celastrol *in vivo* we used kidney-specific, tamoxifen-inducible Cre-*Pkd1*lox mice (iKspCre-*Pkd1*^{lox,lox}).⁴⁻⁵ To inactivate the *Pkd1* gene, mice received 15mg/kg Tamoxifen (in 1% ethanol in sunflower oil, dissolved by sonication) by oral gavage at post-natal day (P)10 and P11. From P13-P27, mice received intraperitoneal injections (i.p.) of either celastrol, pyrinium pamoate (PP) or vehicle (5% DMSO + 10% Kolliphor EL in phosphate buffered saline). After the last injection at P27, blood samples were collected from the tail vein to assess the Blood Urea levels using Reflotron Technology and then the mice were euthanized by cervical dislocation. Kidneys were cut in halves and either snap frozen in liquid nitrogen or fixed in buffered 4% formaldehyde solution for embedding in paraffin. Total image scans of Periodic acid-Schiff (PAS) stained kidney sections (4µm) were processed semi-automatically using Photoshop software by an investigator who was blinded to the treatment, as done previously.⁶ Briefly, a specifically designed colour palette was used for all images to remove all pixels from the lumens/cysts, leaving only the pixels of the actual tissue. From these numbers, the percentage of 'cystic' pixels versus total number of pixels was calculated and defined as the cystic index.

Fibrotic Index

The fibrotic index was calculated as done previously on the basis of Sirius Red staining.⁶ Briefly, tissue sections were stained after deparaffinization with 0.2% phosphomolybdic acid for 1 minute and 0.1% Sirius Red (in picric acid) for 90 minutes. This was followed by saturated picric acid and subsequently by ethanol/xylol washstep. Adobe Photoshop (Adobe Systems, Inc. San Jose, California, USA) was used for the quantification of Sirius Red.

Immunohistochemistry on 3D cyst cultures and tissue sections.

Samples were subjected by O/N Formaldehyde fixation (in buffered 4% Formaldehyde solution) and embedded in paraffin. For immunohistochemical analysis, 4μm sections were deparaffinised and subjected to heat-mediated antigen retrieval (10mM/1mMTris/EDTA) [pH 9.0] for anti-p (Tyr705) STAT3 [no. 9145; Cell Signaling Technology], and 10 mM citrate buffer [pH 6.0] for antiphospho-CREB [Ser133], and anti-phospho-ribosomal protein S6 (Ser240/244) from Cell Signaling Technology (no's. 9198, and 2215 respectively).

Sections were blocked with 0.1% H₂O₂ for 20 min for endogenous peroxidase activity and preincubated for 1 h with 5% normal goat serum in 1% BSA in PBS. Next, the sections were incubated O/N with anti-pSTAT3 (1:75), anti-p-rpS6 (1:100) or anti-pCREB (1:800). After incubation with rabbit Envision horseradish peroxidase (no. K4011;Dako) or rabbit anti-goat horseradish peroxidase (1:100; no. Po449;Dako), immune reactions were revealed using diaminobenzidine as a chromogen, counterstained with hematoxylin, dehydrated, and mounted.

Statistical Analysis

Statistical analyses were performed in Graphpad Prism 7 software, using one-way ANOVA coupled to Dunnett's multiple comparison's adjustment unless otherwise stated. Results were considered statistically significant with $p < 0.05$, and this is further annotated in figure legends.

References belonging to supplemental methods

1. Booi TH, Bange H, Leonhard WN, Yan K, Fokkelman M, Kunnen SJ, Dauwerse J, Qin Y, van de Water B, van Westen GJP, Peters DJM, Price LS: High-throughput phenotypic screening of kinase inhibitors to identify drug targets for polycystic kidney disease. *SLAS Discov (in press)*
2. Booi TH, Klop MJ, Yan K, Szantai-Kis C, Szokol B, Orfi L, van de Water B, Keri G, Price LS: Development of a 3D Tissue Culture-Based High-Content Screening Platform That Uses Phenotypic Profiling to Discriminate Selective Inhibitors of Receptor Tyrosine Kinases. *J Biomol Screen* 21(9): 912-922, 2016
3. Ligges U, Mächler M: Scatterplot3D - an R Package for Visualizing Multivariate Data. *J Stat Soft* 8(11): 1-20, 2003

4. Lantinga-van Leeuwen IS, Leonhard WN, van de Wal A, Breuning MH, Verbeek S, de Heer E, Peters DJ: Transgenic mice expressing tamoxifen-inducible Cre for somatic gene modification in renal epithelial cells. *Genesis* 44(5): 225-232, 2006
5. Lantinga-van Leeuwen IS, Leonhard WN, van der Wal A, Breuning MH, de Heer E, Peters DJ: Kidney-specific inactivation of the Pkd1 gene induces rapid cyst formation in developing kidneys and a slow onset of disease in adult mice. *Hum Mol Genet* 16(24): 3188-3196, 2007
6. Leonhard WN, Kunnen SJ, Plugge AJ, Pasternack A, Jianu SB, Veraar K, El Bouazzaoui F, Hoogaars WM, Ten Dijke P, Breuning MH, De Heer E, Ritvos O, Peters DJ: Inhibition of Activin Signaling Slows Progression of Polycystic Kidney Disease. *J Am Soc Nephrol* 27(12): 3589-3599, 2016

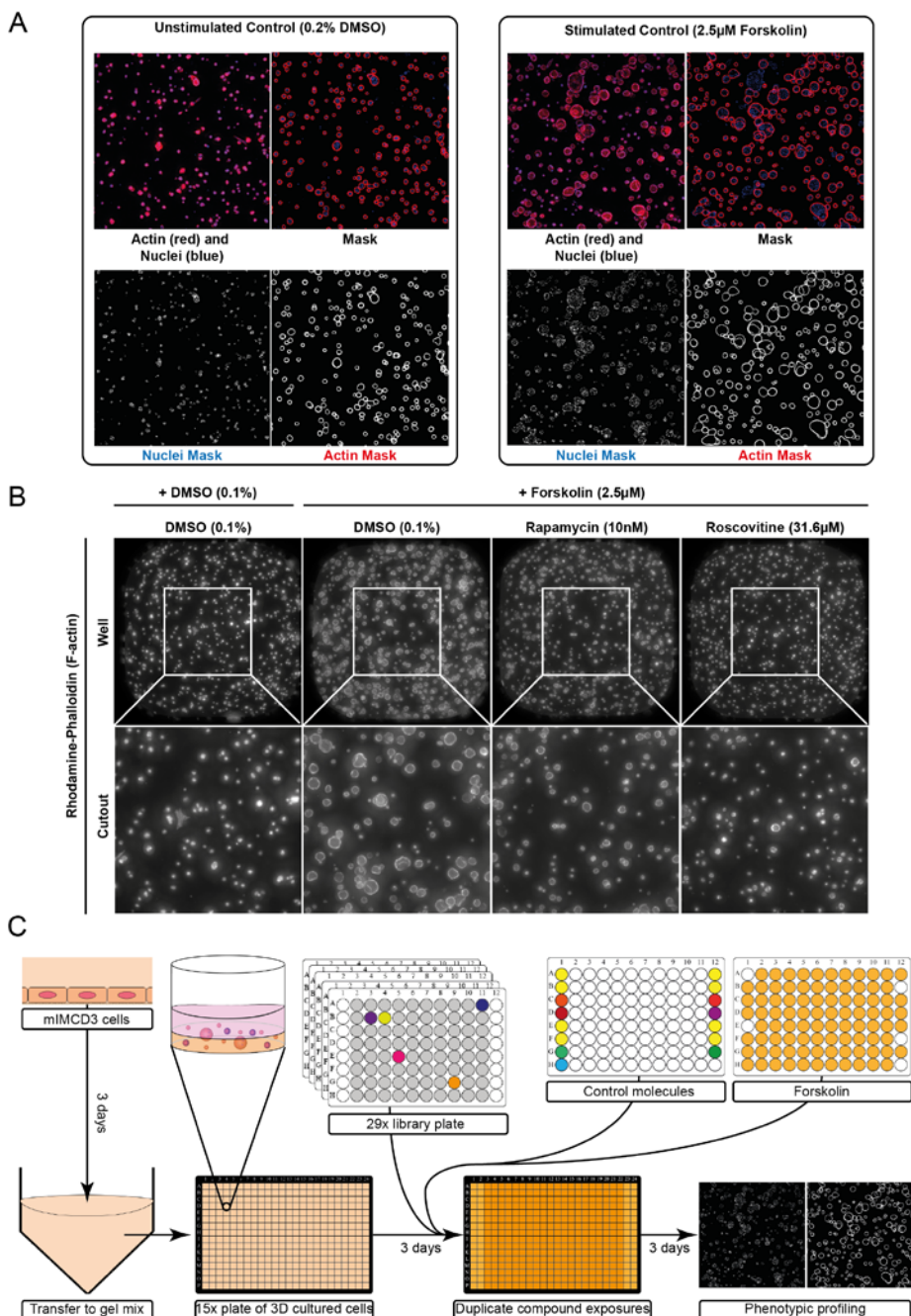
SUPPLEMENTAL MATERIALS

SUPPLEMENTAL TABLE 1 Parameter contributions to LDA

LDA feature coefficients (top 10 negatively ranked)			
LD1		LD2	
Feature Name	Interpretation	Feature Name	Interpretation
nc.Mean(zernike_order_1_1).meas		nc.Mean(std_child_to_par_center_dist).corr.meas	(related to position of nuclei)
actin.Mean(lumen_avg_width).struct.meas	(lumen size)	actin.Mean(lumen_avg_width).struct.meas	(lumen size)
actin.Sum(area).meas	(cyst wall size)	nc.Mean(avg_child_to_par_boundary_dist).corr.meas	(related to position of nuclei)
actin.Mean(zernike_order_2_2).meas		actin.SD(child_count).corr.meas	
actin.Mean(axis_Ratio_Minor_Major).meas	(cyst wall shape related)	actin.Mean(zernike_order_2_2).meas	
nc.Sum(area).meas	(nuclear size)	org.SD(axis_Ratio_Minor_Major).meas	(cyst shape related)
actin.Mean(eccentricity).meas	(cyst wall shape related)	nc.SD(number_of_branches).meas	
org.Count*(area).meas	(number of cysts)	actin.Mean(eccentricity).meas	(cyst wall shape related)
nc.Mean(child_parent_size_ratio).corr.meas	(nuclear size relative to cyst)	nc.Sum(area).meas	(nuclear size)
nc.SD(maximum_intensity).meas		nc.Mean(solidity).meas	(nuclear roundness)
LDA feature coefficients (top 10 positively ranked)			
nc.Mean(maximum_intensity).meas	(staining intensity of nuclei)	nc.Mean(hu_order_1).meas	
org.Mean(number_of_single_junction_points).meas		actin.SD(eccentricity).meas	(cyst wall shape related)
nc.Mean(avg_child_to_par_boundary_dist).corr.meas	(related to position of nuclei)	org.Mean(axis_Ratio_Minor_Major).meas	(cyst shape related)
nc.Mean(number_of_end_points).meas		nc.SD(maximum_intensity).meas	(nuclear intensity)
nc.Mean(hu_order_1).meas		nc.SD(zernike_order_8_2).meas	
actin.Mean(std_intensity).meas	(actin intensity related)	actin.SD(child_parent_size_ratio).corr.meas	(related to thickness of cyst wall)
nc.SD(zernike_order_8_2).meas		actin.Mean(std_intensity).meas	(actin intensity related)
actin.SD(eccentricity).meas	(cyst wall shape related)	org.Mean(feret).meas	
nc.SD(ratio_Area_BoundingBox_Area).meas	(nuclear shape related)	actin.Sum(area).meas	(cyst wall size)
org.Mean(feret).meas	(cyst shape related)	nc.Mean(zernike_order_1_1).meas	

SUPPLEMENTAL TABLE 2 Pathways affected by celastrol

Pathways/Targets	Context	Pubmed ID	DOI
HIF-1, erythropoietin, VEGF, mTOR, p70S6K, eIF4E, Erk	Hepatocellular carcinoma	28242743	10.1124/mol.116.107706
NFκB	Acute hepatic dysfunction	28189063	10.1016/j.etap.2017.02.002
NOX2-derived ROS-dependent PP5-JNK signaling pathway	ROS induced neurodegenerative disorders	28129433	10.1111/jnc.13966
Lipid synthesis, Sirt1		28123944	10.1016/j.molmet.2016.11.002
Nrf2, Erk1/2, Nox2, Angiotensin II type 1 receptor		28119074	10.1016/j.ejphar.2017.01.027
IKKβ		27931154	10.1080/13880209.2016.1241809
Cdc37, Annexin A2, eEF1A		27819370	10.1039/c6mb00691d
HSP90/Cdc37		27398312	10.1002/2211-5463.12081
NF-κappa B, MAPK, JAK/STAT and RANKL/OPG pathways	Autoimmune inflammation	27405485	10.1093/femspd/ftw059
IRAKs to block TLR4-mediated NFκB activation	Autoimmune inflammation	27181127	10.1016/S2095-4964(16)60257-1
miR-21/ERK	Cardiac fibrosis and cardiac dysfunction	27160852	10.1159/000445554
TLR4/MyD88/NFκB	Diabetic liver injury	27057550	10.1155/2016/2641248
AMPK/PGC1α/Sirt3	Diabetic myopathy and oxidative stress	27049825	10.3892/ijmm.2016.2549
miR-21/mTOR/p27	Gastric cancer	26500453	10.1186/s12935-015-0256-3
Autophagy		26473737	10.1371/journal.pone.0140745
HSP90		17010675	10.1016/j.ccr.2006.09.005
Calpain		18726991	10.1002/jcp.21565
hERG channel	Cancer	25866772	10.1155/2015/308475
Apoptosis mediated through mitochondrial dysfunction, Akt, PI3K, 4E-BP1, mTOR. Celastrol also inhibited the Akt/GSK3beta and Akt/NFκB survival pathways	Triple-negative breast cancer	25818165	10.1016/j.yexmp.2015.03.031
CYP1A2, CYP2C19, CYP2D6, CYP2E1 and CYP3A4		25811791	10.3109/00498254.2014.1003113
HIF-1 induction through ROS/Akt/p70S6K		25383959	10.1371/journal.pone.0112470
HSP90		24954307	10.1016/j.bbagen.2014.06.008
HIF-1α pathway by inhibition of mTOR/p70S6K/eIF4E and ERK1/2		24859482	10.3892/or.2014.3211
Cannabinoid receptory type 2	Neuropathic pain	25101848	10.3390/ijms150813637
NFκB	Inflammation	PMC4453024	10.5483/BMBRep.2015.48.3.147
Inhibit proteasome and upregulate <i>hsp30</i> and <i>hsp70</i> gene expression		20188206	10.1016/j.cbpa.2010.02.015
miR-21, PI3K/Akt, NFκB		24434352	doi: 10.1159/000357683
JNK, PTEN-Akt/mTOR pathway	Cadmium-induced neuronal cell death	24111524	10.1111/jnc.12474
Snail/E-cadherin	TGF-beta induced EMT	23850675	10.1016/j.bbrc.2013.06.113
Hsp70, Akt1, p70/S6K, ERK1/2	C2C12 myotube atrophy	23810294	10.1016/j.abb.2013.06.006
LOX-1	Atherosclerosis	23799016	10.1371/journal.pone.0065477
UDP-glucuronosyl transferase (UGT) 1A6 and 2B7		22669039	10.3390/molecules17066832
p-JNK, p-c-Jun, NFκB	Cerebral ischemia	22575561	10.1016/j.brainres.2012.04.054
Estrogen receptor α (ERα)	Breast cancer	20934245	10.1016/j.canlet.2010.09.006
Platelet activation (P-selectin and glycoprotein IIb/IIIa activation)		19661812	10.1097/FJC.0b013e3181b21472
VEGFR		18343027	10.1016/j.canlet.2008.01.043

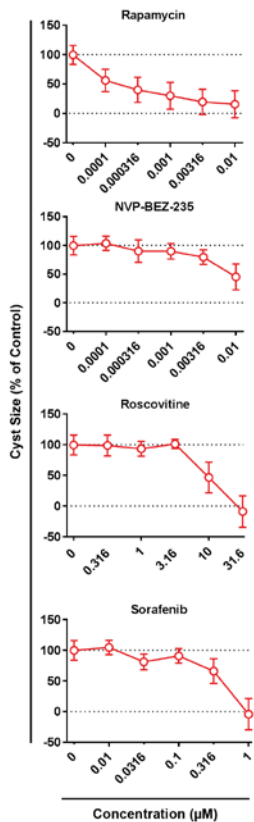


► **SUPPLEMENTAL FIGURE 1** Screening molecule libraries using 3D cultured cysts.

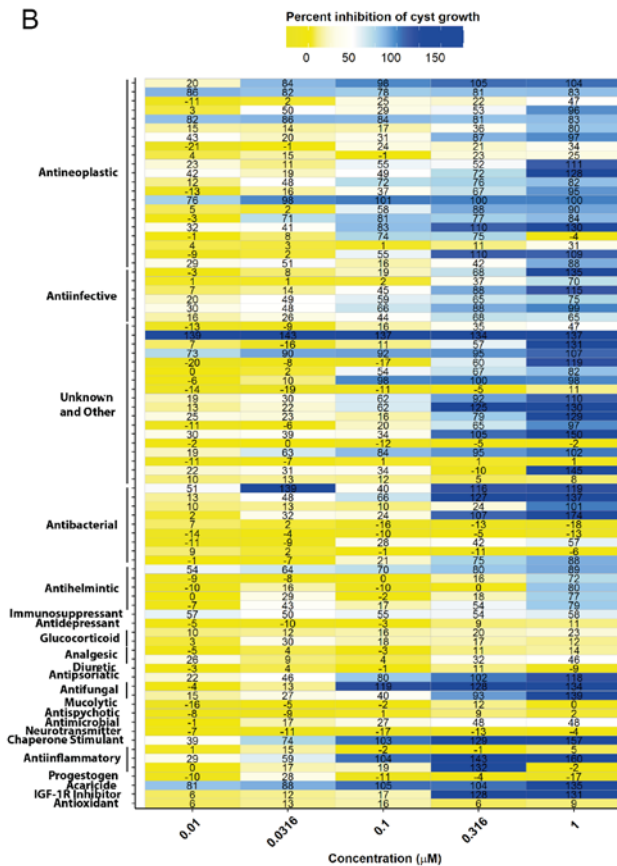
A) mIMCD3 *Pkd1*^{-/-} cysts cultured for 96 hours in Cyst-Gel and exposed to solvent (unstimulated) or forskolin (stimulated). Image stacks of rhodamine-phalloidin and Hoechst 33258-stained cysts (top left images) processed by Ominer software to (legend continues on next page)

generate- and quantify binary masks. **B)** mIMCD3 *Pkd1*^{-/-} cells were cultured for 96 hours in Cyst-Gel and exposed to solvent (DMSO) or control compounds (rapamycin, roscovitine) in the presence of forskolin. Cytoskeleton (F-actin) shown. Upper panel shows projected image stacks of entire well images with an ImageXpress micro XLS imager. Lower panel represents 500x500px cut-out of the centre of the well. Contrast and brightness enhanced for presentation purposes. **C)** Schematic representation of screening pipeline as described under supplemental methods. mIMCD3 *shPkd1* cells were mixed with Cyst-Gel and allowed to develop into small cysts during 72 hours, prior to exposure to the small molecule library. Control molecules were added to the outer plate columns, and forskolin was added to all wells, except for a few wells that served as ‘unstimulated’ controls (16 per plate). Staurosporin was added to the lower right corner of each plate to serve as positive control for cytotoxicity. After 72-hours incubation, cultures were stained, imaged and quantified as described in the supplemental methods section.

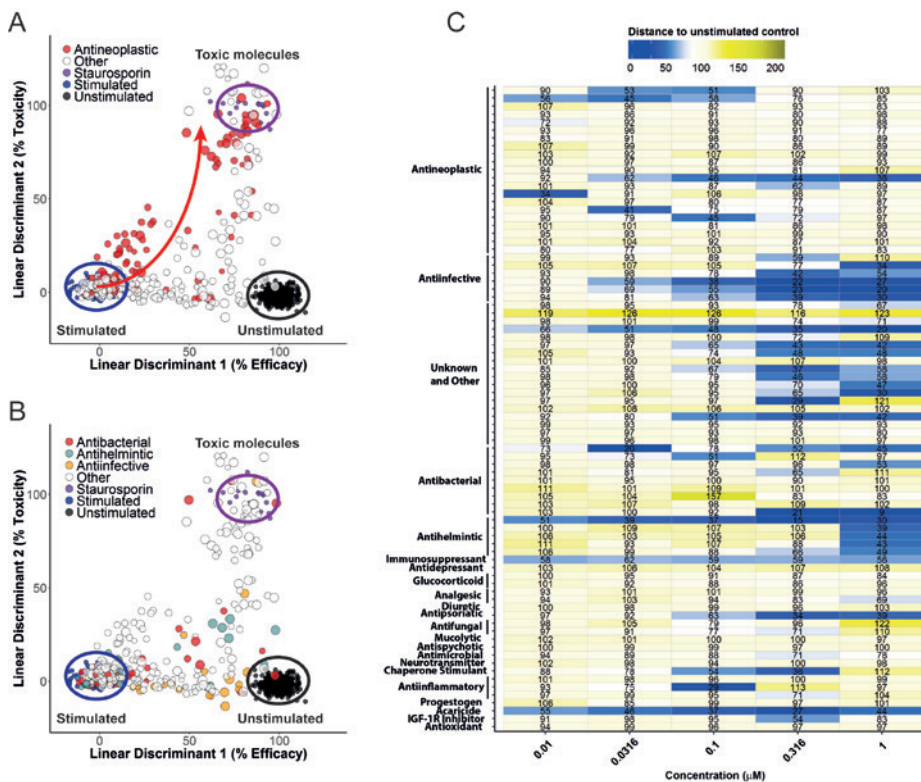
A



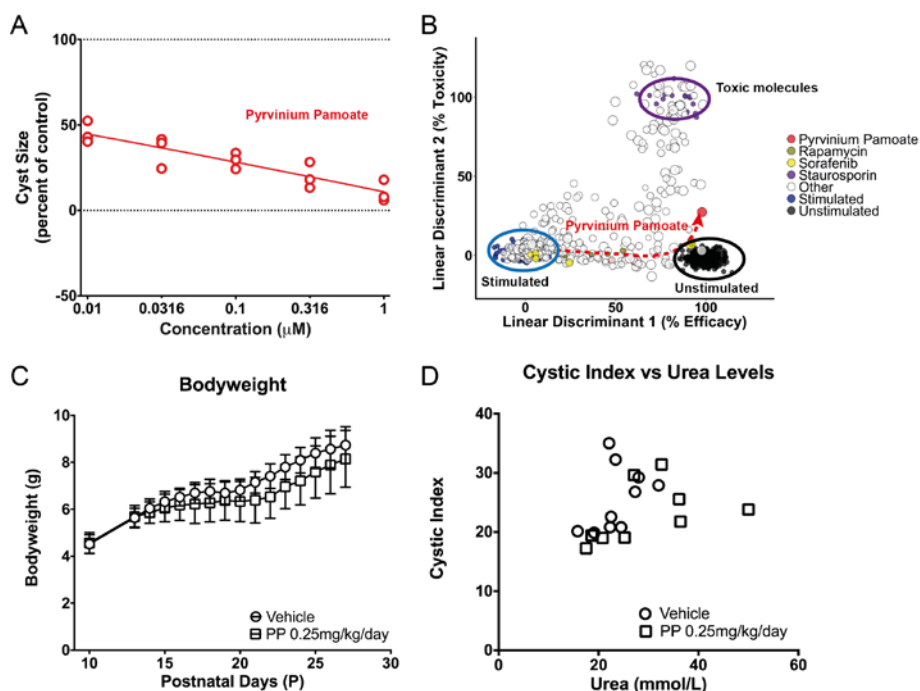
B



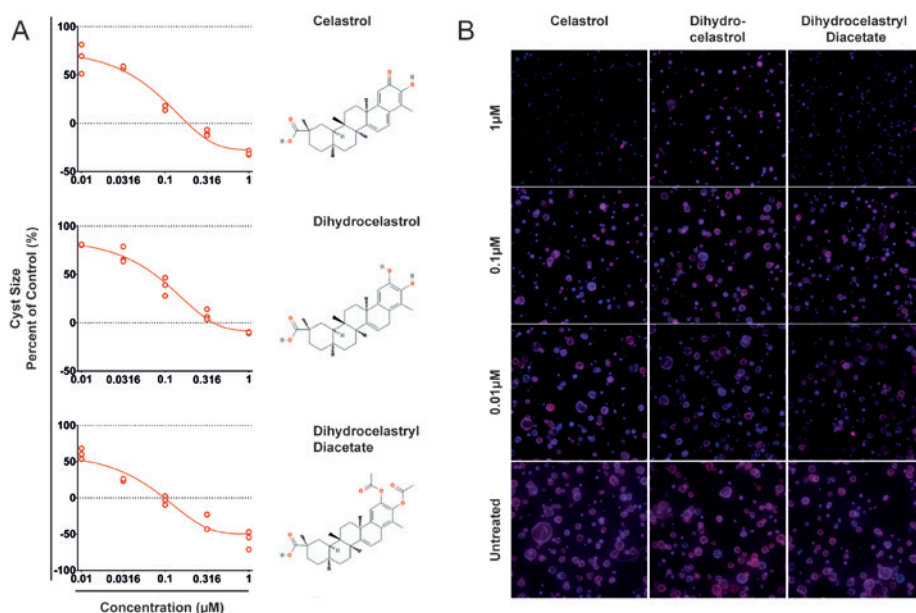
SUPPLEMENTAL FIGURE 2 Screen validation on mIMCD3 *Pkd1*^{-/-} cysts. **A)** Concentration-response curves of positive control molecules in the validation screen. Cyst size was scaled to %cyst growth: 100% represents forskolin-stimulated control (large cysts), 0% represents unstimulated control (small cysts). Means \pm SD shown from triplicate wells. **B)** 81 cyst-growth inhibition molecules rescreened at 5 concentrations. Described bioactivity of the manufacturer's datasheet displayed on y-axis. Potency of molecules represented by percent-inhibition of forskolin-induced cyst growth, as represented by the colour scale and the numbers displayed (means of triplicate wells). 52/81 molecules showed activity $>50\%$ inhibition at 1mM concentration.



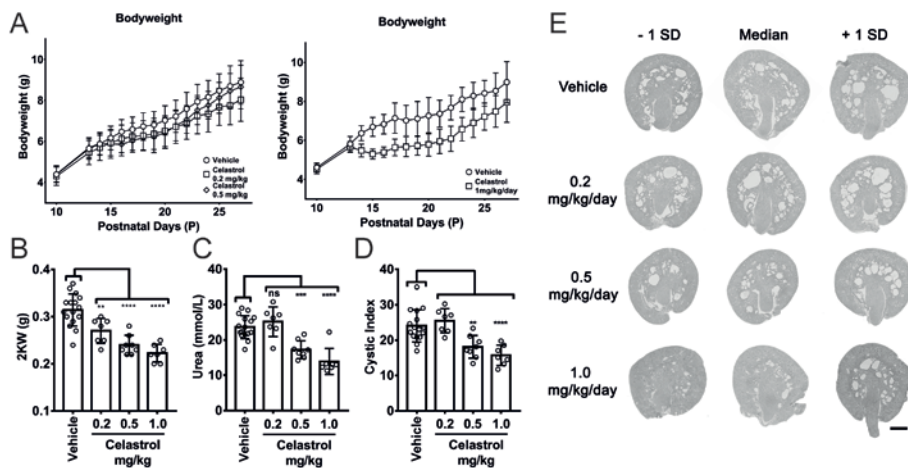
SUPPLEMENTAL FIGURE 3 Linear discriminant analysis discriminates antineoplastic molecules. **A-B)** LDA was trained as described in supplemental methods (using phenotypic parameters with linear correlation <0.85) and could discriminate antineoplastic molecules (A, red circles) from the unstimulated- and stimulated controls, indicated by black and blue circles, respectively, while retaining activity of others such as antibacterial (B, red circles), antihelminthic (B, light blue) or antiinfective molecules (B, yellow). Point size corresponds with concentration and points shown represent means of triplicate wells (except for “Stimulated”, “Unstimulated” and “Staurosporin”: individual datapoints shown). **C)** Measurement of desirable efficacy-similar to supplemental figure 2B, but presenting absolute distance to unstimulated control calculated from supplemental figure 3B, presented as colour scale and numeric values. Blue colours indicate efficacy.



SUPPLEMENTAL FIGURE 4 Pyrvinium Pamoate (PP) shows potent efficacy *in vitro*, but not *in vivo*. **A**) PP inhibits forskolin-induced cyst growth of mIMCD3 *Pkd1*^{-/-} cysts (100%, forskolin-stimulated; 0%, unstimulated). Individual wells shown as red circles. **B**) LDA plot indicates potent desirable efficacy of PP, and indicates no toxic effects. **C**) In total 17 mice received with PP treatment at postnatal day 13. Ten of those started at 1mg/kg/day of which three mice died within 4-6 days after the start of the treatment. As PP was poorly tolerated at 1mg/kg/day, we reduced the dosage for the 7 remaining mice to 0.25mg/kg/day. In order to obtain sufficient group size, 7 mice were included later during the experiment and were only treated with 0.25mg/kg/day. PP did not affect bodyweight at 0.25mg/kg/day. (vehicle n=11, PP n=14, mean \pm SD shown). **D**) At 0.25mg/kg/day, PP did not lower cystic index or urea levels (vehicle n=10 and PP n=9 shown).



SUPPLEMENTAL FIGURE 5 Structural analogues of celastrol also potently inhibit forskolin-induced cyst growth *in vitro* in m1MCD3 *Pkd1*^{-/-} cysts. **A)** Dihydrocelastrol (middle panel) and dihydrocelastryl diacetate (bottom panel) were included in the molecule library and inhibited forskolin-induced cyst growth similarly to celastrol (top panel). Structural formulae shown on the right were obtained from PubChem. **B)** Representative images of celastrol-treated, dihydrocelastrol-treated or dihydrocelastryl diacetate-treated m1MCD3 *Pkd1*^{-/-} cysts. Images shown are collapsed-stack images of nuclei (Hoechst 33258, blue) and F-actin (rhodamine-phalloidin, red) combined. Images show a 500x500px cut-out from the center of the well. Images were taken with the ImageXpress micro XLS imager. Untreated control condition represents forskolin stimulated controls (corresponding with 100% cyst size in figure A).

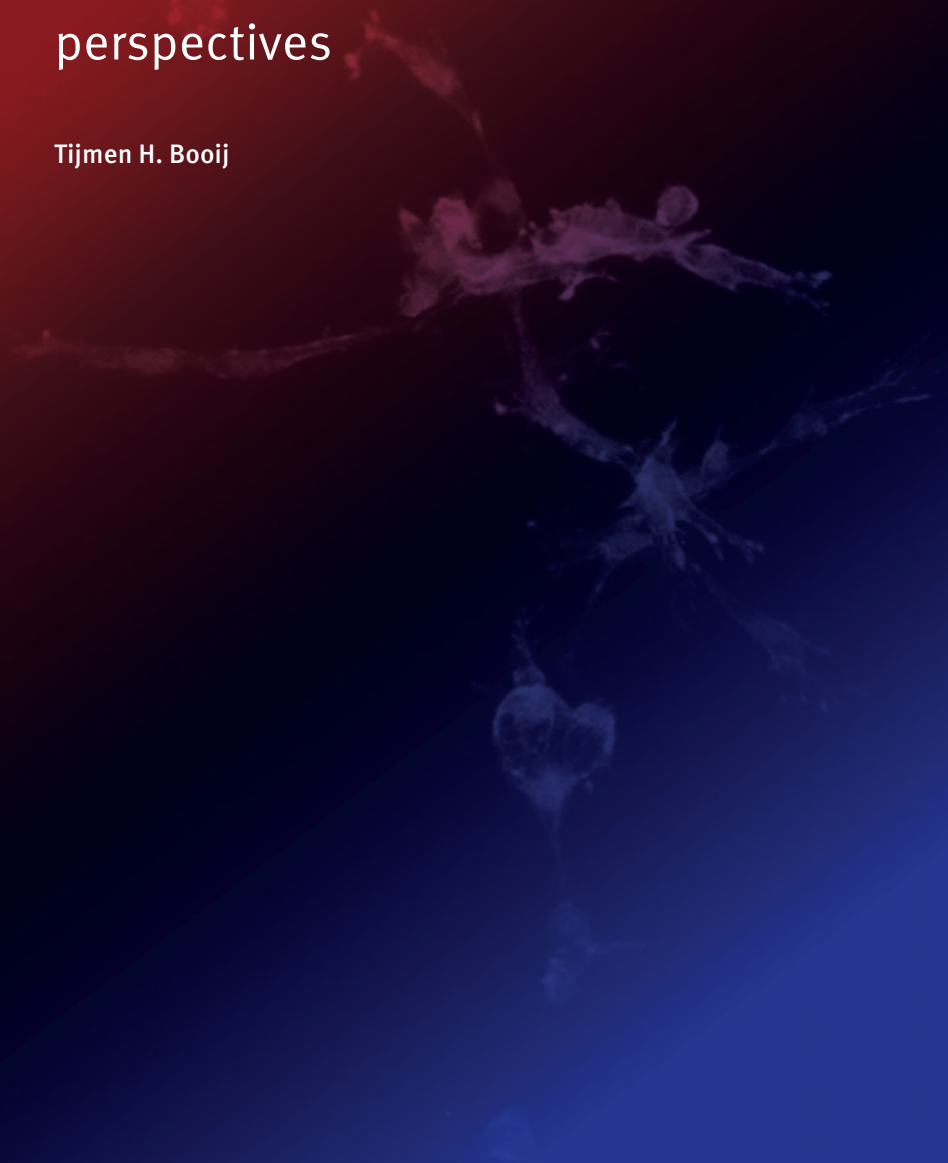


SUPPLEMENTAL FIGURE 6 Celastrol potently inhibits cystogenesis in an *in vivo* model of PKD. **A**) Bodyweight is affected by 1mg/kg/day and 0.5mg/kg/day between P13 and P18. **B-D**) Treatment with 0.5 and 1mg/kg/day celastrol lowers two-kidney weight (**B**), urea levels (**C**) and cystic index (**D**) as compared to vehicle control. For these charts, we pooled the experimental data of two independent experiments (0.2 and 0.5mg/kg/day versus 1mg/kg/day celastrol), because the vehicle controls were highly similar. Mean \pm SD as well as individual mice shown. * $p < 0.05$, ** $p < 0.01$, *** $p < 0.001$, **** $p < 0.0001$ with ordinary one-way ANOVA with Dunnett's multiple comparison's test. **E**) Histology reveals that celastrol potently inhibited cyst growth at 0.5 and 1mg/kg/day. Images displaying cystic index close to median ± 1 SD were selected and presented here.

chapter 7

General discussion and future perspectives

Tijmen H. Booij



Three-dimensional cell culture assays

In order to overcome biological limitations of traditional *in vitro* disease models as discussed in **chapter 1**, three-dimensional (3D) cell culture techniques were developed to bridge the gap between these *in vitro* models and the *in vivo* situation.^{1,2} However, while 3D cell culture techniques provide biological advantages over 2D cell culture models, these are often not exploited to their full potential (**chapter 2**). For example, while more biologically relevant, these *in vitro* models have often not been adapted for routine compound screening due to problems associated with scalability and increased cost of tissue culture reagents.³ As a result, 3D cultures are generally employed to validate findings that were originally observed in two-dimensional (2D) cell culture context, prior to *in vivo* evaluation. While the 3D cell culture models can in this context eliminate false positives prior to animal experiments, it is likely that the lack of relevant biological features of 2D cell cultures causes an increased false-negative rate in the initial observations in 2D cell cultures (**chapter 1**). Advances in laboratory automation have enabled large-scale preparation of 3D cultures for high-throughput screens (HTS), and throughout this thesis I applied this technology, coupled with high-content analysis, to perform screens using 3D cultured micro-tissues.

High-Content Screening (HCS)

Simple biochemical or colorimetric measurements of compound efficacy on cell cultures (e.g. ATPlite or MTT assays) often only provide limited information on the biological context.⁴ While an ATPlite measurement can provide very relevant measurements of ATP content and related general cell health status,^{5,6} a molecule that kills cells is not necessarily a good drug. For example, in **chapter 6**, I described the potent efficacy of antineoplastic drugs at inhibiting 3D cyst growth in the context of polycystic kidney disease (PKD). In the context of cancer, a DNA-intercalating- or otherwise growth-inhibitory drug may be effective at treating or delaying the disease. In the context of PKD, a molecule that inhibits cell growth is also likely to arrest cystogenesis, because increased cell proliferation is an important driver of cyst growth. Importantly, because PKD is a disease with a slow progression, such a therapy is likely to come with severe side effects that limit its use as a drug for PKD patients.

An alternative to using traditional biochemical efficacy measurements is using phenotypic information, often termed high-content analysis (HCA) or HCS in the context of screening⁷⁻⁹ (**chapter 2**). Although HCA currently is more commonly used together with 2D cell culture assays, phenotypic information can also be derived from the individual 3D micro-tissues,¹⁰ where tissues are individually imaged and quantified against a pre-defined set of phenotypic descriptors for various possible characteristics (branching morphology, roundness, size, nuclear elongation, etc.).¹¹⁻¹³ An advantage offered by HCA is that it is possible to conduct drug discovery at a target-agnostic level,⁷ thus opposing target-based drug discovery. Additionally, information on cellular phenotypes can be used to identify potential off-target effects of molecules, or even cytotoxic effects. For example, in **chapter 6**, phenotypic information was used to exclude potentially toxic molecules, and this indeed limited the selection of known antineoplastic

compounds. Throughout this thesis, I applied HCS on different cellular assays, to discriminate selective inhibitors from non-selective inhibitors of receptor tyrosine kinases, to identify modulators of cystogenesis and to find drug candidates that can effectively slow down the growth of renal cysts.

Discriminating small molecule inhibitors by target

In **chapter 3**, I used this high-content analysis, also termed phenotypic profiling, to discriminate epidermal growth factor receptor (EGFR) and c-Met receptor tyrosine kinase inhibitors in the context of tumour cell invasion. Using phenotypic profiling, I could selectively classify molecules that inhibited EGFR or c-Met, and also identified dual inhibitors for these receptors. Interestingly, off-target effects by molecules that inhibited tumour cell invasion through different mechanisms were also observed. Therefore, using phenotypic profiling it is possible to screen for the inhibition of disease phenotypes, while target-based screening can also be performed. One limitation to this approach is that target discrimination relies on the phenotypic manifestation of target inhibition, or activation. However, this phenotypic target-based approach can be of particular interest for the identification of off-target effects,⁷ as these are not commonly captured using traditional biochemical approaches.

Identification of druggable targets for polycystic kidney disease

In **chapters 4 and 5**, a 3D cyst screening platform was used to screen molecule libraries containing kinase inhibitors with pre-determined molecular targets. In these chapters, I related the effects of these molecules to their known molecular targets to identify pathways relevant in cyst growth. This approach led to the selection of targets such as mammalian target of rapamycin (mTOR), which has been extensively described for PKD²⁴⁻²⁶ and can therefore confirm the relevance of this approach. Additionally, we discovered that inhibitors of cyclin-dependent kinases (CDKs) potentially inhibited cyst growth, which is also in line with earlier observations for roscovitine.²¹ Although very potent, PCA analysis could discriminate roscovitine from unstimulated controls in **chapter 4**, indicating that the phenotype of the cysts is altered compared to unstimulated cysts. While the activity of roscovitine in other PKD models has been confirmed, roscovitine has not yet entered clinical trials, possibly related to safety concerns for the use of this type of drugs for PKD.²²⁻²³ This potential for causing side effects is also illustrated by the results I presented in **chapter 5**, where many CDK inhibitors that inhibited cyst growth also affected morphology of 4T1 tumouroids, indicating that these inhibitors do not exclusively target cystogenesis, but may have a broader activity spectrum.

Interestingly, the results presented in **chapter 4 and 5**, and also in **chapter 6** (supplemental figures 2 and 3), have shown that several insulin-like growth factor receptor-1 (IGF-1R) inhibitors delayed cyst growth in our assay. The IGF-1R is a receptor for insulin-like growth factor (IGF) and its signalling is known to contribute to cell proliferation and survival through PI3K, Akt, mTOR and P70S6K.²⁴⁻²⁹ The involvement of IGF-1 in PKD progression has been described previously by other groups,³⁰⁻³² and IGF-1R inhibitors may present an interesting therapeutic option of PKD due to the increase in

IGF-1 expression observed with progression of cystic lesions.^{27, 31} Of note, the IGF-1R inhibitors tested here may also have affinity towards other receptors such as the insulin receptor, which can also bind ligand IGF,^{27, 33} and it is therefore necessary to confirm the involvement of the IGF-1R, potentially using function-blocking antibodies raised against the receptor or by downregulation of receptor expression. The low severity of the side effects (e.g. hyperglycaemia, fatigue, nausea) observed of IGF-1R inhibitors in clinical trials to treat cancer,³⁴ and the absence of dose-limiting toxicity,³⁵ further supports the potential of IGF-1R inhibitors for the treatment of PKD.

Similarly, in **chapter 4 and 5**, I described the efficacy of inhibitors for HER2, an important molecular target in aggressive breast cancer,³⁶ at inhibiting cyst growth in our 3D cyst assay. HER2 was identified as a potential target for PKD more than a decade ago, but was not followed up since.³⁷ Whether HER2-targeted therapy would also be effective in PKD patients would therefore be unclear. HER-2 targeted therapy (generally monoclonal antibodies against HER2 rather than small molecule inhibitors) has been tested in the clinic in the context of different types of cancer, most commonly breast cancer, and is generally combined with chemotherapeutic drugs,³⁸ making it difficult to judge the safety profile, but the most common reported side effects of pertuzumab (a humanized monoclonal antibody against HER2), include diarrhoea, weakness, nausea and rash.³⁹ Although trastuzumab, a monoclonal antibody against HER2 was associated with cardiotoxicity, this was not observed for novel HER2-targeted therapies.⁴⁰ Neratinib, an oral small molecule HER2 inhibitor is also reported to cause diarrhoea,⁴¹ and this may be the result of the presence of ErbB-class receptors on intestinal epithelial cells.⁴¹⁻⁴²

Finally, the results presented in **chapter 4** suggest the importance of spleen tyrosine kinase (Syk) in cyst growth, which has not been previously reported. Syk plays an important role in the immune system⁴³ and has mostly been implied as a target for immune disorders such as asthma⁴⁴ and rheumatoid arthritis,⁴⁵ but has also been proposed as a target in cancer.⁴⁶ However, because of its role in signalling in B-cells, mast cells, macrophages, neutrophils, platelets and erythrocytes,⁴³ targeting Syk for the treatment of PKD may potentially cause side effects that outweigh its use for treating PKD.

While the drug targets described in this section are known to be inhibited by the molecules in the tested compound libraries, it is likely that these molecules also have other molecular targets at the concentrations tested, and it will therefore be important to measure protein phosphorylation levels after compound treatment to ensure that the targets are affected. Additionally, for several receptor tyrosine kinases, such as HER2, function-blocking antibodies were designed that may be more specific to the target. These antibodies may be used to confirm the efficacy of target inhibition on cyst growth.

Finding drug candidates to treat polycystic kidney disease

Currently the only available drug for the treatment of PKD is tolvaptan. While this compound can slow down the growth of renal cysts, its use may be limited because of side effects associated with diuresis. This illustrates that novel therapies are still required.

Chapter 6 described the identification of pyrvinium pamoate and celastrol as inhibitors of cystogenesis *in vitro*. Both compounds were initially selected after a phenotypic screen with 2320 compounds on 3D-cultured mouse inner medullary collecting duct cells with reduced levels of *Pkd1* expression. While this screening setup was highly convenient to screen large compound libraries due to fast cystogenesis and swelling, the choice of a murine collecting duct cell line and also the rapid cystogenesis can potentially limit the relevance of the *in vitro* findings to human disease. Firstly, the cysts in human polycystic kidney disease develop slowly over time, and not in a few days. It is therefore a possibility that proliferation-driven processes are more important in this 3D cyst culture model, compared to human PKD, which could also explain the identification of many antineoplastic molecules as cyst growth inhibitors. Secondly, the cysts developing in PKD do not solely originate from the collecting ducts, but from all segments of the nephron.⁴⁷ It is therefore possible that the effects observed from pyrvinium pamoate and celastrol are nephron-segment specific, potentially limiting therapeutic potential. Finally, the choice of using murine cells may complicate translation of our findings to PKD patients.

Since we were aware of the shortcomings of using a rapid murine *in vitro* model for PKD, the effects of pyrvinium pamoate and celastrol were evaluated in a mouse *in vivo* model for PKD. We found that pyrvinium pamoate displayed a lack of activity in this model and we therefore did not investigate this compound further. In contrast, the *in vivo* activity of celastrol confirmed the *in vitro* discoveries and celastrol could therefore present an interesting therapeutic opportunity. Further supporting the use of celastrol for the treatment of PKD is the finding that two close analogues of celastrol, dihydrocelastrol and dihydrocelastryl diacetate, also induced similar cyst growth inhibition profiles *in vitro*, although the effects of these compounds have not been evaluated *in vivo* due to lack of commercial availability and the low number of scientific publications covering their effects.

Celastrol is a molecule isolated from the thunder god vine, also *Tripterygium Wilfordii*. This vine is promoted in traditional Chinese medicine for use in rheumatoid arthritis,⁴⁸ but its use is not recommended due to safety concerns.⁴⁹ It is important to mention in that context that *Tripterygium Wilfordii* contains many bioactive molecules (~100), potentially explaining the side effects associated with its use.⁵⁰⁻⁵¹ Celastrol has not been previously linked to PKD, but has been implied for several other indications.⁵¹⁻⁵⁶ In **chapter 6**, we evaluated the effects of celastrol on several PKD-associated signalling pathways (pCREB, pS6 and pSTAT3), but observed no effect on these targets. As several publications have previously suggested, celastrol may have many molecular targets such as HSP90/Cdc37,⁵⁷⁻⁵⁸ NFκB⁵⁹ and Nrf2.⁶⁰ HSP90 inhibition has

previously been shown to be an effective strategy to reduce cyst growth *in vivo*, probably because many pathways activated by *PKD1* or *PKD2* inactivation are regulated by HSP90.⁶¹ Additionally, oxidative stress is observed in all stages of ADPKD⁶² and may be a general mechanism in the pathogenesis of PKD.⁶³ Inhibition of NFκB and activation of the Nrf2 by celastrol and the associated antioxidant response could therefore be an important mechanism by which celastrol can inhibit the growth of cysts, although whether this is also the case in our *in vitro* and *in vivo* model remains to be determined. In addition to these targets, celastrol is also known to be able to interact with thiol groups in many proteins^{58, 64} as is the case for many plant extracts (e.g. curcumin⁶⁵), probably giving celastrol a very broad target space that has not yet been completely unravelled. Interestingly, such a broad target specificity also makes it unlikely to identify similar molecules in traditional target-based drug discovery approaches – thereby favouring phenotypic screening techniques. As currently the mechanism by which celastrol inhibits cystogenesis in our model is unclear, an analysis of the transcriptome of 3D-cultured cysts treated with celastrol could shed light on the pathways that are affected.

Very importantly however: a broad target specificity can be beneficial in diseases where many signalling cascades are effected (such as PKD), but it is also a concern for safety, as it is more likely that other organs and physiological processes are affected. Increased insight in the pathways that are affected by celastrol by transcriptomics, as well as the use of fluorescent reporters for cellular stress pathways could be used to predict potential toxicity.⁶⁶⁻⁶⁷ Fortunately, in our *in vivo* experiments, celastrol did not appear to cause many side effects, except for a reduction in body weight between P13 and P18, as was also reported by others for 1mg/kg/day.⁵² While such a reduction in body weight can be related to dose-limiting toxicity or effects on other organs than the kidney, the reduced bodyweight after celastrol treatment are more likely related to its known effects as a leptin sensitizer and its potential use in the treatment of obesity.⁶⁸⁻⁶⁹ Reduced food intake as a result of this effect of celastrol may have biased our findings as food restriction is also known to ameliorate PKD progression.⁷⁰ However, it is unlikely that the effects observed on *in vitro* cultured cysts are the result of this mechanism. One limitation of the *in vivo* PKD model used in **chapter 6** is the rapid disease progression. Because these mice develop renal failure within a few weeks, which does not correspond with the slow disease progression in humans, the efficacy of celastrol in a chronic disease *in vivo* model remains to be determined and will also be critical to detect potential safety concerns associated with long-term administration. Whether celastrol is likely to become a drug for PKD, while maintaining a desirable efficacy profile is therefore, despite the promising results presented in this thesis, still uncertain.

As a result of the many signalling pathways that are deregulated in PKD as described in **chapter 1**, one could argue that a single drug cannot be sufficient to prevent cystogenesis. An interesting approach could therefore be to test drug combinations, for example from the other identified active compounds in **chapter 6**, on 3D cell culture models of cystogenesis. This may potentially identify synergistic effects, allowing for dose reductions of the individual compounds.

The current availability of 3D cell culture matrices and the ability to prepare 3D cultured cells in multi-well plates using automated liquid handlers, has improved the quality of *in vitro* PKD models over the past years, which is now likely to aid in the selection of more effective, and safer drugs. In addition, the *in vitro* selection of better drugs could eventually contribute to a reduction in the required animal experiments, although some hurdles need to be overcome to further improve these models, as discussed below.

Current limitations of 3D HCS technology and future perspectives

In **chapter 2** I discussed limitations of 3D cell culture techniques that have hampered their implementation in routine drug discovery. These difficulties include the use of natural ECM protein matrices for 3D cultures, such as collagen and Matrigel, because these suffer from batch-to-batch variability and also complicate liquid handling because the reagents solidify at room temperature. Currently, synthetic hydrogels generally have limited biocompatibility compared to these natural hydrogels.⁷¹ However, several examples now exist where this type of gel can provide improved biological context due to incorporation of functional groups,⁷²⁻⁷³ and it is possible that such techniques can be incorporated in high-throughput screens and will be more accessible in the future.

Sample preparation from 3D cell cultures, such as the extraction of protein for Western blot or RNA extractions to measure gene expression levels, is also more challenging, and requires additional purification steps compared to regular 2D cell cultures. This is especially important when attempting to extract cellular proteins: Matrigel or collagen-based gels contain high concentrations of proteins that can far exceed the content of cellular proteins, thus requiring removal of proteins from the gel prior to cell lysis. Another challenge lies in performing immunostainings, as antibodies take longer to diffuse through the ECM, requiring longer incubation times and more extensive washing steps. Nevertheless, these problems can probably largely be overcome by setting up standard procedures for these techniques optimized for 3D cell cultures, although whether this is successful will also depend on the type of culture matrix.

Currently, the popularity of immortalized cell lines for high-throughput screens, such as the PC-3, mIMCD3 and 4T1 cell lines used throughout this thesis, can pose a barrier to the physiological relevance of cell culture assays, because organs are comprised of many different cell types that cannot be represented completely by a single cell line.⁷⁴⁻⁷⁵ This means more extensive validations are required to be able to translate findings on immortalized cell lines to the human body. While immortalized cell lines are generally convenient in high-throughput screens due to their ease of culturing and also because of their relative lack of heterogeneity, depending on the research question it is likely that the introduction of multiple cell types in the form of co-cultures may allow us to improve physiological relevance. However, this may also introduce more experimental variation, making implementation in HCS more challenging.

Moving away from immortalized cell lines altogether and instead using patient-derived cells is likely to tremendously enhance physiological relevance of 3D cell-based assays. For example, in the context of PKD, patient-derived induced pluripotent stem cells (iPSCs) can be differentiated to kidney cells⁷⁶⁻⁷⁸ and iPSCs have been generated with mutations relevant to PKD.⁷⁹⁻⁸⁰ A clear advantage of such PKD patient-derived cells is the biological relevance of the mutation. While most generated immortalized cell lines harbour a deletion of an entire gene or large gene fragment, these iPSC-derived tissues retain a disease-causing mutation (although these are patient-, and possibly also species specific – meaning that it may not always be possible to validate findings in animal models⁸¹⁻⁸²). Even though iPSC-derived tissues can be used for high-throughput screening,⁸³ their extensive differentiation procedures and slow growth can pose new challenges, especially for screens of 3D cultures. Therefore, to what extent such cell types can be used in routine high-content screens as 3D culture remains to be determined, but it is likely that such cell types will be used more frequently in the future as an alternative to immortalized cell lines in screening.

It has even proven possible to generate self-organising kidney organoids from pluripotent stem cells.⁸⁴⁻⁸⁵ These kidney organoids can contain many different cell lineages and can more accurately model kidney development.⁸⁶ While these organoids display increased functionality compared to single cell types, they are not currently used in high-throughput phenotypic screens. It is possible that their composition of multiple tissue types may make phenotypic screening more challenging, as the composition of individual organoids may be too variable. The presence of multiple cell types also puts additional strain on image capturing and image analysis, because it may no longer be sufficient to capture a series of xy-images per well. Instead, such organoid cultures are likely to require 3D reconstruction at high magnification to capture sufficient detail. While such organoids may therefore eventually enable screening of molecules for organ toxicity (e.g. nephrotoxicity) or kidney disease, the technology is currently still in its infancy and it is probably going to take another 5 to 10 years before such micro-tissues can be routinely used for phenotypic screens. However, an interesting application of these self-organising kidney organoids, is the development of bioengineered kidneys to treat disease.⁸⁷

In addition to the limitations posed by the cell types used, extraction of phenotypic information from 3D cell cultures is currently limited by computational power and storage capacity. Due to the vast quantity of image data that is typically generated from multi-well plates with 3D micro-tissues (50-100GB per 384 well assay plate), dedicated storage facilities and excellent infrastructure are required. Additionally, the quality of the imager and the image analysis tools can potentially limit the quality of the readout. On the upside, judging from the progress in the last ten years in storage capacity, computational power and quality of the microscopes, this barrier to the implementation of 3D HCS may soon become a thing of the past.

Conclusions

This thesis described various strategies to employ 3D phenotypic screening in a high-throughput setting; ranging from the identification of new drugable targets to the selection of lead molecules. While 3D cell culture-based high-content screening is not yet routinely applied in drug discovery campaigns, the improved biological relevance of these assays is likely to improve translatability of results to the clinic and may drastically reduce the animal experiments that are currently required in drug research, and reduce barriers for more personalized medicine.

References

1. Pampaloni F, Reynaud EG, Stelzer EH: The third dimension bridges the gap between cell culture and live tissue. *Nat Rev Mol Cell Biol* 8(10): 839-845, 2007
2. Birgersdotter A, Sandberg R, Ernberg I: Gene expression perturbation in vitro--a growing case for three-dimensional (3D) culture systems. *Semin Cancer Biol* 15(5): 405-412, 2005
3. Ryan SL, Baird AM, Vaz G, Urquhart AJ, Senge M, Richard DJ, O'Byrne KJ, Davies AM: Drug Discovery Approaches Utilizing Three-Dimensional Cell Culture. *Assay Drug Dev Technol* 14(1): 19-28, 2016
4. Vega-Avila E, Pugsley MK: An overview of colorimetric assay methods used to assess survival or proliferation of mammalian cells. *Proc West Pharmacol Soc* 54 10-14, 2011
5. Riss TL, Moravec RA, Niles AL, Duellman S, Benink HA, Worzella TJ, Minor L: Cell Viability Assays. In: edited by Sittampalam GS, NP Coussens, K Brimacombe, A Grossman, M Arkin, D Auld, C Austin, J Baell, B Bejcek, TDY Chung, JL Dahlin, V Devanaryan, TL Foley, M Glicksman, MD Hall, JV Hass, J Inglese, PW Iversen, M Lal-Nag, Z Li, J McGee, O McManus, T Riss, OJ Trask, Jr., JR Weidner, M Xia and X Xu, Bethesda (MD), Eli Lilly & Company and the National Center for Advancing Translational Sciences, 2004,
6. Adan A, Kiraz Y, Baran Y: Cell Proliferation and Cytotoxicity Assays. *Curr Pharm Biotechnol* 17(14): 1213-1221, 2016
7. Fraietta I, Gasparri F: The development of high-content screening (HCS) technology and its importance to drug discovery. *Expert Opin Drug Discov* 11(5): 501-514, 2016
8. Bickle M: The beautiful cell: high-content screening in drug discovery. *Anal Bioanal Chem* 398(1): 219-226, 2010
9. Bickle M: High-content screening: a new primary screening tool? *IDrugs* 11(11): 822-826, 2008
10. Li L, Zhou Q, Voss TC, Quick KL, LaBarbera DV: High-throughput imaging: Focusing in on drug discovery in 3D. *Methods* 96 97-102, 2016
11. Horvath P, Aulner N, Bickle M, Davies AM, Nery ED, Ebner D, Montoya MC, Ostling P, Pietiainen V, Price LS, Shorte SL, Turcatti G, von Schantz C, Carragher NO: Screening out irrelevant cell-based models of disease. *Nat Rev Drug Discov* 15(11): 751-769, 2016

12. Kriston-Vizi J, Flotow H: Getting the whole picture: High content screening using three-dimensional cellular model systems and whole animal assays. *Cytometry A* 91(2): 152-159, 2017
13. Di Z, Klop MJ, Rogkoti VM, Le Devedec SE, van de Water B, Verbeek FJ, Price LS, Meerman JH: Ultra high content image analysis and phenotype profiling of 3D cultured micro-tissues. *PLoS One* 9(10): e109688, 2014
14. Perico N, Antiga L, Caroli A, Ruggenti P, Fasolini G, Cafaro M, Ondei P, Rubis N, Diadei O, Gherardi G, Prandini S, Panozo A, Bravo RF, Carminati S, De Leon FR, Gaspari F, Cortinovis M, Motterlini N, Ene-Iordache B, Remuzzi A, Remuzzi G: Sirolimus therapy to halt the progression of ADPKD. *J Am Soc Nephrol* 21(6): 1031-1040, 2010
15. Ravichandran K, Zafar I, Ozkok A, Edelstein CL: An mTOR kinase inhibitor slows disease progression in a rat model of polycystic kidney disease. *Nephrol Dial Transplant* 30(1): 45-53, 2015
16. Ruggenti P, Gentile G, Perico N, Perna A, Barcella L, Trillini M, Cortinovis M, Ferrer Siles CP, Reyes Loaeza JA, Aparicio MC, Fasolini G, Gaspari F, Martinetti D, Carrara F, Rubis N, Prandini S, Caroli A, Sharma K, Antiga L, Remuzzi A, Remuzzi G: Effect of Sirolimus on Disease Progression in Patients with Autosomal Dominant Polycystic Kidney Disease and CKD Stages 3b-4. *Clin J Am Soc Nephrol* 11(5): 785-794, 2016
17. Serra AL, Poster D, Kistler AD, Krauer F, Raina S, Young J, Rentsch KM, Spanaus KS, Senn O, Kristanto P, Scheffel H, Weishaupt D, Wuthrich RP: Sirolimus and kidney growth in autosomal dominant polycystic kidney disease. *N Engl J Med* 363(9): 820-829, 2010
18. Shillingford JM, Murcia NS, Larson CH, Low SH, Hedgepeth R, Brown N, Flask CA, Novick AC, Goldfarb DA, Kramer-Zucker A, Walz G, Piontek KB, Germino GG, Weimbs T: The mTOR pathway is regulated by polycystin-1, and its inhibition reverses renal cystogenesis in polycystic kidney disease. *Proc Natl Acad Sci U S A* 103(14): 5466-5471, 2006
19. Stallone G, Infante B, Grandaliano G, Bristogiannis C, Macarini L, Mezzopane D, Bruno F, Montemurno E, Schirinzi A, Sabbatini M, Pisani A, Tataranni T, Schena FP, Gesualdo L: Rapamycin for treatment of type I autosomal dominant polycystic kidney disease (RAPYD-study): a randomized, controlled study. *Nephrol Dial Transplant* 27(9): 3560-3567, 2012
20. Tao Y, Kim J, Schrier RW, Edelstein CL: Rapamycin markedly slows disease progression in a rat model of polycystic kidney disease. *J Am Soc Nephrol* 16(1): 46-51, 2005
21. Bukanov NO, Moreno SE, Natoli TA, Rogers KA, Smith LA, Ledbetter SR, Oumata N, Galons H, Meijer L, Ibraghimov-Beskrovnaya O: CDK inhibitors R-roscovitine and S-CR8 effectively block renal and hepatic cystogenesis in an orthologous model of ADPKD. *Cell Cycle* 11(21): 4040-4046, 2012
22. Cicenas J, Kalyan K, Sorokinas A, Stankunas E, Levy J, Meskinyte I, Stankevicius V, Kaupinis A, Valius M: Roscovitine in cancer and other diseases. *Ann Transl Med* 3(10): 135, 2015

23. Song H, Vita M, Sallam H, Tehranchi R, Nilsson C, Siden A, Hassan Z: Effect of the Cdk-inhibitor roscovitine on mouse hematopoietic progenitors in vivo and in vitro. *Cancer Chemother Pharmacol* 60(6): 841-849, 2007
24. Nakae J, Kido Y, Accili D: Distinct and overlapping functions of insulin and IGF-I receptors. *Endocr Rev* 22(6): 818-835, 2001
25. Tracz AF, Szczyluk C, Porta C, Czarnecka AM: Insulin-like growth factor-1 signaling in renal cell carcinoma. *BMC Cancer* 16 453, 2016
26. Motallebnezhad M, Aghebati-Maleki L, Jadidi-Niaragh F, Nickho H, Samadi-Kafil H, Shamsasenjan K, Yousefi M: The insulin-like growth factor-I receptor (IGF-IR) in breast cancer: biology and treatment strategies. *Tumour Biol* 37(9): 11711-11721, 2016
27. Liu C, Zhang Y, Yuan L, Fu L, Mei C: Rosiglitazone inhibits insulin-like growth factor1-induced polycystic kidney disease cell growth and p70S6 kinase activation. *Mol Med Rep* 8(3): 861-864, 2013
28. Yin Y, Hua H, Li M, Liu S, Kong Q, Shao T, Wang J, Luo Y, Wang Q, Luo T, Jiang Y: mTORC2 promotes type I insulin-like growth factor receptor and insulin receptor activation through the tyrosine kinase activity of mTOR. *Cell Res* 26(1): 46-65, 2016
29. Li H, Batth IS, Qu X, Xu L, Song N, Wang R, Liu Y: IGF-IR signaling in epithelial to mesenchymal transition and targeting IGF-IR therapy: overview and new insights. *Mol Cancer* 16(1): 6, 2017
30. Parker E, Newby LJ, Sharpe CC, Rossetti S, Streets AJ, Harris PC, O'Hare MJ, Ong AC: Hyperproliferation of PKD1 cystic cells is induced by insulin-like growth factor-1 activation of the Ras/Raf signalling system. *Kidney Int* 72(2): 157-165, 2007
31. Nakamura T, Ebihara I, Nagaoka I, Tomino Y, Nagao S, Takahashi H, Koide H: Growth factor gene expression in kidney of murine polycystic kidney disease. *J Am Soc Nephrol* 3(7): 1378-1386, 1993
32. Aukema HM, Housini I: Dietary soy protein effects on disease and IGF-I in male and female Han:SPRD-cy rats. *Kidney Int* 59(1): 52-61, 2001
33. Mulvihill MJ, Cooke A, Rosenfeld-Franklin M, Buck E, Foreman K, Landfair D, O'Connor M, Pirritt C, Sun Y, Yao Y, Arnold LD, Gibson NW, Ji QS: Discovery of OSI-906: a selective and orally efficacious dual inhibitor of the IGF-1 receptor and insulin receptor. *Future Med Chem* 1(6): 1153-1171, 2009
34. Beckwith H, Yee D: Minireview: Were the IGF Signaling Inhibitors All Bad? *Mol Endocrinol* 29(11): 1549-1557, 2015
35. Haluska P, Shaw HM, Batzel GN, Yin D, Molina JR, Molife LR, Yap TA, Roberts ML, Sharma A, Gualberto A, Adjei AA, de Bono JS: Phase I dose escalation study of the anti insulin-like growth factor-I receptor monoclonal antibody CP-751,871 in patients with refractory solid tumors. *Clin Cancer Res* 13(19): 5834-5840, 2007
36. Labidi S, Mejri N, Lagha A, Daoud N, El Benna H, Afrit M, Boussen H: Targeted Therapies in HER2-Overexpressing Metastatic Breast Cancer. *Breast Care (Basel)* 11(6): 418-422, 2016
37. Wilson SJ, Amsler K, Hyink DP, Li X, Lu W, Zhou J, Burrow CR, Wilson PD: Inhibition of HER-2(neu/ErbB2) restores normal function and structure to polycystic kidney disease (PKD) epithelia. *Biochim Biophys Acta* 1762(7): 647-655, 2006

38. Sini V, Cassano A, Corsi D, De Laurentiis M, Gamucci T, Mauri M, Naso G, Roselli M, Ruggeri EM, Tonini G, Vici P, Zampa G, Marchetti P: Bevacizumab as first-line treatment in HER2-negative advanced breast cancer: pros and cons. *Tumori* 102(5): 472-480, 2016
39. Capelan M, Pugliano L, De Azambuja E, Bozovic I, Saini KS, Sotiriou C, Loi S, Piccart-Gebhart MJ: Pertuzumab: new hope for patients with HER2-positive breast cancer. *Ann Oncol* 24(2): 273-282, 2013
40. Sendur MA, Aksoy S, Altundag K: Cardiotoxicity of novel HER2-targeted therapies. *Curr Med Res Opin* 29(8): 1015-1024, 2013
41. Chan A: Neratinib in HER-2-positive breast cancer: results to date and clinical usefulness. *Ther Adv Med Oncol* 8(5): 339-350, 2016
42. Van Sebillie YZ, Gibson RJ, Wardill HR, Bowen JM: ErbB small molecule tyrosine kinase inhibitor (TKI) induced diarrhoea: Chloride secretion as a mechanistic hypothesis. *Cancer Treat Rev* 41(7): 646-652, 2015
43. Kaur M, Singh M, Silakari O: Inhibitors of switch kinase 'spleen tyrosine kinase' in inflammation and immune-mediated disorders: a review. *Eur J Med Chem* 67 434-446, 2013
44. Ulanova M, Duta F, Puttagunta L, Schreiber AD, Befus AD: Spleen tyrosine kinase (Syk) as a novel target for allergic asthma and rhinitis. *Expert Opin Ther Targets* 9(5): 901-921, 2005
45. Nijjar JS, Tindell A, McInnes IB, Siebert S: Inhibition of spleen tyrosine kinase in the treatment of rheumatoid arthritis. *Rheumatology (Oxford)* 52(9): 1556-1562, 2013
46. Krisenko MO, Geahlen RL: Calling in SYK: SYK's dual role as a tumor promoter and tumor suppressor in cancer. *Biochim Biophys Acta* 1853(1): 254-263, 2015
47. Devuyt O, Burrow CR, Smith BL, Agre P, Knepper MA, Wilson PD: Expression of aquaporins-1 and -2 during nephrogenesis and in autosomal dominant polycystic kidney disease. *Am J Physiol* 271(1 Pt 2): F169-183, 1996
48. Tao X, Younger J, Fan FZ, Wang B, Lipsky PE: Benefit of an extract of *Tripterygium Wilfordii* Hook F in patients with rheumatoid arthritis: a double-blind, placebo-controlled study. *Arthritis Rheum* 46(7): 1735-1743, 2002
49. Canter PH, Lee HS, Ernst E: A systematic review of randomised clinical trials of *Tripterygium wilfordii* for rheumatoid arthritis. *Phytomedicine* 13(5): 371-377, 2006
50. Liu Z, Ma L, Zhou GB: The main anticancer bullets of the Chinese medicinal herb, thunder god vine. *Molecules* 16(6): 5283-5297, 2011
51. Wong KF, Yuan Y, Luk JM: *Tripterygium wilfordii* bioactive compounds as anticancer and anti-inflammatory agents. *Clin Exp Pharmacol Physiol* 39(3): 311-320, 2012
52. Kim JE, Lee MH, Nam DH, Song HK, Kang YS, Lee JE, Kim HW, Cha JJ, Hyun YY, Han SY, Han KH, Han JY, Cha DR: Celastrol, an NF-kappaB inhibitor, improves insulin resistance and attenuates renal injury in db/db mice. *PLoS One* 8(4): e62068, 2013
53. Venkatesha SH, Dudics S, Astry B, Moudgil KD: Control of autoimmune inflammation by celastrol, a natural triterpenoid. *Pathog Dis* 74(6), 2016

54. Salminen A, Lehtonen M, Paimela T, Kaarniranta K: Celastrol: Molecular targets of Thunder God Vine. *Biochem Biophys Res Commun* 394(3): 439-442, 2010
55. Kannaiyan R, Shanmugam MK, Sethi G: Molecular targets of celastrol derived from Thunder of God Vine: potential role in the treatment of inflammatory disorders and cancer. *Cancer Lett* 303(1): 9-20, 2011
56. Allison AC, Cacabelos R, Lombardi VR, Alvarez XA, Vigo C: Celastrol, a potent antioxidant and anti-inflammatory drug, as a possible treatment for Alzheimer's disease. *Prog Neuropsychopharmacol Biol Psychiatry* 25(7): 1341-1357, 2001
57. Hieronymus H, Lamb J, Ross KN, Peng XP, Clement C, Rodina A, Nieto M, Du J, Stegmaier K, Raj SM, Maloney KN, Clardy J, Hahn WC, Chiosis G, Golub TR: Gene expression signature-based chemical genomic prediction identifies a novel class of HSP90 pathway modulators. *Cancer Cell* 10(4): 321-330, 2006
58. Zhou Y, Li W, Wang M, Zhang X, Zhang H, Tong X, Xiao Y: Competitive profiling of celastrol targets in human cervical cancer HeLa cells via quantitative chemical proteomics. *Mol Biosyst* 13(1): 83-91, 2016
59. Lee JH, Koo TH, Yoon H, Jung HS, Jin HZ, Lee K, Hong YS, Lee JJ: Inhibition of NF-kappa B activation through targeting I kappa B kinase by celastrol, a quinone methide triterpenoid. *Biochem Pharmacol* 72(10): 1311-1321, 2006
60. Divya T, Dineshbabu V, Soumyakrishnan S, Sureshkumar A, Sudhandiran G: Celastrol enhances Nrf2 mediated antioxidant enzymes and exhibits anti-fibrotic effect through regulation of collagen production against bleomycin-induced pulmonary fibrosis. *Chem Biol Interact* 246 52-62, 2016
61. Seeger-Nukpezah T, Proia DA, Egleston BL, Nikonova AS, Kent T, Cai KQ, Hensley HH, Ying W, Chimmanamada D, Serebriiskii IG, Golemis EA: Inhibiting the HSP90 chaperone slows cyst growth in a mouse model of autosomal dominant polycystic kidney disease. *Proc Natl Acad Sci U S A* 110(31): 12786-12791, 2013
62. Menon V, Rudym D, Chandra P, Miskulin D, Perrone R, Sarnak M: Inflammation, oxidative stress, and insulin resistance in polycystic kidney disease. *Clin J Am Soc Nephrol* 6(1): 7-13, 2011
63. Maser RL, Vassmer D, Magenheimer BS, Calvet JP: Oxidant stress and reduced antioxidant enzyme protection in polycystic kidney disease. *J Am Soc Nephrol* 13(4): 991-999, 2002
64. Liby KT, Yore MM, Sporn MB: Triterpenoids and rexinoids as multifunctional agents for the prevention and treatment of cancer. *Nat Rev Cancer* 7(5): 357-369, 2007
65. Leonhard WN, van der Wal A, Novalic Z, Kunnen SJ, Gansevoort RT, Breuning MH, de Heer E, Peters DJ: Curcumin inhibits cystogenesis by simultaneous interference of multiple signaling pathways: in vivo evidence from a Pkd1-deletion model. *Am J Physiol Renal Physiol* 300(5): F1193-1202, 2011
66. Wink S, Hiemstra S, Herpers B, van de Water B: High-content imaging-based BAC-GFP toxicity pathway reporters to assess chemical adversity liabilities. *Arch Toxicol* 91(3): 1367-1383, 2017

67. Wink S, Hiemstra S, Huppelschoten S, Danen E, Niemeijer M, Hendriks G, Vrieling H, Herpers B, van de Water B: Quantitative high content imaging of cellular adaptive stress response pathways in toxicity for chemical safety assessment. *Chem Res Toxicol* 27(3): 338-355, 2014
68. Greenhill C: Celastrol identified as a leptin sensitizer and potential novel treatment for obesity. *Nat Rev Endocrinol* 11(8): 444, 2015
69. Liu J, Lee J, Salazar Hernandez MA, Mazitschek R, Ozcan U: Treatment of obesity with celastrol. *Cell* 161(5): 999-1011, 2015
70. Warner G, Hein KZ, Nin V, Edwards M, Chini CC, Hopp K, Harris PC, Torres VE, Chini EN: Food Restriction Ameliorates the Development of Polycystic Kidney Disease. *J Am Soc Nephrol* 27(5): 1437-1447, 2016
71. Cushing MC, Anseth KS: Materials science. Hydrogel cell cultures. *Science* 316(5828): 1133-1134, 2007
72. Malkoch M, Vestberg R, Gupta N, Mespouille L, Dubois P, Mason AF, Hedrick JL, Liao Q, Frank CW, Kingsbury K, Hawker CJ: Synthesis of well-defined hydrogel networks using click chemistry. *Chem Commun (Camb)* (26): 2774-2776, 2006
73. Engler AJ, Sen S, Sweeney HL, Discher DE: Matrix elasticity directs stem cell lineage specification. *Cell* 126(4): 677-689, 2006
74. Masters JR, Stacey GN: Changing medium and passaging cell lines. *Nat Protoc* 2(9): 2276-2284, 2007
75. Nestor CE, Ottaviano R, Reinhardt D, Cruickshanks HA, Mjoseng HK, McPherson RC, Lentini A, Thomson JP, Dunican DS, Pennings S, Anderton SM, Benson M, Meehan RR: Rapid reprogramming of epigenetic and transcriptional profiles in mammalian culture systems. *Genome Biol* 16 11, 2015
76. Lam AQ, Freedman BS, Bonventre JV: Directed differentiation of pluripotent stem cells to kidney cells. *Semin Nephrol* 34(4): 445-461, 2014
77. Thatava T, Armstrong AS, De Lamo JG, Edukulla R, Khan YK, Sakuma T, Ohmine S, Sundsbak JL, Harris PC, Kudva YC, Ikeda Y: Successful disease-specific induced pluripotent stem cell generation from patients with kidney transplantation. *Stem Cell Res Ther* 2(6): 48, 2011
78. Xia Y, Nivet E, Sancho-Martinez I, Gallegos T, Suzuki K, Okamura D, Wu MZ, Dubova I, Esteban CR, Montserrat N, Campistol JM, Izpisua Belmonte JC: Directed differentiation of human pluripotent cells to ureteric bud kidney progenitor-like cells. *Nat Cell Biol* 15(12): 1507-1515, 2013
79. Freedman BS, Lam AQ, Sundsbak JL, Iatrino R, Su X, Koon SJ, Wu M, Daheron L, Harris PC, Zhou J, Bonventre JV: Reduced ciliary polycystin-2 in induced pluripotent stem cells from polycystic kidney disease patients with PKD1 mutations. *J Am Soc Nephrol* 24(10): 1571-1586, 2013
80. Freedman BS, Brooks CR, Lam AQ, Fu H, Morizane R, Agrawal V, Saad AF, Li MK, Hughes MR, Werff RV, Peters DT, Lu J, Baccei A, Siedlecki AM, Valerius MT, Musunuru K, McNagny KM, Steinman TI, Zhou J, Lerou PH, Bonventre JV: Modelling kidney disease with CRISPR-mutant kidney organoids derived from human pluripotent epiblast spheroids. *Nat Commun* 6 8715, 2015

81. Saha K, Jaenisch R: Technical challenges in using human induced pluripotent stem cells to model disease. *Cell Stem Cell* 5(6): 584-595, 2009
82. Freedman BS: Modeling Kidney Disease with iPS Cells. *Biomark Insights* 10(Suppl 1): 153-169, 2015
83. Yang YM, Gupta SK, Kim KJ, Powers BE, Cerqueira A, Wainger BJ, Ngo HD, Rosowski KA, Schein PA, Ackeifi CA, Arvanites AC, Davidow LS, Woolf CJ, Rubin LL: A small molecule screen in stem-cell-derived motor neurons identifies a kinase inhibitor as a candidate therapeutic for ALS. *Cell Stem Cell* 12(6): 713-726, 2013
84. Little MH, Takasato M: Generating a self-organizing kidney from pluripotent cells. *Curr Opin Organ Transplant* 20(2): 178-186, 2015
85. Takasato M, Little MH: A strategy for generating kidney organoids: Recapitulating the development in human pluripotent stem cells. *Dev Biol* 420(2): 210-220, 2016
86. Takasato M, Er PX, Chiu HS, Maier B, Baillie GJ, Ferguson C, Parton RG, Wolvetang EJ, Roost MS, Chuva de Sousa Lopes SM, Little MH: Kidney organoids from human iPS cells contain multiple lineages and model human nephrogenesis. *Nature* 526(7574): 564-568, 2015
87. Little MH, Combes AN, Takasato M: Understanding kidney morphogenesis to guide renal tissue regeneration. *Nat Rev Nephrol* 12(10): 624-635, 2016

chapter 8

Appendices

Tijmen H. Booij

LIST OF ABBREVIATIONS

	2D	Two-dimensional
	2KW	Two-kidney weight
	3D	Three-dimensional
	8-Br-cAMP	Membrane-permeable cAMP
A	AC	Adenylyl cyclase
	AC-VI	Adenylyl cyclase 6
	ADP	Adenosine diphosphate
	ADPKD	Autosomal dominant polycystic kidney disease
	AMP	Adenosine monophosphate
	AMPK	5'AMP-activated protein kinase
	ANOVA	Analysis of variance
	ARPKD	Autosomal recessive polycystic kidney disease
	ArQ-197	Tivantinib
	ATM	Ataxia-telangiectasia mutated
	ATP	Adenosine triphosphate
	ATR	Ataxia telangiectasia and Rad3-related protein
	AVP	Antidiuretic hormone arginine vasopressin
B	BCA assay	Bicinchoninic acid assay
	BM	Basement membrane
	BSA	Bovine serum albumin
	BUN	Blood urea nitrogen
	BW	Bodyweight
C	c-Met	Tyrosine-protein kinase Met/HGF receptor
	cAMP	3', 5' Cyclic adenosine monophosphate
	Cdc2	Cell division cycle protein 2 (CDK1)
	CDDP	Cis- diamminedichloroplatinum(II), cisplatin
	CDK	Cyclin dependent kinase
	CFTR	Cystic fibrosis transmembrane conductance regulator
	CI	Combination index
	CREB	cAMP response element-binding protein
	Ctrl1	high affinity copper uptake protein 1
D	DMEM	Dulbecco's modified eagle medium
	DMSO	Dimethyl sulfoxide
	DNA	Deoxyribonucleic acid
	DNA-PK	DNA-dependent protein kinase
E	ECM	Extracellular matrix
	EDTA	Ethylenediaminetetraacetic acid
	EGF	Epidermal growth factor
	EGFR	Epidermal growth factor receptor
	EHS	Engelbreth-Holm-Swarm
	EMA	European medicines agency
	EMT	Epithelial- to mesenchymal transition

	ER	Endoplasmic reticulum
	ERK	Extracellular regulated kinase
	ESRD	End-stage renal disease
E	FBS	Fetal bovine serum
	FGFR	Fibroblast growth factor receptor
	Flt3	Fms-like tyrosine kinase 3, Fetal liver kinase 2, CD135
G	GB	Gigabyte
	GPCR	G-protein-coupled receptor
	GSK3	Glycogen synthase kinase 3
H	HCA	High-content analysis
	HCS	High-content screening
	HDM	Hanging-drop microtiter (plate)
	HER2	Human epidermal growth factor receptor 2
	HGF	Hepatocyte growth factor
	Hsp90	Heat shock protein 90
	HTS	High-throughput screening
I	IBMX	3-isobutyl-1-methylxanthine
	IGF-1(R)	Insulin-like growth factor 1 (receptor)
	IKK β	Inhibitor of nuclear factor kappa-B kinase subunit beta
	IP3	Inositol triphosphate
	iPSC	Induced pluripotent stem cell
	IR	Insulin receptor
K	K-NN	K-nearest neighbor
	Klf4	Kruppel-like factor 4
	KNIME	Konstanz Information Miner
	KO	knockout
L	LDA	Linear discriminant analysis
M	MAD	Median absolute deviation
	MEK	Mitogen-activated protein-kinase/ERK kinase
	mIMCD3	Mouse inner medullary collecting duct 3
	mRNA	Messenger ribonucleic acid
	mTOR	Mammalian Target of Rapamycin
N	NF- κ B	Nuclear factor kappa B
	NPI	Normalized-percent inhibition
	NVP-BEZ-235	Dactolisib
	NVP-BKM120	Buparlisib
O	OCT2	Organic cation transporter 2, SLC22A2
	Oct4	Octamer-binding transcription factor 4
P	PAS	Periodic acid-Schiff
	PBS	Phosphate-buffered saline
	PC	Principal component
	PC1	Polycystin-1

	PC2	Polycystin-2
	PCA	Principal component analysis
	PCP	Planar cell polarity
	PDE (PDE1/4c)	cAMP-dependent phosphodiesterases
	PDGFR	Platelet-derived growth factor receptor
	PDX	Patient-derived xenograft
	PEG	Poly-ethylene glycol
	PI3K	Phosphatidylinositol-4,5-bisphosphate 3-kinase
	PKA	protein kinase A
	PKD	Polycystic kidney disease
	Pkd1	Gene encoding polycystin-1 (mouse)
	PKD1	Gene encoding polycystin-1 (human)
	Pkd2	Gene encoding polycystin-2 (mouse)
	PKD2	Gene encoding polycystin-2 (human)
	PKHD1	Gene encoding fibrocystin/polyductin (human)
	PLC	Phospholipase c
	px	Pixels
R	R&D	Research & development
	R788	Fostamatinib
	RNA	Ribonucleic acid
	ROCK	Rho kinase
	ROI	Regions of interest
S	SD	Standard deviation
	Sox2	SRY (Sex determining region Y)-box 2
	SSTR	Somatostatin receptor
	STAT3	Signal transducer and activator of transcription 3
	Syk	Spleen tyrosine kinase
T	TBS	This-buffered saline
	TBS-T	Tris-buffered saline/Tween 20
	TKI	Tyrosine kinase inhibitor
	TNFR	TNF receptor
	TNF α	Tumour necrosis factor alpha
	TRPP2	Transient receptor potential polycystic 2 (polycystin-2)
	TSC1	Hamartin
	TSC2	Tuberin
V	V1R	Vasopressin V1 receptor
	V2R	Vasopressin V2 receptor
	V2RA	V2R antagonist
	VEGFR	Vascular endothelial growth factor receptor
W	WNT	Refers to Wnt signalling pathway

ENGLISH SUMMARY

Traditional drug discovery approaches have been hampered by (*in vitro*) cell culture models that poorly represent the situation in the human body. Principally, cells grow in the body in a three-dimensional (3D) environment that cannot generally be captured using cell culture methods. For this reason, cell culture models have been developed where cells grow in a 3D environment, which allows them to form structures that are more comparable to tissue in the body. However, the full complexity of these advanced cell culture models can only be fully used for routine drug testing if the cell culture model can be used on a large scale (also termed high-throughput screening or HTS), and if the readout can capture all of the biological complexity reflected by the 3D-cultured cells (high-content screening or HCS), as discussed in chapter 2. Due to these technological limitations, 3D cellular models are not yet routinely applied in drug and drug-target discovery.

In order to underline the importance of measuring the biological complexity exerted by 3D-cultured cells, **chapter 3** describes the development and use of a 3D cell culture model that simulates the process of tumour cell invasion, a process that precedes metastasis. This model was used to test different types of molecules that may prevent this process through different mechanisms. By using phenotypic measurements on these 3D-cultured prostate cancer cells, the molecules could be classified by mechanism-of-action, and off-target activity. The classification of these molecules according to phenotype was confirmed to be correct by comparison with enzyme activity measurements.

In a similar approach, **chapter 4** describes the development of a 3D cell culture model that can mimic the development of renal cysts as observed in polycystic kidney disease (PKD). This disease is characterized by the development of fluid-filled renal cysts that cause a progressive decline of kidney function. As a result of the lack of relevant cell models, only one drug was recently admitted onto the market, and this is associated with side-effects that may limit its use. The model we developed uses 3D-cultured renal cells that form cysts. The enlargement of these cysts can be influenced or reduced by adding molecules that affect relevant disease targets. In order to find these relevant disease targets, this developed 3D cyst culture model was employed to test a library of molecules for which molecular targets were known. This allowed us to relate efficacy of the molecules at inhibiting growth of cysts to molecular targets, leading to the identification of mTOR, HER2, IGF-1R, CDK, Aurora A kinase and Syk, but surprisingly not PI3K and EGFR as relevant disease targets. Some of these molecular targets have been extensively described in literature (mTOR, CDK) for PKD, confirming the relevance of this approach.

In order to follow up on the identified molecular targets, in **chapter 5**, we tested another molecule library with known target specificity and affinity in the 3D cyst culture model. The phenotypic changes that the molecules induced on the 3D cultured cysts

were compared to the changes induced by a model compound for cytotoxicity. Using this approach, we were able to exclude potentially toxic molecules and retain molecules that only reduced cyst enlargement. We discovered that also these molecules are known to inhibit CDKs, but also again found Aurora A kinase, HER2 and IGF-1R inhibitors among the active molecules. Having confirmed our previous findings, we decided to compare the activity of these molecules on invasive tumour cells. This allowed us to select molecules that only influenced the growth of cysts, but not the phenotype of tumour cells. An IGF-1R and Akt1 inhibitor, VCC55, strongly reduced cyst swelling without killing cells, and could therefore be an interesting treatment candidate.

In **chapter 6**, we identified two effective molecules, pyrvinium pamoate and celastrol, after a large screen with 2320 molecules. These molecules showed desirable effects in our 3D cyst culture platform and were therefore tested in a mouse model of PKD. Whereas pyrvinium pamoate failed to show effect, celastrol potently reduced cyst burden and improved kidney function in these mice. It is currently unclear through which molecular mechanism celastrol influences cyst growth, but it likely involves multiple molecular targets. Celastrol is a molecule that is isolated from the thunder god vine, which is extensively described in (traditional Chinese-) medicine for its anti-inflammatory, anti-obesity and potential anti-cancer effects.

In summary, this thesis describes how 3D cell culture techniques, coupled with phenotypic profiling, can be used to advance drug discovery. The use of 3D cell-based assays can enhance physiological relevance of *in vitro* research and may thereby lead to improved drug selection and safety. In addition, by using more biologically relevant cell culture models, there may be a possibility to reduce the number of animal studies required, prior to clinical evaluation of drugs, due to increased success rates.

NEDERLANDSE SAMENVATTING

De ontwikkeling van nieuwe medicijnen wordt gelimiteerd door de beperkte fysiologische relevantie van traditionele celweekmodellen in preklinisch *in vitro* onderzoek. In het menselijk lichaam groeien cellen in een driedimensionale (3D) omgeving die niet kan worden weergegeven door deze celweekmodellen. Om over deze beperking heen te komen zijn 3D celweeksystemen ontwikkeld, waarbij cellen een structuur kunnen vormen die fysiologisch relevanter is en meer lijkt op weefsels in het lichaam. Een probleem is dat om gebruik te maken van alles wat deze weefsels te bieden hebben, het celweekmodel geschikt moet zijn voor het testen van medicijnen op grote schaal (high-throughput screening of HTS) en dat alle biologische complexiteit correct moet worden gemeten (high-content screening of HCS). Dit wordt verder besproken in **hoofdstuk 2**. Door deze problemen worden 3D celkweeken nog niet routinematig gebruikt in het medicijnonderzoek.

Om het belang van het meten van de biologische complexiteit van 3D celkweeken te benadrukken laat **hoofdstuk 3** de ontwikkeling van een 3D celweek model zien dat het proces van kankercel-invasie simuleert (een proces dat voorafgaat aan het uitzaaien of metastaseren van kanker). We hebben dit celweek model gebruikt om moleculen die dit proces op verschillende manieren beïnvloeden te testen. Door de structuur en vorm van de 3D prostaatkanker-celstructuren te bepalen konden deze moleculen geclassificeerd worden naar mechanisme en konden daarnaast moleculen geïdentificeerd worden die niet specifiek waren. De correctheid van deze classificatie aan de hand van het fenotype hebben we ten slotte bevestigd door het meten van enzymactiviteit.

Op een vergelijkbare wijze laten we in **hoofdstuk 4** de ontwikkeling van een 3D celweek model zien waarin we de ontwikkeling van cysten, zoals bij de humane ziekte cystenieren (ook wel PKD), simuleren. Bij deze erfelijke ziekte vormen tijdens het leven vocht-gevulde cysten in de nieren waardoor de nierfunctie sterk achteruit gaat. Doordat er voor het onderzoek naar geneesmiddelen voor deze ziekte geen relevante celkweeken zijn die gebruikt kunnen worden om op grote schaal stoffen kunnen testen, is er nu slechts één geneesmiddel op de markt, dat ook lastige bijwerkingen heeft. Het model dat wij beschrijven in dit hoofdstuk gebruikt niercellen die in een 3D omgeving cysten kunnen vormen. Door moleculen toe te voegen aan deze cysten kunnen we onderzoeken of de moleculen die voor cystenieren relevante aangrijpingspunten (ook wel: moleculaire targets) hebben, cystegroei vertragen. Om te onderzoeken welke aangrijpingspunten binnen de cel relevant zijn voor cystenieren, hebben we dit 3D celweek model gebruikt om een verzameling moleculen, waarvan de moleculaire targets bekend waren, te testen. Hierdoor was het mogelijk om het effect van de moleculen op cyste groei te relateren aan de moleculaire targets. Naar aanleiding hiervan identificeerden wij mTOR, HER2, IGF-1R, CDK, Aurora A kinase en Syk, maar tot onze verbazing niet PI3K of EGFR, als eiwitten die mogelijk van belang zijn bij het

remmen van cyste groei. Doordat een aantal van deze targets eerder beschreven waren in de literatuur (mTOR, CDK) voor cystenieren, bevestigt dit de relevantie van dit model.

Om volgens deze strategie verder te gaan, hebben we in **hoofdstuk 5** een andere verzameling moleculen getest, waarvan de precieze affiniteit voor de targets van bekend was. Hierbij hebben we de fenotypische veranderingen van de cysten na de behandeling met deze moleculen vergeleken met een toxische stof. Door moleculen, die een fenotype veroorzaakte dat erg lijkt op het fenotype geïnduceerd door de toxische stof, uit te sluiten hebben we moleculen kunnen selecteren die minder toxisch zijn. Ook hier vonden wij dat de moleculen die cyste groei remden CDK, Aurora A kinase, HER2 en IGF-1R als targets hadden. Doordat dit ook onze bevindingen in het vorige hoofdstuk bevestigde, hebben we de activiteit van deze moleculen vergeleken op een model voor kankercel invasie. Hierdoor konden we moleculen selecteren die alléén een effect hadden op cyste groei, en niet op deze andere cellen, waardoor er mogelijk een gericht effect is op cystenieren. VCC55 is een IGF-1R en Akt1 remmer die cyste groei sterk verminderde zonder cellen te doden, waardoor dit mogelijk een kandidaat zou zijn voor vervolgonderzoek.

Hoofdstuk 6 beschrijft de ontdekking van twee zeer effectieve moleculen, pyrvinium pamoate en celastrol, na een grote screen met 2320 moleculen in het 3D celkweek model voor cystenieren. Door de sterke activiteit van deze moleculen in ons 3D celkweek model hebben we besloten deze stoffen te testen in een muismodel voor cystenieren, waarin we zagen dat pyrvinium pamoate geen gunstige effecten op het ziekteverloop had. Daarentegen bleek celastrol een zeer effectieve stof; na behandeling hadden de muizen een verbeterde nierfunctie en ook een kleiner aantal cysten. Op dit moment is onbekend waarom celastrol de groei van cysten vertraagt, maar dit komt waarschijnlijk door meerdere moleculaire targets. Celastrol kan worden geëxtraheerd uit *tripterygium wilfordii*, een plant die vaak in (traditionele Chinese-) geneeskunde wordt gebruikt ter genezing van ontstekingen en vanwege mogelijke werkingen tegen obesitas en tumoren.

Samenvattend; in dit proefschrift laten we zien hoe 3D celkweek modellen, gecombineerd met fenotypische analyse, gebruikt kan worden om het *in vitro* medicijnonderzoek te verbeteren, zodat de bevindingen relevanter zijn voor diermodellen en voor patiënten, met als resultaat mogelijk veiligere geneesmiddelen met minder bijwerkingen. Doordat deze nieuwere celkweek methoden kunnen bijdragen aan een grotere kans op succes voor geneesmiddelen, is het mogelijk dat uiteindelijk het aantal dierproeven, dat nodig is voordat geneesmiddelen in mensen getest kunnen worden, kan worden teruggedrongen.

LIST OF PUBLICATIONS

High-throughput phenotypic screening of kinase inhibitors to identify drug targets for polycystic kidney disease

Booij, T.H., Bange, H., Leonhard, W.N., Yan, K., Fokkelman, M., Kunnen, S.J., Dauwerse, J.G., Qin, Y., van de Water, B., van Westen, G.J.P., Peters, D.J.M., Price, L.S.

SLAS Discovery, Sep. 2017; 22(8): 974-84

8

Development of a 3D tissue culture-based high-content screening platform that uses phenotypic profiling to discriminate selective inhibitors of receptor tyrosine kinases

Booij, T.H.#, Klop M.J.#, Yan, K., Szántai-Kis, C., Szokol, B., Orfi, L., van de Water, B. Keri, G. and Price, L.S.

Journal of Biomolecular Screening, Oct. 2016; 21(9): 912-22

MEK inhibition induces apoptosis in osteosarcoma cells with constitutive ERK1/2 phosphorylation

Baranski, Z., Booij, T.H., Kuijjer, M.L., de Jong, Y., Cleton-Jansen, A.M., Price, L.S., van de Water, B., Bovée, J.V., Hogendoorn, P.C. and Danen, E.H.

Genes Cancer, Nov. 2015; 6(11-12): 503-12

Aven-mediated checkpoint kinase control regulates proliferation and resistance to chemotherapy in conventional osteosarcoma

Baranski, Z., Booij, T.H., Cleton-Jansen, A.M., Price, L.S., van de Water, B., Bovée, J.V., Hogendoorn, P.C., Danen, E.H.

Journal of Pathology, Jul. 2015; 236(3): 348-59

Epac-Rap signaling reduces oxidative stress in the tubular epithelium

Stokman G.#, Qin, Y.#, Booij, T.H., Ramaiahgari, S., Lacombe, M., Dolman, M.E., van Dorenmalen, K.M., Teske, G.J., Florquin, S., Schwede, F., van de Water, B., Kok, R.J., Price, L.S.

Journal of the American Society of Nephrology, Jul. 2014; 25(7): 1474-85

In vitro 3D phenotypic drug screen identifies celastrol as an effective in vivo inhibitor of polycystic kidney disease

Booij, T.H.#, Leonhard, W.N.#, Yan, K., Fokkelman, M., Plugge, A.J., Veraar, K.A.M., Dauwerse, J.G., van Westen, G.J.P., van de Water, B., Price, L.S.¥, Peters, D.J.M.¥

Manuscript submitted and under revision

Getting the most out of 3D cell based assays with high content image analysis and phenotypic profiling

Booij, T.H., Herpers, B., Yan, K., Price, L.S.

Manuscript in preparation

Phenotypic profiling of 3D-cultured micro-tissues to identify selective inhibitors of cyst growth

Booij, T.H., Kaczmarczyk, A., Bange, H., van Asten, S.D., Yan, K., van de Water, B., Peters, D.J.M., Price, L.S.

Manuscript in preparation

^{#/¥}These authors contributed equally

CURRICULUM VITAE

Tijmen Harmen Booij was born on November 26th, 1988 in Den Helder, the Netherlands. Between 2001 and 2007 he went to the Mummellius Gymnasium in Alkmaar, also in the Netherlands.

Greatly fascinated by (cell-) biology and medicine, he decided in 2007 to pursue his Bachelor's degree in Bio-Pharmaceutical Sciences at the University of Leiden, the Netherlands. During his Bachelor's studies, he was first introduced to cell culture and 3D-cell culture technologies, the latter of which were, back then, used only in small-scale experiments.

Fascinated by the improved physiological relevance of complex multicellular structures that developed when cells were cultured in extracellular matrix, and by the potential of such cell culture assays to transform and enhance preclinical drug research, Tijmen pursued his Master's degree in Bio-Pharmaceutical Sciences at the University of Leiden from 2010. He joined the Division of Toxicology of the Leiden Academic Centre for Drug Research (LACDR) for his master's internship, where he miniaturized 3D cell culture assays to enable their use for high-throughput drug evaluation under supervision of Dr. Leo S. Price and Prof. Dr. Bob van de Water. For this work, Tijmen later received the Suzanne Hovinga Award for best master's internship project at the LACDR in 2013. During his master's studies, he also worked as a student assistant in this laboratory to screen molecule libraries in close collaboration with pharmaceutical industry. He later joined the Eidgenössische Technische Hochschule (ETH) in Zürich, Switzerland, to study the role of matrix metalloproteases on wound healing as part of his master's education.

Tijmen's great interest in developing physiologically relevant *in vitro* culture systems that can improve the quality of *in vitro* drug research and may eventually reduce or replace required animal experiments, motivated him in 2013 to pursue his PhD research at the division of Toxicology of the LACDR under supervision of Dr. Leo S. Price, Prof. Dr. Dorien J.M. Peters and Prof. Dr. Bob van de Water. During his PhD studies, he developed 3D cell culture-based screening assays with many different cell types. His PhD studies have resulted in the establishment of 3D cell-culture based phenotypic screening technology that can be used to identify new drug targets or potential new drug candidates as described in this thesis. During his PhD studies, Tijmen received two awards to attend scientific conferences (SLAS Tony B. Travel Awards 2013 and 2016).

After his PhD studies in 2017, Tijmen will combine his interests in developing (physiologically relevant) cell-based assays, laboratory automation technology and compound screening, as lab automation and screening specialist at NEXUS Personalized Health Technologies at the ETH in Zürich.

